

EVALUATING AND COMPARING LONGITUDINAL CONTROL STRATEGIES FOR
AUTONOMOUS VEHICLES

BY

LOUIS SUNGWOO CHO

THESIS

Submitted in partial fulfillment of the requirements
for the degree of Master of Science in Civil Engineering
in the Graduate College of the
University of Illinois Urbana-Champaign, 2025

Urbana, Illinois

Adviser:

Assistant Professor Alireza Talebpour

Abstract

Maintaining appropriate inter-vehicle distances is crucial in enhancing safety and efficiency of traffic flow for autonomous vehicles. Various control spacing control policies affect traffic stability and vehicle dynamics, impacting road capacity and driving patterns. This comparative study analyzes Constant Spacing Policy (CSP), Constant Time Headway (CTH), Traffic Flow Stability (TFS), Constant Safety Factor (CSF), and the Intelligent Driver Model (IDM) by calibrating the genetic algorithm for optimizing the parameters of each spacing policy using highway datasets from I294, I90-94 and Waymo's Phoenix data. Simulation results show that CSP and CSF models had the most robust performance, achieving the lowest RMSE and highest R^2 values. The CSP model achieved stability under low-density highway conditions by maintaining consistent vehicle spacing with minimal perturbations. The CSF policy was determined to be the most optimal policy for high-density traffic, effectively managing safety-critical scenarios involving abrupt acceleration and braking. The CTH model showed reliable performance in stable conditions but sensitive to speed fluctuations, resulting in higher errors during dynamic traffic scenarios. The TFS model consistently had higher errors, reflecting its limited adaptability to congested or complex traffic environments. The IDM model demonstrated strong adaptability and realistic driving behavior across diverse conditions but required precise calibration to achieve optimal performance in high-density and unpredictable scenarios.

Acknowledgments

I would like to thank many people who have always encouraged me to be motivated to work on this thesis along my academic journey. I would like to sincerely thank all the faculty members and students in transportation engineering at the Department of Civil and Environmental Engineering at the University of Illinois at Urbana-Champaign. I would also like to thank the U.S. National Science Foundation under the Centers of Research Excellence in Science and Technology (CREST) program, award number 2112650 for supporting this research.

I am sincerely grateful for my advisor Professor Alireza Talebpour for funding my research and my education, and my colleague Gihyeob An in my research lab for mentoring me throughout the research. This research would not have been attainable without the support of my advisor and my colleague Gihyeob An.

I would also like to express my gratitude to all my friends in Illinois for generously sharing their personal experiences on coping with academic stress and managing mental health during challenging times in life. All the support from my friends have been invaluable to me in navigating difficult circumstances.

I dedicate my thesis work to my family and relatives in South Korea, who have been giving me love, encouragement, and support throughout my adventurous academic journey. Special thanks to my parents for offering me prudent advice on situations where I encountered dilemma in my personal life.

Finally, I extend my gratitude to Lord Jesus Christ, Saint Mary, and the Holy Spirit, who have brought me joy throughout this difficult journey. I am also deeply thankful to everyone who has supported me, especially the fathers of Saint John's Catholic Newman Center, for their spiritual guidance and encouragement.

Table of contents

Chapter 1	Introduction	1
Chapter 2	Background Study	3
Chapter 3	Data Description	13
Chapter 4	Mathematical Formulation	14
Chapter 5	Parameter Optimization	18
Chapter 6	Results and Discussion	22
Chapter 7	Conclusion	226
References	228

Chapter 1: Introduction

1.1 Motivation

Controlling inter-vehicular spacing between vehicles is essential to maintain safety for autonomous vehicles. Various research done by transportation engineers integrate concepts from macroscopic and microscopic traffic properties to safely guide self-driving vehicles along the road while mitigating the risk of major roadway accidents. However, real-world driving maneuvers are overlooked by existing control policies in complex traffic conditions, limiting the ability to adapt to scenarios such as sudden lane changes, varying vehicle interactions, or abrupt braking events. Addressing these challenges requires robust calibration methods that can accurately replicate observed vehicular behavior, ensuring both reliability and safety.

One significant challenge is the procedure of accurately calibrating the spacing policies to replicate the vehicle trajectories. Existing models overlook the intricate interactions between kinematic variables such as acceleration, spacing, and relative speed leading to discrepancies between predicted maneuvers and the actual maneuver. The aforementioned challenges of the control spacing models undermine the reliability in complex traffic scenarios.

This study addresses these challenges by leveraging vehicular trajectory data from Interstate highways to calibrate the most optimal parameters for each control spacing policy by using the genetic algorithm. This approach provides a robust framework for optimizing model parameters, and replicating the observed behavior. The results from this sophisticated calibration process contribute to the development of more reliable and adaptable control spacing policies, paving the way for safer and more efficient autonomous systems.

1.2 Research Objective

The primary objective of this study is to evaluate the performance of various control spacing models used for safely and efficiently maintaining spacings between autonomous vehicles. The goal is to assess the ability of the control spacing models capturing critical driving dynamics such as vehicle speed, spacing, acceleration, and relative speed which could be used for autonomous vehicles. The genetic algorithm calibrates the most optimal parameter values needed for each control spacing policy. By fine-tuning the parameters for control spacing policies, the results were calibrated to closely align the simulated trajectories with the observed vehicle trajectories, ensuring improved accuracy and consistency with real-world vehicular trajectory data.

To evaluate the performance of each model, the calibrated parameters were validated by comparing the predicted trajectories generated by the model against the actual observations for a comprehensive assessment of the model's accuracy and reliability. Additionally, the study examined how each control spacing model performed under varying traffic conditions, from free-flowing scenarios to congested scenarios. This in-depth analysis highlights the strengths and limitations of each control spacing model under various traffic conditions.

1.3 Outline of the Study

The remainder of this study focuses on the calibration results of control spacing models for vehicles. Chapter 2 provides an overview of the background and a comprehensive literature review of various control models used for modeling vehicles. Chapter 3 provides a description of the data utilized for calibration. In Chapter 4, the mathematical formulations for the control models used in this study are shown. Chapter 5 summarizes the results from the calibration process. Finally, Chapter 6 concludes the study with a summary and recommendations for future research in refining the control spacing policies.

Chapter 2: Background Study

2.1 Control Spacing Policies

Various research studies on control spacing models for car-following behavior in autonomous vehicles have been conducted in recent years [1]. These models can be broadly categorized into those that rely on Vehicle-to-Vehicle (V2V) communication, those that function independently of communication systems, and hybrid approaches that integrate multiple strategies [2]. Communication-based models leverage real-time data exchange by getting information through sensors to enhance vehicle coordination and string stability, while non-communication-based approaches rely on predefined control spacing laws to safely maneuver diverse traffic scenarios. Hybrid models aim to balance the advantages of both, improving adaptability under varying traffic conditions.

The selection and fine-tuning of control parameters are critical in optimizing vehicle safety, improving traffic flow efficiency, and maintaining stability across various driving conditions. It is important to meticulously adjust the parameters that govern control spacing policies to enable Adaptive Cruise Control (ACC) systems to adapt to diverse traffic environments. These refined adjustments help mitigate stop-and-go oscillations, enhance traffic safety, and improve overall traffic flow. Furthermore, precise tuning ensures a smoother transition between acceleration and deceleration, reducing abrupt braking events and minimizing perturbations in vehicle platoons. This process is critical in maintaining string stability, preventing abrupt changes in the vehicle's behavior in small speed fluctuations that could propagate through traffic and lead to unnecessary congestion.

The most commonly studied spacing policies for vehicles are Constant Spacing Policy (CSP), Constant Time Headway (CTH), and Traffic Flow Stability (TFS). The Intelligent Driver Model (IDM), developed by Treiber, Hennecke, and Helbing [3], is a widely used car-following model for microscopic traffic flow simulations. The model provides a robust framework for modeling vehicle interactions under various driving conditions, making it useful in research

related to traffic flow dynamics. In addition to these commonly used control spacing policies, Constant Safety Factor (CSF) policy is essential for adjusting inter-vehicle spacing based on safety margins such as adjusting safety factor to take into account of variations in speed, time headway, and braking. These safety measures are critical to allow ACC systems to operate safely and mitigate collisions. Thus, the Constant Factor Safety (CSF) policy was also used to compare the calibration among the aforementioned commonly used control spacing policies.

Additionally, other approaches such as Variable Time Headway (VTH), Cooperative Adaptive Cruise Control (CACC) with String Stability, Model Predictive Control (MPC), Lateral and Longitudinal Control, and Closed-Loop Dynamics have been explored to optimize vehicle interactions and traffic efficiency. The control spacing models for car-following behavior can further be classified based on their reliance on communication systems: those that operate with Vehicle-to-Vehicle (V2V) communication, those without communication, and hybrid approaches that integrate both strategies.

2.2 Models with Communication

Models that incorporate communication-based control strategies have various approaches to simulate the car-following behavior of vehicles. Model Predictive Control (MPC) can help mitigate traffic flow disturbances caused by lane-changing maneuvers while maintaining CTH [4]. The proposed approach optimizes both the lateral trajectory of a lane-changing Connected Automated Vehicles (CAV) and the longitudinal control of a Connected and Automated Vehicles (CAV) in the target lane for simulation. The study proposed a MPC framework for the target-lane vehicle to effectively respond to lane changes, while a predefined set of lateral trajectories was evaluated for the vehicle changing lanes. The optimal trajectory was selected based on its ability to minimize the required deceleration of the impacted vehicle, reducing acceleration disturbances and shockwave propagation. Analytical and simulation results show that the integrated control strategy enhances traffic stability and abate perturbations in the vehicle platooning system.

Gap regulation and gap-closing controllers to enhance string stability in traffic flow [5] was analyzed in another study. These two main controllers take advantage of the Vehicle-to-Vehicle (V2V) communication to enhance coordination between autonomous vehicles. The Cooperative Adaptive Cruise Control (CACC) system that augments traditional Adaptive Cruise Control (ACC) was used to model the vehicles by integrating wireless Vehicle-to-Vehicle communication. One controller was in charge of managing in scenarios where a vehicle joins

the platoon. The other controller regulated the car-following behavior. The Infiniti M56s cars were used for experimental validation to demonstrate the capability of the proposed CACC system being able to significantly improve traffic stability and coordination.

Tuning control model parameters is a commonly used approach to enhance overall system stability for car-following behavior. One study optimizes the ACC system parameters by leveraging the Controller Area Network (CAN) communication framework to improve car-following behavior and to preclude fatal traffic collisions [6]. The proposed ACC system integrates collision avoidance system by classifying driving scenarios into safe, warning, and dangerous modes using a non-dimensional warning index and time to collision metrics. Various control strategies are utilized based on the classifications. The parameters for the optimization process were fine-tuned through a confusion-matrix method using manual-driving data in scenarios with no traffic accidents. The study compares the vehicle-following characteristics of the system to real-world manual driving to emphasize that integrating both ACC and collision avoidance systems can successfully replicate human-driving behavior in both high-speed cruising and low-speed stop-and-go traffic scenarios. Additionally, experimental validation in real-vehicle tests corroborates that the system effectively prevents vehicles from following too close to each other enhancing both safety and driver comfort across various driving conditions.

A study on Semi-Autonomous Adaptive Cruise Control (SAACC) systems explores the integration of a radio-frequency communication framework to enhance highway safety and traffic flow capacity [7]. Unlike traditional Adaptive Cruise Control (ACC) or fully automated highway systems (AHS) that rely on tightly coordinated vehicle platoons, SAACC operates without having to form vehicle platoons or be too dependent on dynamic frequency allocation. The system consistently maintains a user-defined cruising speed until a target vehicle is detected in the same lane. Under this condition, the system adjusts the ego vehicle's following distance based on real-time communication signals. The proposed SAACC approach enables vehicles to maintain smaller time gaps safely while ensuring string stability and minimizing actuator input efforts compared to standard autonomous ACC systems. Simulation results demonstrate that SAACC are more accurate and smoother in tracking vehicles, mitigates control efforts, and increases robustness to variations in vehicle dynamics, making it a viable solution for mixed-traffic environments.

One study examines truck platooning with Cooperative Adaptive Cruise Control (CACC), emphasizing the benefits and challenges of using the Constant Time Headway (CTH) model in uphill driving conditions [8]. The study highlights critical issues where truck platoons

controlled by the CACC model become asymptotically unstable on steep grades due to the limited acceleration capabilities of heavy vehicles. This instability prevents trucks from tracking the vehicle platoon after an uphill terrain, leading to spacing errors. In order to resolve this issue, the study proposes new control strategies to complement existing controllers and enhance stability. These strategies mitigate the adverse effects of low crawl speeds and ensure that truck platoons remain string stable irrespective of uphill grades. The results underscore the need for refined control policies in uneven road conditions where elevation changes impact the overall dynamics of the vehicle and traffic flow.

One study explores the Variable Time Headway (VTH) concept. This method dynamically adjusts the inter-vehicle headway. The headway is increased during acceleration and decreased during deceleration [9]. This adaptive spacing policy enhances string stability, ensuring that perturbations are not amplified during vehicle platooning. Unlike constant spacing policies, which require inter-vehicle communication to maintain string stability, VTH allows autonomous vehicles to achieve stability without explicit coordination by adjusting the time headway based on velocity errors. This modification significantly abates transient spacing errors, improves responsiveness to traffic fluctuations, and minimizes the risk of traffic shockwaves propagating in the vehicle platoon and mitigates stop-and-go congestion. Additionally, VTH allows for smaller inter-vehicle distances in autonomous platoon operation.

Constant spacing with communication is a widely used control model for enhancing vehicle coordination in platooning. Several studies have investigated this approach, including the integration of Adaptive Cruise Control (ACC), spacing policies, and Cooperative Adaptive Cruise Control (CACC) to improve string stability [10]. One study proposes a decentralized CACC controller that relies on a wireless communication link with the nearest preceding vehicle, allowing vehicles to maintain small inter-vehicle spacings. To take into consideration of vehicles with possibly different characteristics, a frequency-domain condition for the string stability system was derived. The study demonstrates that a velocity-dependent inter-vehicle spacing policy, supported by wireless communication, enables stable platooning, whereas a constant spacing system that is independent of velocity may lead to instability.

One study explores the use of linear kinetic properties in Adaptive Cruise Control (ACC) and Cooperative Adaptive Cruise Control (CACC) systems to optimize inter-vehicle spacing in platoons [11]. The proposed spacing control algorithm leverages on-board sensors and communicates only with the preceding vehicle to regulate following distances. The study evaluates string stability by leveraging a frequency-domain analysis and Nyquist diagrams.

The control algorithm ensures that each vehicle maintains a stable spacing while mitigating perturbations that could propagate through the platoon. Numerical simulations demonstrate the model's potential for improving platoon coordination and roadway capacity.

Traffic flow stability analysis was conducted in this research by leveraging deterministic acceleration models and Vehicle-to-Vehicle (V2V) communication [12]. The study proposed a simulation framework that differentiates between connectivity and automation, modeling various vehicle types with distinct communication capabilities. A stability analysis of mixed traffic streams demonstrates that CAVs significantly enhance string stability, with automation proving more effective than connectivity alone in preventing shockwave formation and propagation, underscoring the potential of V2V communication and automation in optimizing highway traffic flow and mitigating congestion.

Model Predictive Control (MPC) is also a widely-known controller to address complex traffic scenarios. These studies have experimented how MPC can be used in multi-stage lane-changing movements of vehicles in dynamic traffic conditions [13], predictive optimization of lane-changing decisions through the integration of game theory and MPC [14], and Distributed MPC for heterogeneous vehicle platoons, which tracks leader speed and maintains desired gaps under unidirectional topologies [15]. MPC enhances Adaptive Cruise Control (ACC) and Cooperative Adaptive Cruise Control (CACC) strategies, allowing vehicles while maintaining traffic stability to adjust their speed and spacing dynamically. Some studies have also integrated learning-based approaches with MPC to improve adaptability in uncertain environments, where vehicles must anticipate and react to unpredictable traffic fluctuations. These findings underscore the importance of optimizing vehicle control and coordination in scenarios where lane-changing behavior happens frequently.

This study proposes a data-driven, stochastic optimization-based Model Predictive Control (MPC) framework that enhances stability, robustness, and safety in longitudinal cooperative driving by incorporating Vehicle-to-Vehicle (V2V) communication [16]. To address uncertainties in traffic dynamics, the framework integrates an online learning-based driving dynamics prediction model that anticipates the uncertain states of preceding vehicles. The predictions were incorporated into a constrained finite horizon optimal control problem to optimize the acceleration and deceleration commands for CAVs. The study calibrates the Distributionally Robust Stochastic Optimization (DRSO) model with Distributionally Robust Chance Constraints (DRCC) to ensure reliable control under uncertain conditions. Additionally, Semi-definite Programming (SDP) relaxation technique was applied to perform real-time

computation. Experimental validation using Next Generation Simulation (NGSIM) data demonstrates that the proposed approach maintains string stability and robust cooperative driving performance under various traffic conditions by properly tuning key parameters such as prediction horizon length and time headway parameters.

Hybrid models incorporating communication have been analyzed. One study integrates Adaptive Cruise Control (ACC) and Model Predictive Control (MPC) to enable smooth platoon merging through vehicle platooning control [17]. Another study examines the impact of Vehicle-to-Vehicle (V2V) communication on traffic flow stability, analyzing how information availability influences critical density and percolation within vehicular networks [18].

Cooperative Adaptive Cruise Control (CACC) has also been studied for its effects on traffic-flow stability and throughput. By leveraging V2V communication, CACC systems provide reference values that enhance traffic characteristics, such as string stability, particularly in mixed traffic conditions [19]. Another study integrates lateral and longitudinal controllers and develops a finite state system to improve autonomous vehicle platooning. The longitudinal control system consists of upper and lower-level controllers, while the lateral controller ensures safe lane-changing behavior [20].

2.3 Models without Communication

Constant Time Headway (CTH) can be used by models without having to rely on communication between vehicles. One study analyzes the vehicle dynamics using a continuous-time deterministic car-following model by leveraging Pipe's Model to simulate steady-state car-following behavior [21]. The study explores the effects of multiple driver reaction and actuation delays on stability, providing a comprehensive characterization of stability regions within the delay parameter space. By running the frequency-sweeping algorithms, the research simplifies the stability analysis and analyzes how drivers' behavior, decision-making delays, and response times affect the overall traffic flow stability.

A research on how string stability can be achieved without relying Vehicle-to-Vehicle (V2V) communication was conducted by leveraging a kinematic linear model with multi-anticipation [22]. The study highlights that most commercially available ACC systems are unstable. While increasing time headway intervals can stabilize traffic, it reduces roadway capacity. To address this major issue, the study proposed an alternative solution that utilizes recent advancements in RADAR sensing technology. By monitoring the behaviors of two vehicles downstream, the

proposed multi-anticipative ACC system ensures string stability across a wide range of traffic conditions without requiring inter-vehicle communication. Analytical and simulation-based evaluations demonstrate that this approach not only enhances traffic stability overall, but also increases road capacity, even in the presence of external perturbations. Furthermore, Pareto optimization was performed to derive the optimal tuning conditions for the time headway policies. The results suggest that multi-anticipative ACC provides a viable solution for mitigating congestion and improving traffic flow without having to build connectivity-based infrastructure.

Additionally, the performance of commercially available Adaptive Cruise Control (ACC) systems has been analyzed, revealing significant limitations in achieving string stability [23]. A large-scale experiment involving ACC-equipped vehicles was conducted to study their car-following behavior under real-world driving conditions. The study evaluates how target time gaps were maintained based on observed distributions across different vehicle brands. Results indicate that current ACC implementations struggle to maintain consistent inter-vehicle spacing, leading to string instability and disruptions in traffic flow. This instability arises due to variations in control logic among different manufacturers and the inability of ACC systems to adapt dynamically to changes in vehicle ordering and settings. The findings underscore the critical role of Constant Time Headway (CTH) policies in mitigating these issues, highlighting the need for more robust control strategies to ensure stable car-following behavior and prevent unintended traffic disturbances as ACC adoption increases.

A study examining Constant Time Headway (CTH) policies proposed a novel framework for designing and evaluating spacing policies [24]. The research assesses spacing policies in terms of string stability, traffic flow stability, and roadway capacity. While the standard CTH policy guarantees string stability, findings indicate that this policy does not perform well in reduced traffic capacity and can cause instability in traffic flow. To address these limitations, the study introduces an "ideal" spacing policy, formulated as a nonlinear function of speed, which improves both string and traffic flow stability while enhancing overall capacity.

Several studies have used constant spacing approaches. One study explores intelligent cruise control strategies within an Automated Vehicle Control System (AVCS) framework. A commonly used controllers for autonomous vehicles called PID controllers were used to adjust the inter-vehicle spacings effectively [25]. Multiple control system tests were performed by using a validated nonlinear longitudinal vehicle model before implementation in real-world vehicles. The proposed control approach ensures smooth and reliable vehicle following by utilizing on-

board sensors that measure relative distance and speed without relying on Vehicle-to-Vehicle (V2V) communication. The overall stability is maintained through a meticulously designed throttle and brake control systems in conjunction with the Constant Time Headway (CTH) policy. Simulation and experimental results emphasize that the integrated system provides stable and responsive vehicle spacing, even in scenarios where the lead vehicle exhibits erratic speed variations.

Another study utilizes partial differential equations (PDEs) to model traffic flow stability in intelligent cruise control systems operating under constant spacing policies [26]. The study distinguishes between two fundamental stability concepts in traffic flow analysis: string stability, which ensures predictable inter-vehicle spacing in a platoon, and traffic flow stability, which accounts for velocity and density variations due to vehicles entering or leaving the flow. The study also highlights that traffic flow stability depends not only on vehicle-following control laws but also on the spacing policy leveraged by the control system. By analyzing the coupled equations governing automatic vehicle following and traffic density, the study investigates the critical role of constant spacing policies in determining highway capacity and traffic stability.

Additionally, a comparative study evaluates various spacing policies, focusing on the impact on safety, traffic flow efficiency, and user acceptance [27]. The study examines the stability of highway traffic under Adaptive Cruise Control (ACC) systems. This study shows that traffic flow stability under a CTH policy is highly dependent on boundary conditions at highway inlets and exits. Furthermore, the research proposes an unconditionally stable spacing policy, which guarantees stability under all boundary conditions. Simulation results highlight the practical consequences of instability, showing that alternative spacing policies outperform the CTH policy in maintaining smooth and efficient traffic flow. One key finding from this study is that the ACC systems should not rely only on the CTH policy.

Other studies have utilized Model Predictive Control (MPC). One study investigates distributed MPC for managing headway and cruise control in vehicle platooning [28]. Another study focuses on adjusting ACC parameters to alleviate traffic congestion and improve flow efficiency [29]. Additionally, predictive optimization and non-linearity compensation were applied to enhance the longitudinal dynamics of vehicular systems [30].

Furthermore, additional studies include a physics-based lumped mass model that incorporates braking and aerodynamic forces for control optimization [31], and a bidirectional control

approach utilizing decentralized dynamics for improved stability [32]. Another study presents a microscopic traffic flow model that integrates both lateral and longitudinal dynamics to address two-dimensional traffic flow challenges. This model effectively handles collision avoidance, lane-changing, and lateral friction [33].

2.4 Alternative Models

Several studies analyze the performance of Adaptive Cruise Control (ACC) and Cooperative Adaptive Cruise Control (CACC) systems. One of the studies analyzes how the Constant Time Headway (CTH) approach can be integrated with ACC and CACC models under uncertainty conditions [34]. One research study leverages a rolling horizon stochastic optimal control strategy, taking into consideration for uncertainties in system dynamics and sensor measurements. Modeling uncertainties were perceived as normally distributed disturbances in both the state and measurement equations. A multi-objective function was defined by incorporating bounded acceleration limits and collision protection constraints. The resulting optimization problem was formulated as a linearly constrained Linear Quadratic Gaussian (LQG) problem, which is solved using the separation principle.

One study analyzed how traffic flow stability can be induced by the Constant Time Headway (CTH) policy using three different modeling paradigms: a microscopic model, a spatially discrete model, and a spatially continuous model [35]. The analysis shows that traffic stability properties can vary across these paradigms unless the control policy and traffic dynamics are consistently formulated. To ensure consistency, a biasing strategy was introduced, determining whether the feedback control being applied to the system is downstream, upstream, or collocated with respect to the vehicle. According to the study results, it was determined that for ACC-equipped vehicles utilizing forward-looking sensors, a downstream biasing strategy results in exponentially stable traffic flow on circular highways. Furthermore, traffic stability can be maintained on open highways if entry and exit conditions follow the downstream biasing strategy.

A research on integrating Adaptive Cruise Control (ACC) and Cooperative Adaptive Cruise Control (CACC) traffic dynamics into a Gas-Kinetic (GKT) macroscopic traffic flow model was conducted [36]. In this approach, an acceleration/deceleration term to simulate the dynamics of ACC and CACC vehicles on traffic flow was proposed. In addition to this, a novel relaxation-based approach that tracks the time/space-gap principle was also introduced. This

method assigns relaxation time to multiple CACC leading vehicles and only the direct leader was assigned to ACC leading vehicles. The partial differential equations for the nonlinear system were used for numerical approximation using a high-resolution finite volume scheme with a weighted essentially non-oscillatory (WENO) discretization method. The calibrated results calcify corroborates that CACC enhances traffic flow stability, particularly in response to perturbations on a ring road and merging flows at an on-ramp. Compared to ACC, the CACC model enhances dynamic equilibrium capacity and mitigates congestion more effectively, particularly in bottleneck locations.

Human drivers tend to drive relying on the speed and position of the preceding and following vehicles to adjust the state and control inputs of the vehicle. Longitudinal vehicle models can be used to simulate real-world traffic maneuvers by incorporating engine, throttle, and brake dynamics to replicate human-driving behaviors [37]. This study proposed an Autonomous Intelligent Cruise Control (AICC) system, where the relative speed and inter-vehicle spacing determines the actions the following vehicle can take to maintain a desired spacing between the vehicles, ensuring platoon stability bi-directionally. This system has been effective in controlling time headway between vehicles and maintaining constant inter-vehicle spacings.

One study [38] leverages a hierarchical control approach to Adaptive Cruise Control (ACC) as part of an Advanced Driver Assistance System (ADAS). The System-of-Systems (SOS) framework to unify multiple ADAS functionalities was proposed. The ACC system was structured into High-Level Control (HLC), Low-Level Control (LLC), and sensor units to enhance adaptability and efficiency. Using a finite state machine, the HLC dynamically adjusts the vehicle's speed, either by maintaining a minimum safe following distance or by tracking a desired velocity. The Model Predictive Controller (MPC) tracks the movement of the target vehicle and generate optimal control actions for the distance control state. The throttle and brake actions are maneuvered by the LLC. By leveraging the hierarchical structure, the proposed ACC system enhances vehicle response, enhances safety, and facilitates integration with other ADAS technologies such as collision avoidance and blind spot detection.

Chapter 3: Data Description

The high-fidelity Third Generation Simulation (TGSIM) dataset [39] was utilized for analyzing vehicle trajectories [40], [41]. The holistic dataset focuses on complex urban, multi-modal road networks capable of traffic simulations of control algorithms [41] to be conducted. For this research, datasets from the I90/94, and level 1 autonomy vehicles in I294 were utilized with bi-directional lanes represented by positive and negative signs for each lane number.

Each control model in this study was calibrated using the dataset's high-resolution, 10 Hz data, offering an intricate perspective on vehicular movements [41]. The datasets include important trajectory attributes such as time in seconds, longitudinal and lateral coordinates in meters respectively, velocity in meters per second, and acceleration in meters per second squared, enabling a comprehensive analysis of movement patterns and vehicle dynamics for control. In addition to this, the datasets are utilized to track each vehicle's motion in highways.

In addition to the TGSIM datasets, the Phoenix dataset was also used for running simulations. The Phoenix dataset has trajectory data including key attributes such as lateral and longitudinal coordinates in meters, speed in meters per second, acceleration in meters per second squared collected by the LiDAR sensors in the Waymo self-driving cars. By comparing simulations in the Phoenix dataset with the TGSIM datasets, the simulated environments were analyzed to evaluate the interactions between the ego vehicle and the surrounding vehicles in varying traffic conditions [42].

Chapter 4: Mathematical Formulation

This study analyzes Constant Spacing Policy (CSP), Constant Time Headway (CTH), Traffic Flow Stability (TFS), Constant Safety Factor (CSF), and the Intelligent Driver Model (IDM). The aforementioned control spacing policies are widely used to safely maintain the distance between vehicles which can be potentially used for safe autonomous driving.

The CSP model maintains fixed longitudinal gaps between the ego and the leader vehicles, commonly used in vehicle platooning. The CTH model dynamically adjusts the following distance based on the time interval between vehicles. The TFS policy aims to stabilize traffic flow and mitigate stop-and-go traffic waves. The CSF policy prioritizes maintaining safety and to mitigate collision avoidance by dynamically adjusting inter-vehicle spacings. Lastly, the IDM dynamically adjusts inter-vehicle gaps based on the velocity difference to the leading vehicle, incorporating both acceleration and deceleration dynamics to model realistic driving behavior.

This study conducts an in-depth analysis of optimizing the calibration performance of control spacing models, providing a comprehensive assessment of vehicle interactions on roadways. By examining dynamic behavior, the study evaluates how various control strategies influence traffic flow efficiency, safety, and stability.

4.1 Constant Spacing Policy

The Constant Spacing Policy (CSP) maintains a constant spacing between the vehicles from the preceding vehicle with a low computation load [2]. The spacing error variable δ_i for the Constant Spacing Policy can be defined as:

$$\delta_i = x_i - x_{i-1} + L$$

where x_i is the position of the ego vehicle and x_{i-1} is the position of the leading vehicle, and L being the desired spacing. The control law used in this policy is defined as [43] :

$$\ddot{x}_i = -k_v \dot{\delta}_i - k_p \delta_i$$

where k_v, k_p are constants and $\dot{\delta}_i$ is the relative speed between the ego and the leader vehicles.

4.2 Constant Time Headway Policy

To ensure that the desired spacing increases proportionally with the speed, the Constant Time Headway (CTH) dynamically adjusts inter-vehicle spacing in proportion to vehicle speed based on the time headway between the ego and the leader vehicles. [2]. The spacing error variable δ_i for the Constant Time Headway policy can be defined as:

$$\delta_i = x_i - x_{i-1} + hv_i + d_{min}$$

where d_{min} is the safety distance between the ego and the leader vehicles, h is the time headway between two vehicles, and v_i is the speed of the i-th vehicle,. The control law used in this policy is defined as [44]:

$$\ddot{x}_i = -\frac{1}{h}(\dot{\epsilon}_i + \lambda \delta_i)$$

where $\dot{\epsilon}$ is the rate of change for the spacing error, and λ is an arbitrary constant.

4.3 Traffic Flow Stability Spacing Policy

However, the main challenge of the CTH spacing policy is that the stabilizing the traffic flow is not guaranteed. To resolve this issue, the Traffic Flow Stability (TFS) spacing policy was devised. The TFS spacing policy was designed based on the Greenshield's relation, providing better traffic flow stabilization while ensuring safety [2]. The spacing error variable δ_i used for the Traffic Flow Stability spacing policy can be defined as:

$$\delta_i = x_i - x_{i-1} + \frac{1}{\rho_m(1 - \frac{v_h}{v_f})}$$

where ρ_m is the traffic density, v_f is the speed parameter, v_i is the speed of the i-th vehicle. The control law used in this policy is defined as [45] :

$$\ddot{x}_i = -\rho_m(v_f - v_i)(1 - \frac{v_i}{v_f})(\dot{\epsilon}_i + \lambda \delta_i)$$

where $\dot{\epsilon}$ is the rate of change of spacing error, λ is the control gain and δ_i is the spacing error of the i -th vehicle.

4.4 Constant Safety Factor Policy

Safety is an inevitable factor that must be taken account for autonomous driving. To mitigate the possibility of road collisions and to improve driving safety, the Constant Safety Factor (CSF) spacing policy was proposed. Specifically, the emergency braking process was meticulously analyzed for the CSF policy [2]. The spacing error variable δ_i used for the Constant Safety Factor policy can be defined as:

$$\delta_i = x_i - x_{i-1} + d_{min} + t_d v + K D_{stop}$$

where t_d is the time delay, K is the safety factor and the stopping distance D_{Stop} defined as:

$$D_{stop} = -\frac{v_i^2}{2j_i}$$

where j_i is the max deceleration value of the i -th value set as -7.32 m/s^2 . The control law used in this policy is defined as [46] :

$$\ddot{x}_i = -\frac{\dot{\epsilon}_i + \lambda \delta_i}{t_d - \frac{\gamma}{j_i} \dot{x}_i}$$

where λ is a positive control gain, t_d is the time delay in the longitudinal control system, γ is the safety coefficient, and j_i is the average deceleration value of the i -th vehicle during the maximum brake action.

4.5 Intelligent Driver Model

The Intelligent Driver Model (IDM) is a widely-known model to emulate human driving behavior using microscopic traffic properties. The spacing s between the ego vehicle and the leader vehicle can be defined as [3]:

$$s = x_i - x_{i-1}$$

where x_i and x_{i-1} are the position of the ego vehicle and the leader vehicle respectively. The relative velocity Δv is defined as:

$$\Delta v = v_i - v_{i-1}$$

where v_i is the speed of the ego vehicle and v_{i-1} is the speed of the leader vehicle. The acceleration formula can be defined as:

$$\dot{v} = a \left(1 - \left(\frac{v}{v_0} \right)^4 - \left(\frac{s^*(v, \Delta v)}{s} \right)^2 \right)$$

where v is the velocity of the ego vehicle, v_0 is the desired velocity, T is the safe time headway, a is the maximum acceleration, s is the spacing between vehicles. The desired spacing $s^*(v, \Delta v)$ can be calculated by using the following formula below:

$$s^*(v, \Delta v) = s_0 + T v - \frac{v \Delta v}{2\sqrt{ab}}$$

where s_0 is the minimum safe distance between vehicles, and b is the comfortable deceleration.

The analysis of the aforementioned spacing policies evaluate the ability to emulate real-world traffic dynamics effectively. This includes assessing the holistic impact on traffic flow stability, safety, efficiency, and adaptability to diverse traffic conditions. By analyzing the various spacing policies, the study provides a comprehensive analysis of each model's performance with the requirements of modern control systems, offering guidance for optimizing control strategies in both normal and complex driving scenarios to enhance the overall safety and efficiency of simulating trajectories for autonomous vehicles.

Chapter 5: Parameter Optimization

The genetic algorithm was leveraged in this study to determine the optimal parameters for each control spacing policy to model the car-following simulation. The algorithm iteratively evaluates possible solutions based on a fitness function that minimizes speed deviation between the simulated follower and the target follower. Through selection, crossover, and mutation, the population evolves over multiple generations to converge toward an optimal set of control parameters for each control spacing policy during calibration.

5.1 Fitness Function

The fitness function evaluates the effectiveness of the car-following model parameters by comparing simulated speed profiles with target speeds and minimizing the difference between the two variables. Multiple error metrics, such as mean squared error (MSE) and root mean squared error (RMSE), were integrated to quantify the deviation between the simulated follower generated by the control parameters and the target follower. Lower deviation indicates better adherence to the desired trajectory, leading to a higher fitness score. This approach ensures that the optimized parameters conduce to optimal results.

$$\Delta v = v_{sim} - v_{target} \quad (5.1)$$

where v_{sim}, v_{target} are the speed of the simulated follower and the target follower respectively. In addition to this, the error metrics are calculated as follows:

- Mean Squared Error (MSE):

$$MSE = \frac{1}{N} \sum_{i=1}^N (\Delta v_i)^2 \quad (5.2)$$

- Root Mean Squared Error (RMSE):

$$\text{RMSE} = \sqrt{\text{MSE}} \quad (5.3)$$

- Mean Absolute Error (MAE):

$$\text{MAE} = \frac{1}{N} \sum_{i=1}^N |\Delta v_i| \quad (5.4)$$

- Mean Absolute Percentage Error (MAPE):

$$\text{MAPE} = \frac{100}{N} \sum_{i=1}^N \left| \frac{\Delta v_i}{v_{target}} \right| \quad (5.5)$$

- Normalized Root Mean Squared Error (NRMSE):

$$\text{NRMSE} = \frac{\text{RMSE}}{\max(v_{target}) - \min(v_{target})} \quad (5.6)$$

- Sum of Squared Errors (SSE):

$$\text{SSE} = \sum_{i=1}^N (\Delta v_i)^2 \quad (5.7)$$

- R-squared Value:

$$R^2 = 1 - \frac{\text{SSE}}{\sum_{i=1}^N (v_{target_i} - \bar{v}_{target})^2} \quad (5.8)$$

- Speed Deviation Penalty:

$$\sigma = \sum_{i=0}^N (v_{sim_i} - v_{target_i})^2 \quad (5.9)$$

- Total Difference:

$$\text{Total Difference} = \sum_{i=1}^N |\Delta v_i| \quad (5.10)$$

The fitness function $f(x)$ is defined as:

$$f(x) = \frac{1}{\sigma + 10^{-6}} \quad (5.11)$$

5.2 Genetic Algorithm

The genetic algorithm used in this study initializes a certain number of individuals with random values within the specified parameter ranges given an appropriate population size. For each iteration, the genetic algorithm runs for a set number of generations, computing fitness values and ranking individuals accordingly. The top $\frac{N}{2}$ individuals are selected, and the crossover operation is performed by swapping segments between two parents. The mutation step introduces a random adjustment of either -0.1 or 0.1 to the offspring to introduce noise. The new population was formed with these offspring, iteratively refining the parameters during the optimization process. This calibration effectively optimizes the parameters needed for the car-following model for each spacing policy [47].

Algorithm 1 Genetic Algorithm for Car-Following Model Optimization

```
1: Input: Population size  $N$ , number of generations  $G$ 
2: Initialize: Generate  $N$  individuals with random values in the parameter ranges:
3: for each generation  $g = 1$  to  $G$  do
4:   Evaluate fitness: Compute fitness for each individual
5:   Sort population: Rank individuals based on fitness
6:   Select parents: Choose top  $N/2$  individuals
7:   Crossover: Generate offspring by swapping parts of two parents
8:   for each offspring do
9:     Select crossover point randomly
10:    Create child solutions:
          child1 = (parent1[: crossover_point], parent2[crossover_point :])
          child2 = (parent2[: crossover_point], parent1[crossover_point :])
11:   end for
12:   Mutation:
13:   for each child  $i$  do
14:     if random probability < mutation rate then
15:       child $i$  = child $i$  +  $\delta$ ,  $\delta \sim U(-0.1, 0.1)$ 
16:     end if
17:   end for
18:   Replace population: Form the new population with parents and offspring
19: end for
20: Return: Best individual and associated error metrics
```

5.3 Car-following Behavior

The car-following behavior calculates the desired position depending on the control spacing policy being used initially, then the gap distance between the ego and the leader vehicle is calculated by using the following formula:

$$\Delta_i = x_i - x_{i-1}$$

where x_i is the ego vehicle and x_{i-1} is the leader vehicle. The safety distance is then calculated based on the control spacing model being used. The parameters are then fed into the function which calculates the acceleration a of the vehicle for the specific control policy being leveraged. The respective position and the speed are updated using the calibrated values. The speed of the simulated vehicle is updated by the following equation:

$$v_{i+1} = v_i + at$$

where v_i is the previous speed of the vehicle at time t seconds and the acceleration a is calibrated using the respective control spacing policy. The position of the vehicle is then updated by the following equation:

$$x_{i+1} = x_i + v_i t + \frac{1}{2} a t^2$$

where x_{i+1} is the updated position of the simulated vehicle, and x_i is the previous position of the simulated vehicle during the simulation process. The car-following model is called through the optimization process, where the genetic algorithm calibrates the most optimal parameters for the five of the control spacing policies.

The calibration process iteratively refines the parameters by minimizing the error between simulated trajectories and the ground truth trajectory by calling the fitness function, allowing the control spacing models to adapt to various traffic conditions and maintain stability to mitigate sudden fluctuations in position and speed.

Chapter 6: Results and Discussion

For each control spacing policy, the genetic algorithm was used to calibrate the car-following model. The sophisticated calibration process fine-tunes the optimal parameters for each of the control spacing policies by taking into account of the dynamic responses of surrounding vehicles under various driving conditions. The I294, I90/94 and the Phoenix Waymo datasets were used for calibrating the optimal parameters and simulating the trajectories generated by each control spacing policy. The overall process is critical to enhance safety and maximize efficiency of traffic flow for autonomous vehicles.

6.1 Parameter Bound Selection and Limits

To maintain consistency throughout the genetic algorithm calibration process, key parameters such as population size, number of generations, and mutation rate were standardized across all control spacing models analyzed in this study, as shown in Table 6.1. By fixing these parameters needed for the genetic algorithm, this ensures that there are no inconsistencies in the optimization process.

In addition to predetermining the parameters for the genetic algorithm, the parameter bounds for each control spacing model were meticulously selected. The bounds were adjusted to preclude unrealistic acceleration values from being used for the calibration process which could result in the simulated vehicle making impulsive behavior or instability.

Standardizing the parametric limits ensures that comparisons between different control spacing models remain valid and to prevent fluke during the calibration process. Additionally, maintaining fixed parameter boundaries prevent anomalies during the calibration process, reducing the likelihood of convergence to unrealistic or non-generalizable solutions. This approach enhances the reliability of the simulated results.

Table 6.1: Constant parameters for simulating the genetic algorithm.

Parameter	Range
Population Size	100
Number of Generations	100
Mutation Rate	0.1

6.1.1 CSP Parameter Ranges

For the Constant Spacing Policy (CSP), the position tracking constant (k_p), speed correction coefficient (k_v), and desired spacing in meters ($S_{desired}$) parameters were optimized. The parameters were assigned with appropriate ranges to facilitate the search for an optimal solution, as presented in Table 6.2. The position tracking constant (k_p) adjusts the position relative to the target spacing. The lower bound prevents slow reactions to ensure that the vehicle does not respond slowly to changes in the leader vehicle's movement. The upper bound prevents excessive oscillations which could lead to unstable behavior. The speed correction coefficient (k_v) adjusts the influence of the speed differences between the ego and the leader vehicle. The minimum value ensures that the speed correction is gradual while the upper value prevents the aggressive speed changes of the ego vehicle which could lead to abrupt acceleration and deceleration cycles. The desired spacing ($S_{desired}$) ensures the safe distance between the ego and the leader vehicle. The range allows the ego vehicle not to follow too closely with the leader vehicle or unnecessarily slow down if the gap between the ego and the leader vehicle is sufficient enough.

Table 6.2: Parameter ranges for Constant Spacing Policy.

Parameter	Range
k_p	(0.01, 1.5)
k_v	(0.01, 0.9)
$S_{desired}$	(2.5, 10.0)

6.1.2 CTH Parameter Ranges

For the Constant Time Headway policy (CTH), the time headway in seconds (t_h), the minimum safety distance in meters (d_{min}), and damping factor (λ) parameters were optimized. The parameters were given an appropriate range respectively to ease finding an optimal solution shown in Table 6.3. The time headway (t_h) represents the time interval between the ego and the leader vehicles to ensure safe following distance. The lower bound prevents the ego vehicle

from dangerously following closely to the leader vehicle. The upper bound ensures that the ego vehicle does not unnecessarily slow down which could lead to big gaps causing inefficient traffic flow. The minimum safety distance (d_{min}) is the safety buffer between the ego and the leader vehicles. The lower bound is the minimum safe distance to ensure collisions and the upper bound prevents the ego vehicle from unnecessarily slowing down. The damping factor (λ) stabilizes the vehicle's response to speed fluctuations and time interval adjustments. The lower bound ensures that the damping factor is not too weak while the upper bound prevents the adjustments being too aggressive, allowing smooth transitions in vehicle dynamics.

Table 6.3: Parameter ranges for Constant Time Headway policy.

Parameter	Range
t_h	(1.5, 2.0)
d_{min}	(2.5, 3.5)
λ	$(1.0 \times 10^{-5}, 1.0 \times 10^{-4})$

6.1.3 TFS Parameter Ranges

For the Traffic Flow Stability policy (TFS), the traffic density in vehicles per meter (ρ_m), damping factor (λ), and free flow speed in meters per second (v_f) parameters were optimized. The parameters were given an appropriate range respectively to find an optimal solution shown in Table 6.4. The traffic density (ρ_m) ranges have been adjusted to ensure that the vehicle does not fall into unrealistic free-flow speed conditions. The range was chosen to replicate the typical traffic density along the freeways. The range for the damping factor (λ) balances the transient oscillations of the model and to stabilize traffic flow. The lower bound of the free flow speed (v_f) reflects the moderate traffic conditions and the upper bound represents the traffic conditions under optimal conditions.

Table 6.4: Parameter ranges for Traffic Flow Stability policy.

Parameter	Range
ρ_m	(0.10, 0.15)
λ	(0.10, 0.40)
v_f	(25.00, 35.00)

6.1.4 CSF Parameter Ranges

For the Constant Safety Factor (CSF) policy, the safe distance in meters (d_{min}), damping factor (λ), and braking dynamics coefficient (γ) were optimized to ensure safe and efficient car-following behavior. The maximum deceleration for the i -th vehicle was set to -7.32 m/s^2 , while the time delay was fixed at 0.05 seconds to account for realistic driver response times. Each parameter was assigned an appropriate range to facilitate the search for an optimal solution, as presented in Table 6.5. By calibrating these parameters using a genetic algorithm, the CSF policy enhances stability and responsiveness, particularly in scenarios involving sudden braking or dense traffic conditions. The range for the minimum safe distance (d_{min}) is slightly less than for other control spacing policies because the safety factor (K) and braking dynamics coefficient (γ) were taken into account for the CSF model. The damping factor smooths out the speed variations in response to the changes in leader vehicle's movement. This range was chosen to enhance stability in both dense traffic conditions and to prevent excessive stop-and-go oscillations. The lower bound of the safety factor (K) ensures the vehicle reacts appropriately to speed changes while the upper bound prevents aggressive responses to speed changes. The braking coefficient (γ) adjusts how aggressively the braking is applied on the vehicle. The lower bound allows gradual braking adjustments while the upper bound ensures braking in unprecedented situations.

Table 6.5: Parameter ranges for Constant Safety Factor policy.

Parameter	Range
d_{min}	(2.50, 3.00)
λ	(0.01, 0.40)
K	(0.50, 3.00)
γ	(0.10, 0.50)

6.1.5 IDM Parameter Ranges

Finally, for the Intelligent Driver Model (IDM), key parameters such as the minimum safe distance (s_0) in meters, free-flow speed (v_0) in meters per second, time headway (T) in seconds, maximum acceleration (a_{max}) in m/s^2 , and comfortable deceleration (b) in m/s^2 were optimized to ensure safe and efficient car-following behavior. Each parameter was assigned a carefully chosen range to balance realism and computational efficiency, facilitating the search for an optimal solution, as presented in Table 6.6.

The chosen parameter ranges reflect realistic driving conditions and vehicle dynamics. The maximum acceleration range of 0.1 to 3.0 m/s^2 accounts for the diversity in vehicle performance, from low-powered cars to high-performance vehicles. The desired velocity (v_0) is set between 10.0 and 30.0 m/s to cover typical urban and highway speed limits. The minimum spacing (s_0) is constrained between 3.0 and 6.0 meters, ensuring that vehicles maintain a reasonable gap even at low speeds. A time headway (T) range of 0.5 to 3.0 seconds accommodates variations in driver behavior, from aggressive to conservative following. Finally, the comfortable deceleration (b) is limited between 0.5 and 3.0 m/s^2 to capture a balance between smooth and emergency braking scenarios. By calibrating the chosen ranges for the parameters using a genetic algorithm, the IDM framework enhances stability and responsiveness, particularly in challenging traffic conditions such as sudden braking events or high-density congestion.

Table 6.6: Parameter ranges for Intelligent Driver Model.

Parameter	Range
a_{max}	(0.1, 3.0)
v_0	(10.0, 30.0)
s_0	(3.0, 6.0)
T	(0.5, 3.0)
b	(0.5, 3.0)

After determining the appropriate parameter ranges for optimization, the genetic algorithm calibrated the car-following model for each control spacing policy. High-fidelity Interstate highway datasets were utilized to model the simulated trajectories, ensuring realistic traffic conditions. Through iterative evolution, the genetic algorithm performed multiple mutations and crossovers, refining the intrinsic parameter values to achieve optimal performance. The final set of optimized parameters was selected based on their ability to enhance vehicle stability, responsiveness, and overall traffic efficiency.

6.2 Simulated Trajectories

The position-versus-time and speed-versus-time graphs were plotted to visualize the behavior of the simulated follower vehicle in relation to both the leader vehicle and the target vehicle under the various control spacing policies implemented. The following plots illustrate how the follower vehicle adjusts its position and velocity over time in response to changes in the leader's motion, allowing for a comparative analysis of the effectiveness of each spacing policy.

Each graph assesses the ability of each policy to maintain safe following distances, minimizing speed fluctuations, and ensuring smooth acceleration and deceleration transitions.

6.2.1 CSP I294 Simulated Results

For the Constant Spacing Policy (CSP), the simulated results for I294 are illustrated in Figures [6.1](#), [6.2](#), [6.3](#), [6.4](#), [6.5](#), [6.6](#), [6.7](#), [6.8](#), [6.9](#), [6.10](#), [6.11](#), [6.12](#), [6.13](#), [6.14](#), [6.15](#), [6.16](#), [6.16](#), [6.17](#), [6.18](#), [6.19](#), [6.20](#), [6.21](#), [6.22](#), [6.23](#), [6.24](#), [6.25](#) and [6.26](#). Overall, the CSP policy effectively aligns the simulated trajectories with the target trajectories, demonstrating strong consistency in position tracking. However, speed deviations were observed during simulation, where the model occasionally followed the leader vehicle's speed pattern or slightly deviated from the target vehicle's speed profile. These variations indicate potential minor adjustments in the CSP model's responsiveness, particularly in adapting to dynamic traffic conditions.

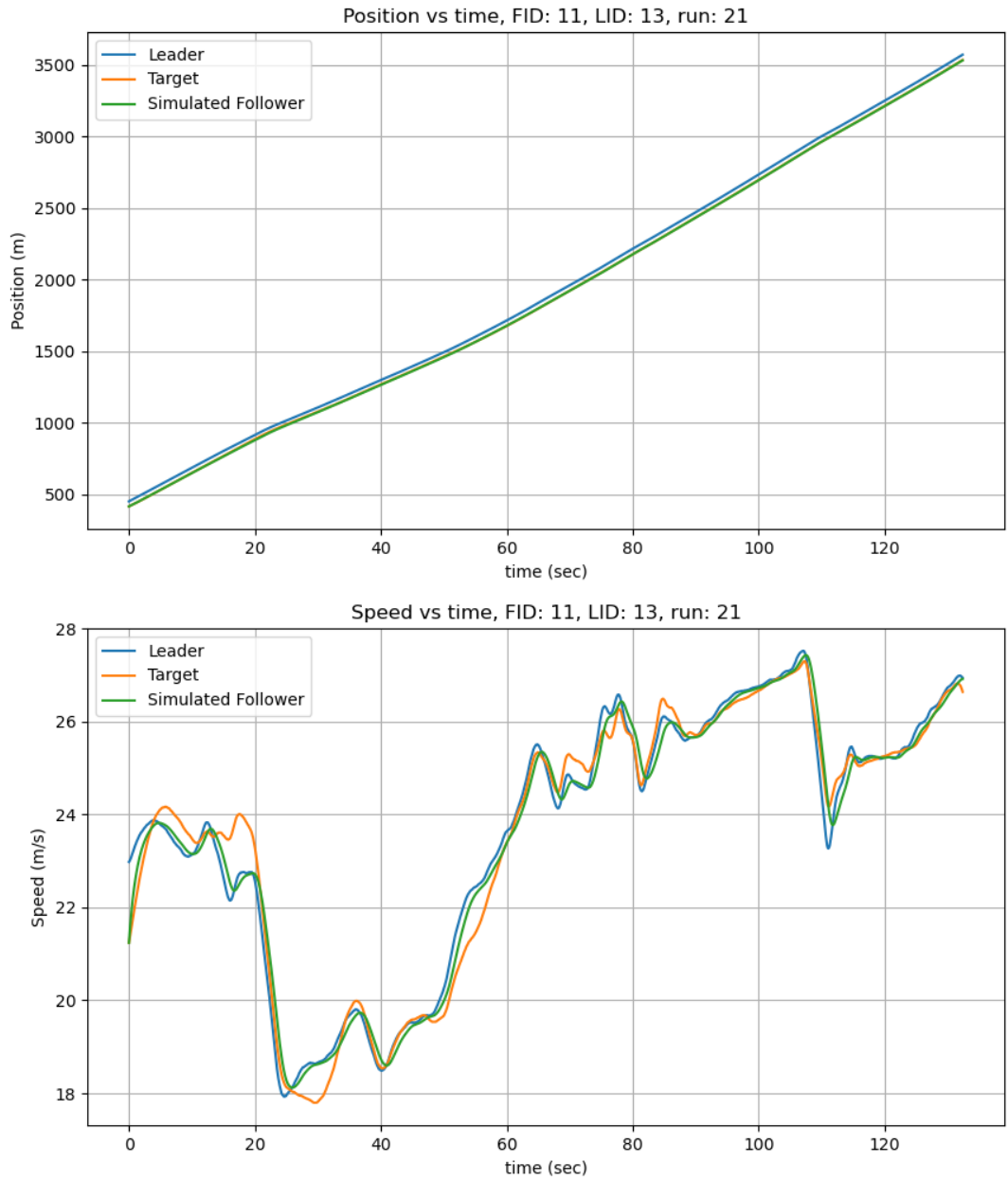


Figure 6.1: Position and speed for CSP for vehicle 11 in run 21 I294L1 dataset.

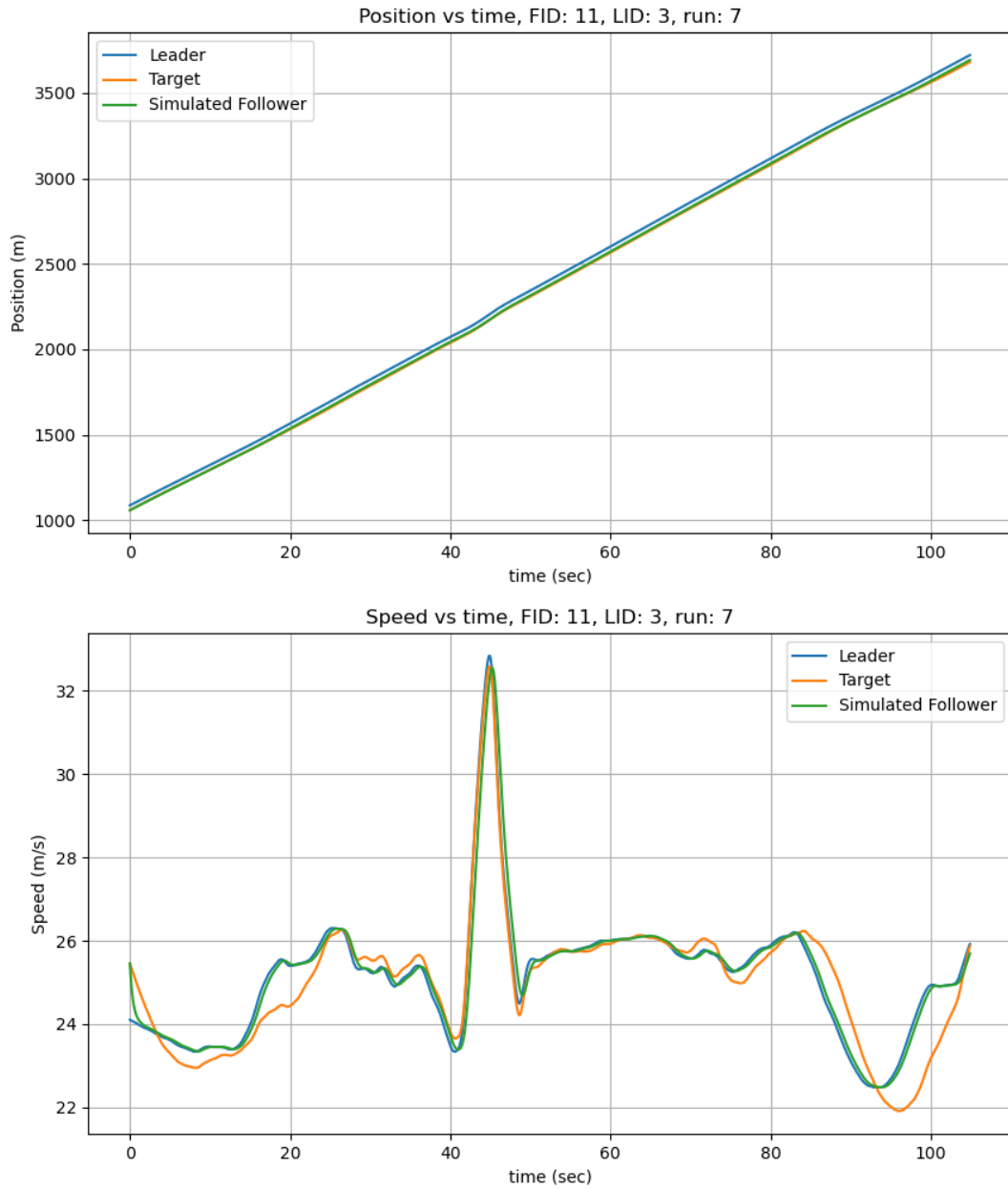


Figure 6.2: Position and speed for CSP for vehicle 11 in run 7 I294L1 dataset.

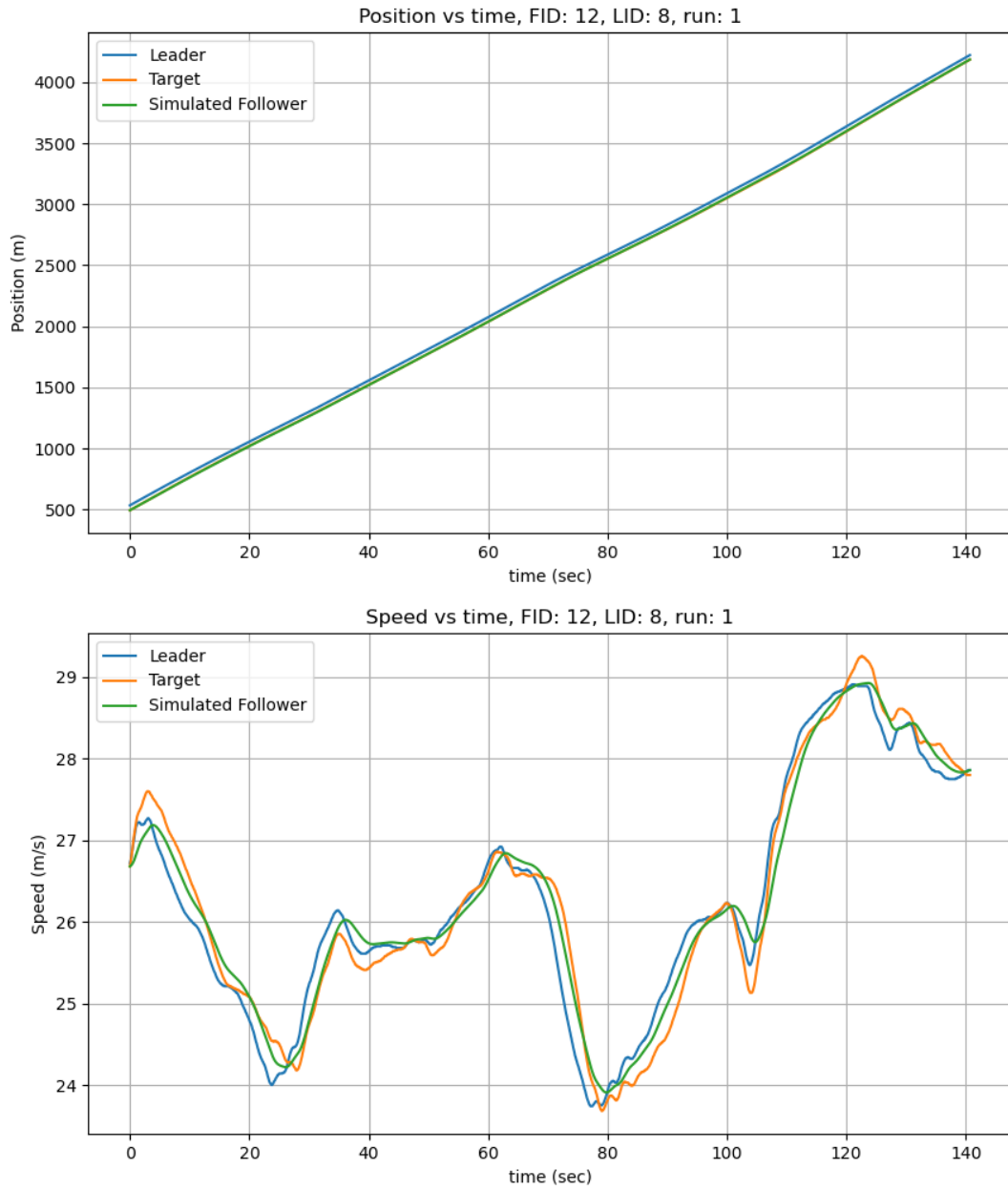


Figure 6.3: Position and speed for CSP for vehicle 12 in run 1 I294L1 dataset.

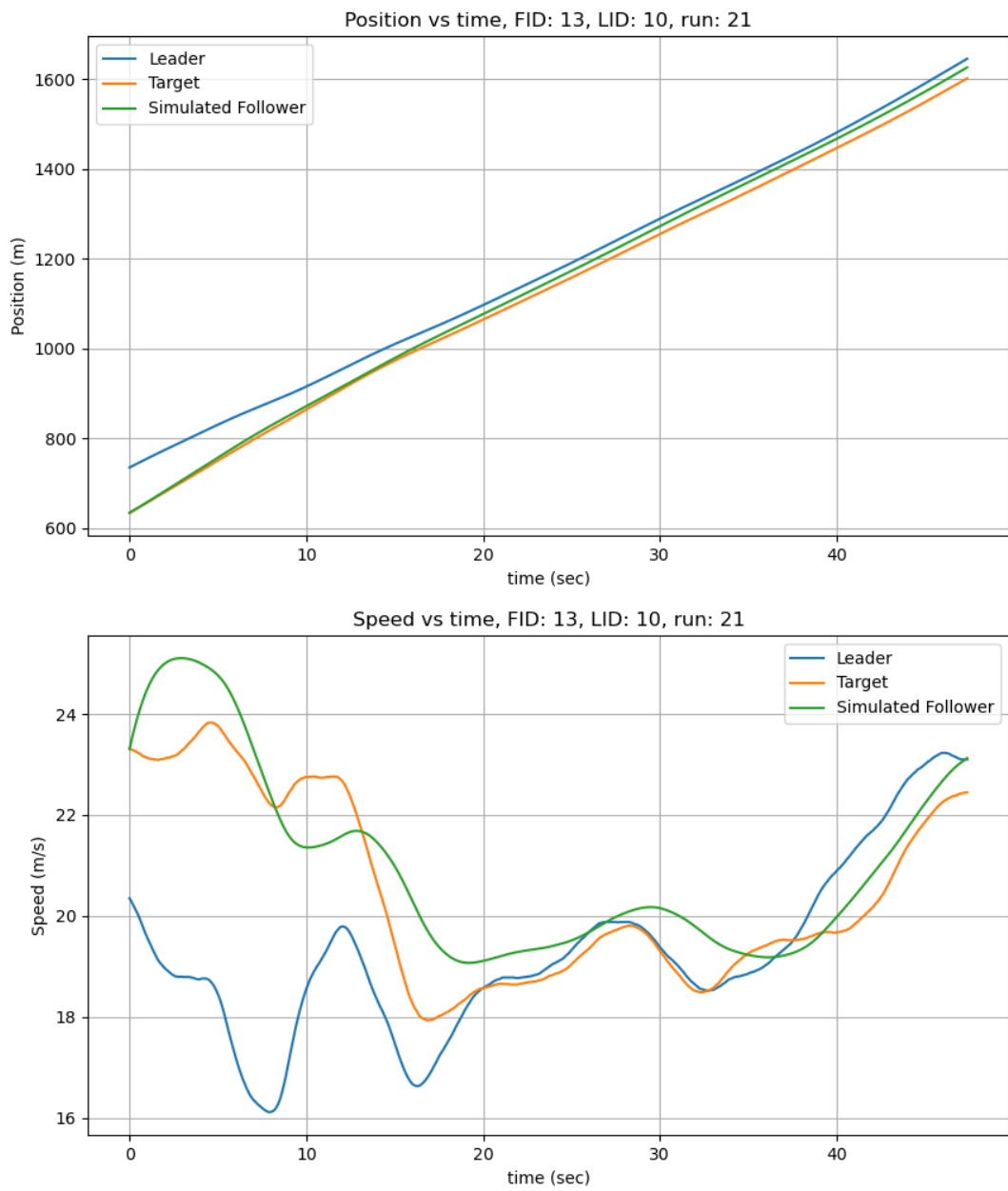


Figure 6.4: Position and speed for CSP for vehicle 13 in run 21 I294L1 dataset.

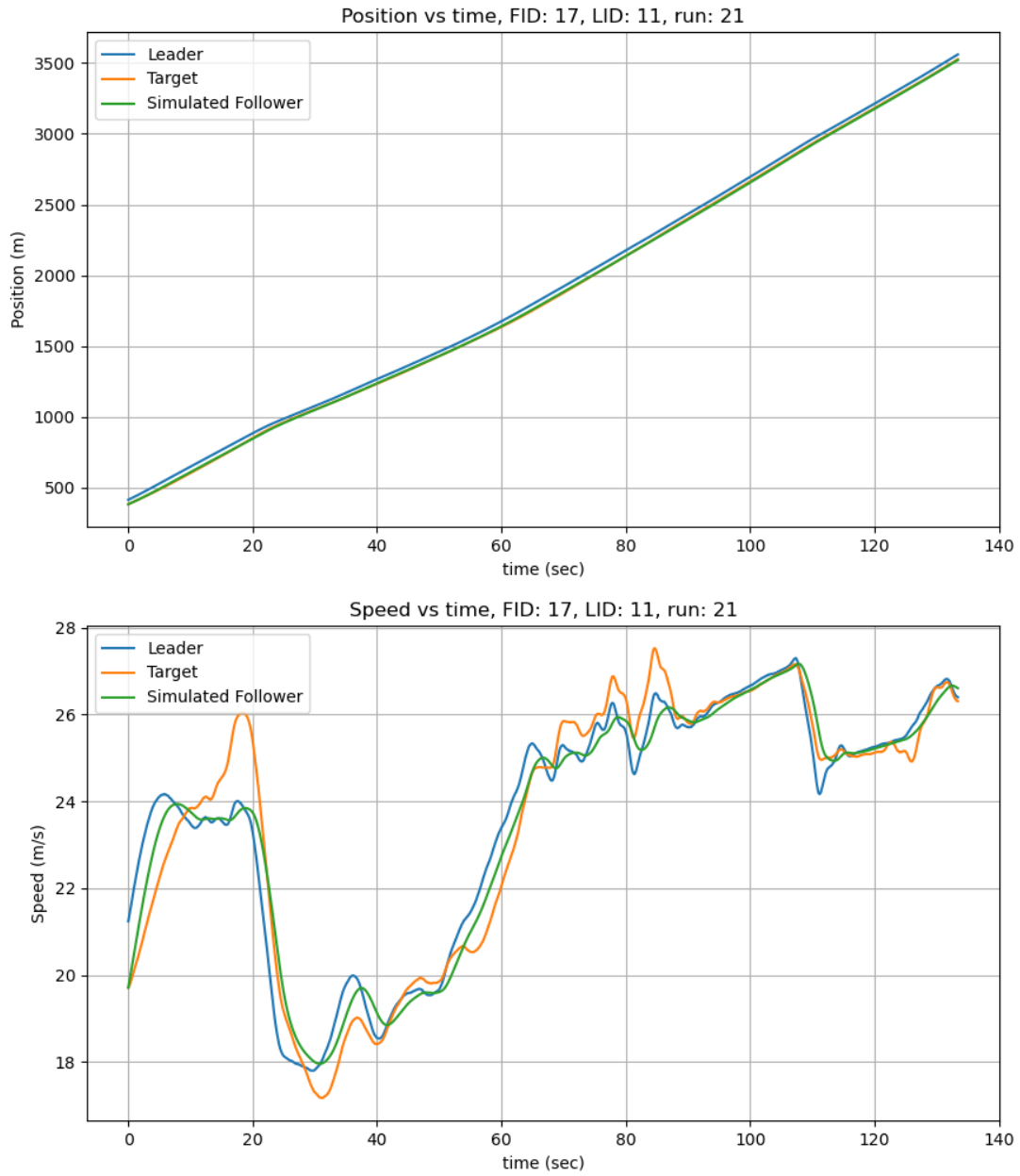


Figure 6.5: Position and speed for CSP for vehicle 17 in run 21 I294L1 dataset.

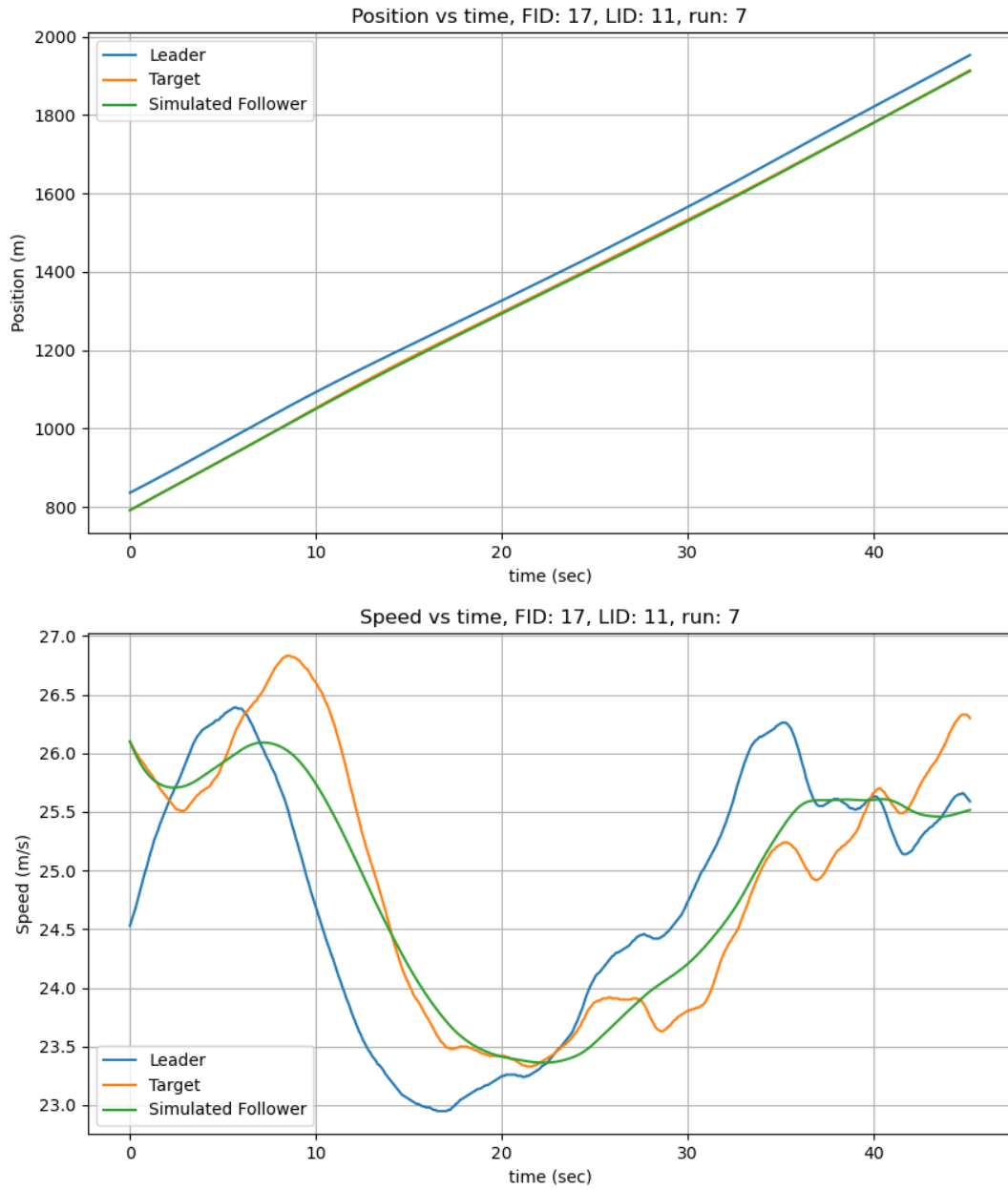


Figure 6.6: Position and speed for CSP for vehicle 17 in run 7 I294L1 dataset.

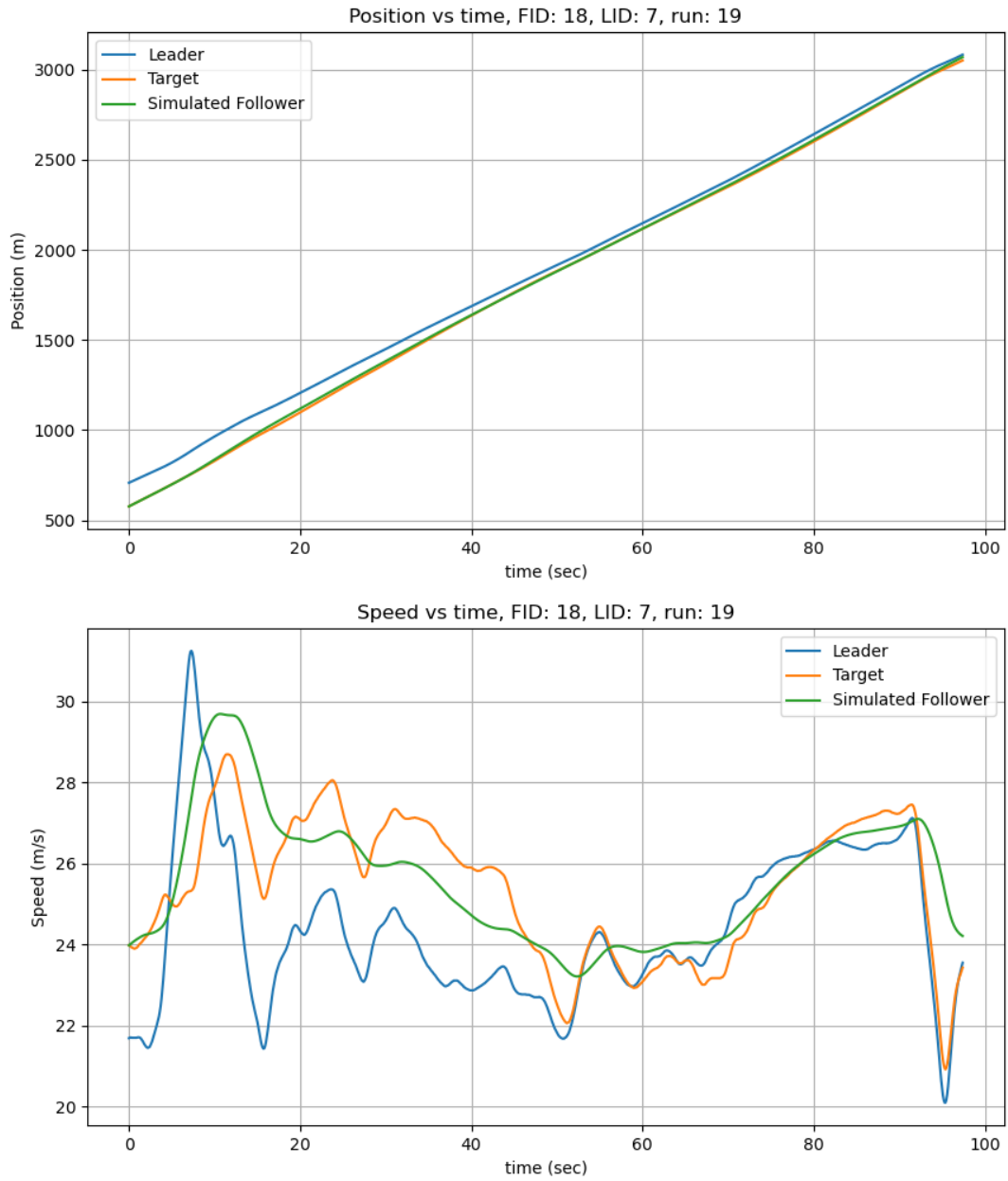


Figure 6.7: Position and speed for CSP for vehicle 18 in run 19 I294L1 dataset.

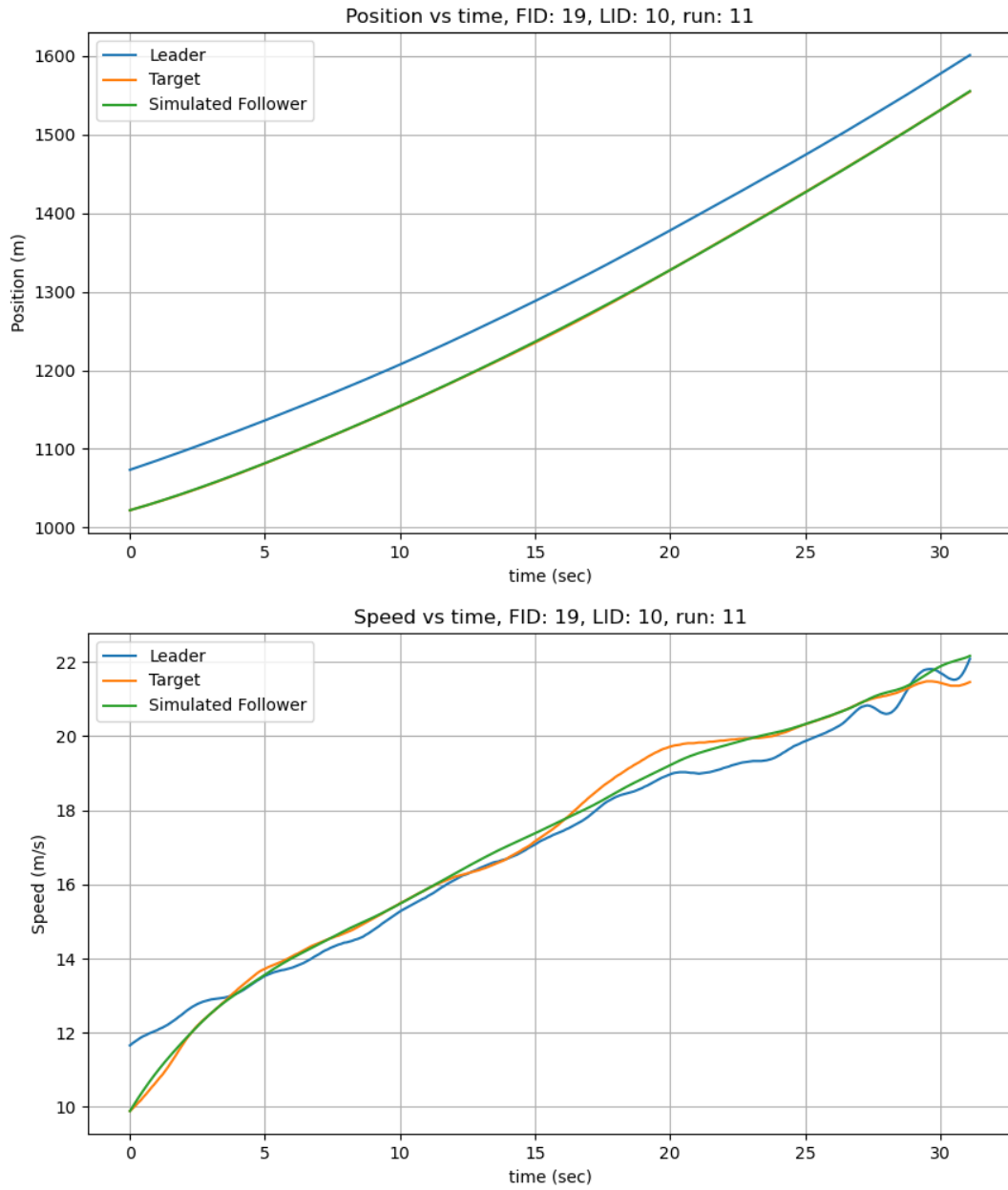


Figure 6.8: Position and speed for CSP for vehicle 19 in run 11 I294L1 dataset.

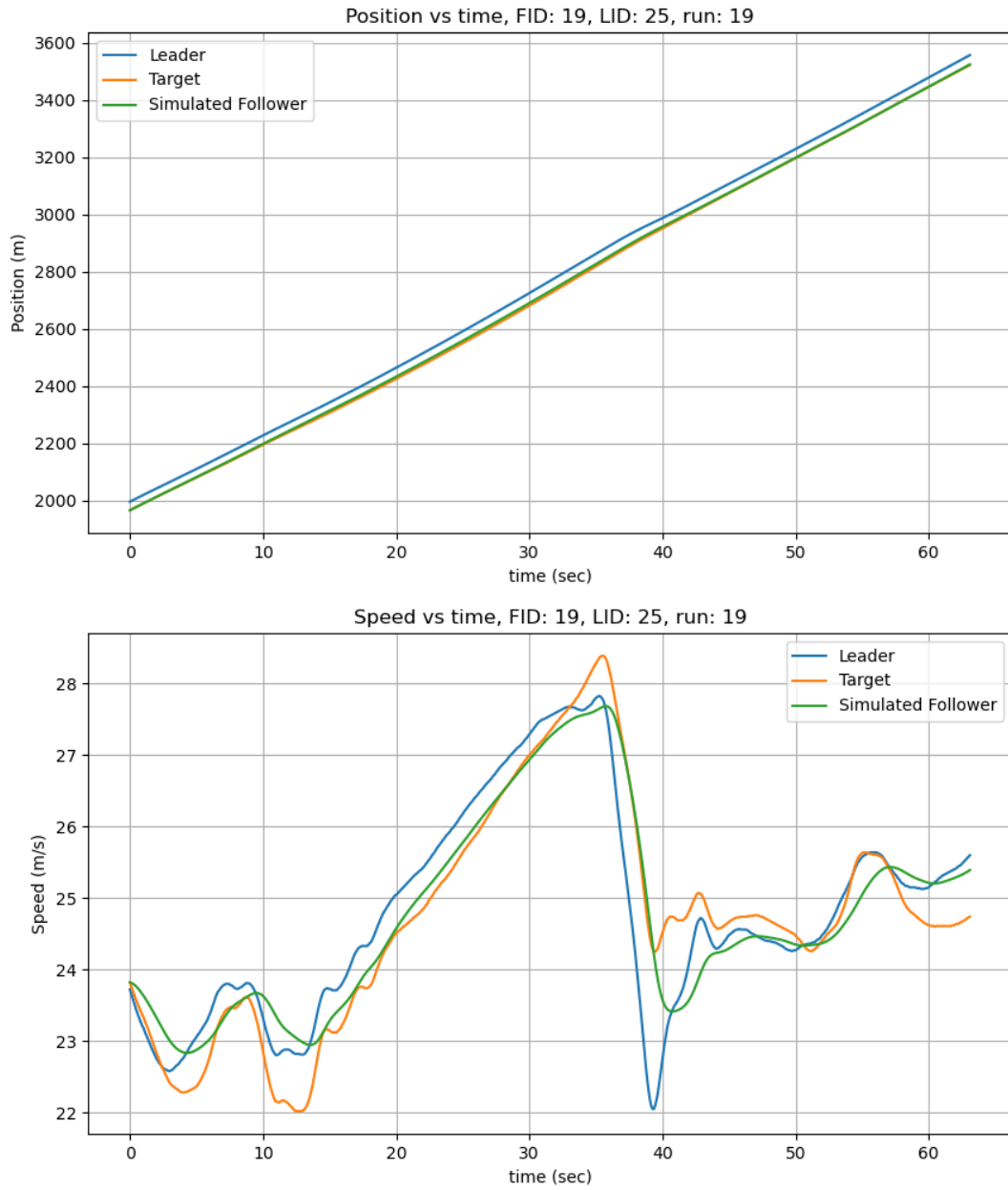


Figure 6.9: Position and speed for CSP for vehicle 19 in run 19 I294L1 dataset.

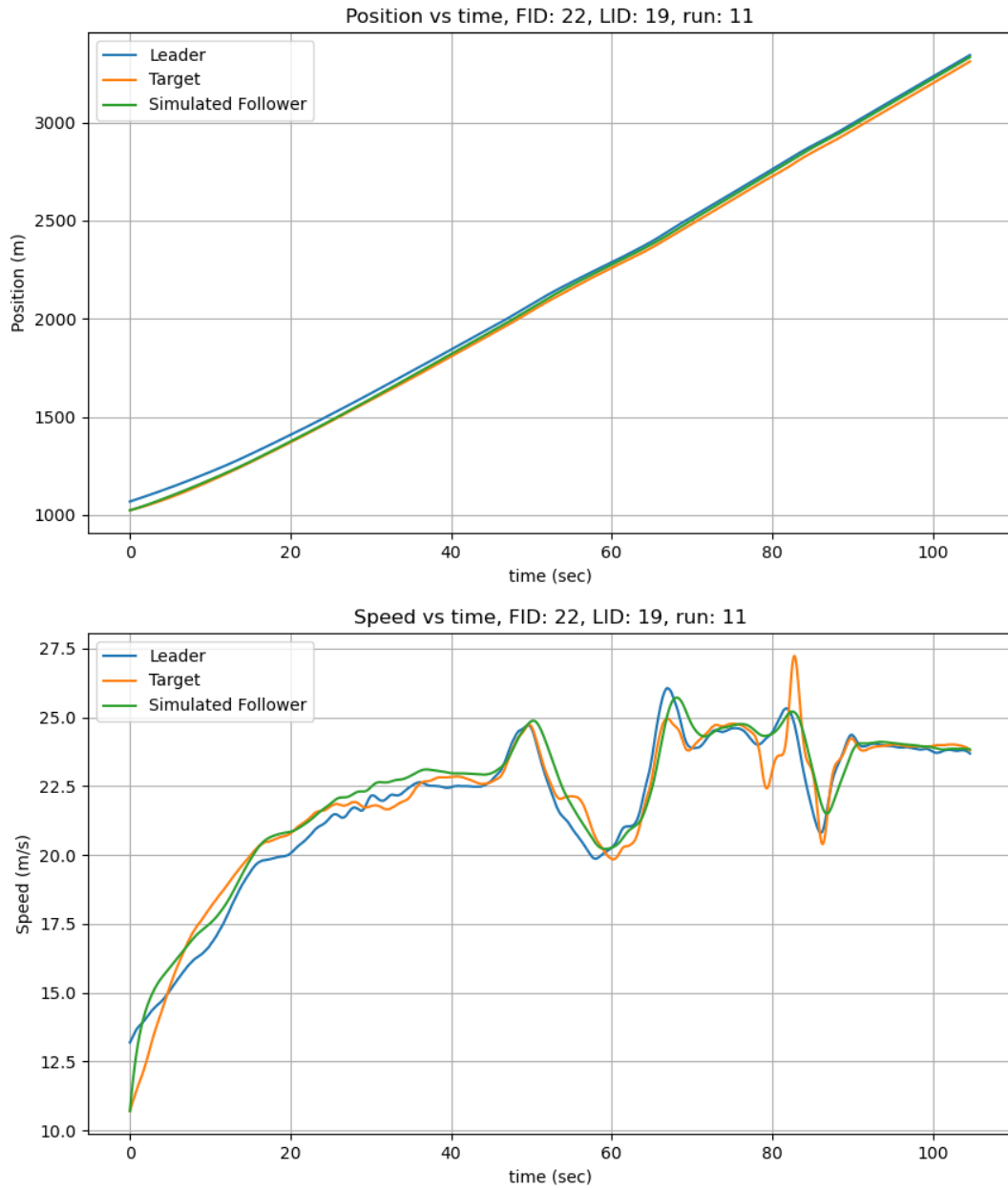


Figure 6.10: Position and speed for CSP for vehicle 22 in run 11 I294L1 dataset.

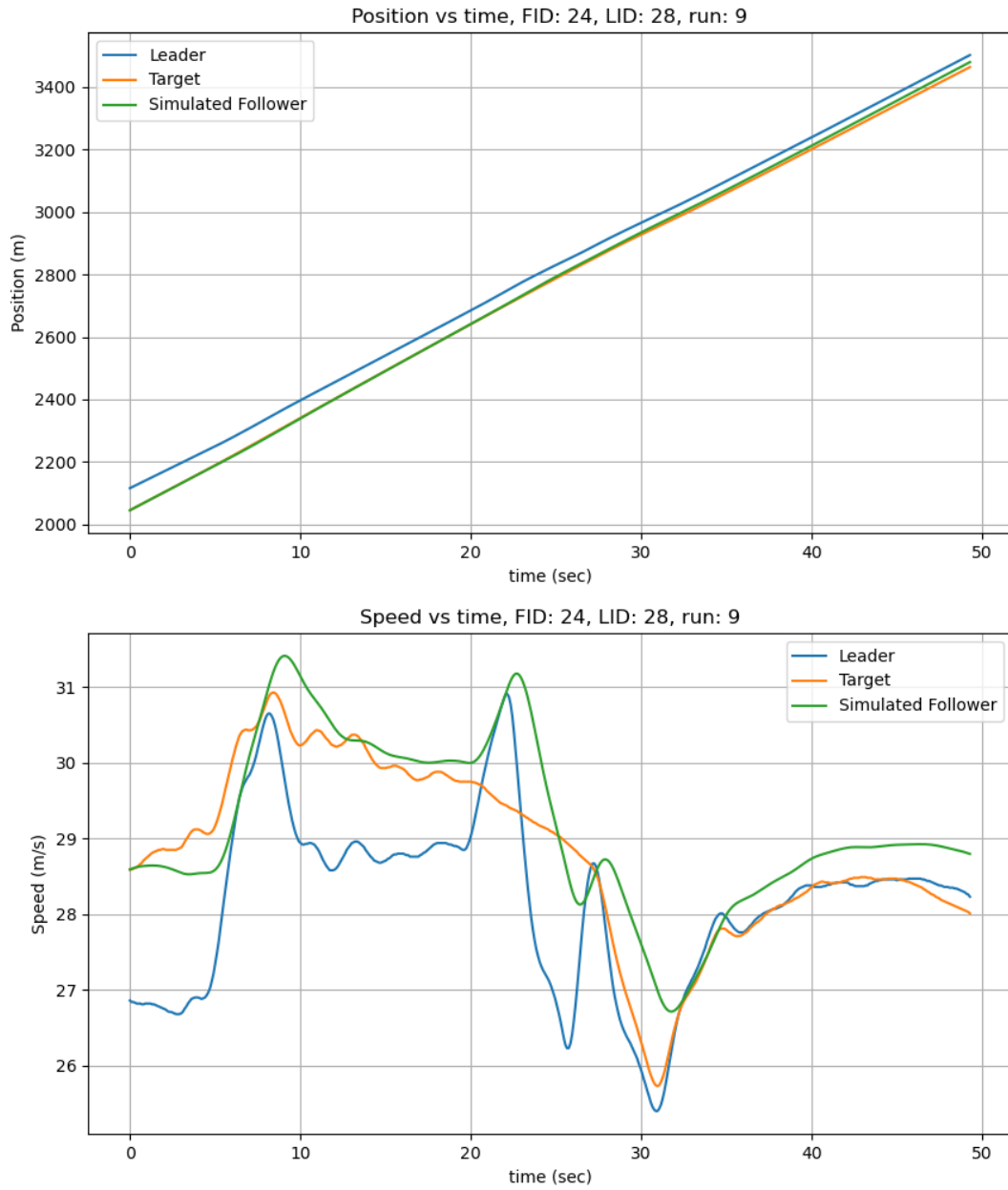


Figure 6.11: Position and speed for CSP for vehicle 24 in run 9 I294L1 dataset.

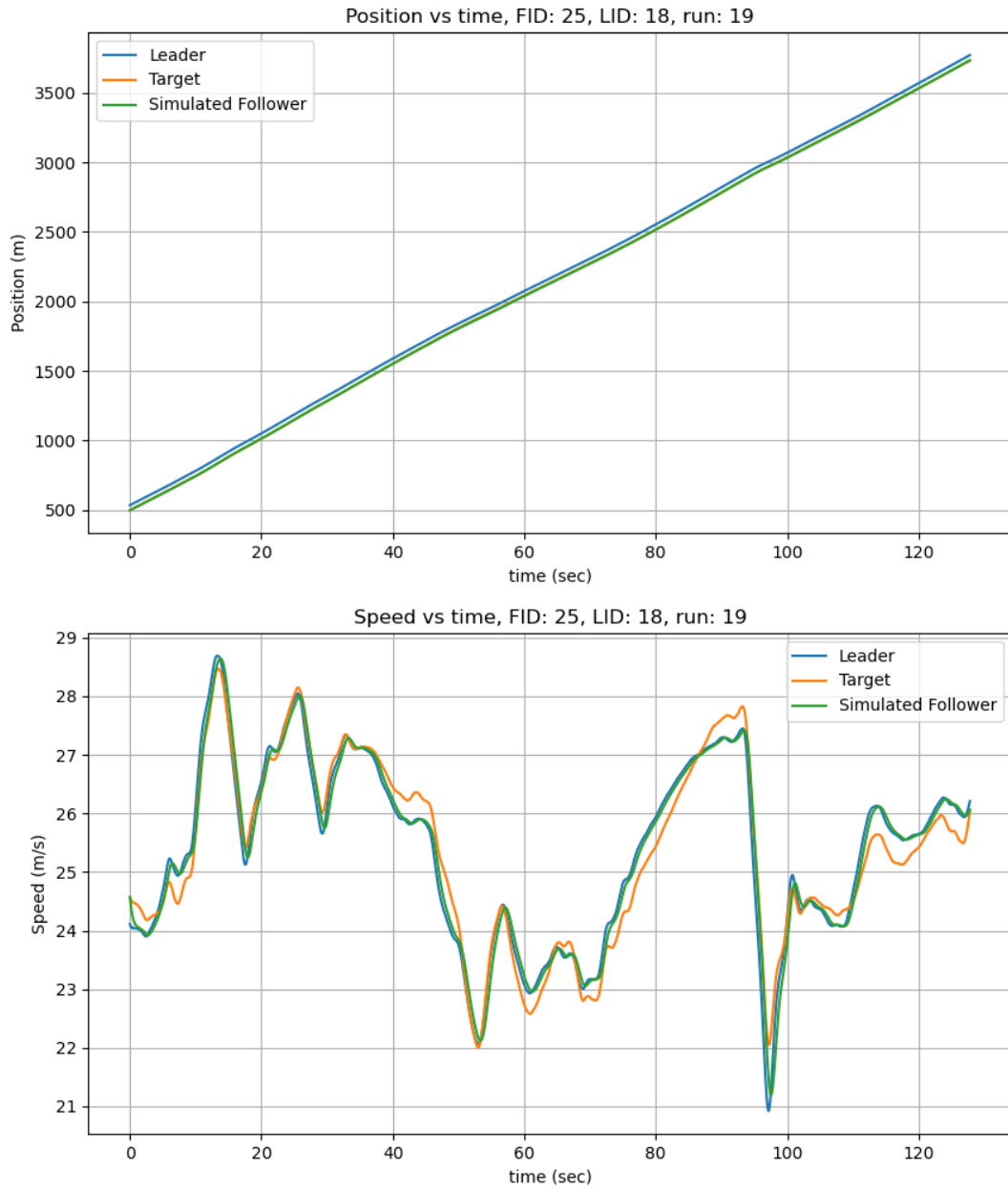


Figure 6.12: Position and speed for CSP for vehicle 25 in run 19 I294L1 dataset.

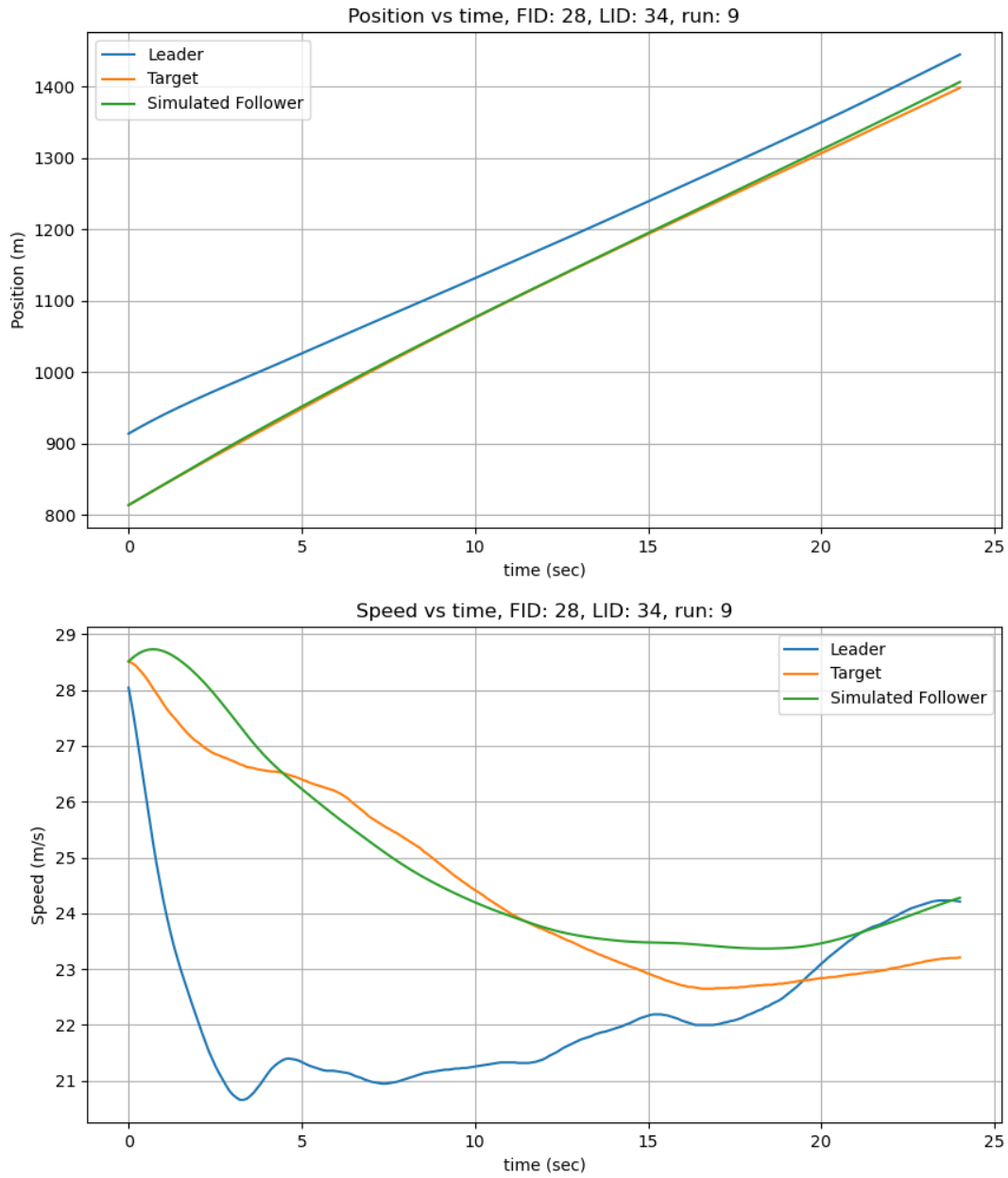


Figure 6.13: Position and speed for CSP for vehicle 28 in run 9 I294L1 dataset.

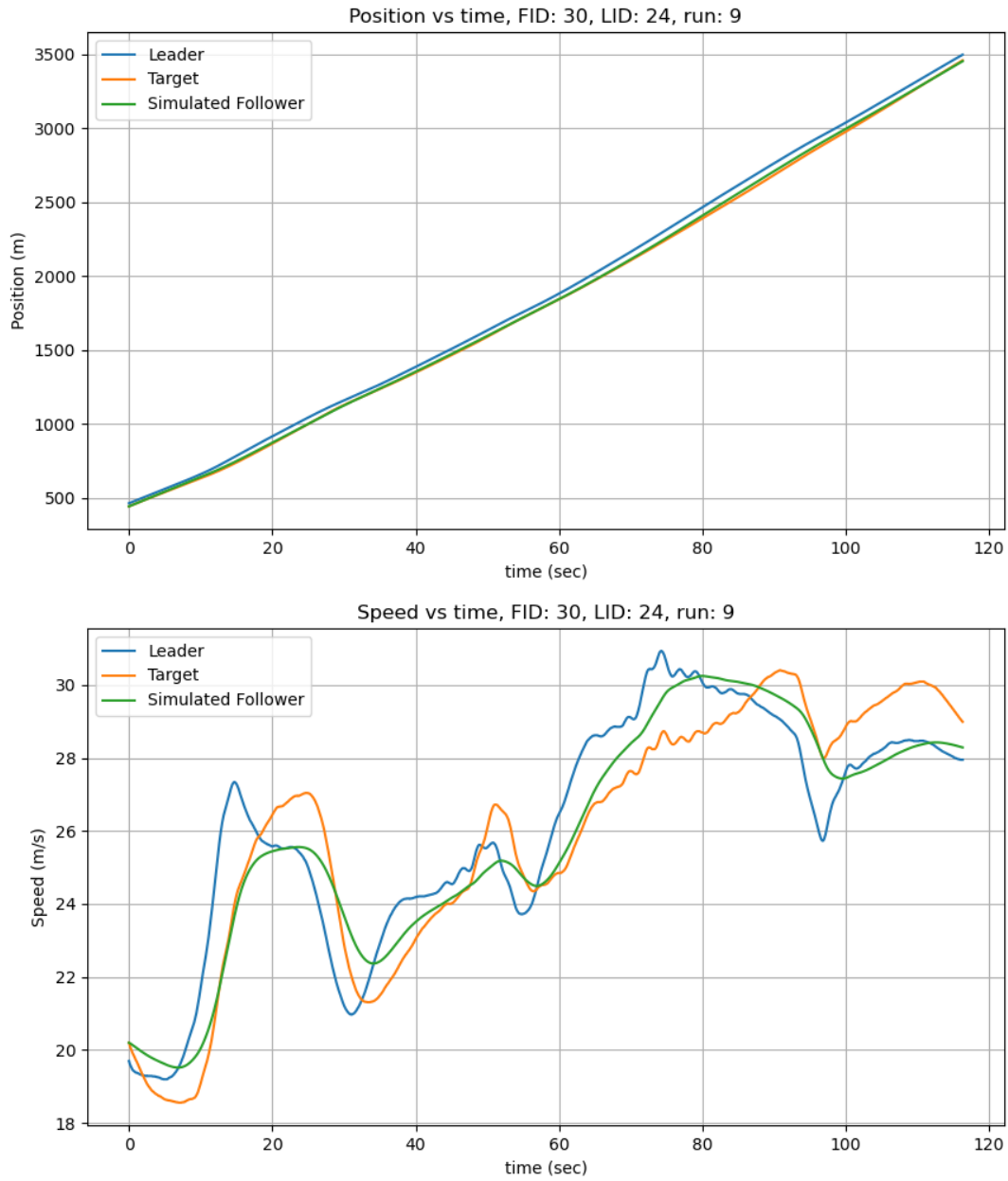


Figure 6.14: Position and speed for CSP for vehicle 30 in run 9 I294L1 dataset.

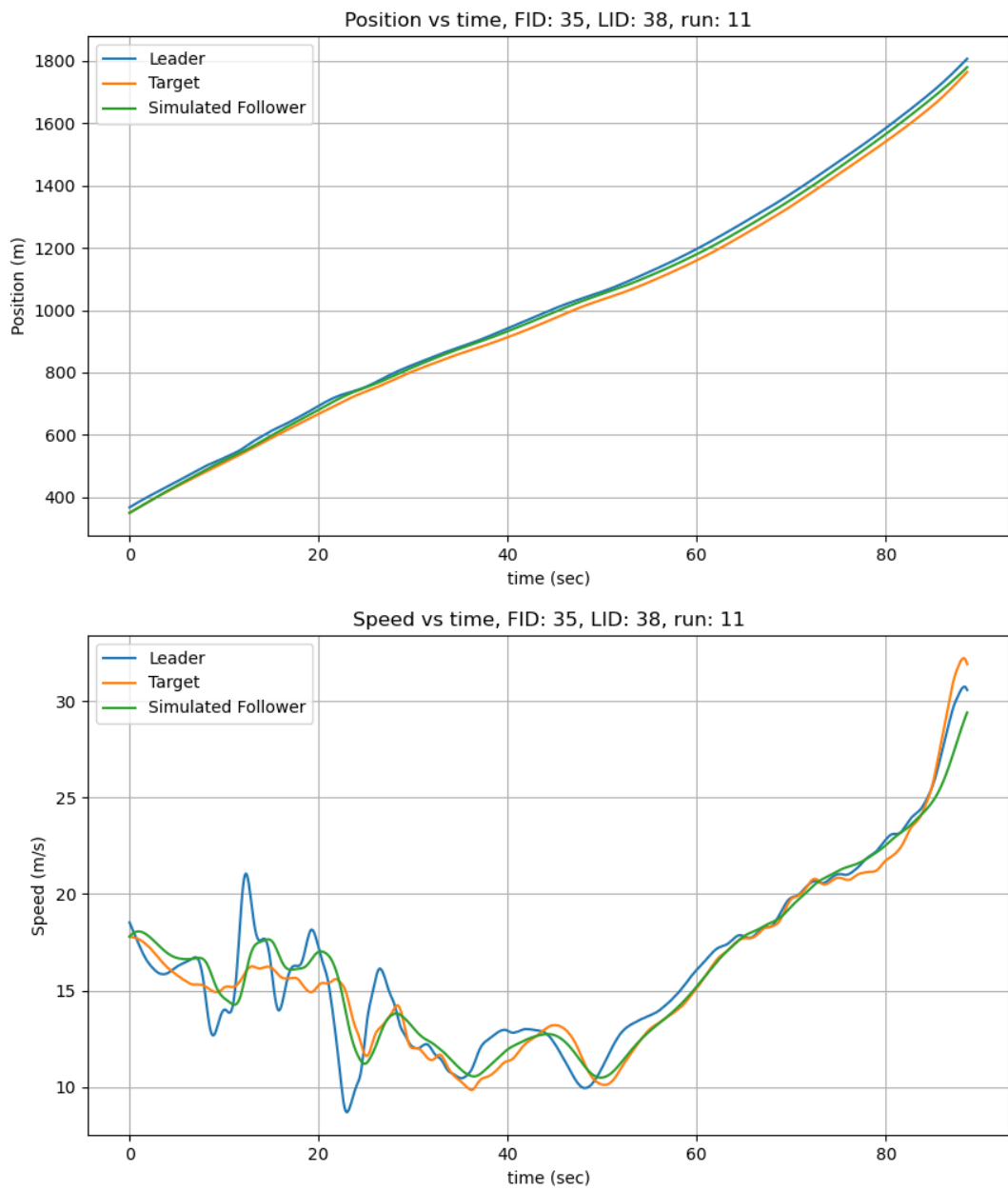


Figure 6.15: Position and speed for CSP for vehicle 35 in run 11 I294L1 dataset.

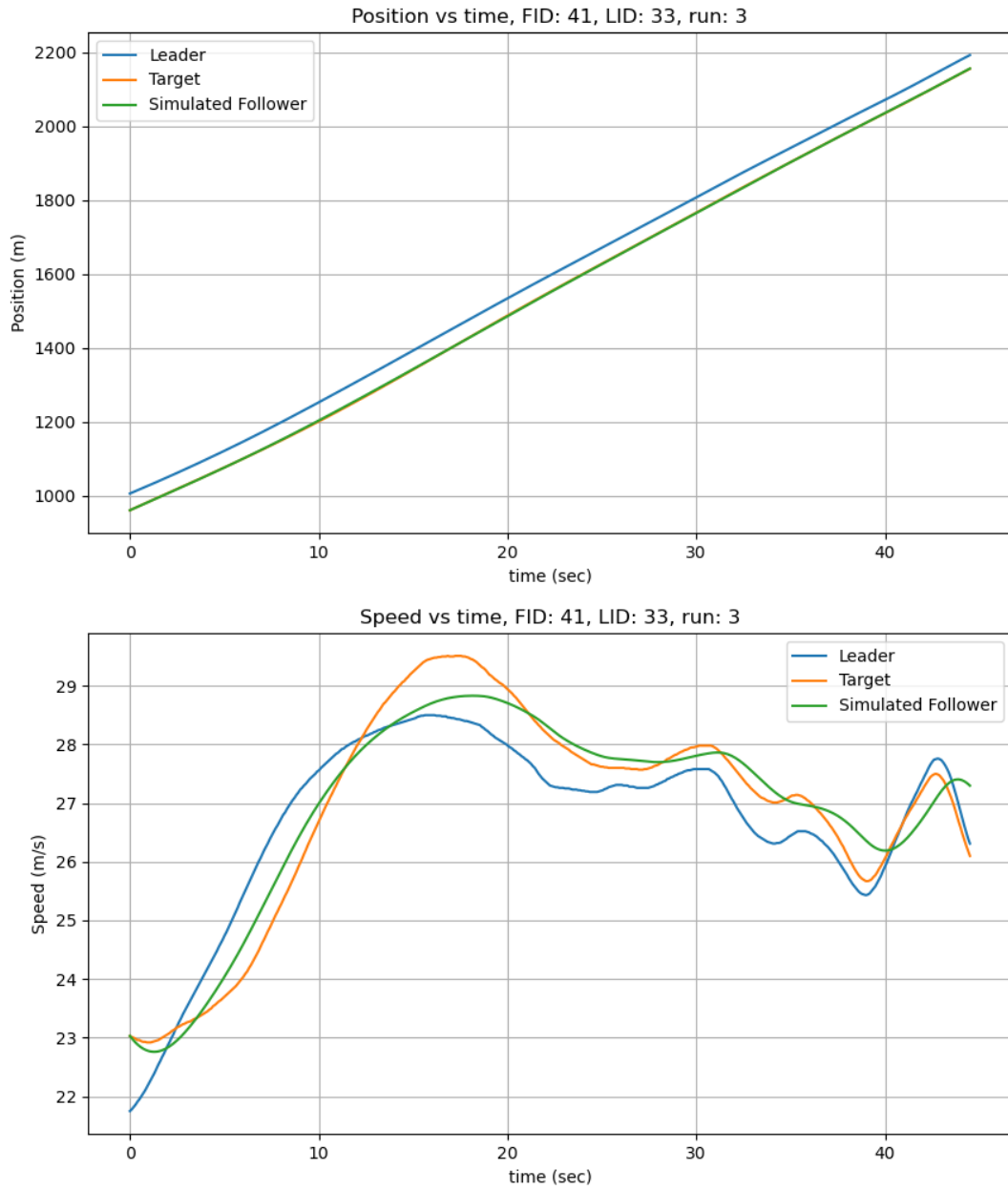


Figure 6.16: Position and speed for CSP for vehicle 41 in run 3 I294L1 dataset.

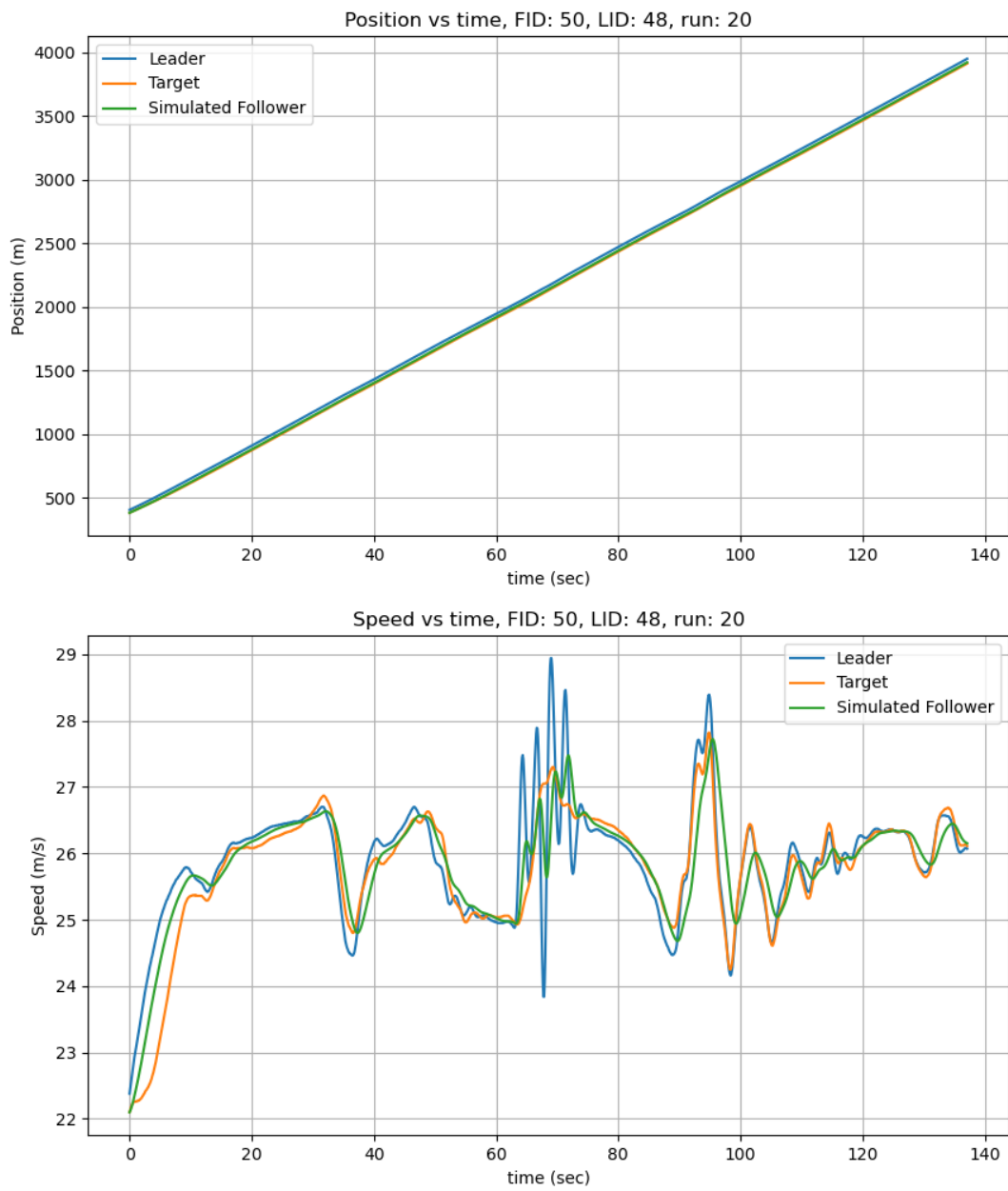


Figure 6.17: Position and speed for CSP for vehicle 50 in run 20 I294L1 dataset.

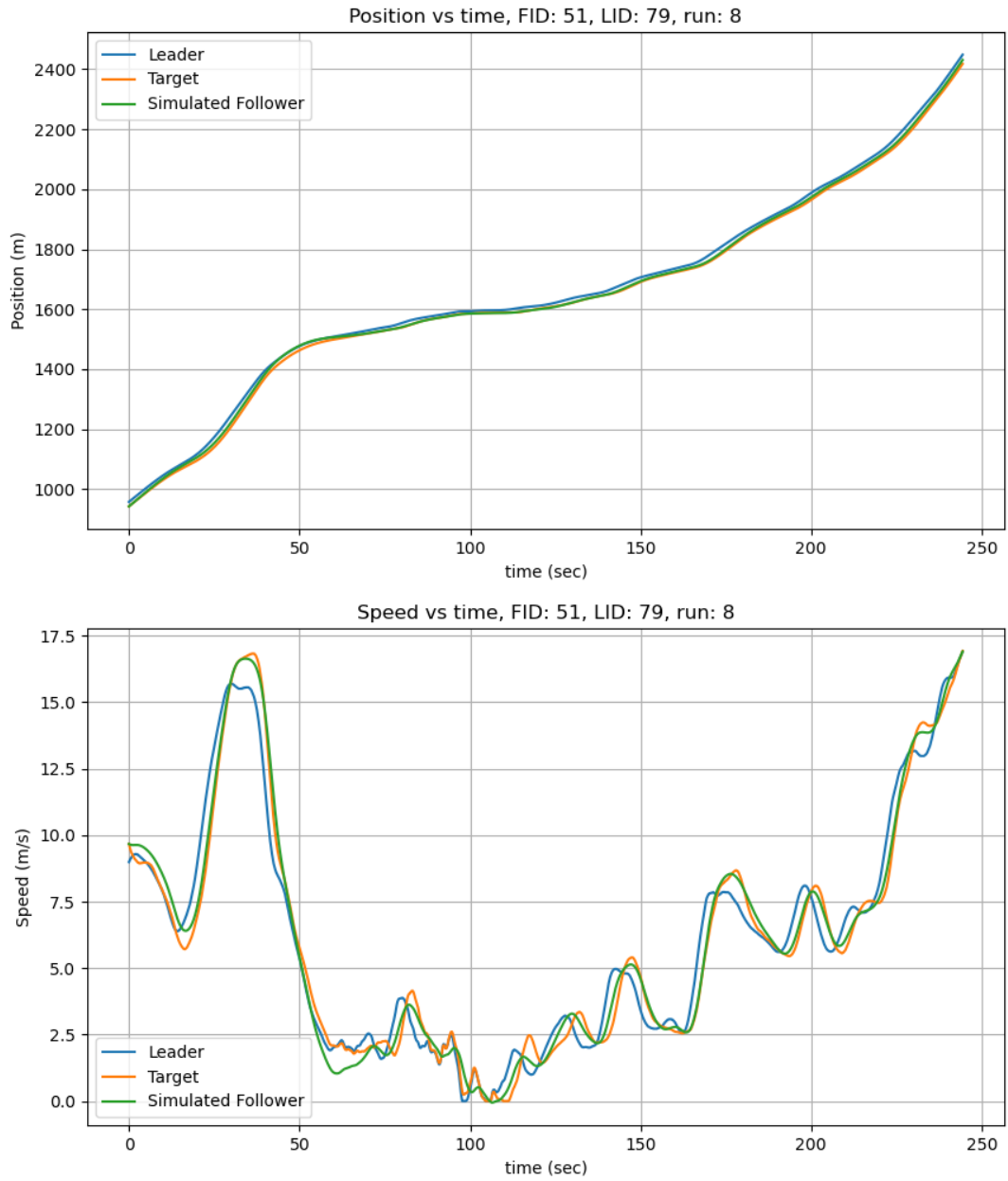


Figure 6.18: Position and speed for CSP for vehicle 51 in run 8 I294L1 dataset.

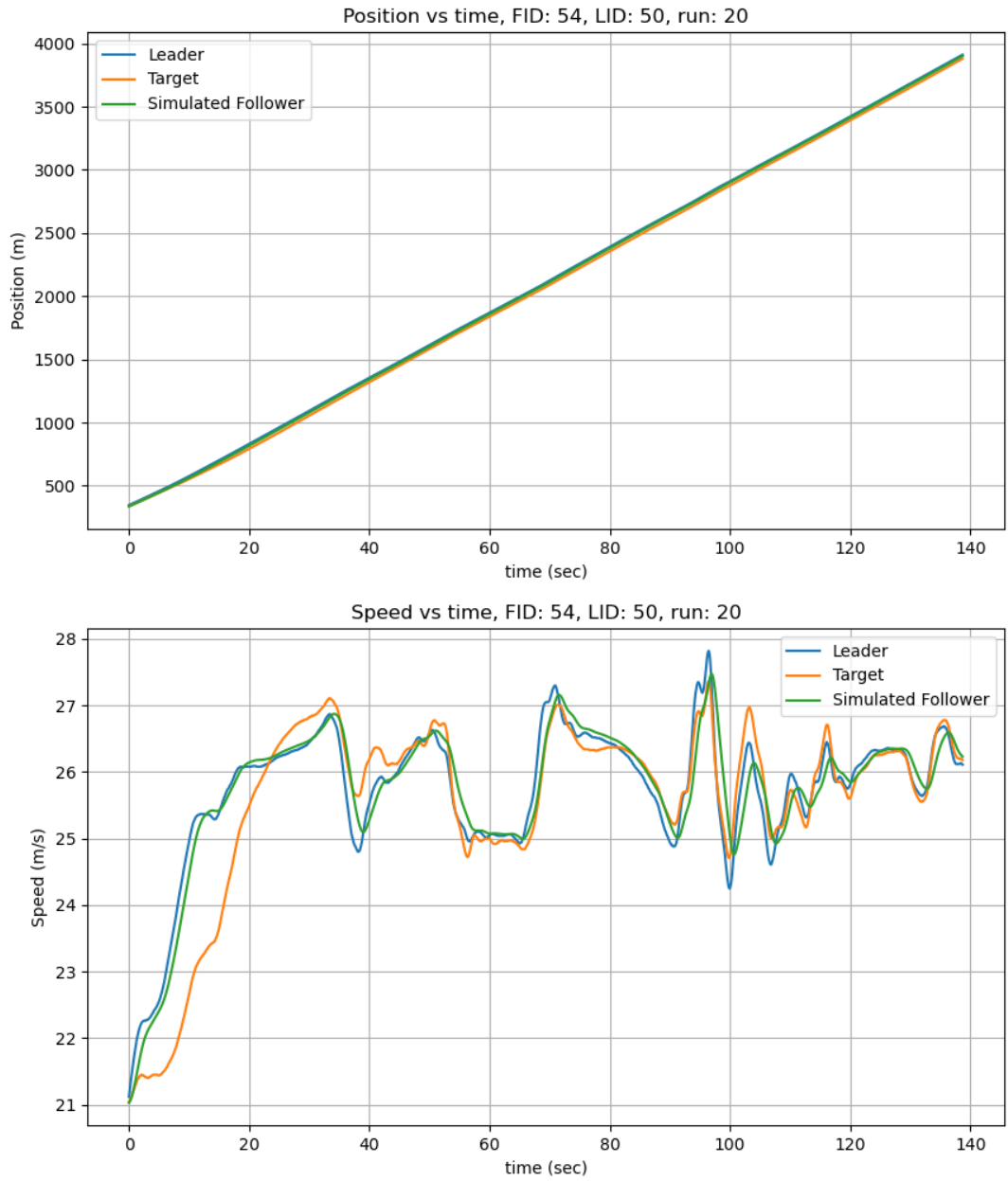


Figure 6.19: Position and speed for CSP for vehicle 54 in run 20 I294L1 dataset.

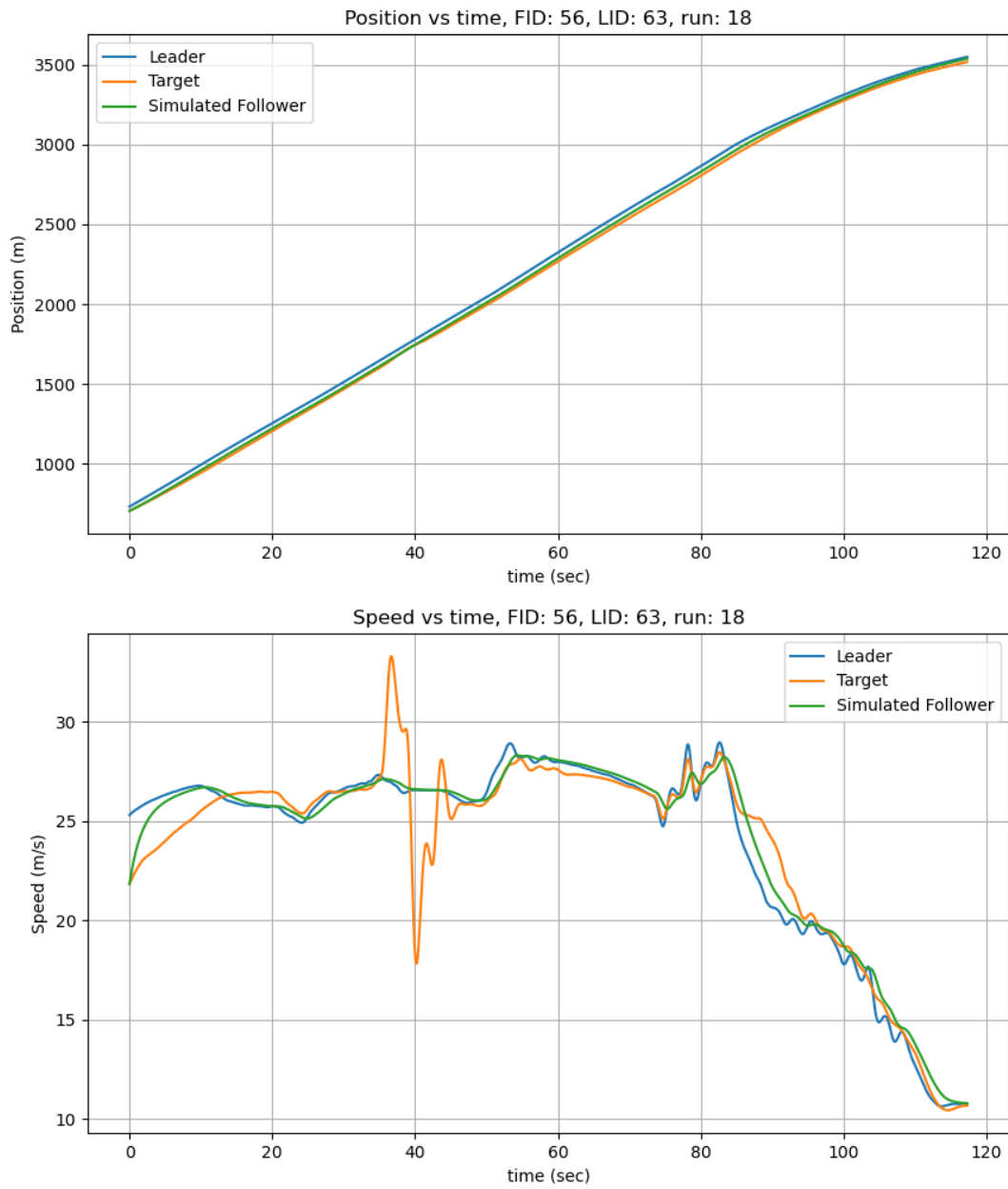


Figure 6.20: Position and speed for CSP for vehicle 56 in run 18 I294L1 dataset.

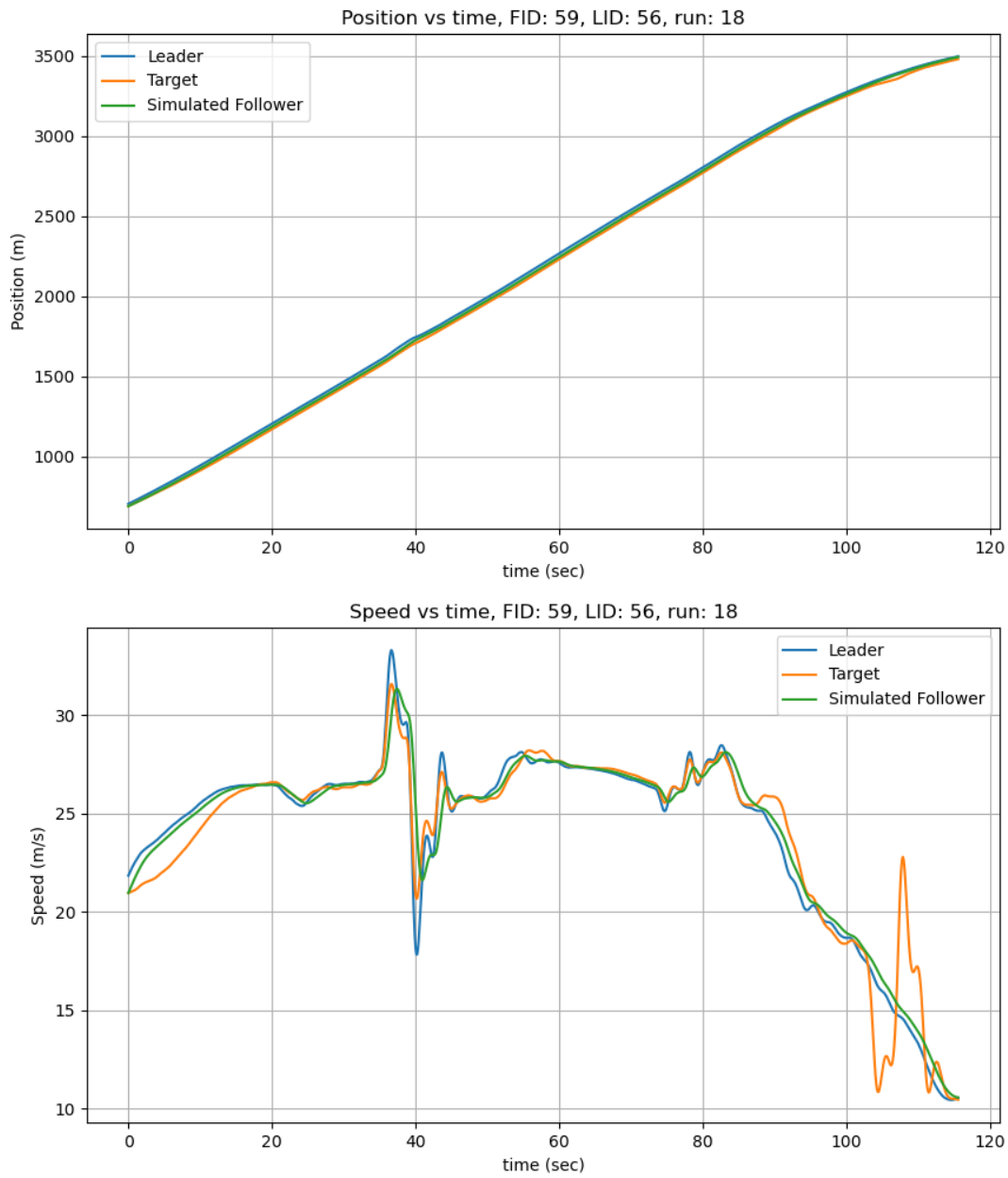


Figure 6.21: Position and speed for CSP for vehicle 59 in run 18 I294L1 dataset.

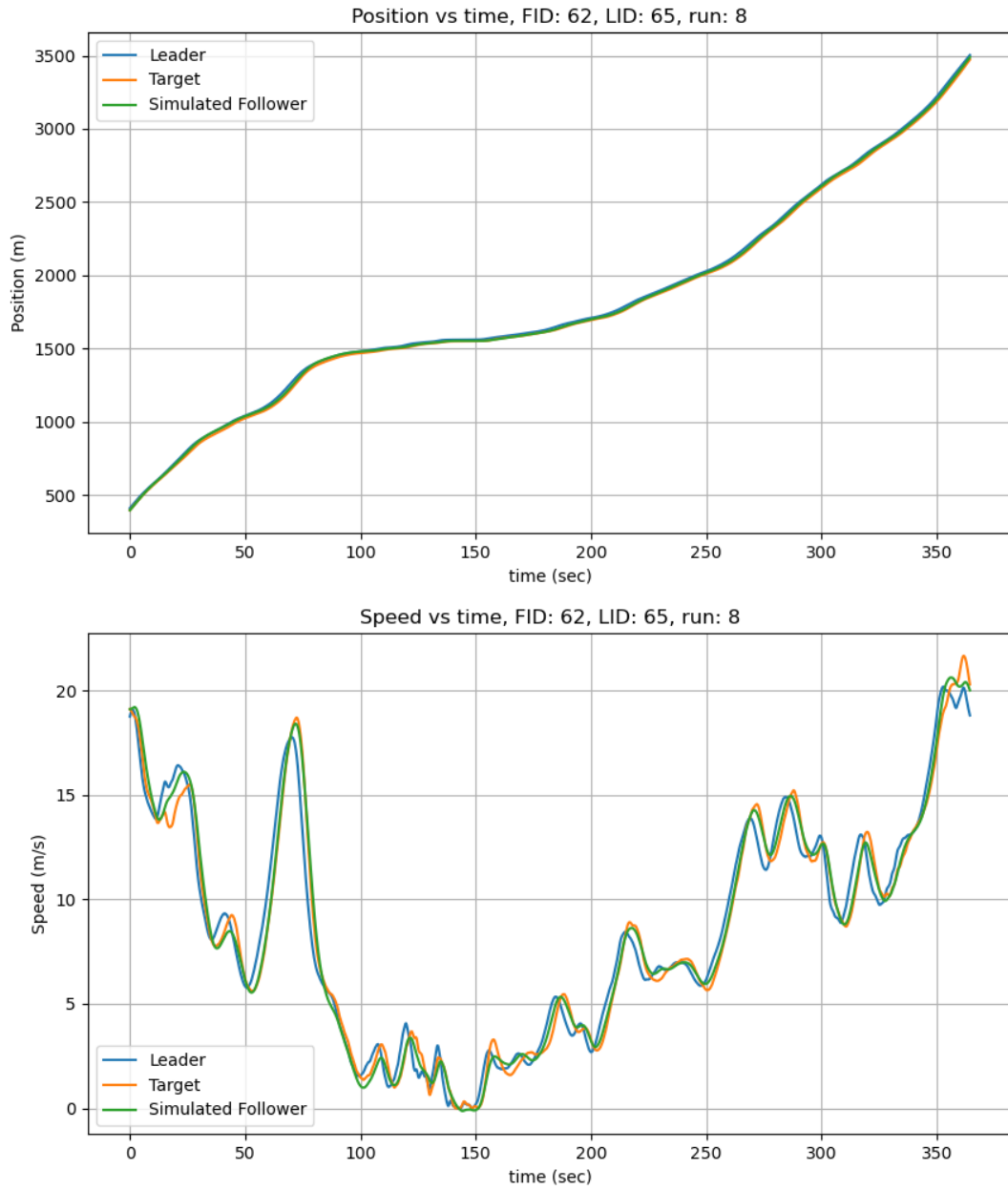


Figure 6.22: Position and speed for CSP for vehicle 62 in run 8 I294L1 dataset.

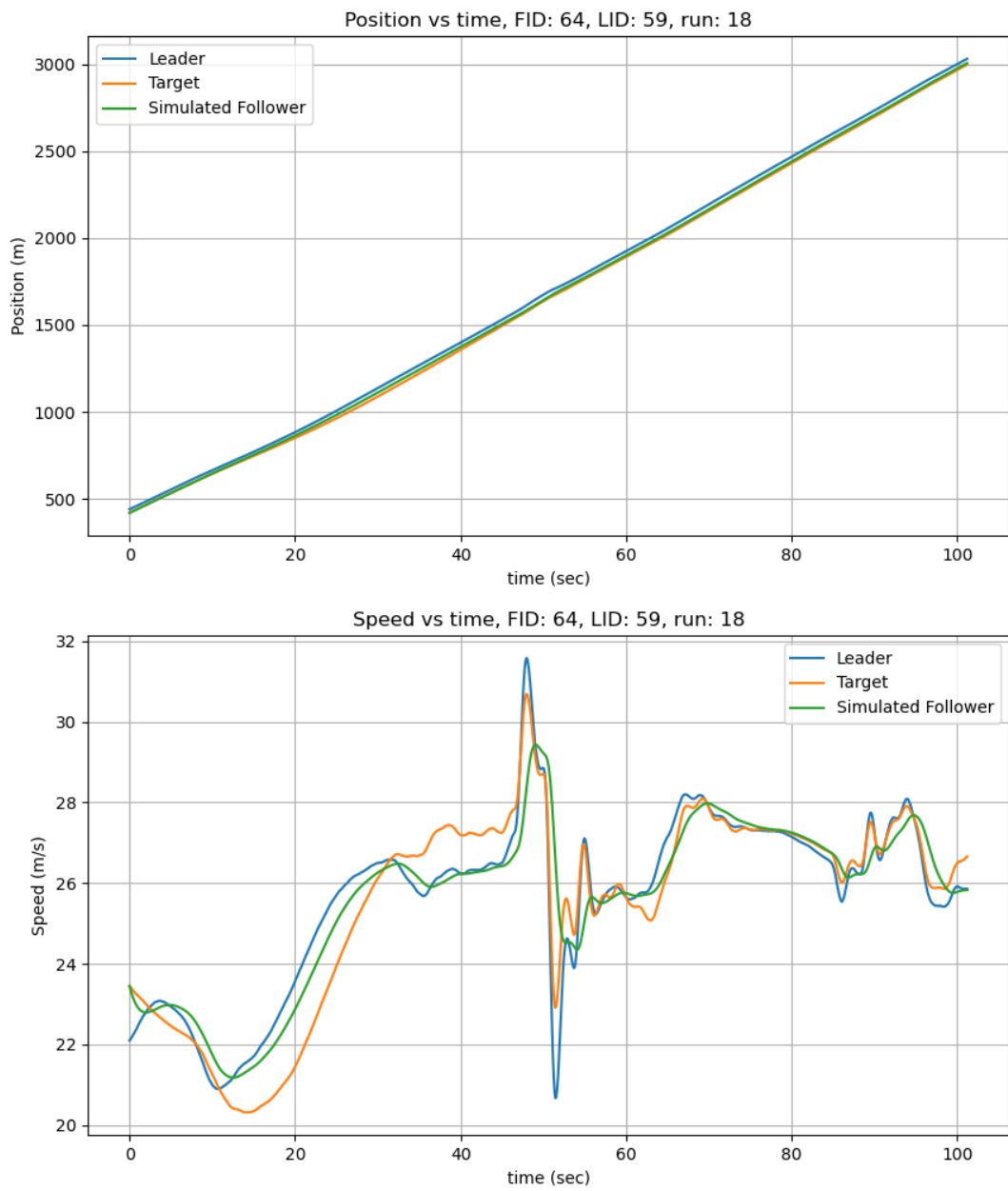


Figure 6.23: Position and speed for CSP for vehicle 64 in run 18 I294L1 dataset.

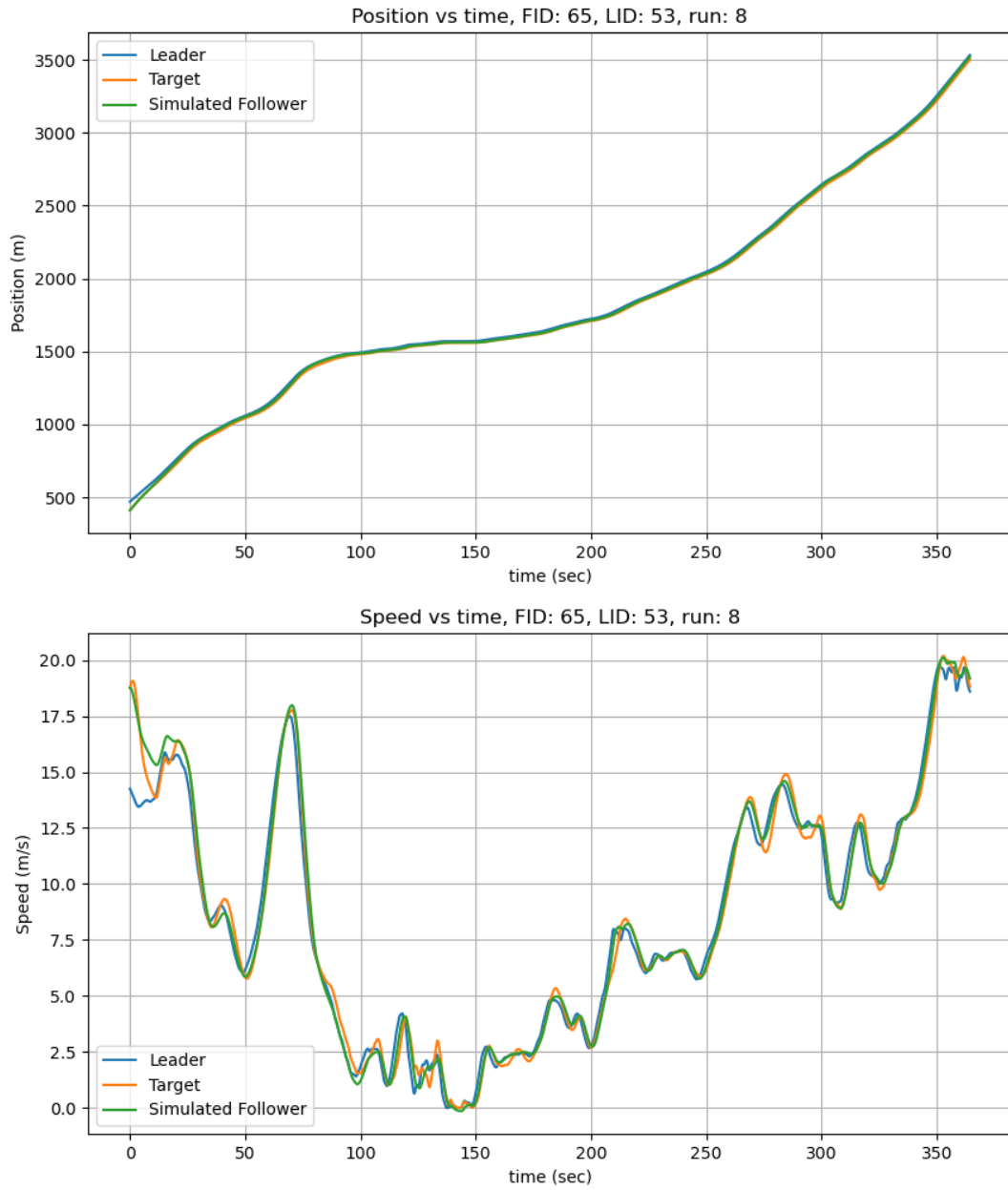


Figure 6.24: Position and speed for CSP for vehicle 65 in run 8 I294L1 dataset.

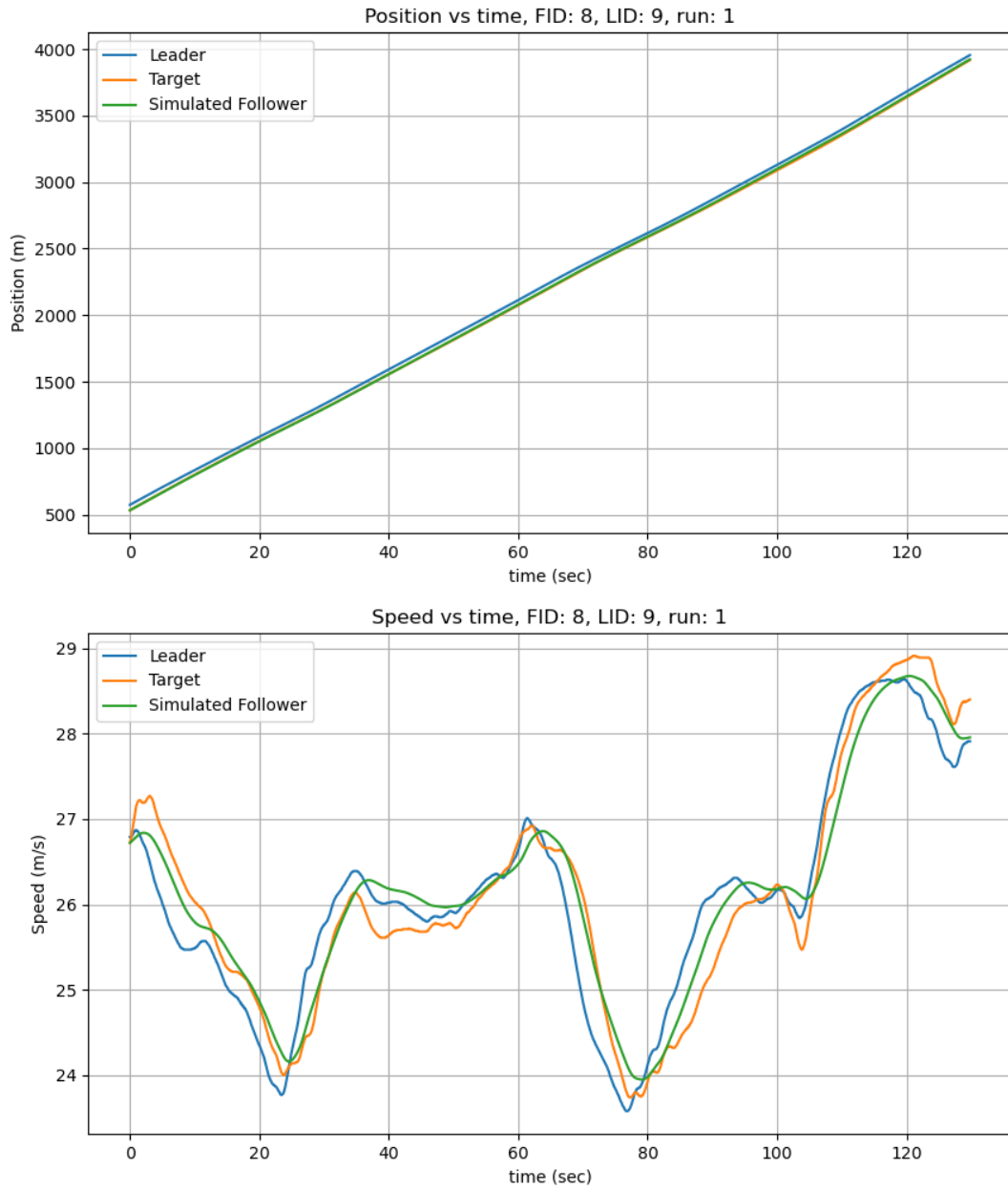


Figure 6.25: Position and speed for CSP for vehicle 8 in run 1 I294L1 dataset.

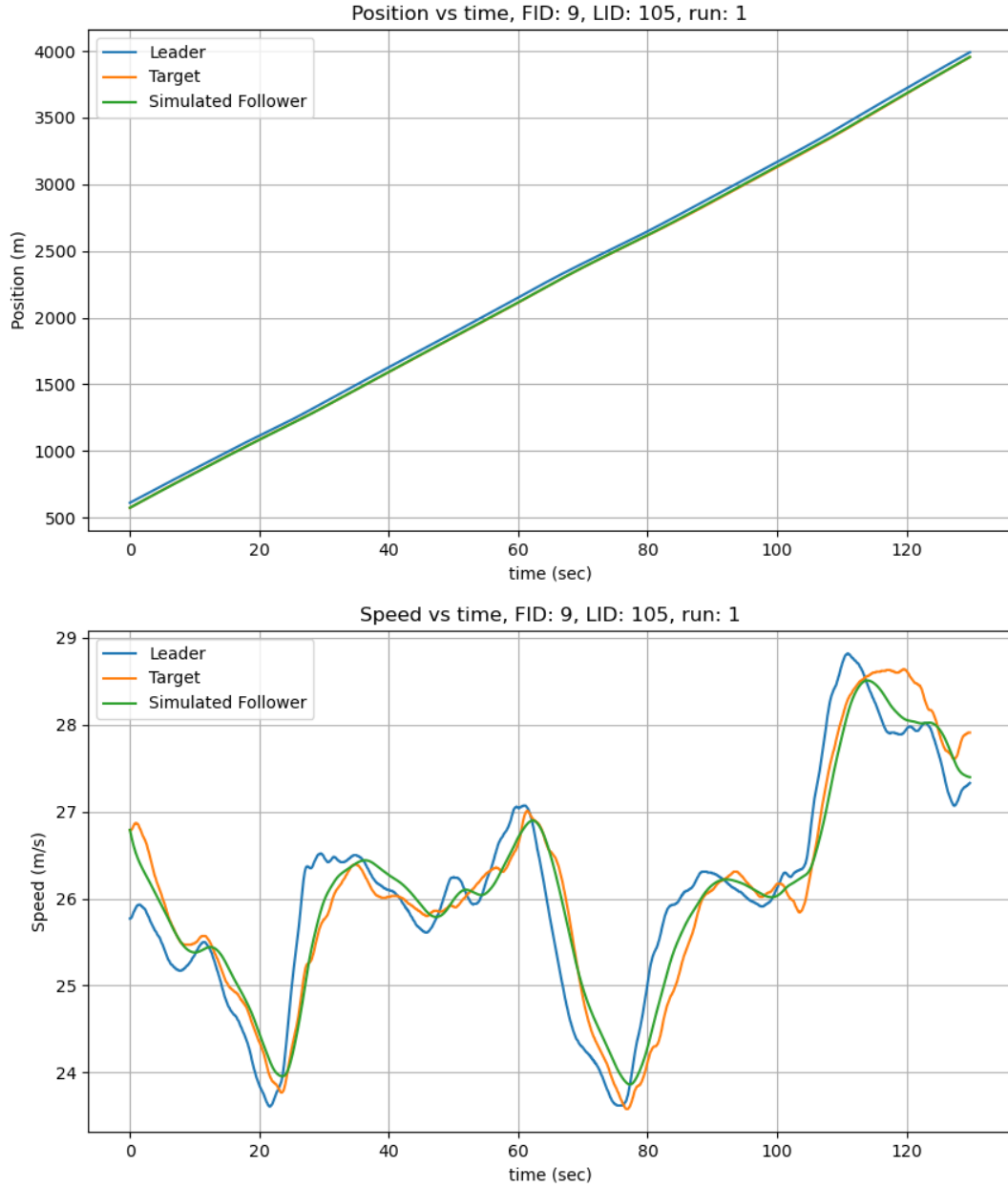


Figure 6.26: Position and speed for CSP for vehicle 9 in run 1 I294L1 dataset.

The optimized parameter ranges for the CSP policy in the I294 dataset are shown in Figure 6.27. The desired spacing ($S_{desired}$) had the largest range, strongly indicating variability

among the optimized values and suggesting that vehicle spacing preferences fluctuate across different driving conditions. Conversely, the control gains (k_v) and (k_p) were tightly clustered at lower values, ensuring consistent stability in vehicle acceleration and deceleration behavior.

Figure 6.28 shows that the distributions of (k_v) and (k_p) are skewed to the right, indicating that most optimized values are concentrated near the lower end of the range but with occasional higher values. The ($S_{desired}$) is skewed to the left, showing that while some vehicles can maneuver traffic with relatively smaller gaps, in some situations, the vehicles may need larger spacing. The wide spread in ($S_{desired}$) suggests that variations in traffic density and driving behavior strongly influence optimal spacing. These observations indicate that CSP maintains consistent vehicle control while allowing adaptive spacing flexibility, making it suitable for highway driving scenarios with varying traffic densities.

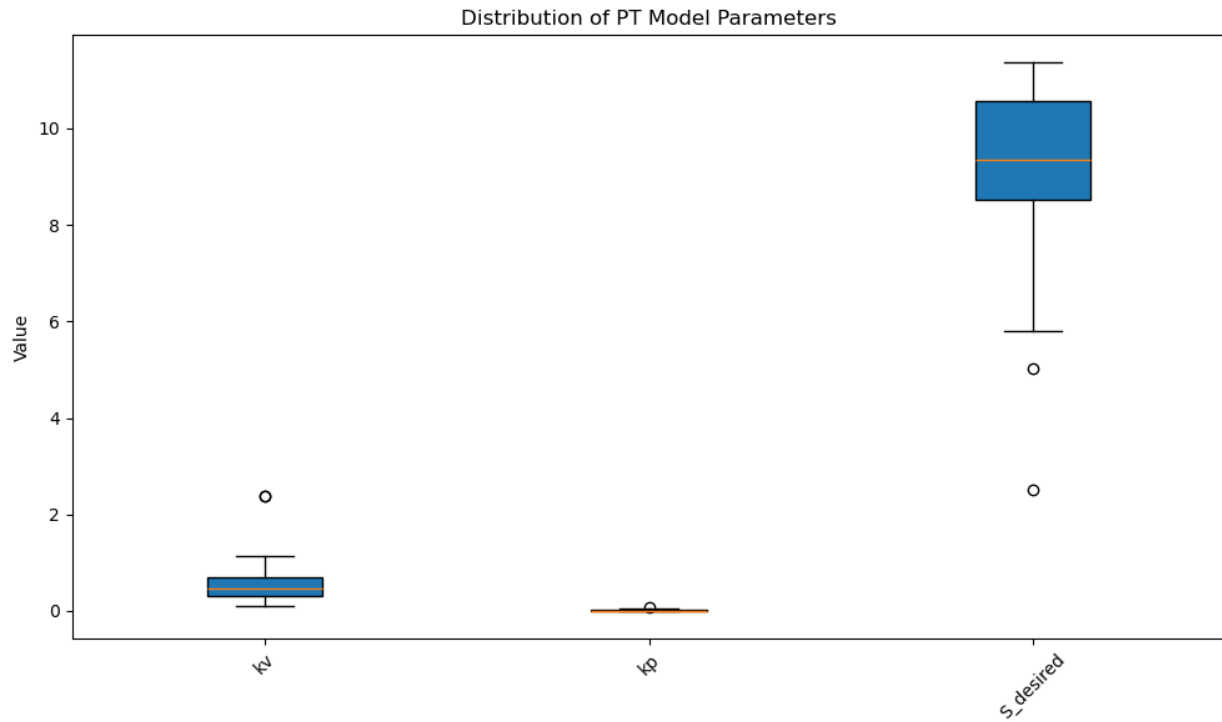


Figure 6.27: Parameter ranges for CSP in I294L1 dataset.

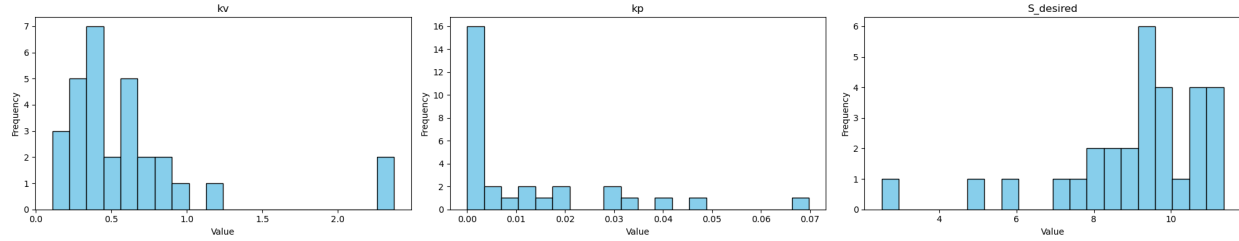


Figure 6.28: Parameter histogram for CSP in I294L1 dataset.

6.2.2 CSP I90/94 Simulated Results

The simulated results for I90/94 are presented in Figures 6.29 6.30, and 6.31 using the Constant Spacing Policy. From Figure 6.29, the simulated follower tracks the target follower with minimum deviation. This shows that the CSP model performs well on the I90-94 highway dataset. Although there is a slight position deviation for vehicle 195 shown in Figure 6.30, the simulated follower closely tracks the simulated speed overall. Despite the speed deviation between the simulated follower and the target follower for vehicle 286 shown in Figure 6.31, the simulated follower's position is well aligned with the target follower's position.

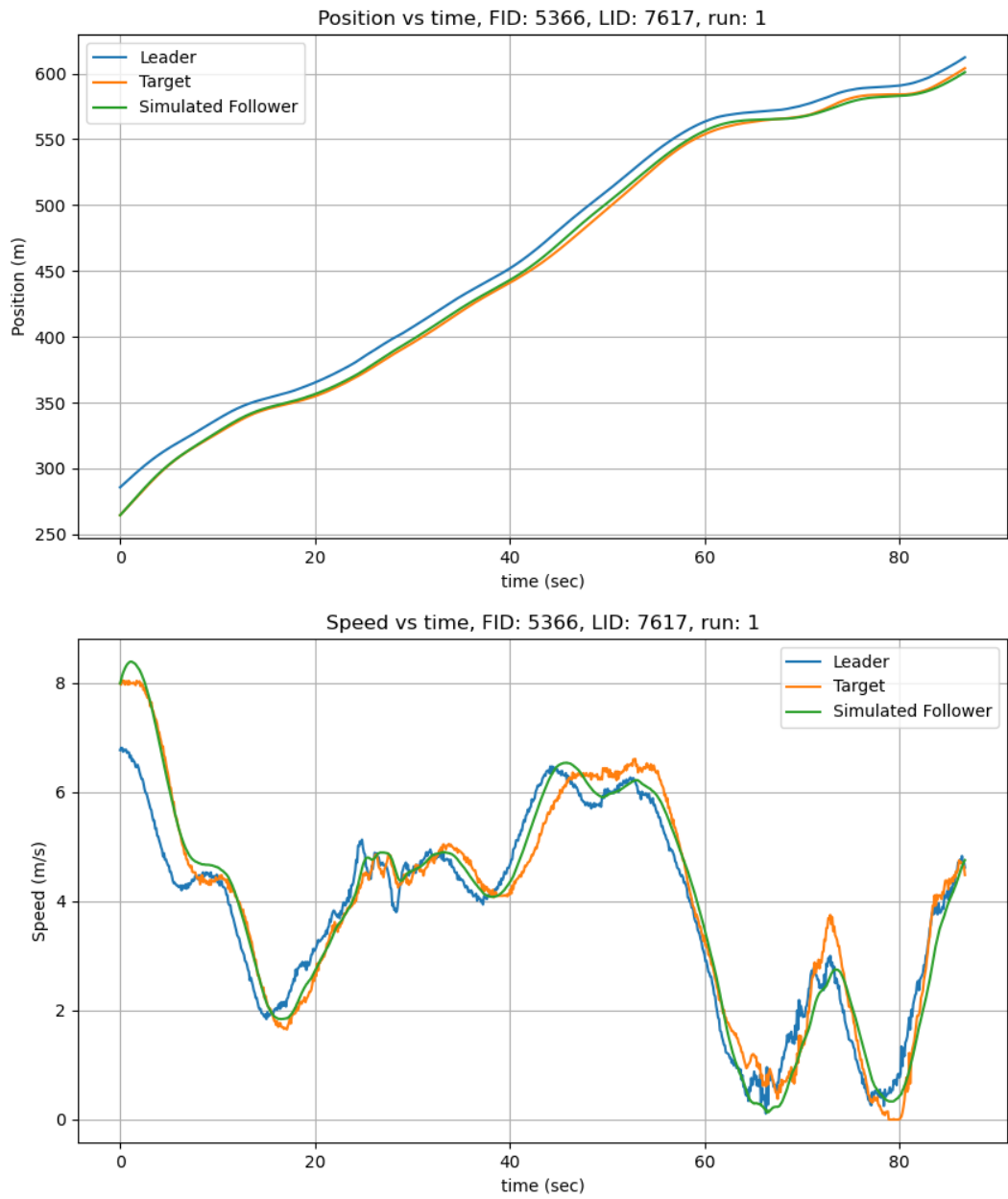


Figure 6.29: Position and speed for CSP for vehicle 5366 in I90/94 dataset.

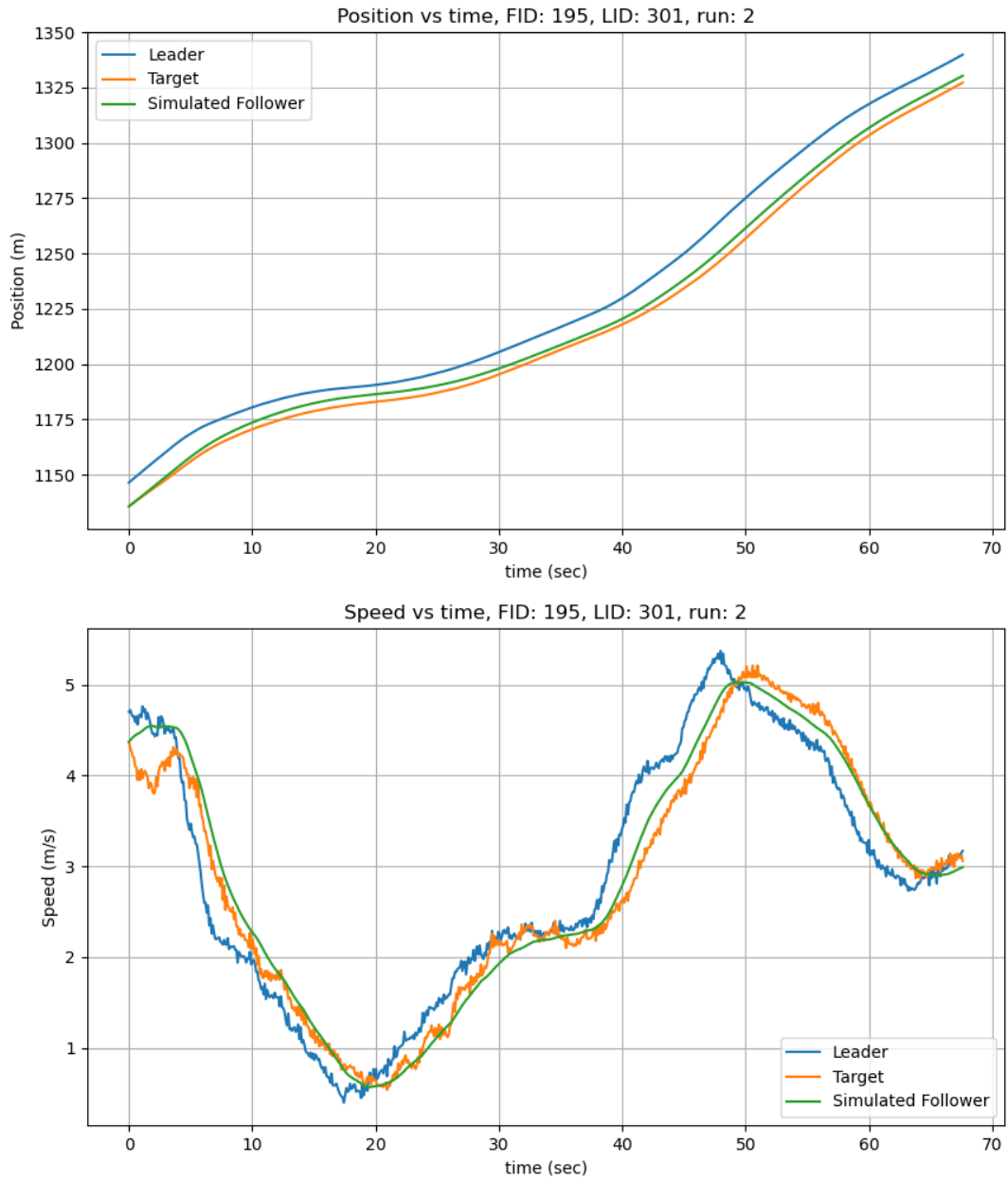


Figure 6.30: Position and speed for CSP for vehicle 195 in I90/94 dataset.

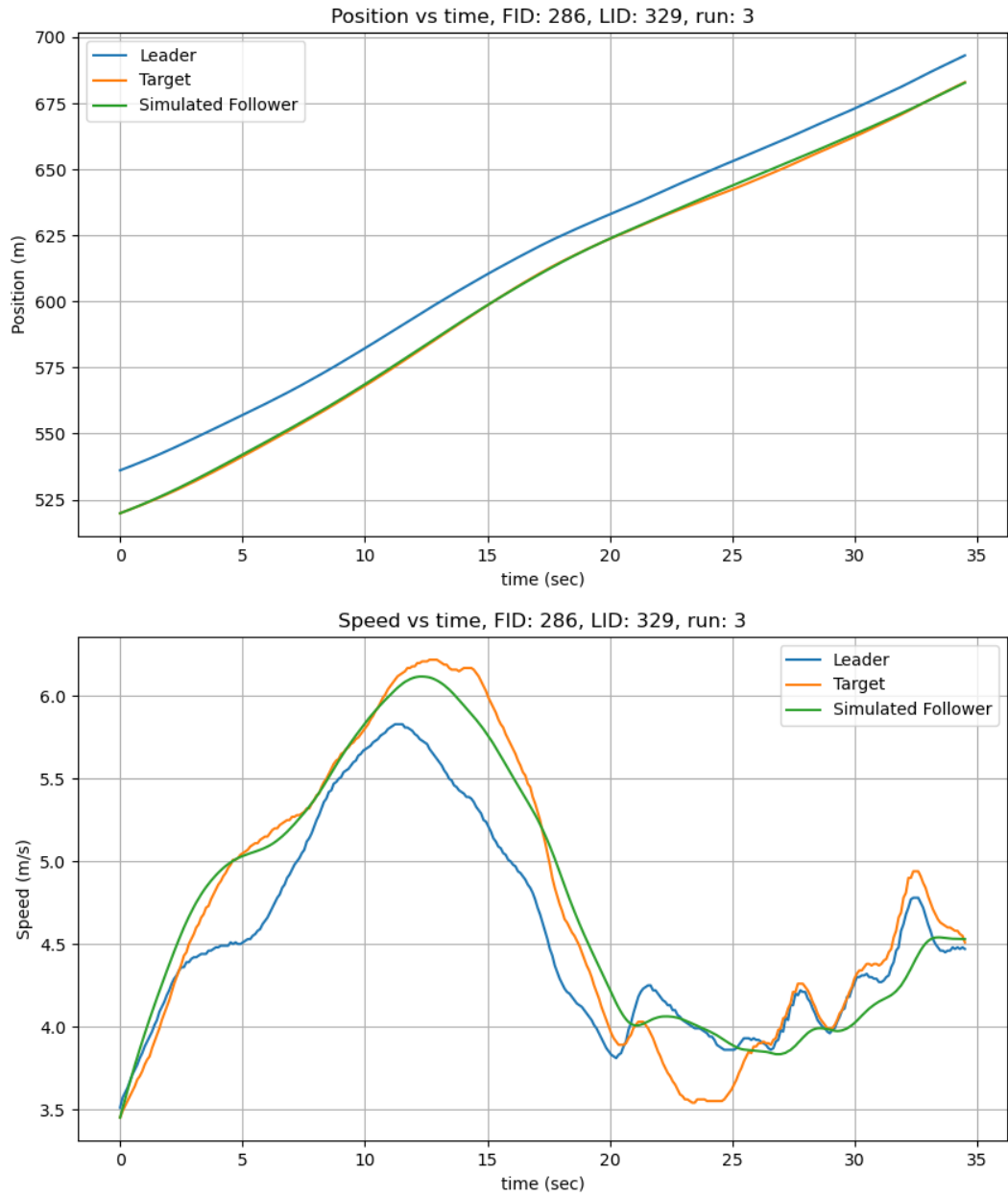


Figure 6.31: Position and speed for CSP for vehicle 286 in I90/94 dataset.

The optimized parameter ranges for the I90/94 dataset using the CSP policy, illustrated in Figure 6.32, presents a significant variation across parameters. The desired spacing ($S_{desired}$)

shows the largest range, suggesting variability in vehicle gap preferences, which could be influenced by traffic density and individual driving behaviors. In contrast, the control gains (k_v) and (k_p) remain tightly clustered, indicating consistent vehicle response and stability in acceleration and deceleration adjustments.

Figure 6.33 further reveals that the parameters follow discrete distributions, highlighting the presence of distinct optimized values rather than a continuous spread. The narrow range of (k_v) and (k_p) ensures the uniformity in control behavior, ensuring reliable adjustments in response to speed changes. Meanwhile, the broader distribution of ($S_{desired}$) suggests that while most vehicles maintain a consistent following distance, some scenarios demand significantly larger gaps to ensure safe and stable car-following behavior. These findings indicate that CSP effectively maintains consistent vehicle dynamics while allowing adaptability in spacing preferences, ensuring reliability for highway driving conditions.

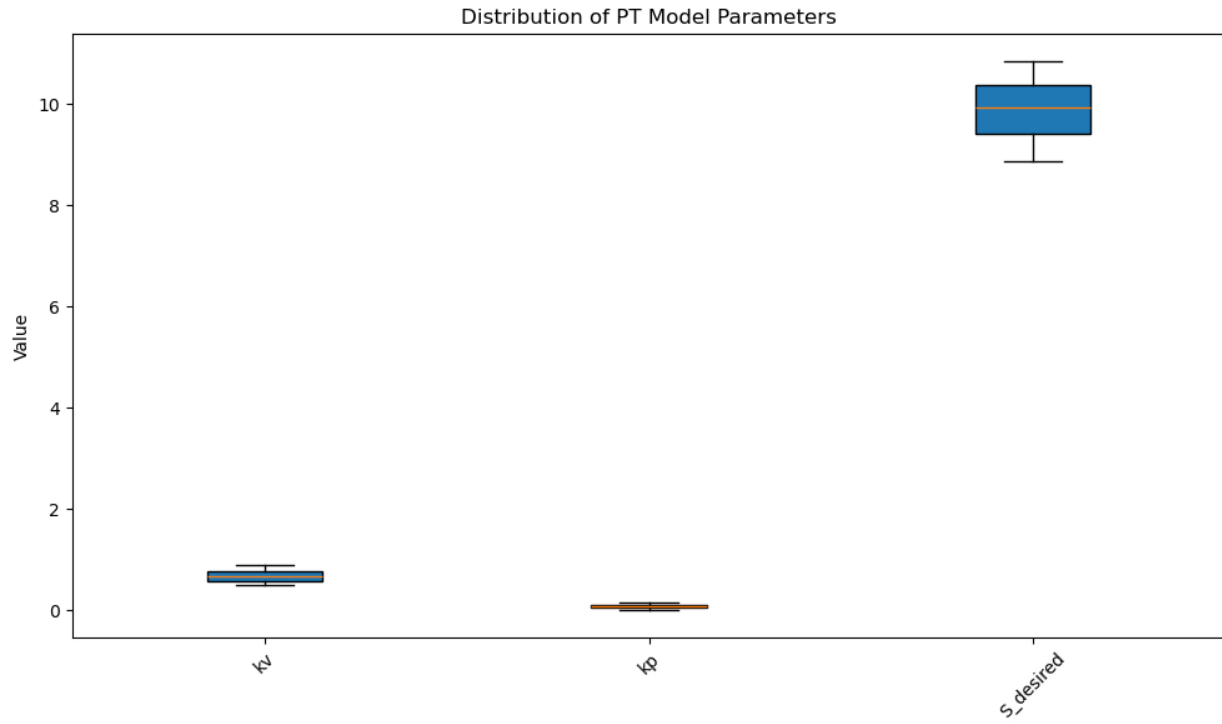


Figure 6.32: Parameter ranges for CSP in I90/94.

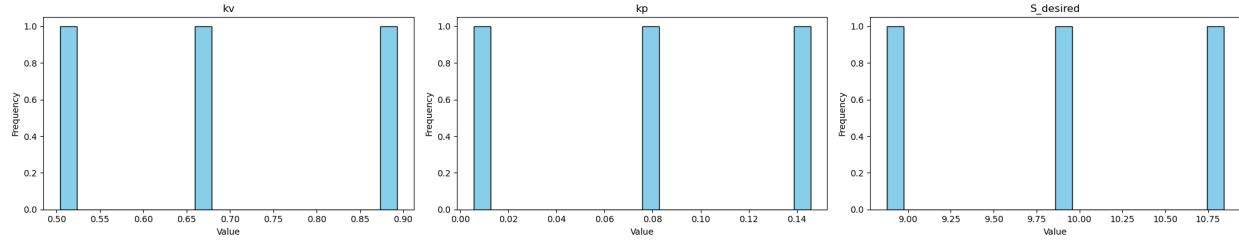


Figure 6.33: Parameter histogram for CSP in I90/94.

6.2.3 CSP Phoenix Simulated Results

The simulated results for the Phoenix dataset are presented in Figures 6.34, 6.35, 6.36, and 6.37. The simulated follower closely aligns with the calibrated position and speed of the target follower, as shown in Figures 6.34 and 6.37 for vehicles 13 and 2 in run 9NS. However, noticeable speed deviations are observed for vehicles 31 and 2 in run 9ES, as illustrated in Figures 6.35 and 6.36. These deviations suggest that certain factors, such as acceleration responsiveness or varying traffic conditions, may have influenced the model's performance in maintaining a consistent speed.

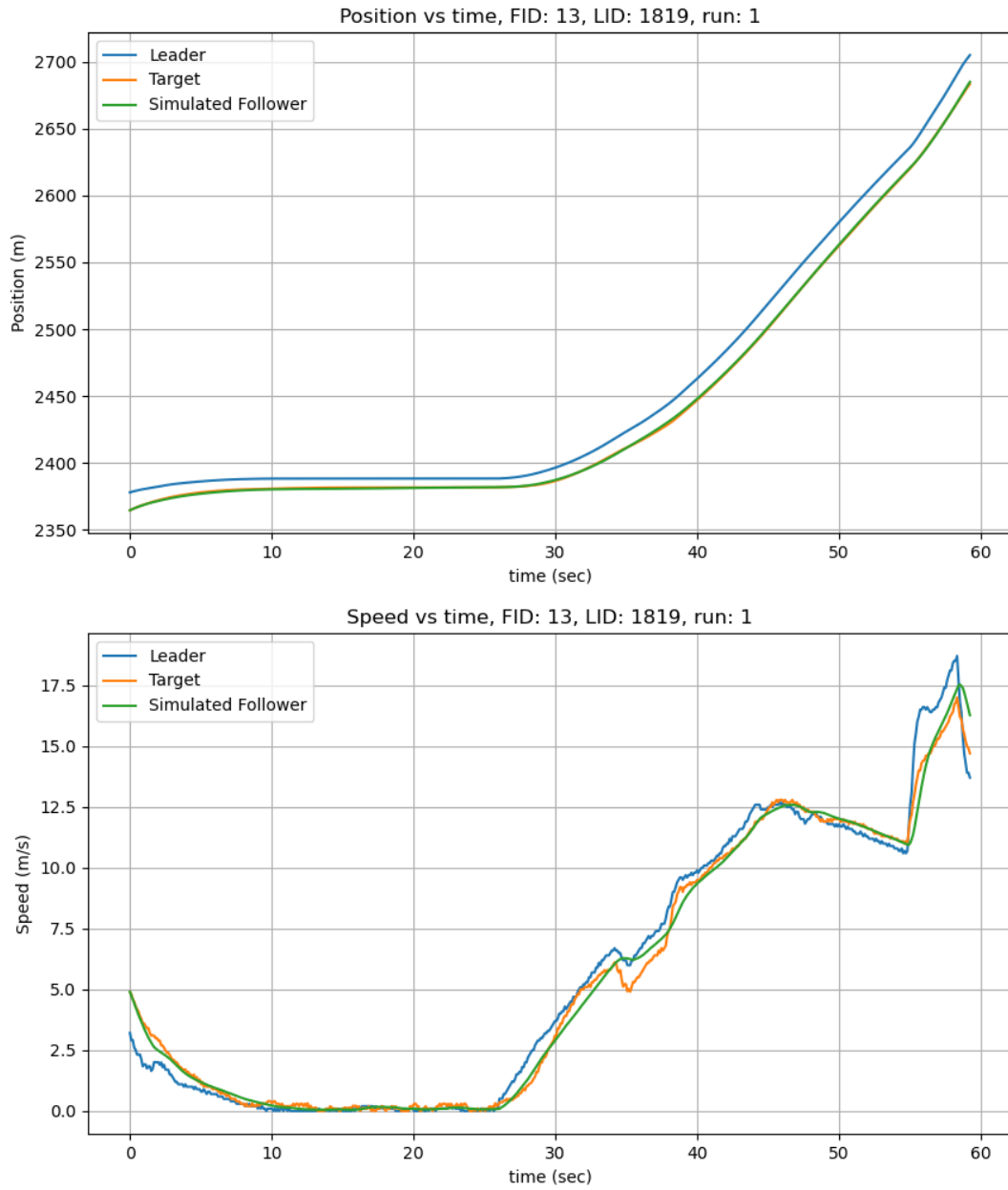


Figure 6.34: Position and speed for CSP for vehicle 13 in Phoenix data H1A3 run 6.

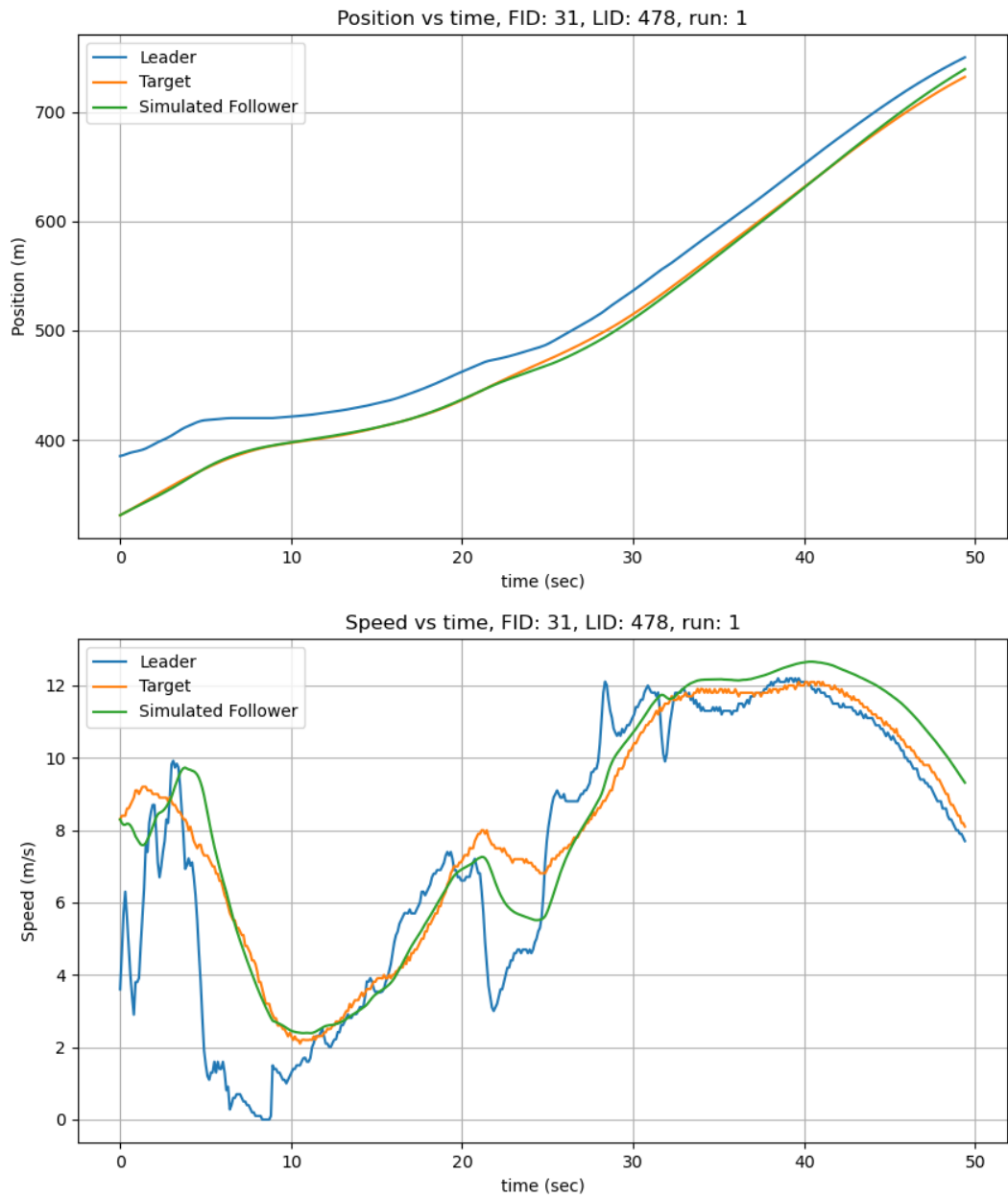


Figure 6.35: Position and speed for CSP for vehicle 31 in Phoenix data H1A3 run 1.

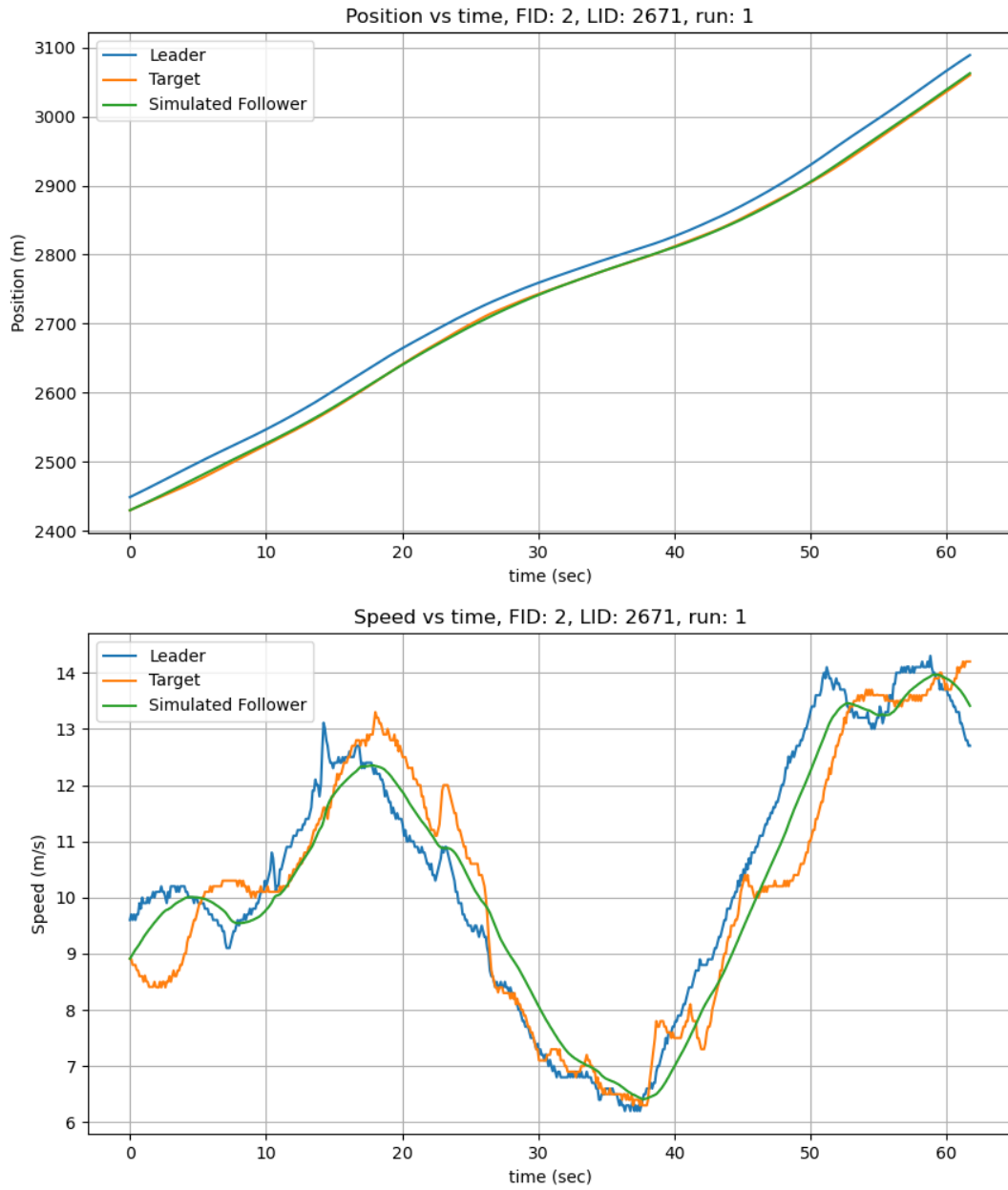


Figure 6.36: Position and speed for CSP for vehicle 2 in Phoenix data H1A3 run 9 ES.

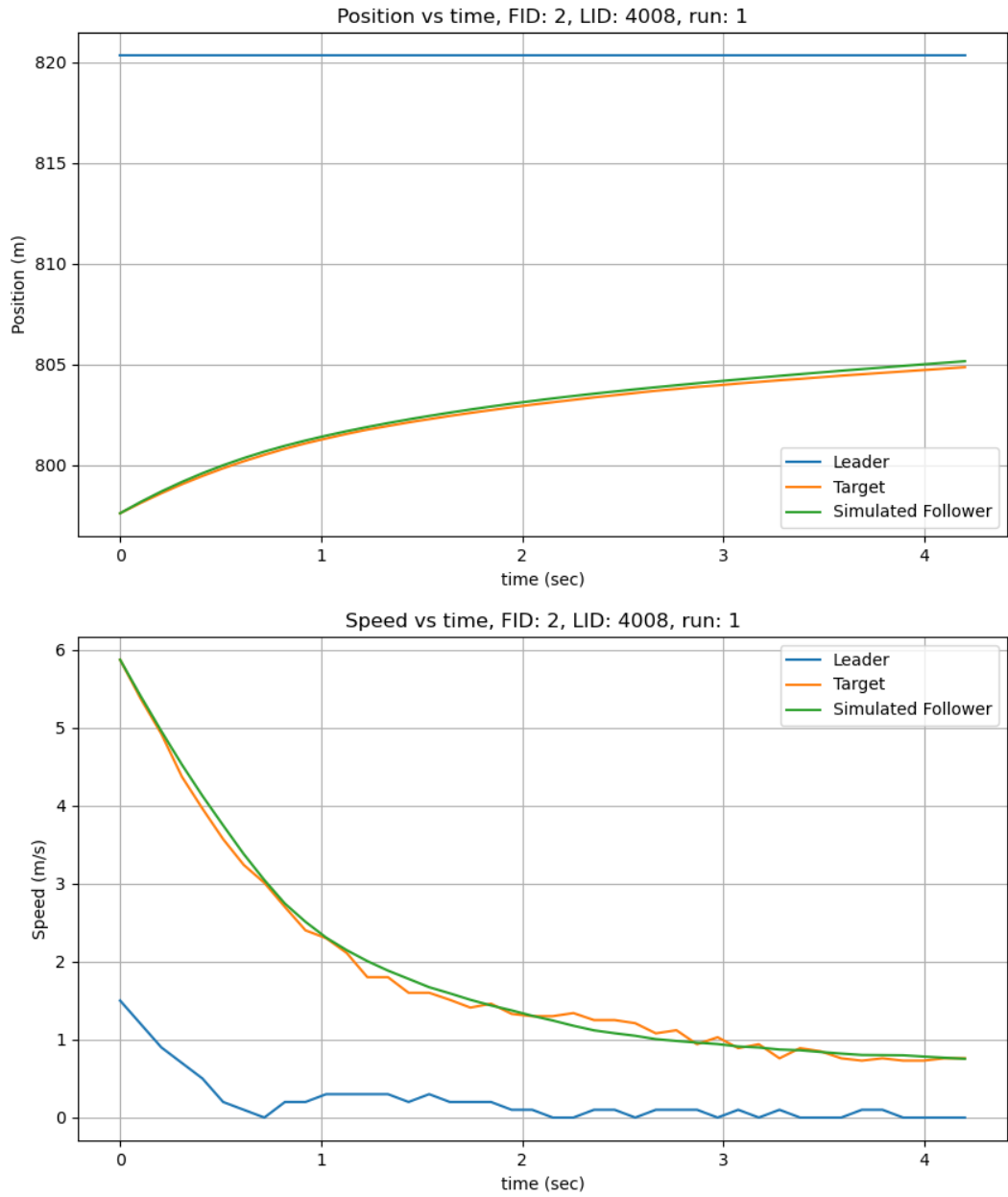


Figure 6.37: Position and speed for CSP for vehicle 2 in Phoenix data H1A3 run 9 NS.

The optimized parameter ranges for the CSP policy in the Phoenix dataset, as shown in Figure 6.38, highlight contrasts in parameter ranges. The desired spacing ($S_{desired}$) exhibits wider

range compared to the tightly clustered values of the control gains (k_v) and (k_p). This suggests that vehicles demonstrate more variability in maintaining inter-vehicle distances, potentially due to differences in traffic flow conditions and driver behaviors unique to the Phoenix dataset.

Figure 6.39 shows that the optimized parameters follow discrete distributions, with values concentrated at specific points rather than being continuously spread. The clustering of (k_v) and (k_p) indicates that acceleration and speed control adjustments remain relatively stable across different scenarios, ensuring uniform response characteristics. Conversely, the broader distribution of ($S_{desired}$) implies that spacing preferences are more dynamic, possibly adapting to varying traffic densities and driving patterns. These findings suggest that while CSP effectively maneuvers the vehicle control dynamics, allowing flexibility in spacing between vehicles under the Phoenix dataset.

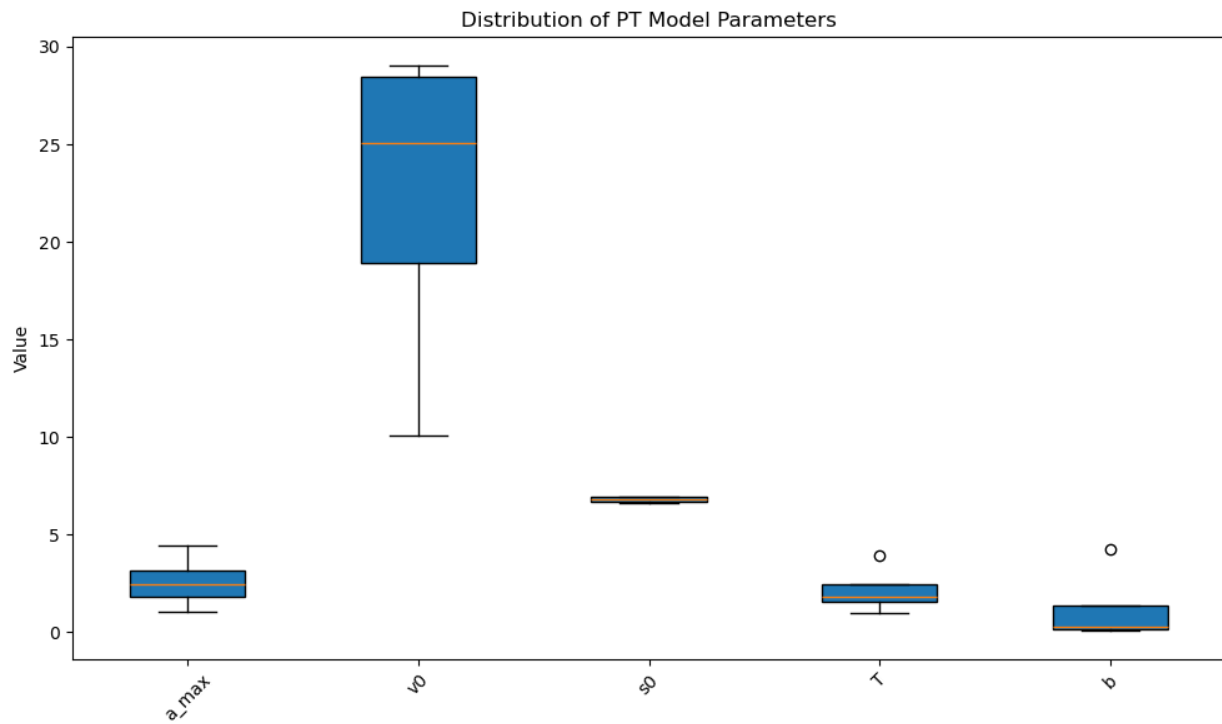


Figure 6.38: Parameter ranges for CSP in Phoenix.

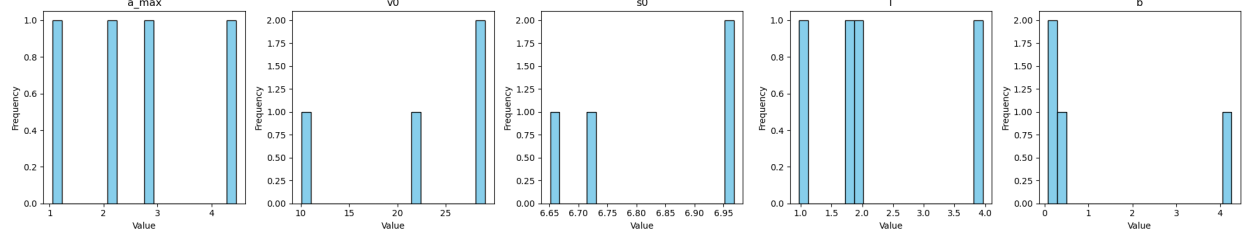


Figure 6.39: Parameter histogram for CSP in Phoenix.

6.2.4 CTH I294 Simulated Results

For Constant Time Headway policy (CTH), the simulated results for I294 are presented in Figures 6.40, 6.41, 6.42, 6.43, 6.44, 6.45, 6.46, 6.47, 6.48, 6.49, 6.50, 6.51, 6.52, 6.53, 6.54, 6.55, 6.55, 6.56, 6.57, 6.58, 6.59, 6.60, 6.61, 6.62, 6.63, 6.64 and 6.65. By dynamically adjusting the time intervals, the simulated trajectories generated by the CTH policy was able to closely track the target trajectories. Despite some speed variations between the simulated follower and target follower, the position was closely aligned.

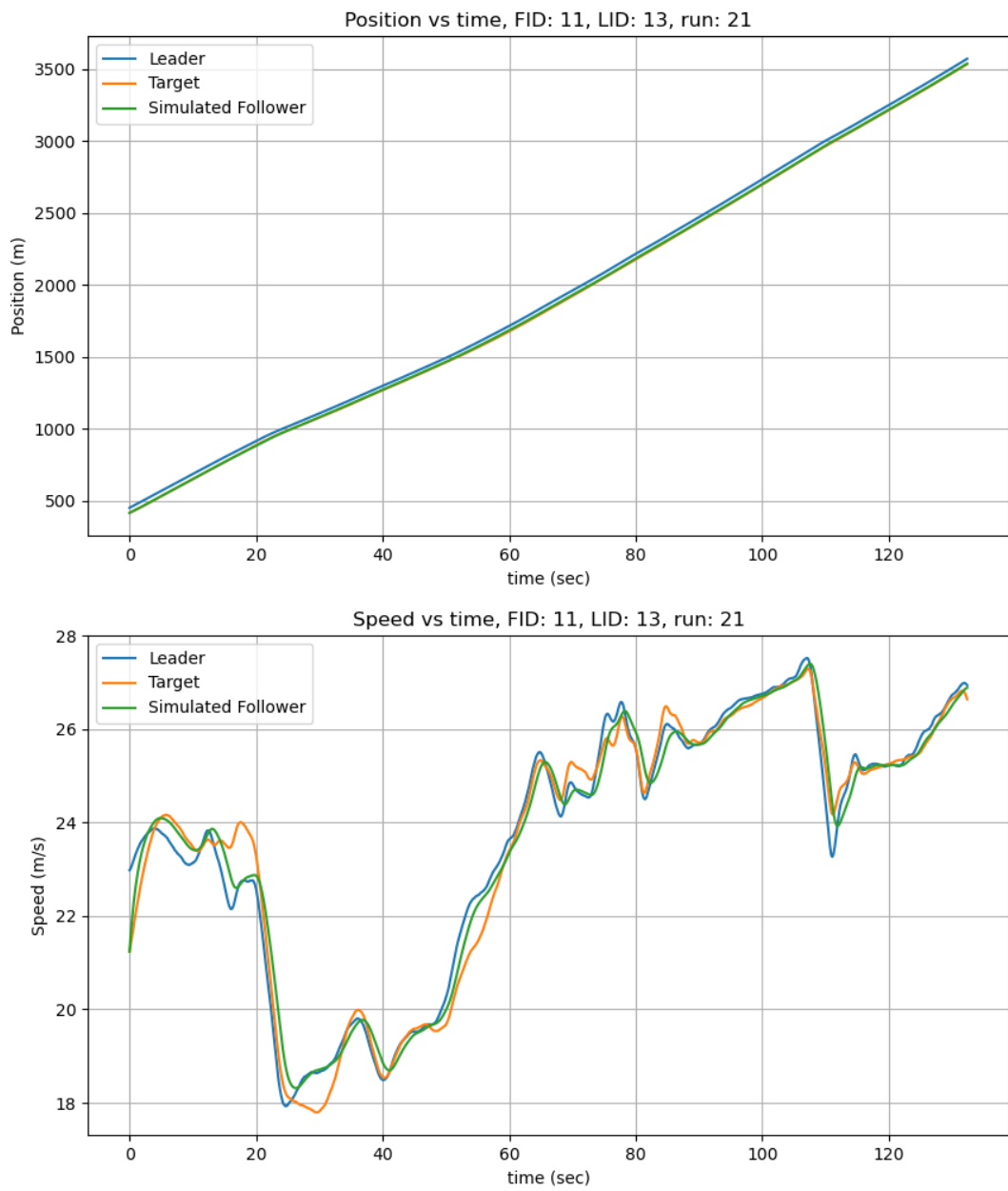


Figure 6.40: Position and speed for CTH for vehicle 11 in run 21 I294L1 dataset.

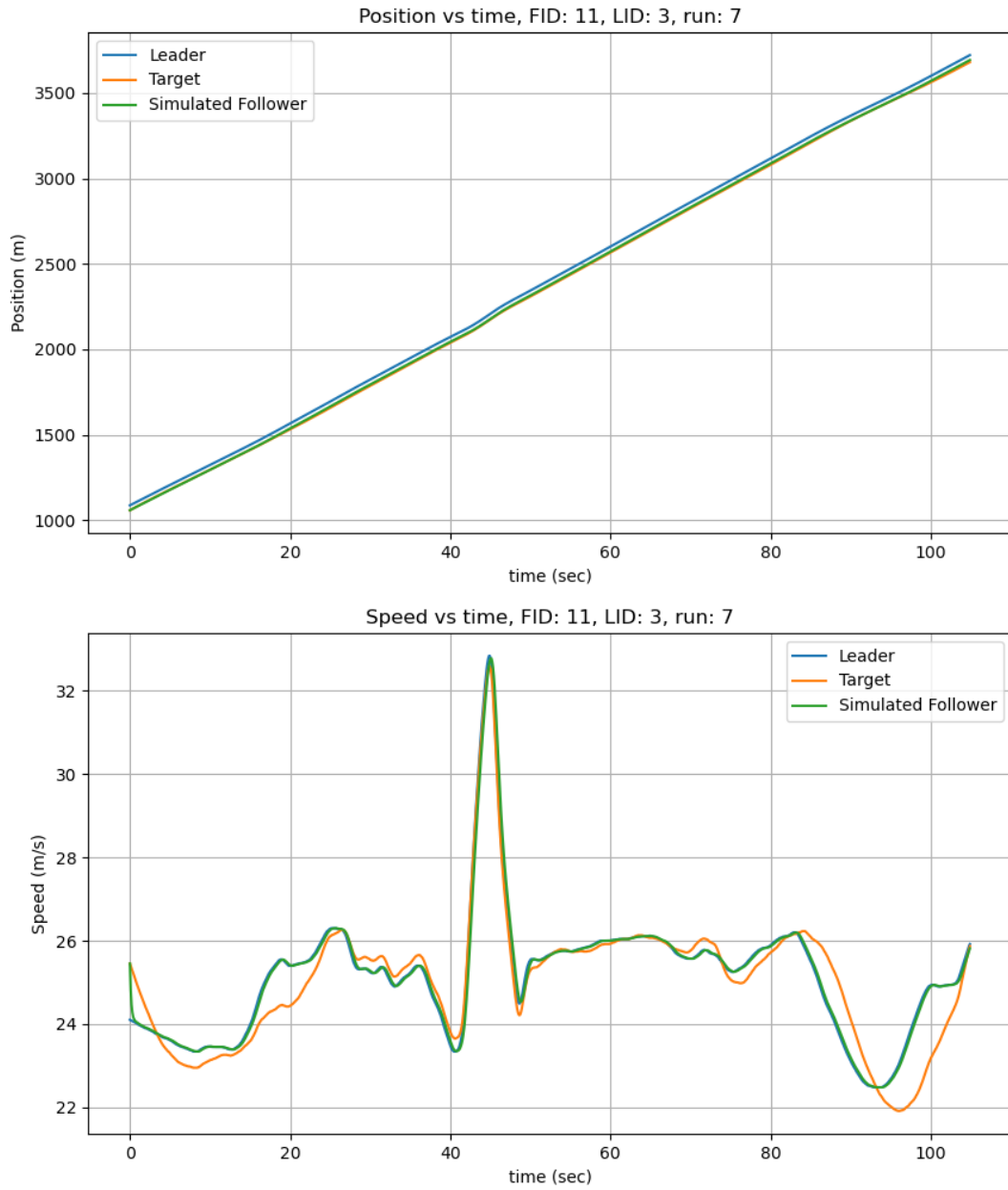


Figure 6.41: Position and speed for CTH for vehicle 11 in run 7 I294L1 dataset.

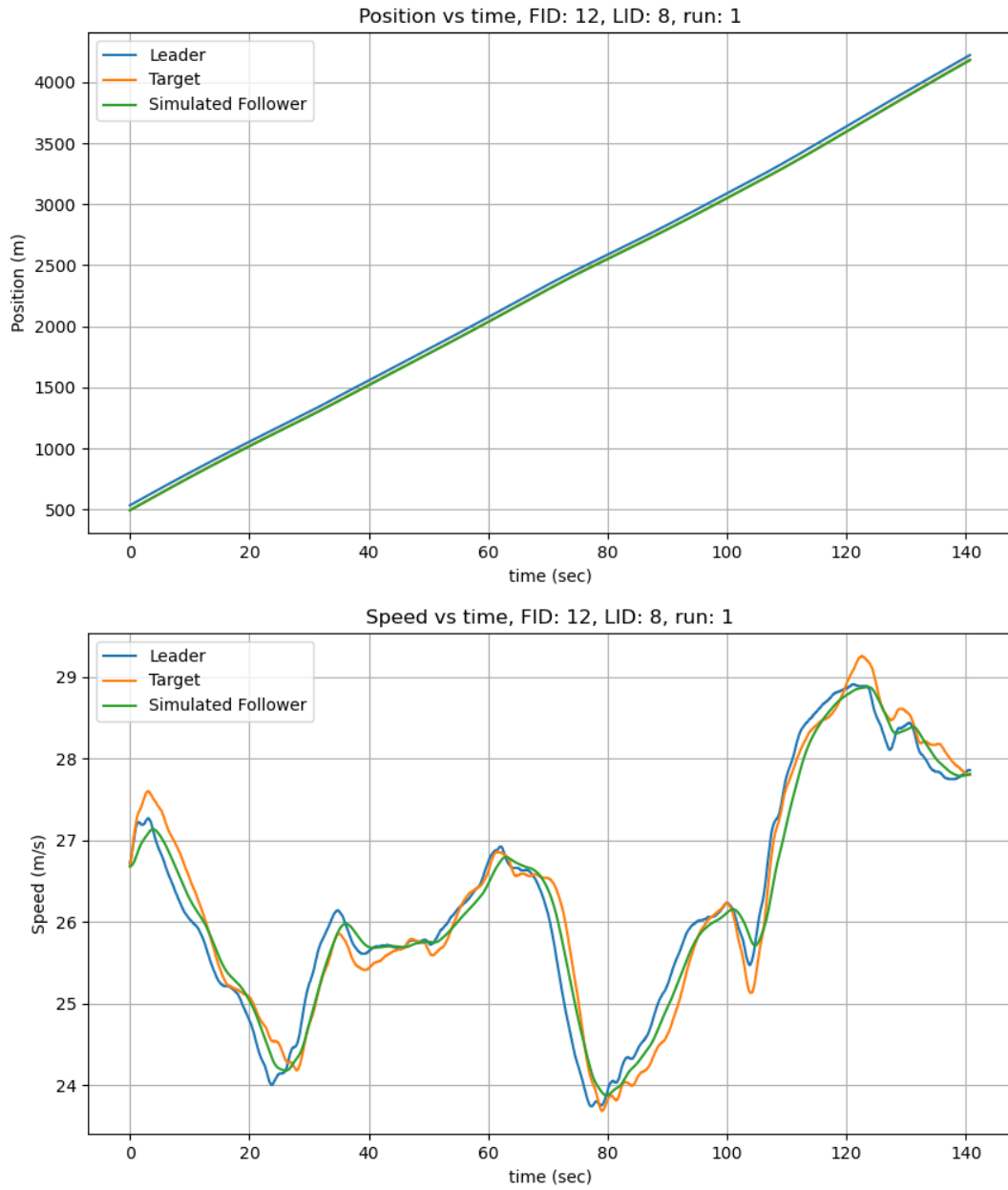


Figure 6.42: Position and speed for CTH for vehicle 12 in run 1 I294L1 dataset.

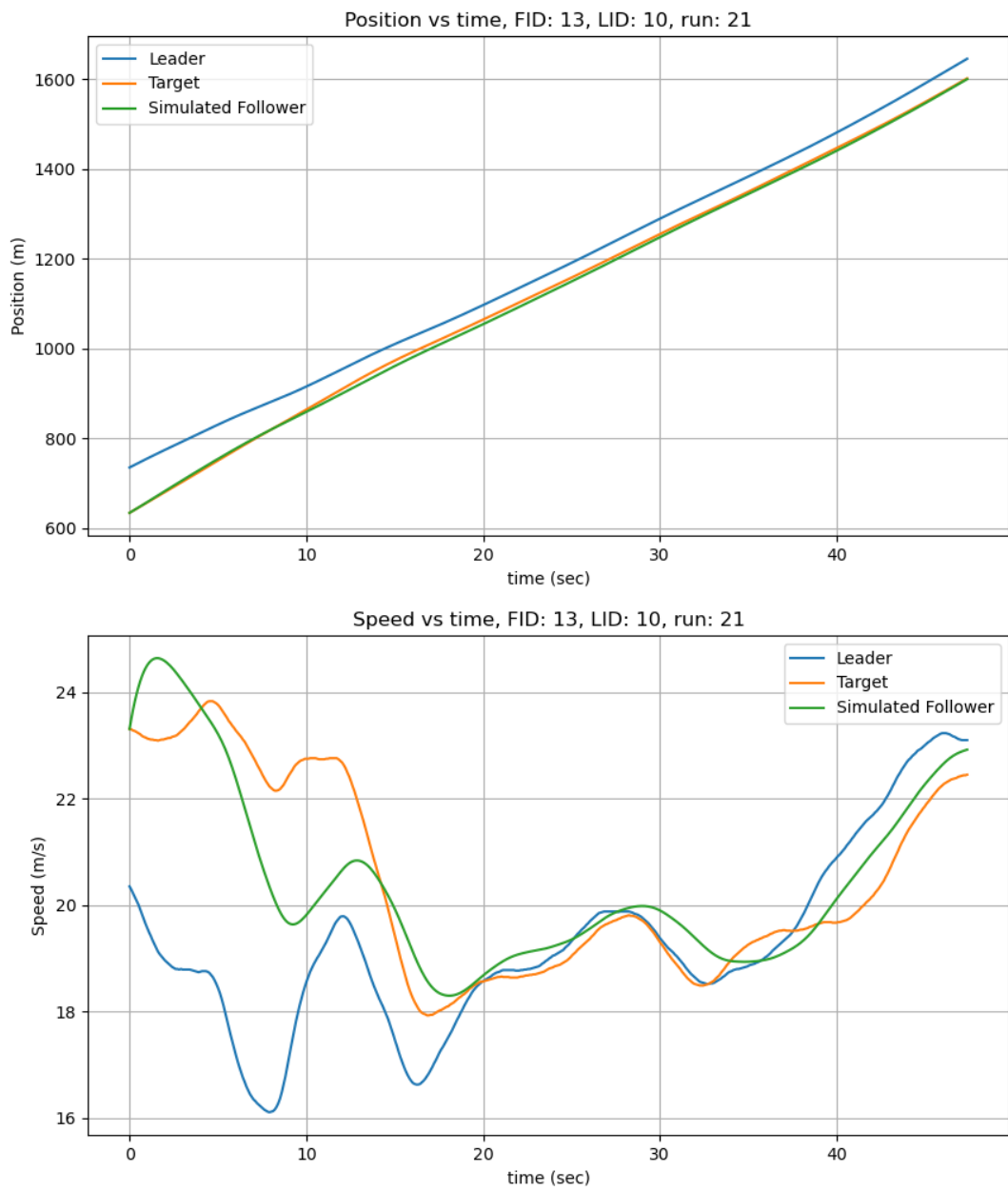


Figure 6.43: Position and speed for CTH for vehicle 13 in run 21 I294L1 dataset.

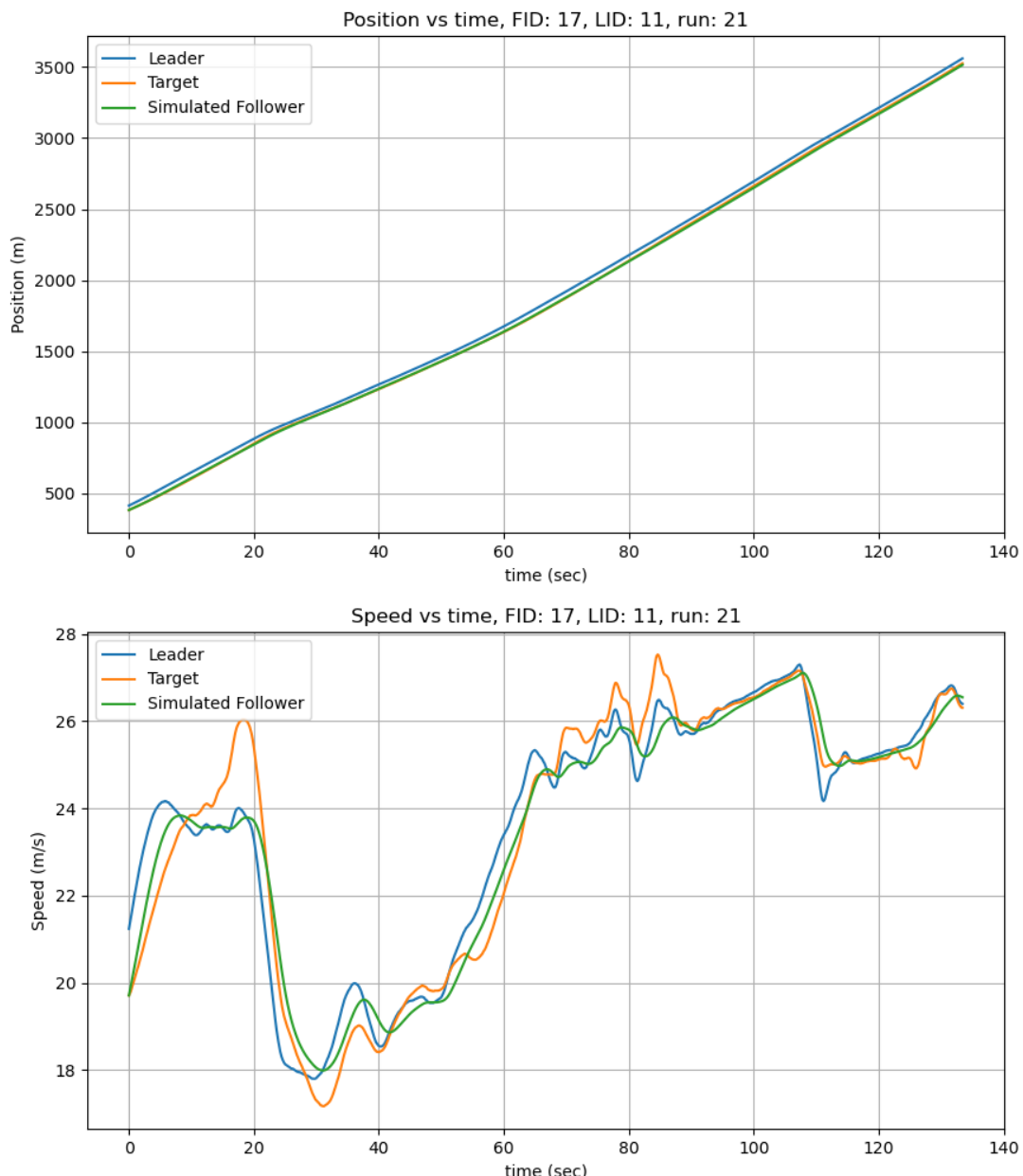


Figure 6.44: Position and speed for CTH for vehicle 17 in run 21 I294L1 dataset.

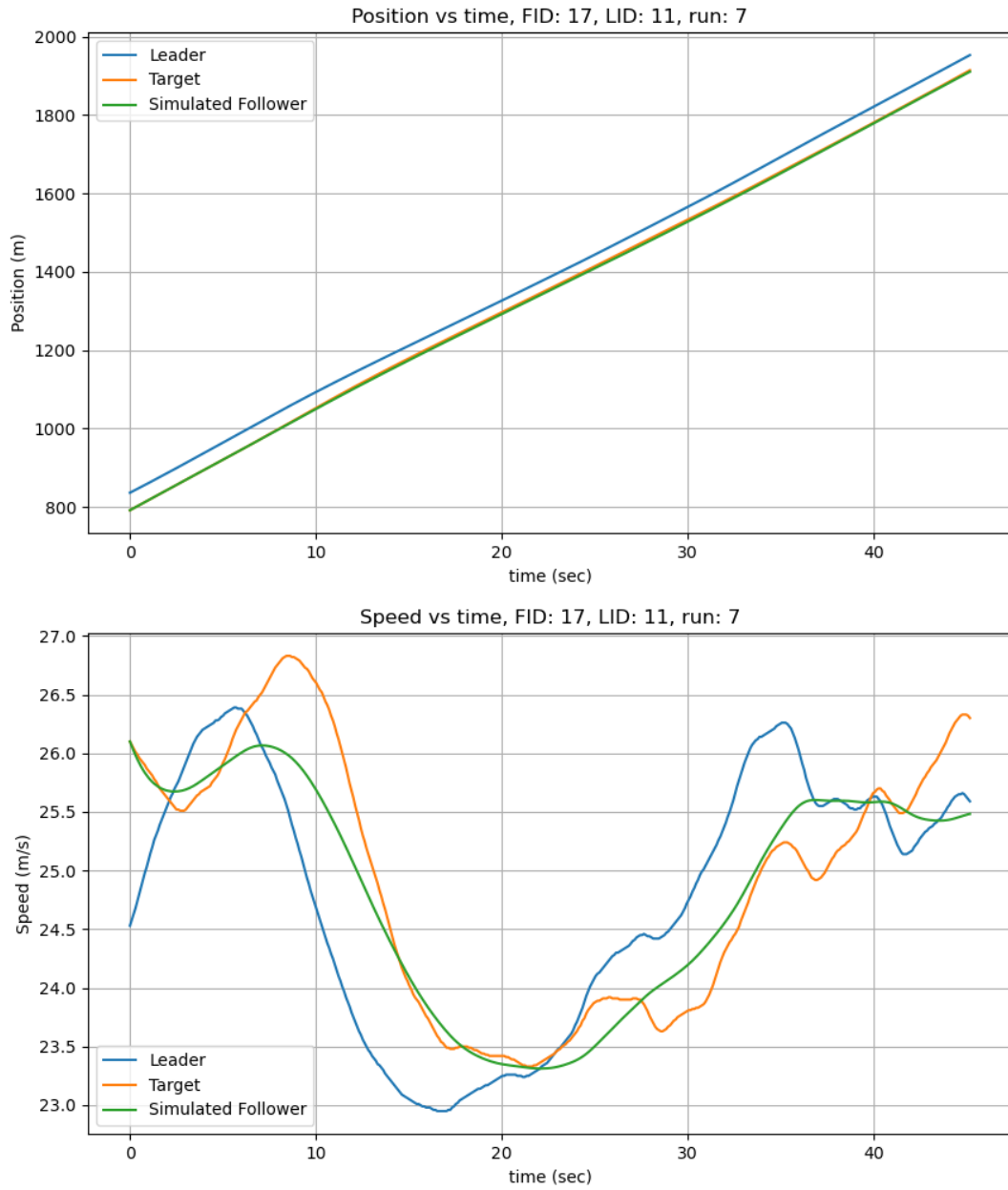


Figure 6.45: Position and speed for CTH for vehicle 17 in run 7 I294L1 dataset.

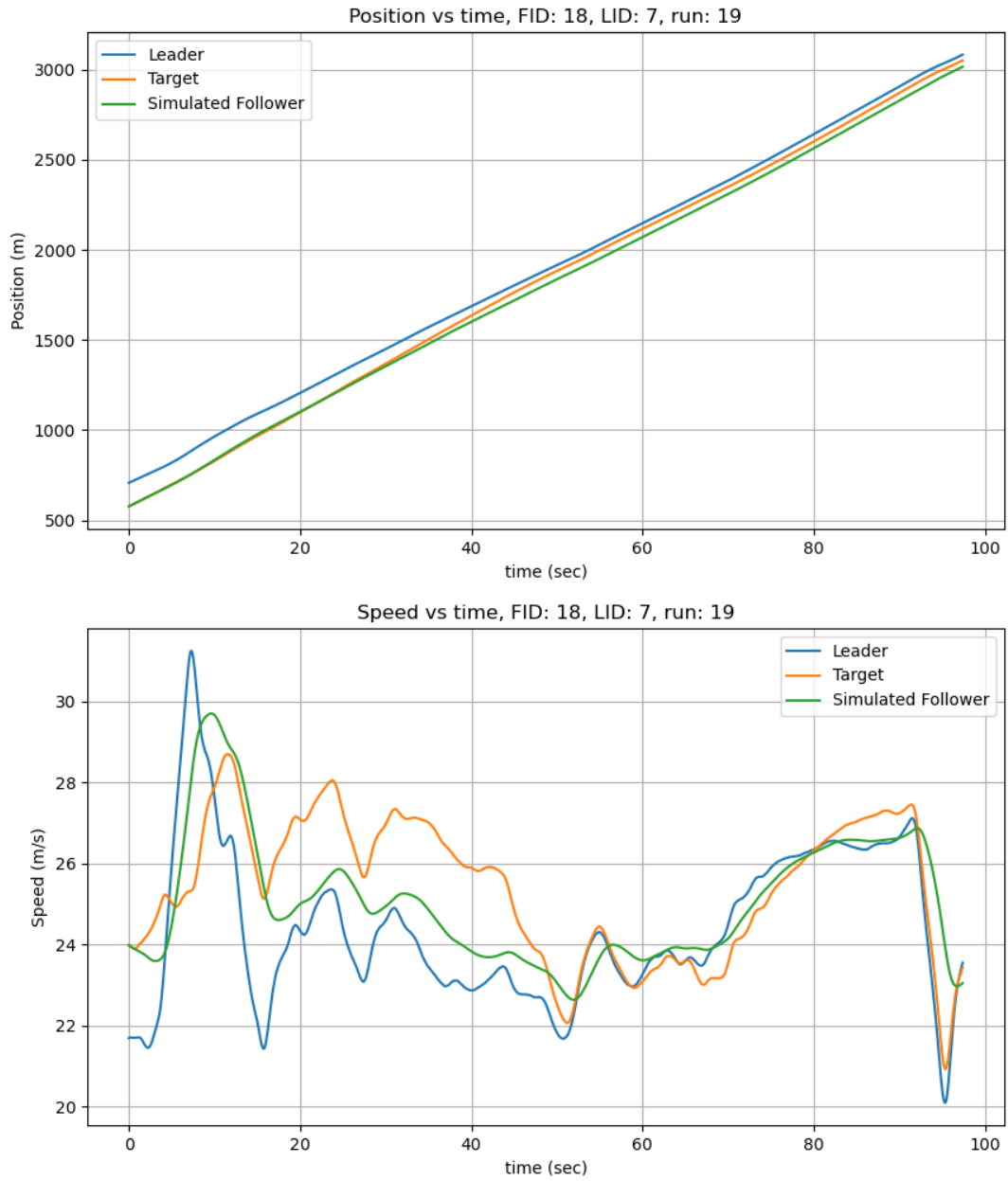


Figure 6.46: Position and speed for CTH for vehicle 18 in run 19 I294L1 dataset.

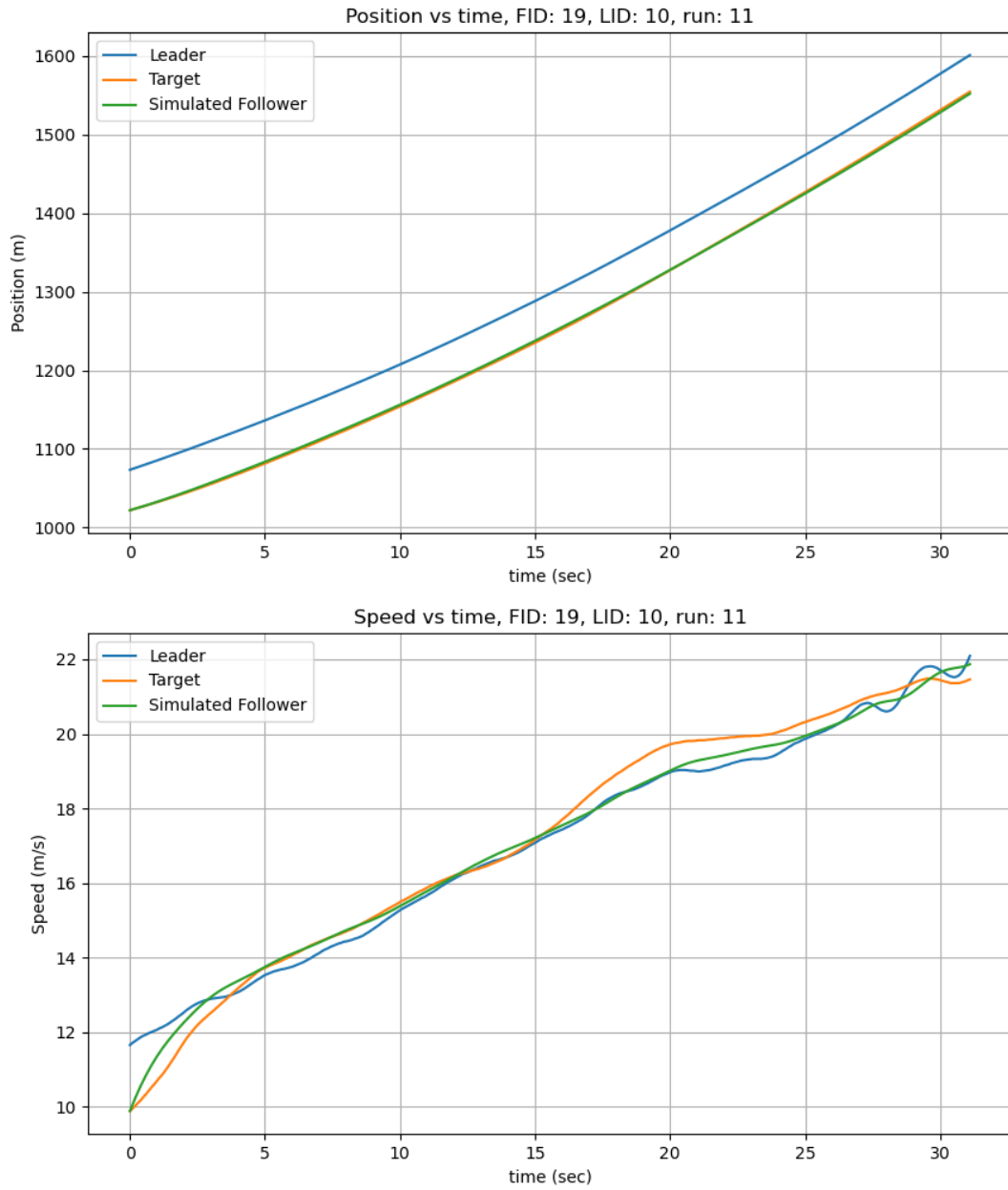


Figure 6.47: Position and speed for CTH for vehicle 19 in run 11 I294L1 dataset.

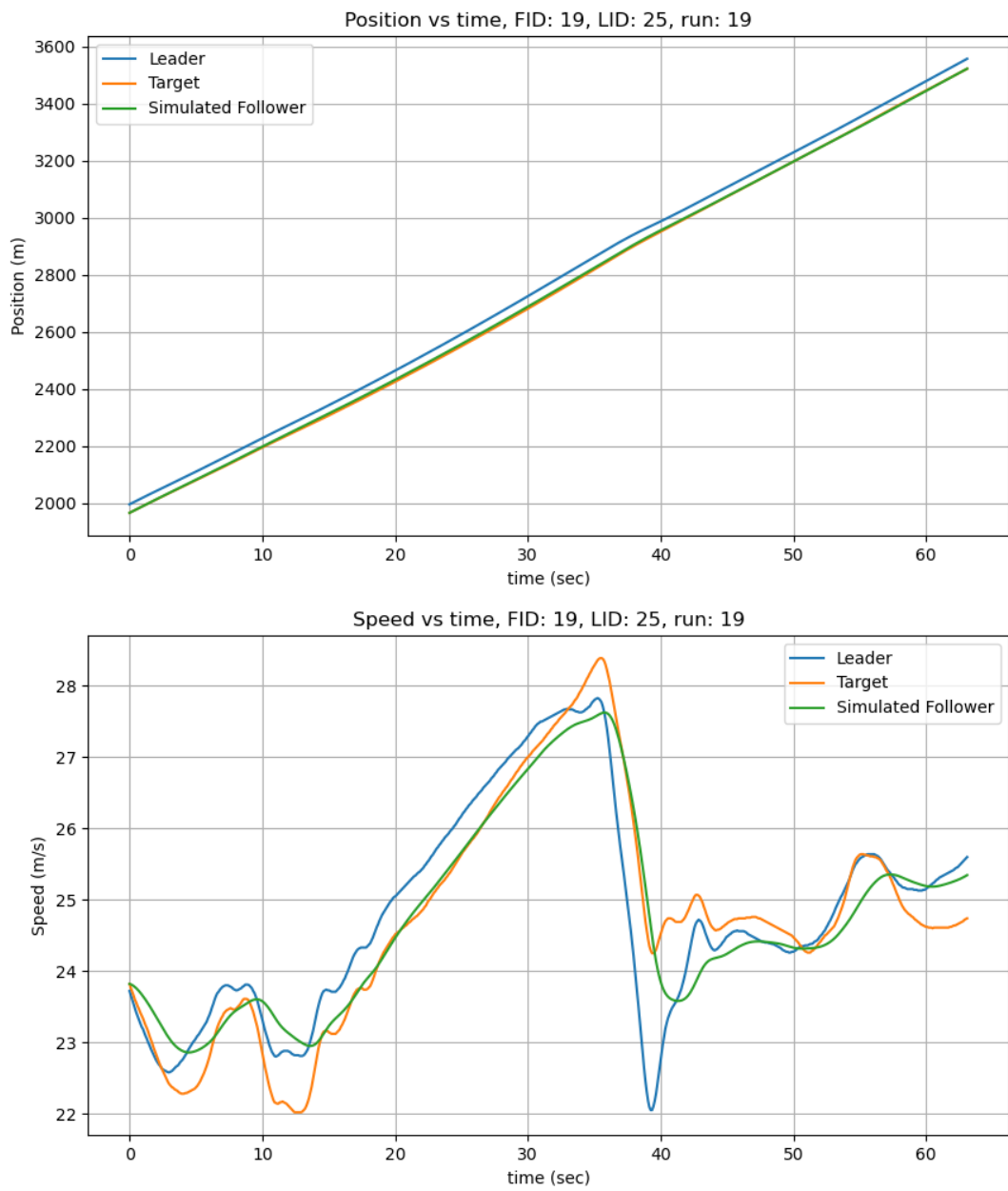


Figure 6.48: Position and speed for CTH for vehicle 19 in run 19 I294L1 dataset.

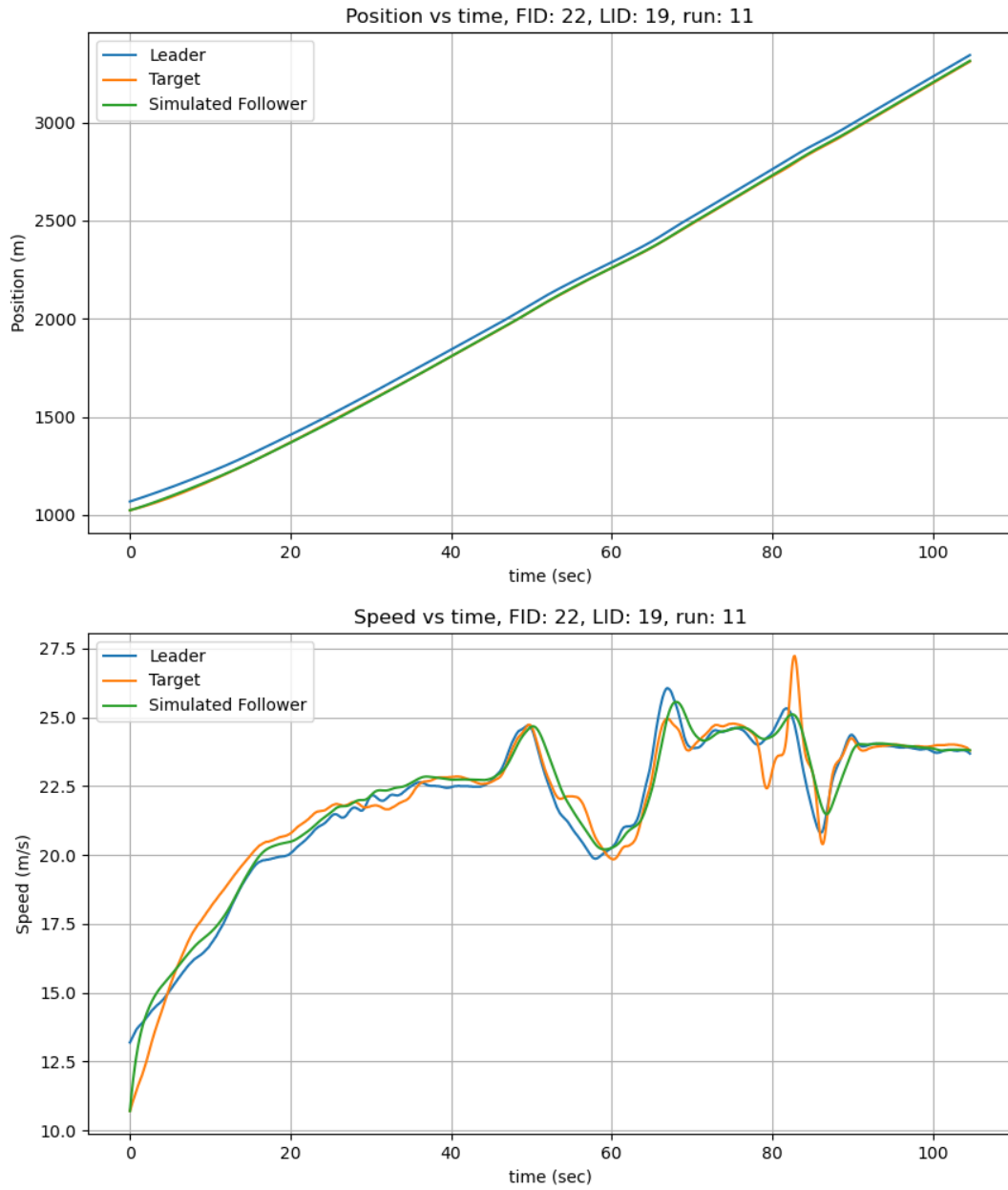


Figure 6.49: Position and speed for CTH for vehicle 22 in run 11 I294L1 dataset.

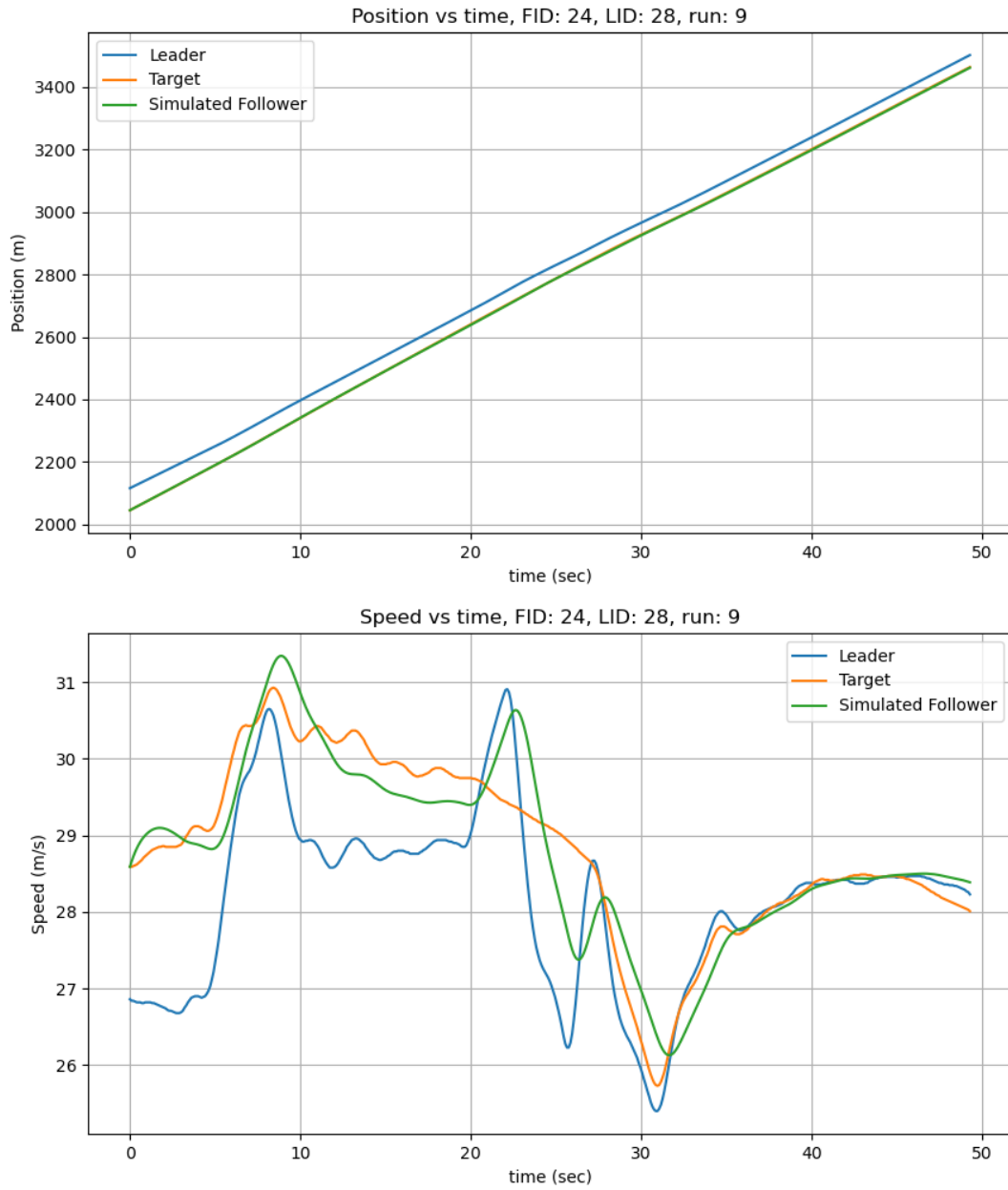


Figure 6.50: Position and speed for CTH for vehicle 24 in run 9 I294L1 dataset.

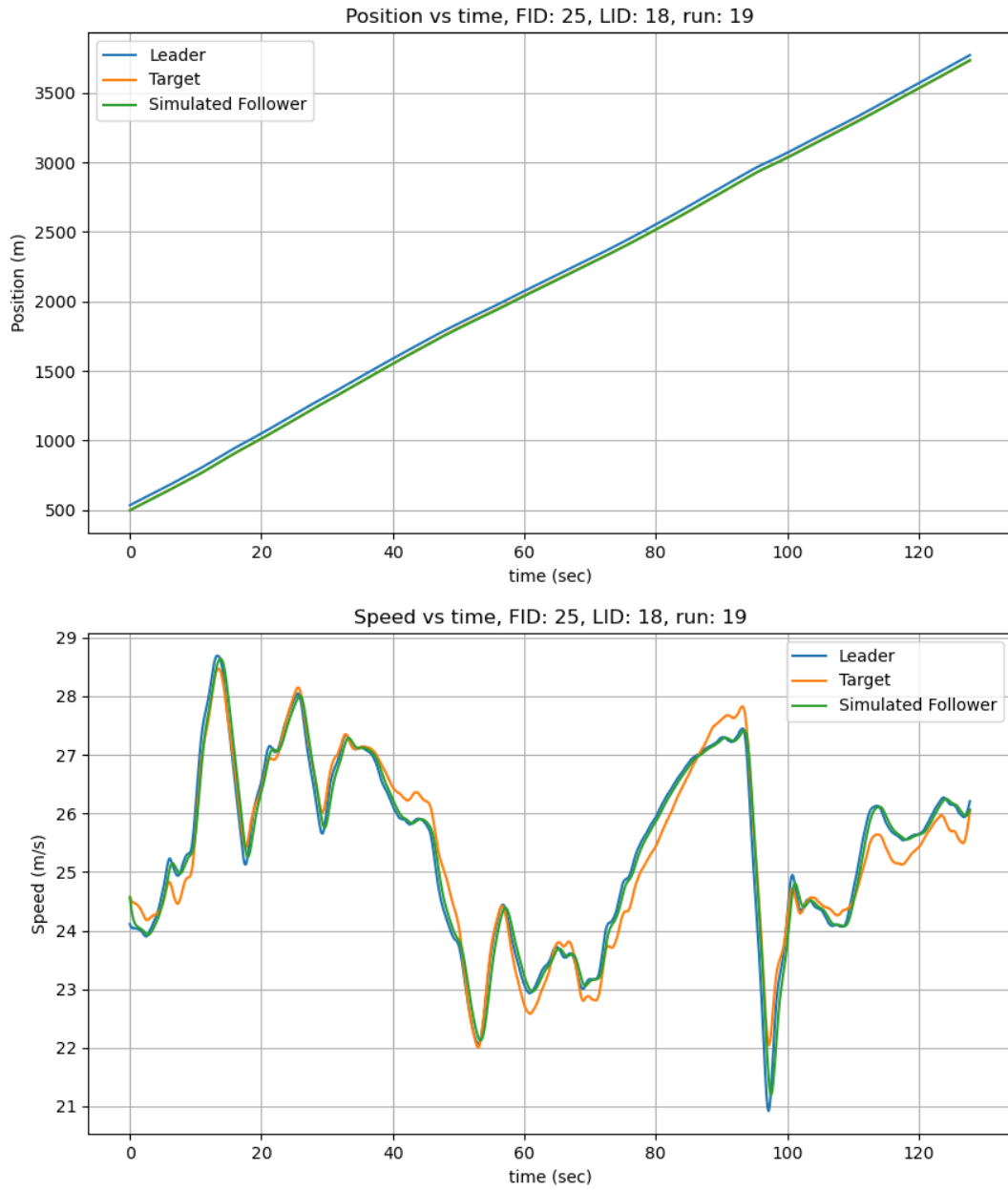


Figure 6.51: Position and speed for CTH for vehicle 25 in run 19 I294L1 dataset.

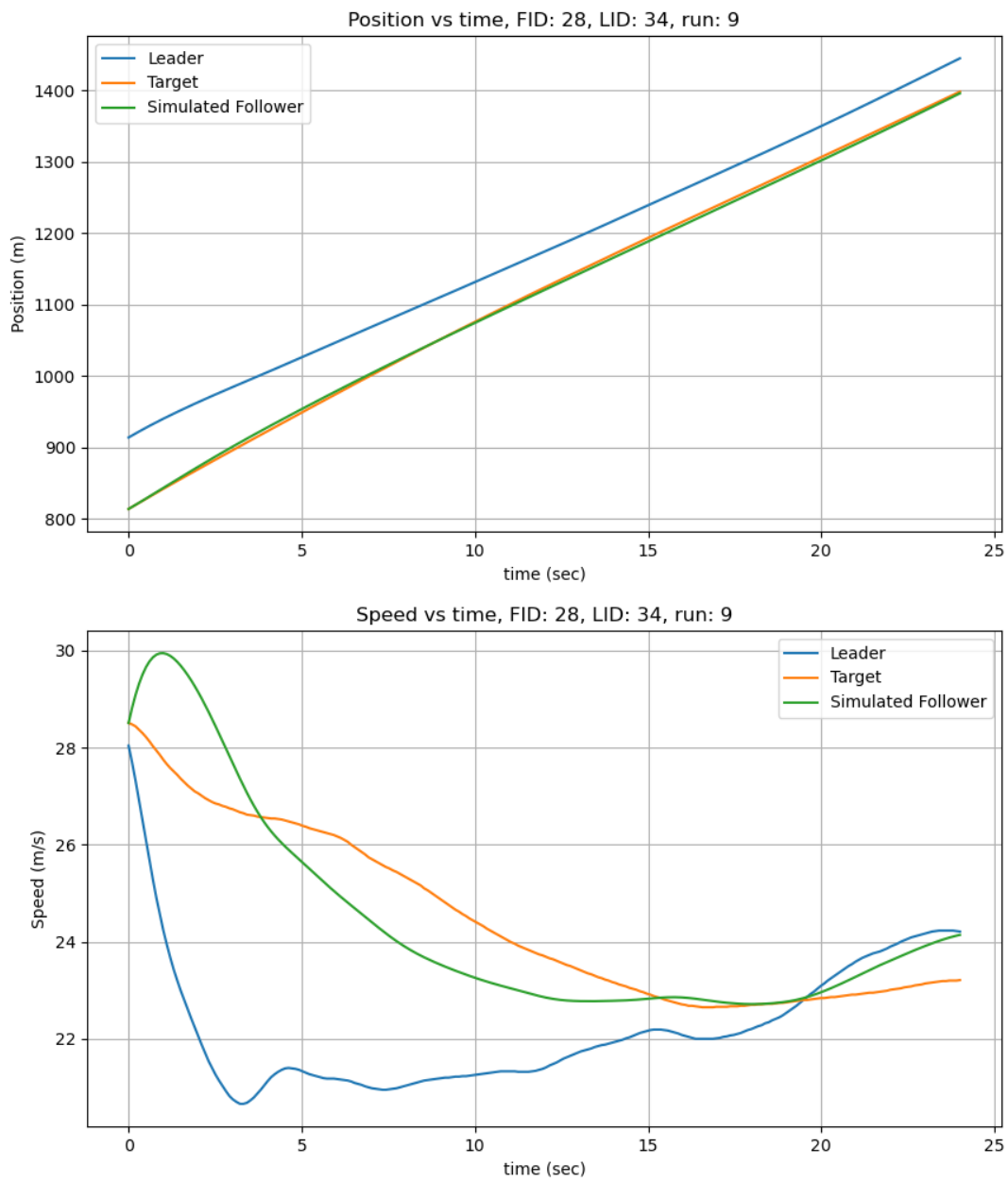


Figure 6.52: Position and speed for CTH for vehicle 28 in run 9 I294L1 dataset.

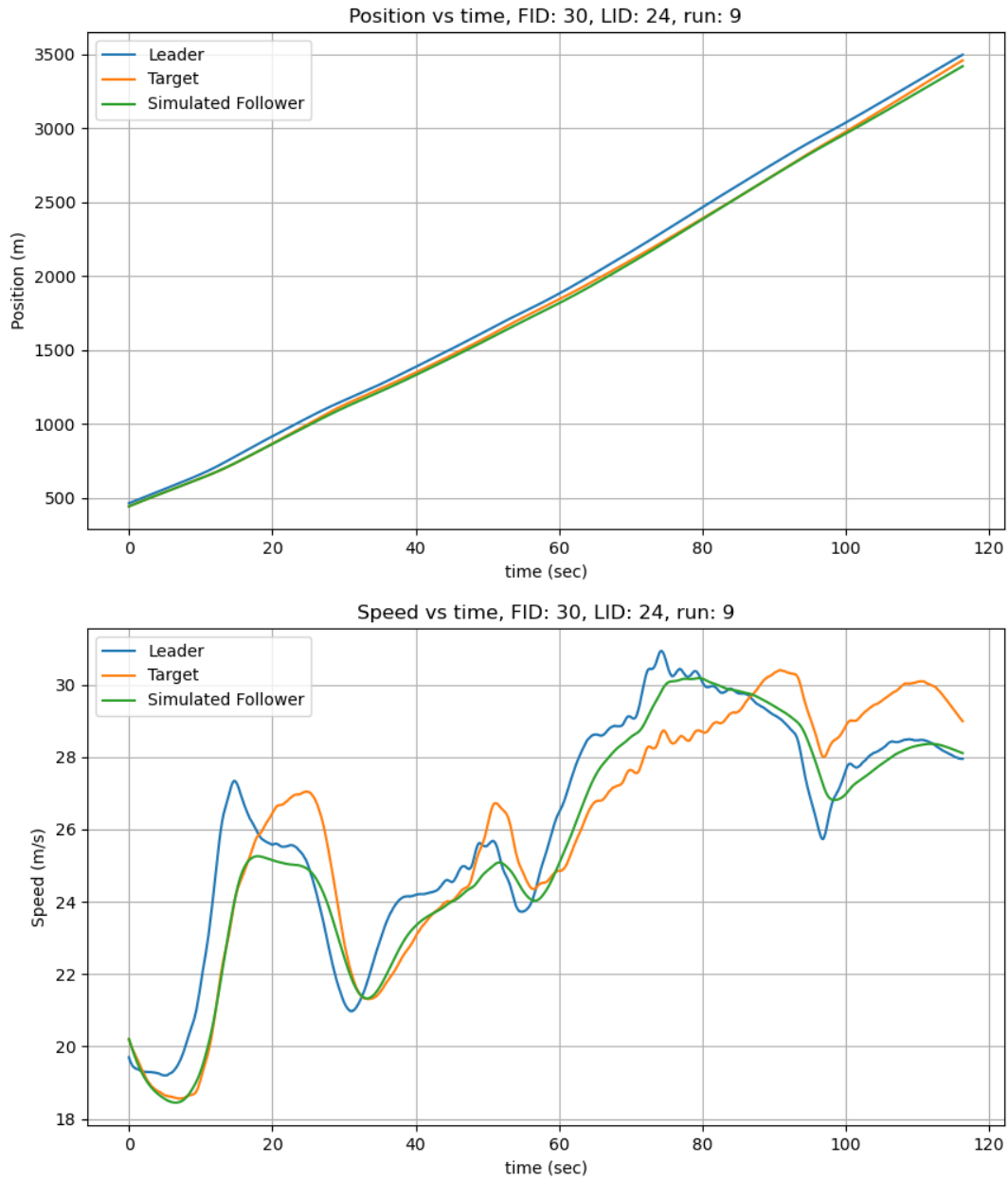


Figure 6.53: Position and speed for CTH for vehicle 30 in run 9 I294L1 dataset.

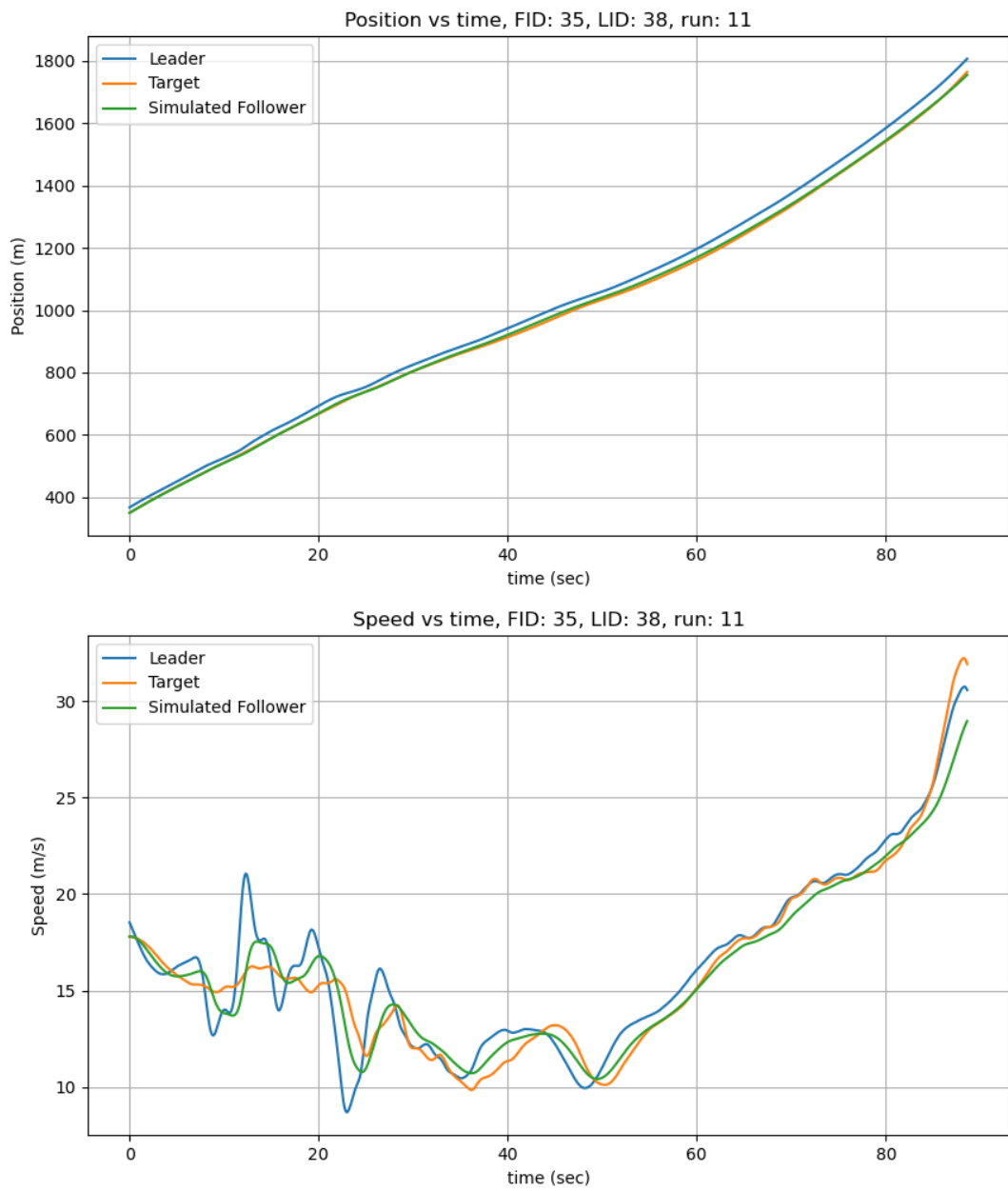


Figure 6.54: Position and speed for CTH for vehicle 35 in run 11 I294L1 dataset.

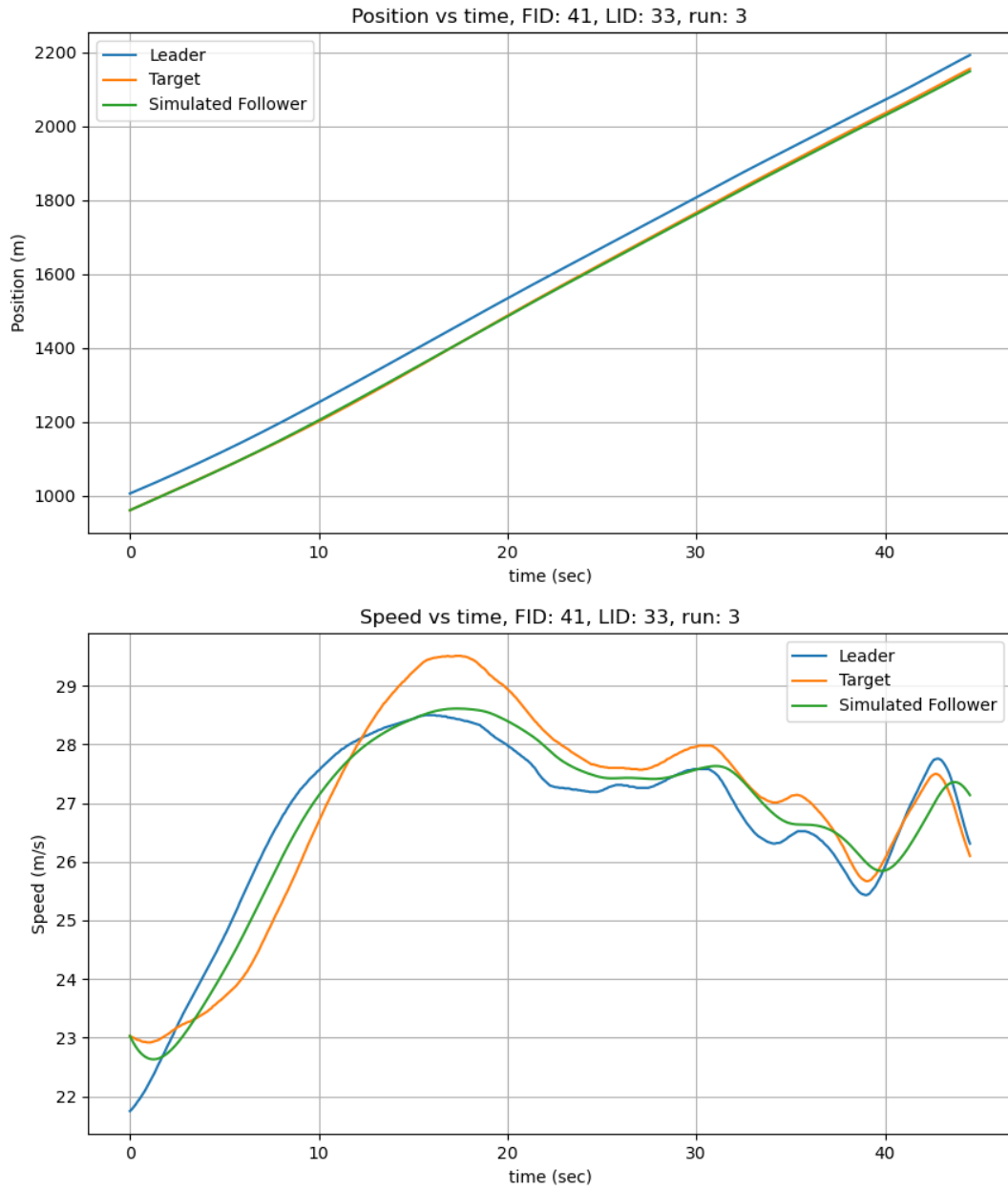


Figure 6.55: Position and speed for CTH for vehicle 41 in run 3 I294L1 dataset.

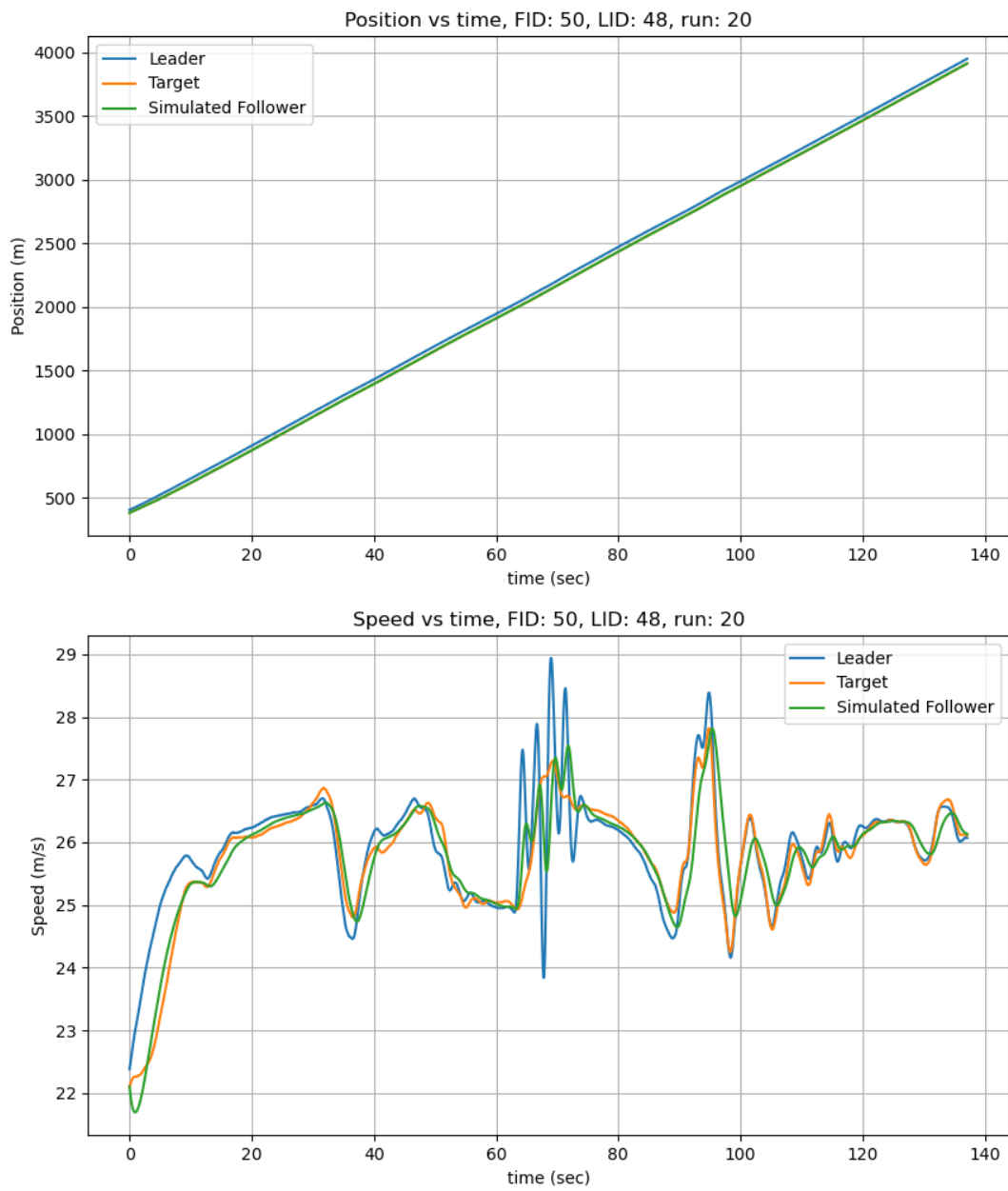


Figure 6.56: Position and speed for CTH for vehicle 50 in run 20 I294L1 dataset.

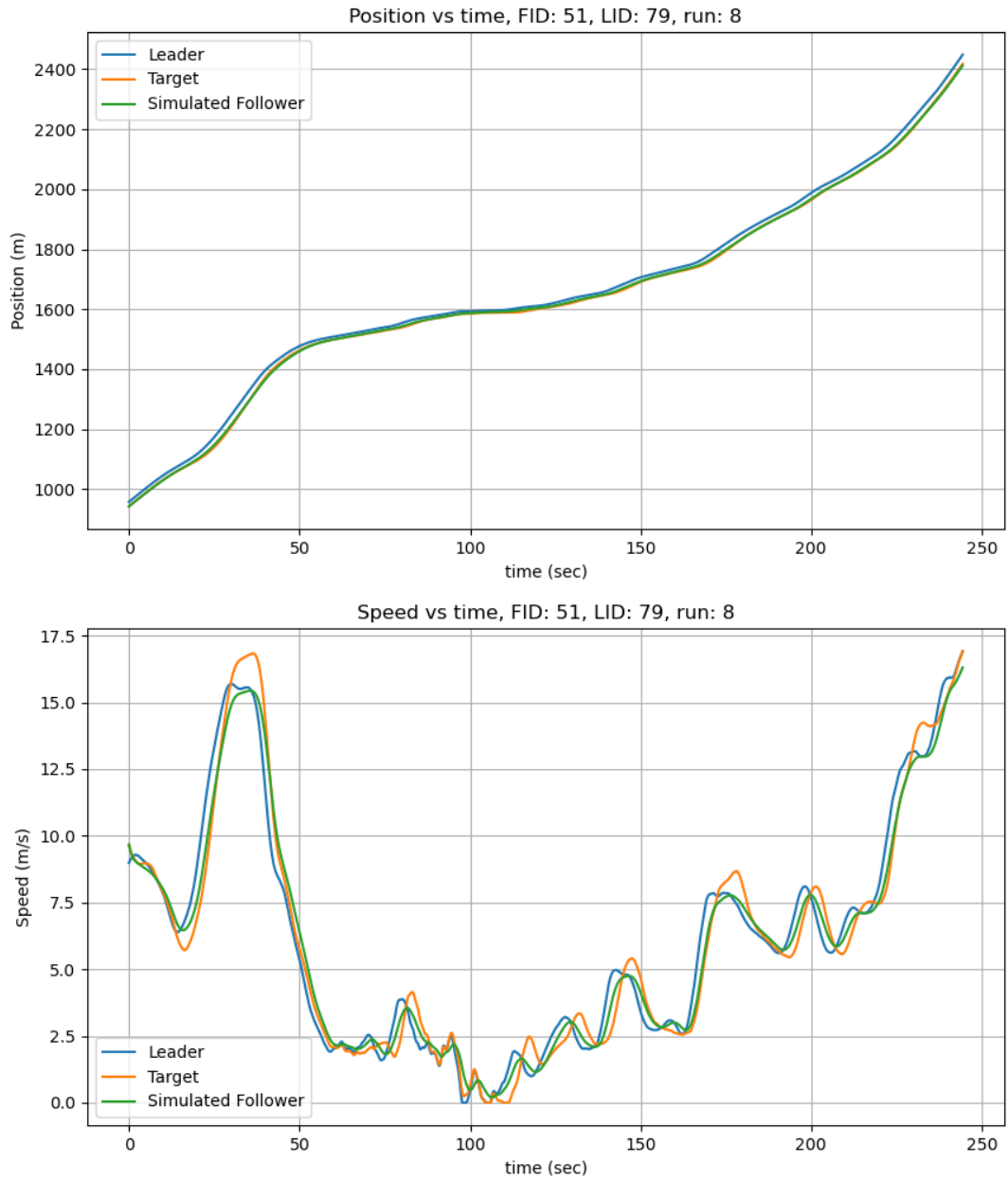


Figure 6.57: Position and speed for CTH for vehicle 51 in run 8 I294L1 dataset.

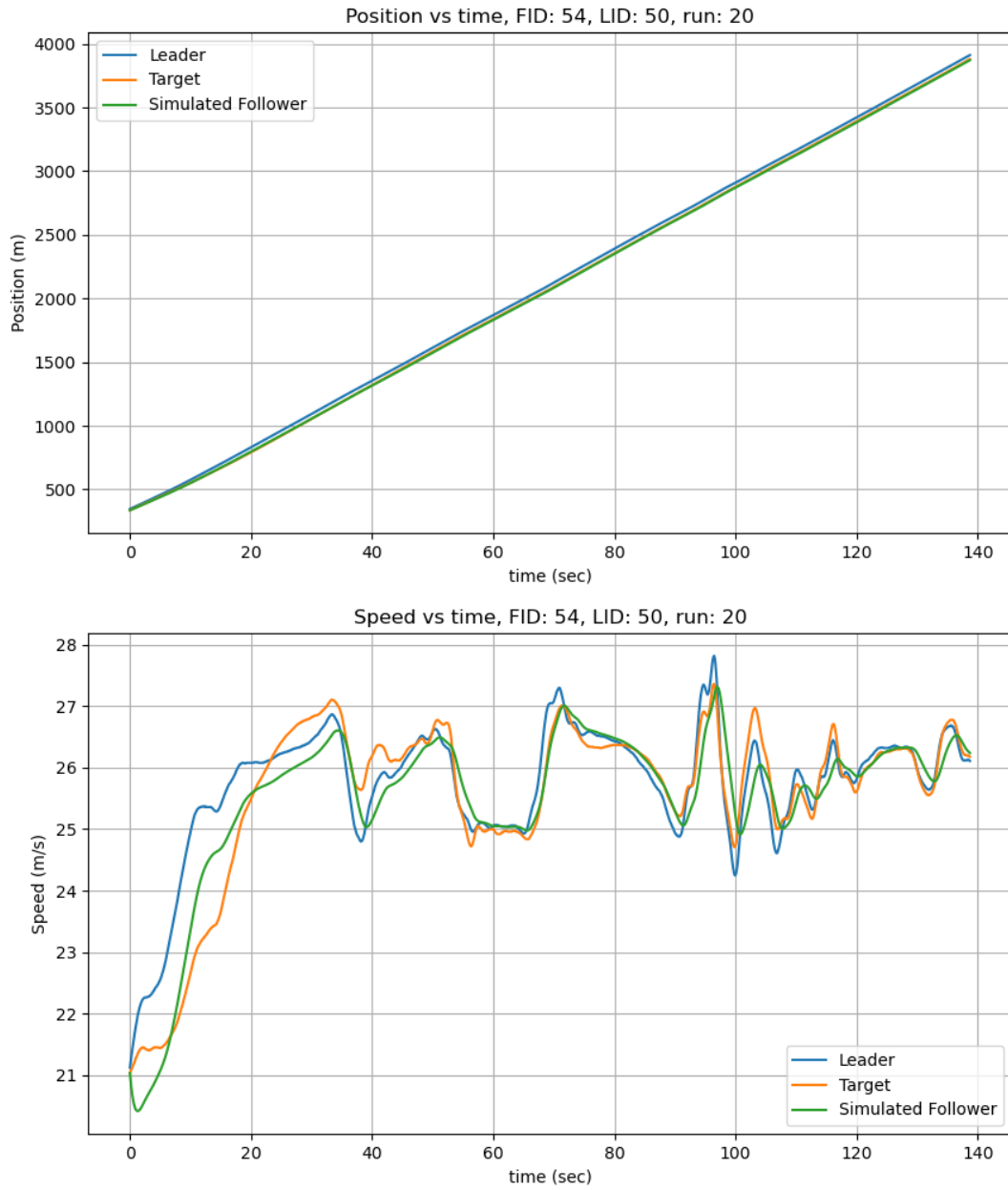


Figure 6.58: Position and speed for CTH for vehicle 54 in run 20 I294L1 dataset.

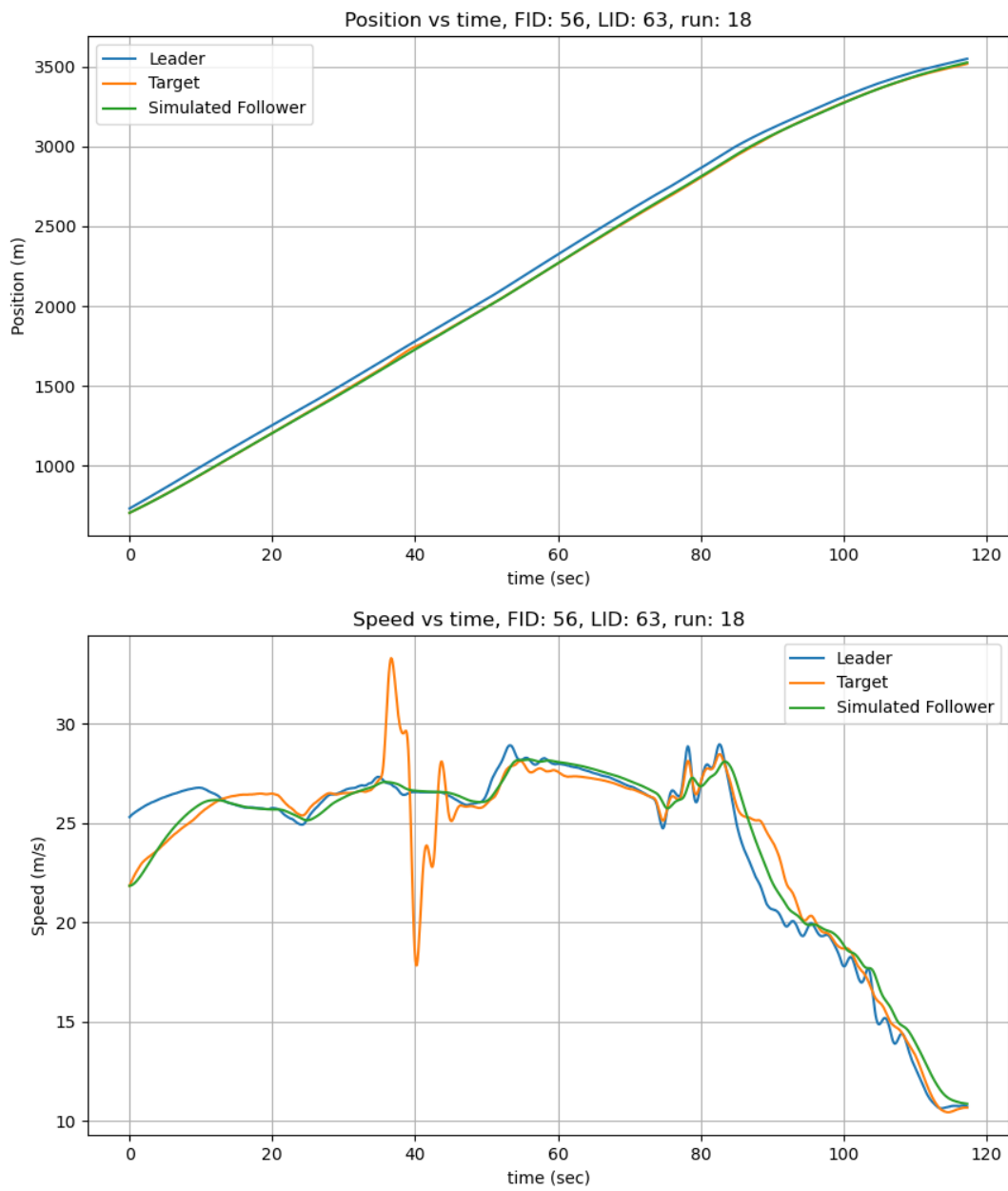


Figure 6.59: Position and speed for CTH for vehicle 56 in run 18 I294L1 dataset.

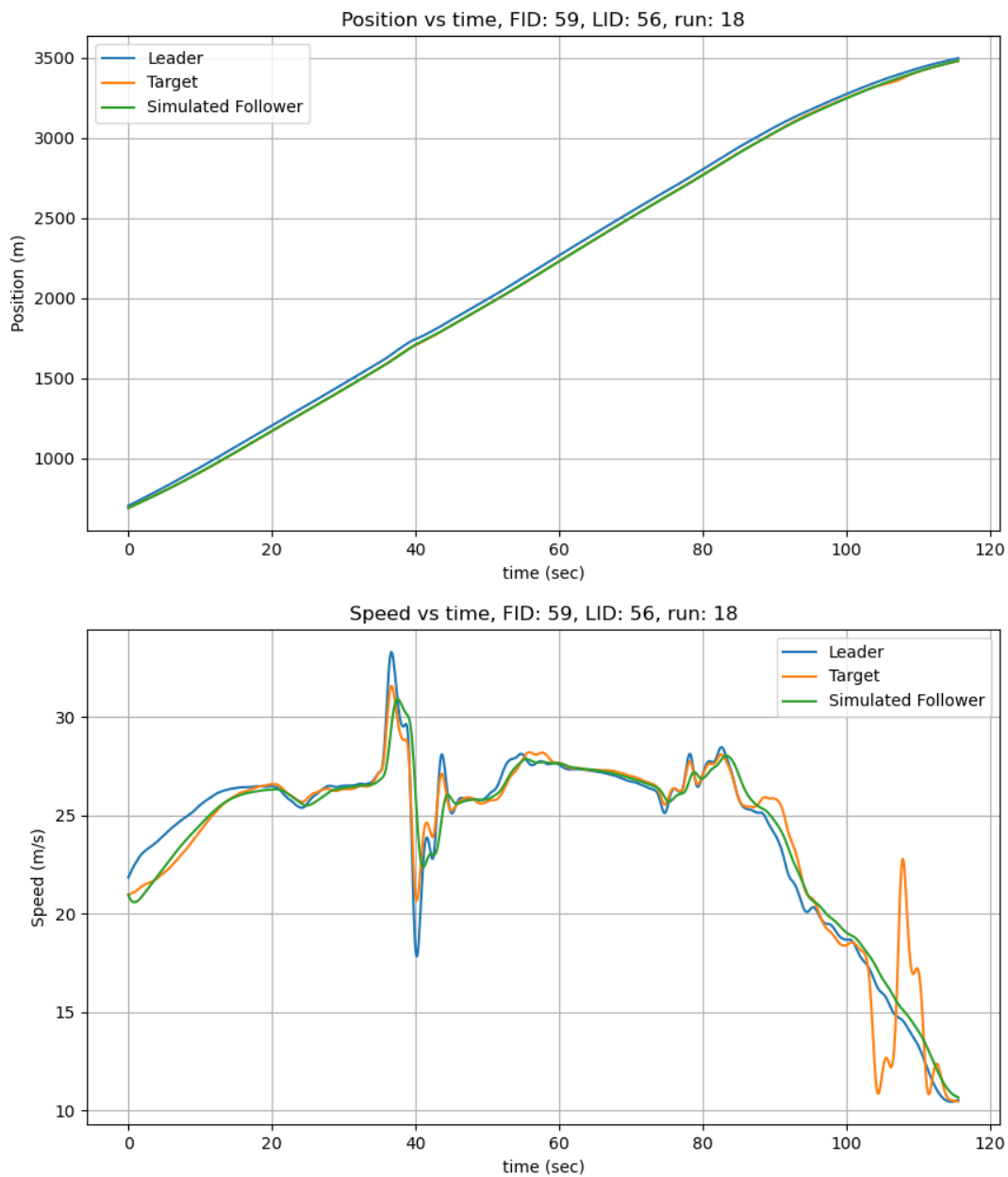


Figure 6.60: Position and speed for CTH for vehicle 59 in run 18 I294L1 dataset.

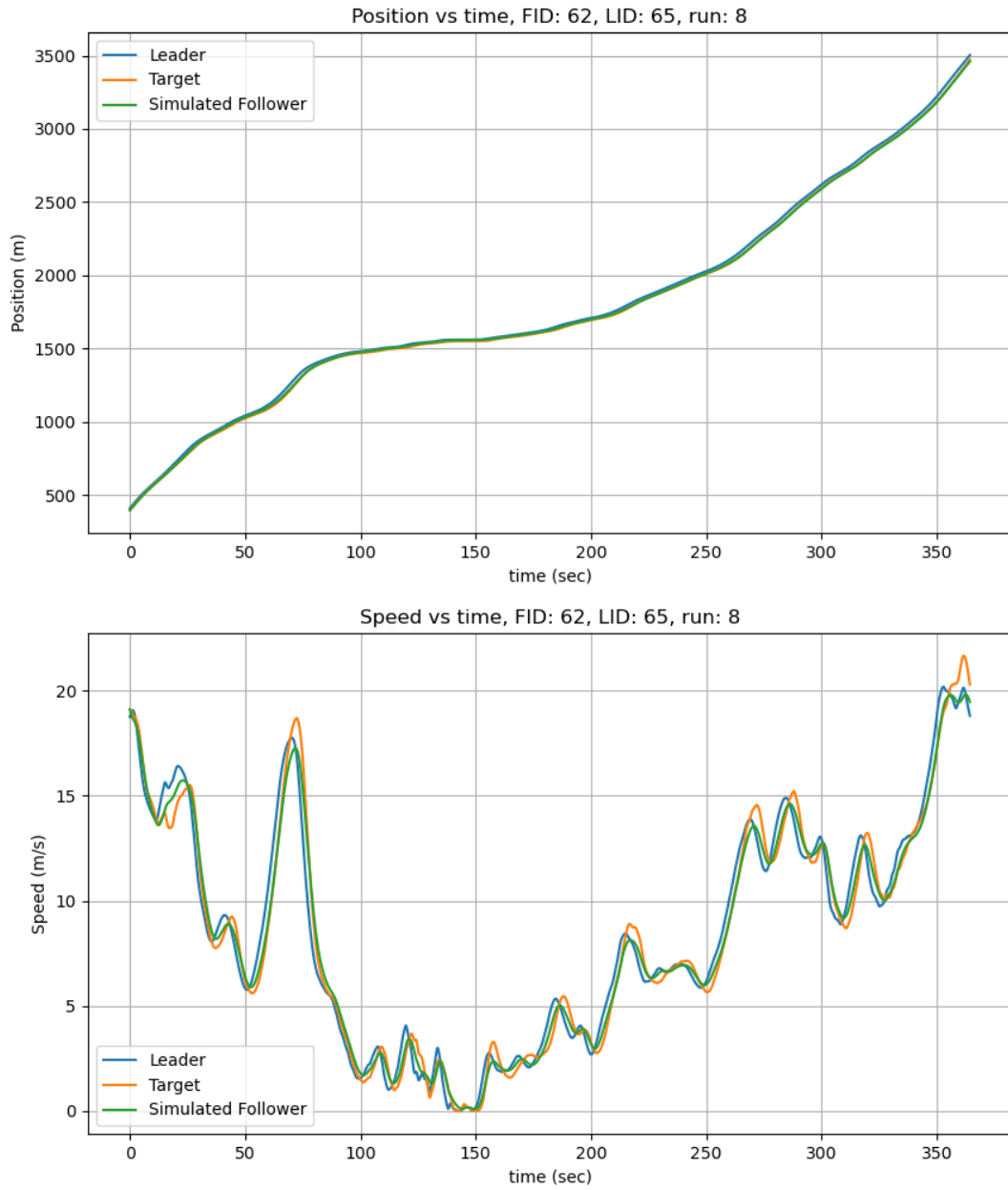


Figure 6.61: Position and speed for CTH for vehicle 62 in run 8 I294L1 dataset.

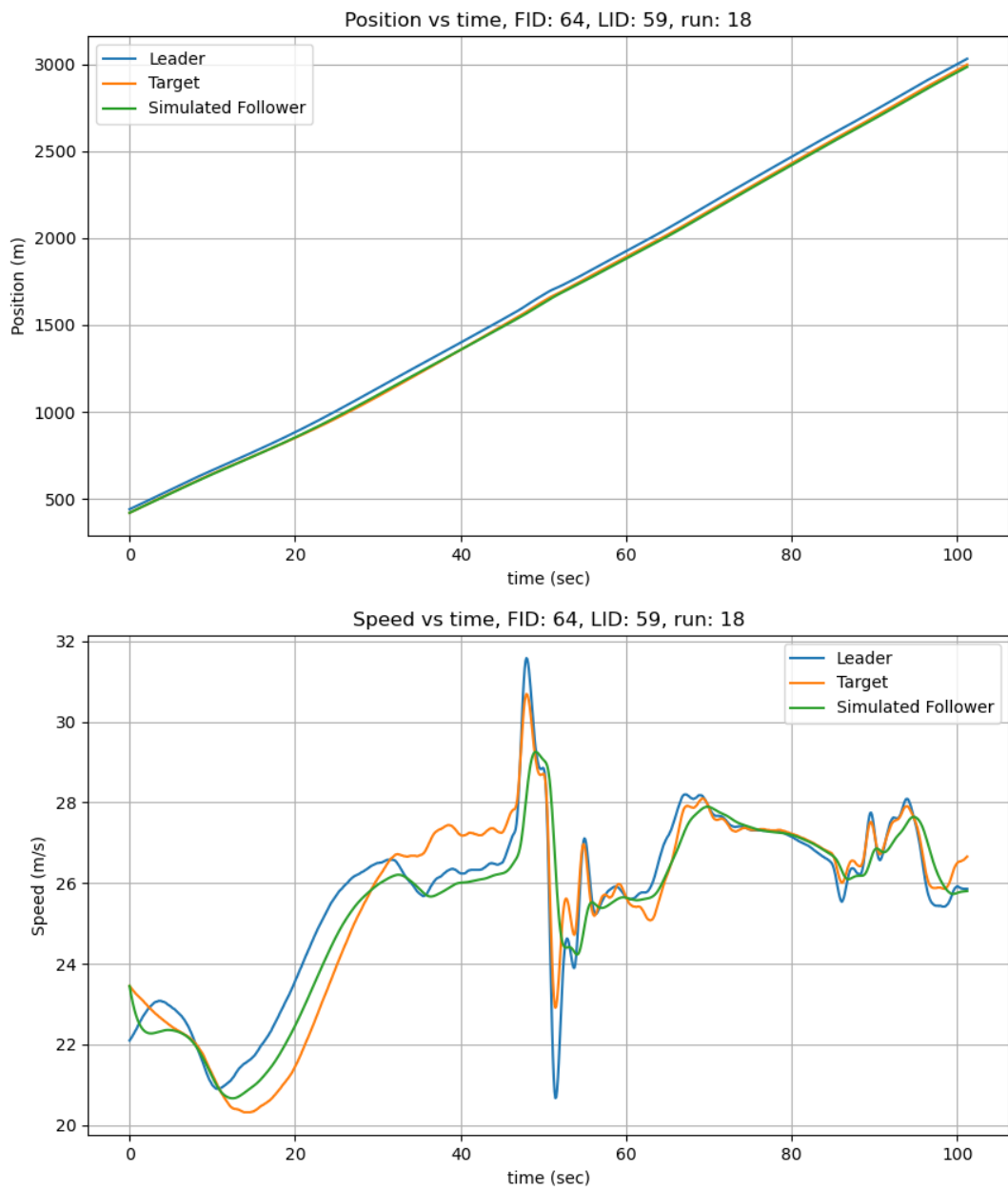


Figure 6.62: Position and speed for CTH for vehicle 64 in run 18 I294L1 dataset.

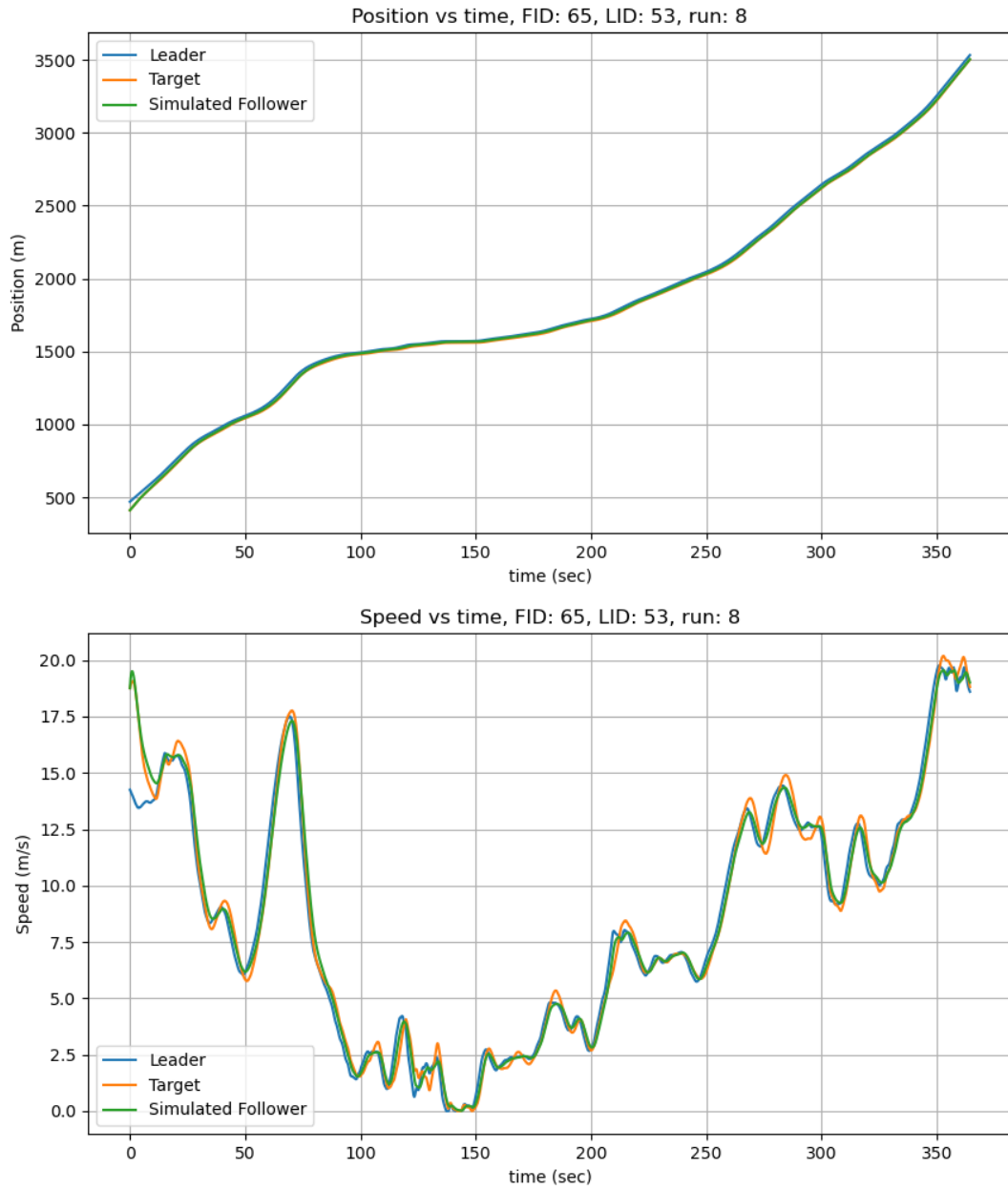


Figure 6.63: Position and speed for CTH for vehicle 65 in run 8 I294L1 dataset.

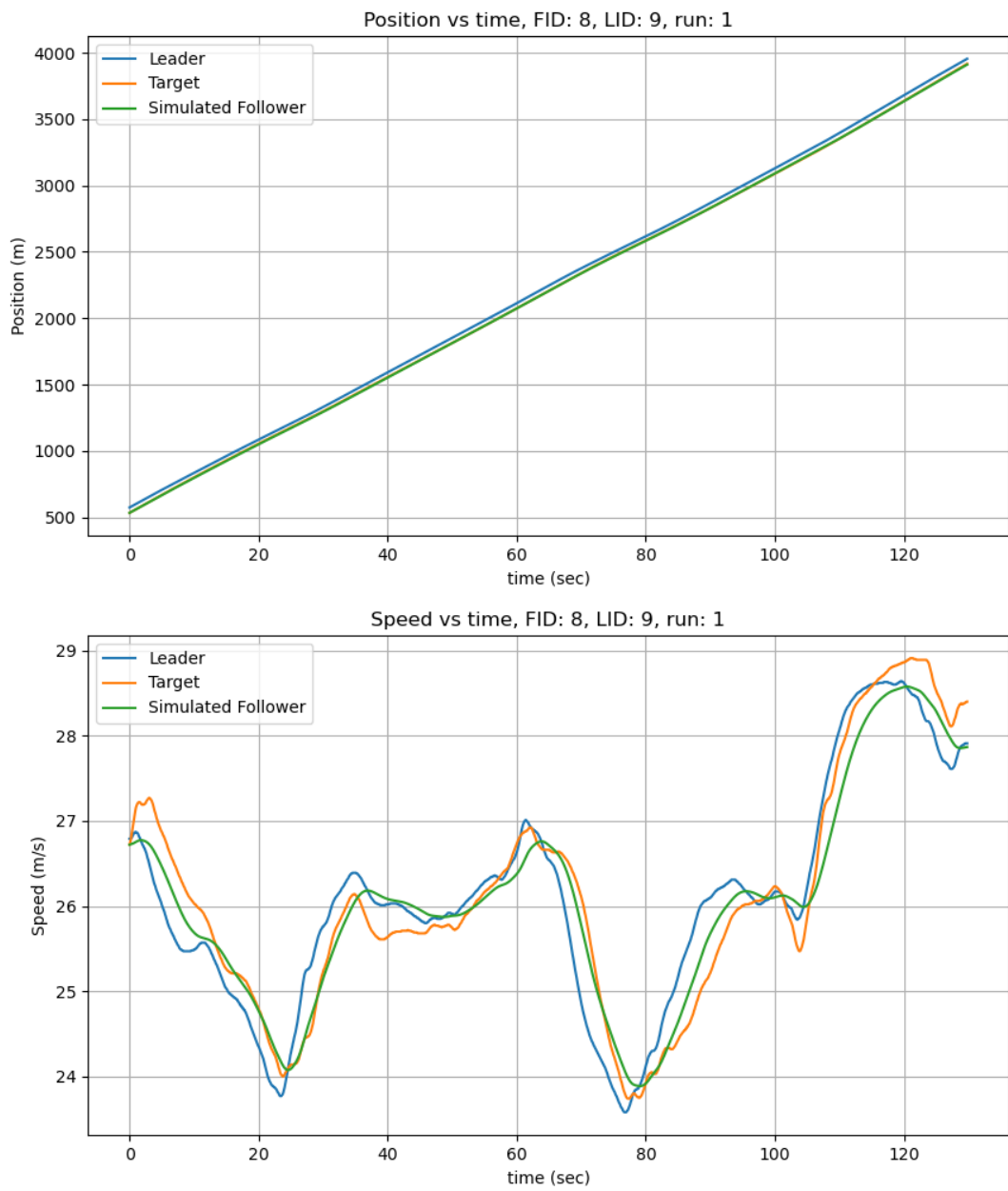


Figure 6.64: Position and speed for CTH for vehicle 8 in run 1 I294L1 dataset.

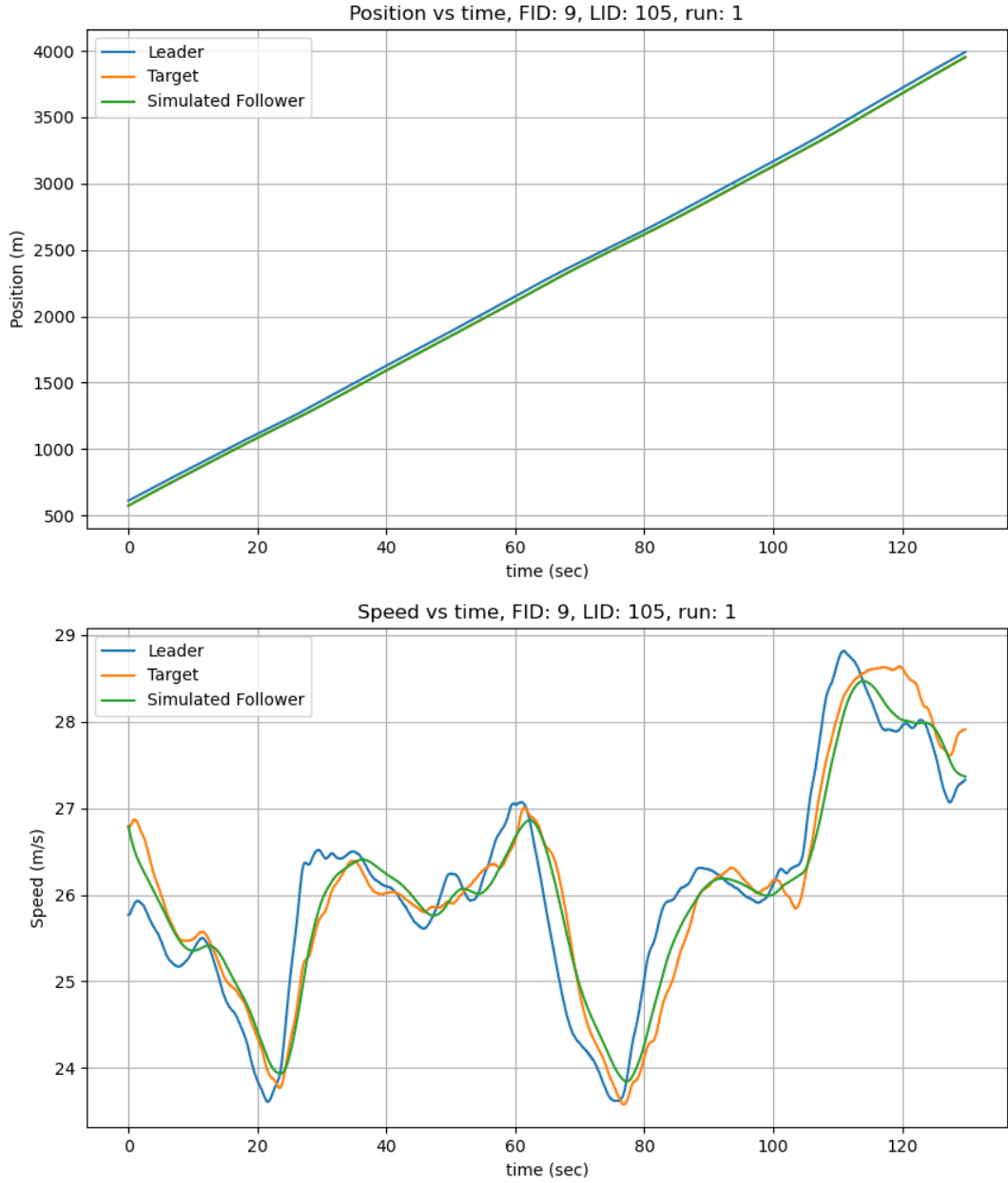


Figure 6.65: Position and speed for CTH for vehicle 9 in run 1 I294L1 dataset.

The optimized parameter ranges for the CTH model in the I294 dataset, as shown in Figure 6.66, strongly indicate variation among key parameters used for optimization. The parameters

(t_h) and d_{min} exhibit broad ranges, suggesting significant tuning variability in time headway and minimum distance settings. In contrast, (λ) is tightly clustered around low values, indicating a high degree of stability and minimal fluctuation during optimization.

Figure 6.67 illustrates the skewed distributions of (t_h) and (d_{min}) , where certain values appear more frequently than others, implying potential biases toward specific parameter configurations. The distribution of (λ) is notably sparse. This suggests that while (t_h) and d_{min} require more flexible adjustments to accommodate diverse traffic conditions, (λ) remains relatively fixed to ensure consistency in the CTH model's control strategy, indicating that the CTH model effectively adapts to different traffic dynamics.

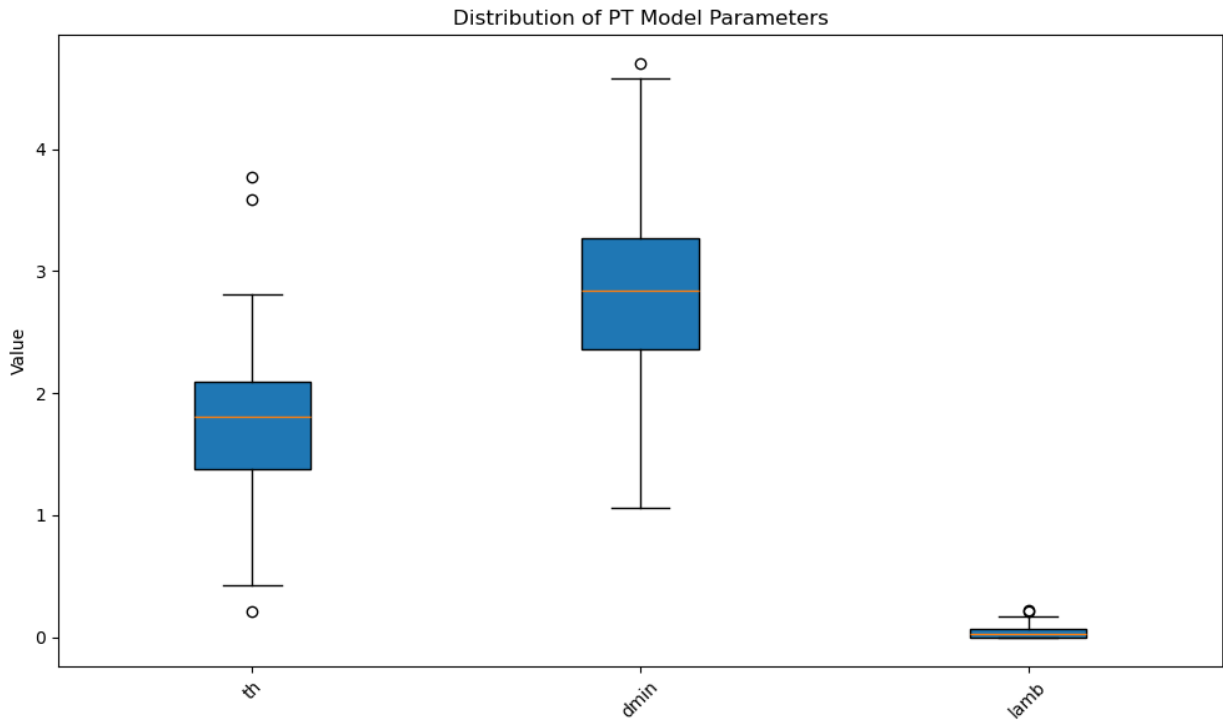


Figure 6.66: Parameter ranges for CTH in I294L1 dataset.

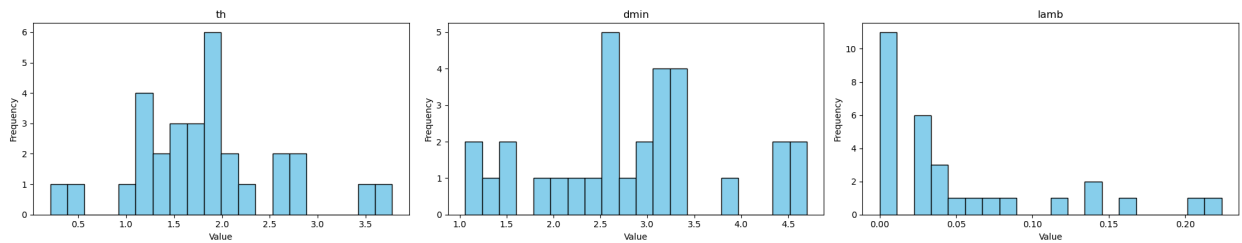


Figure 6.67: Parameter histogram for CTH in I294L1 dataset.

6.2.5 CTH I90/94 Simulated Results

The simulated results for I90/94 are presented in Figures 6.68 6.69, and 6.70 using the CTH policy. For vehicle 5366 and 195, it can be determined that the controller can track the position with minimum speed pattern deviations shown in Figures 6.68 and 6.69. There is a deviation with speed patterns for vehicle 286 shown in Figure 6.70 although the simulated position closely aligns with the target position.

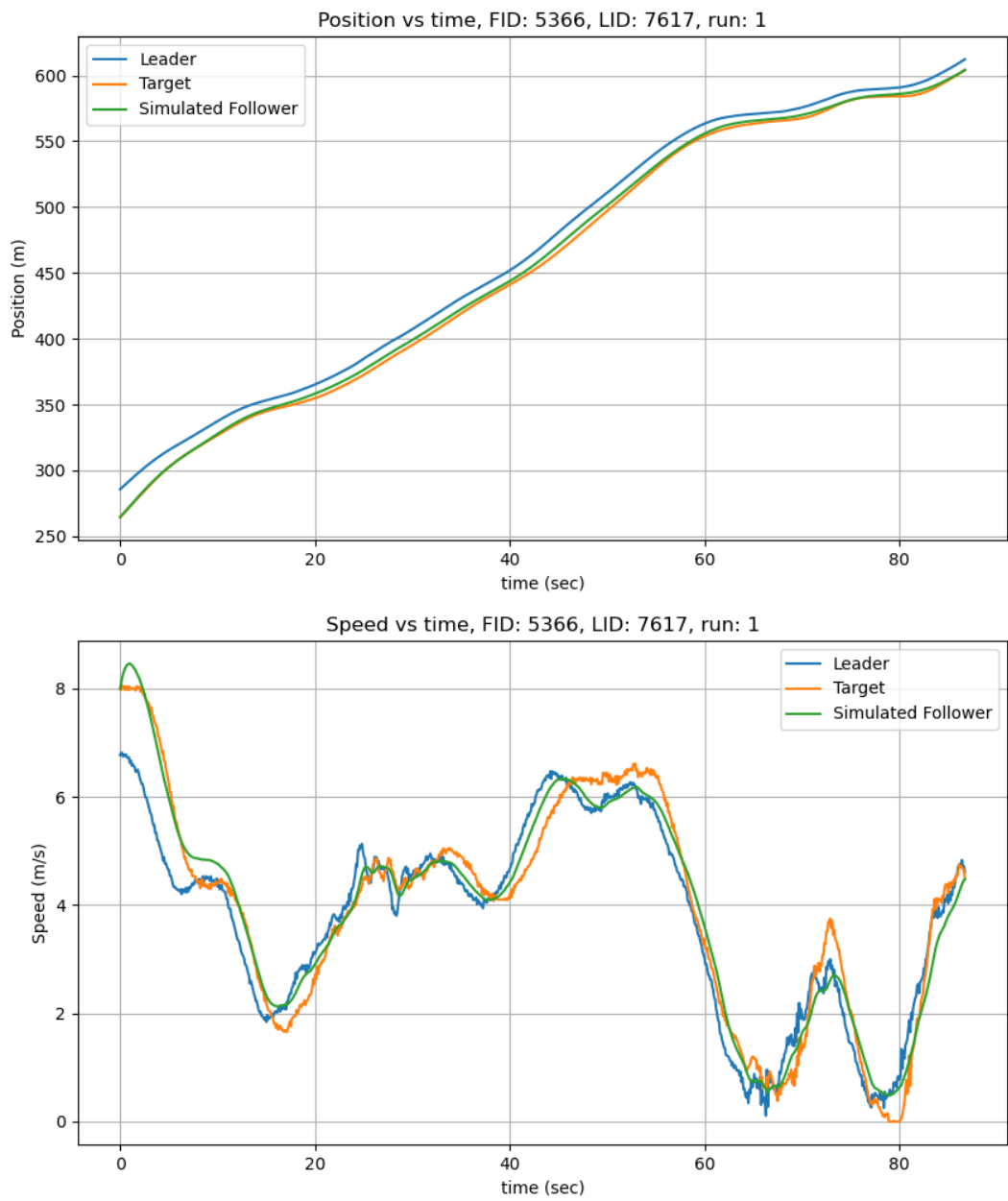


Figure 6.68: Position and speed for CTH for vehicle 5366 in I90/94 dataset.

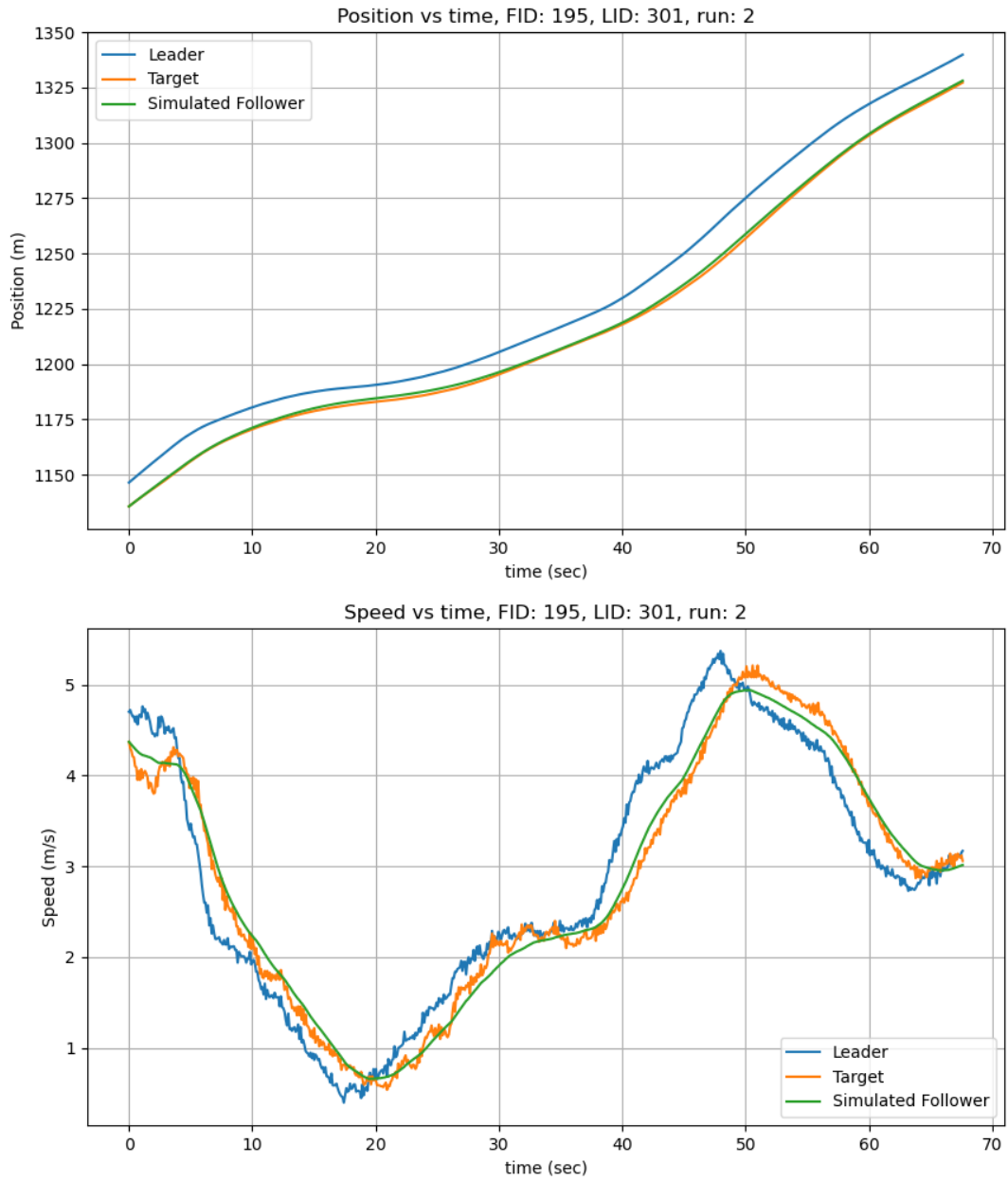


Figure 6.69: Position and speed for CTH for vehicle 195 in I90/94 dataset.

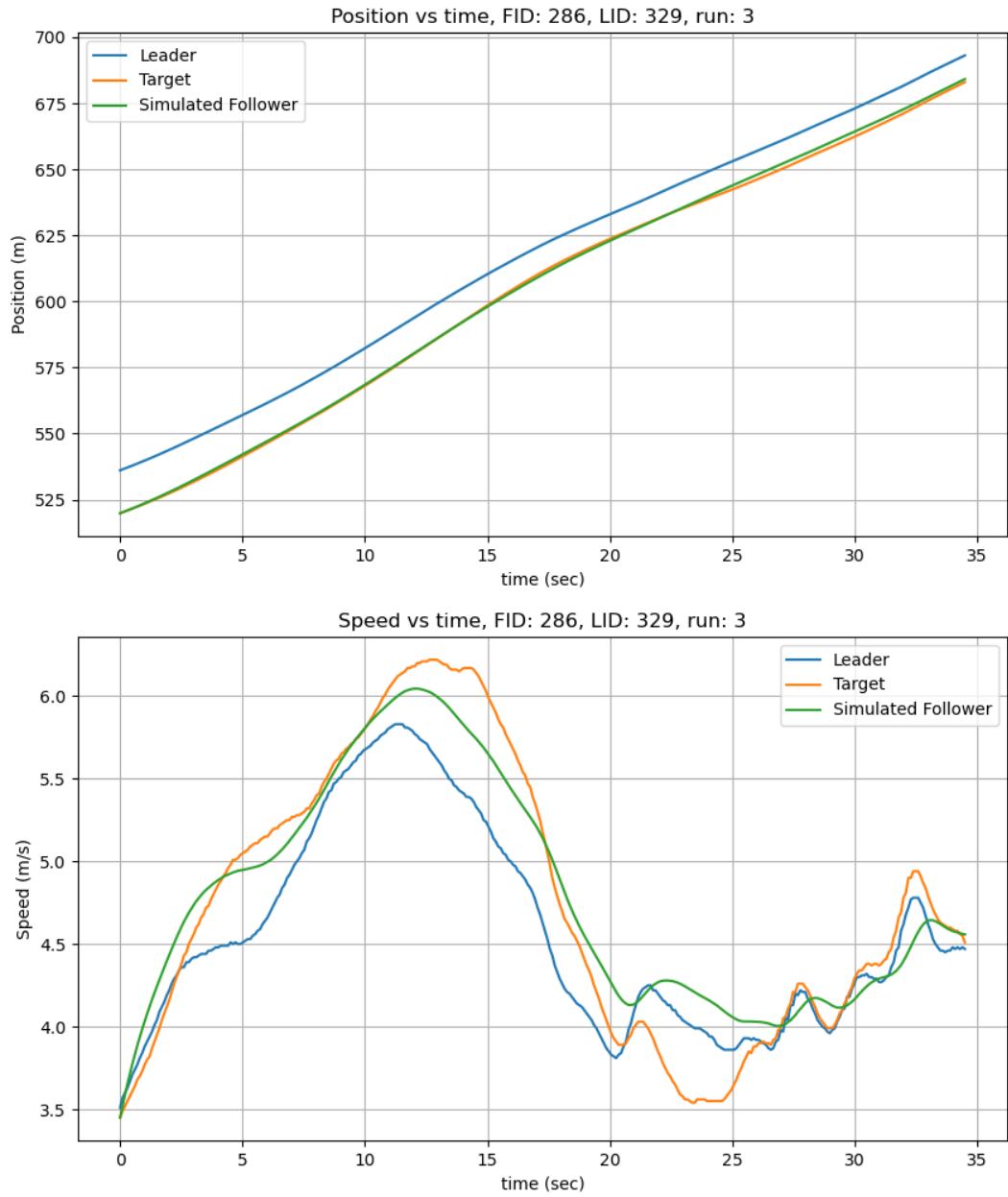


Figure 6.70: Position and speed for CTH for vehicle 286 in I90/94 dataset.

The optimized parameter ranges for the CTH model in the I90/94 dataset illustrates variations across different parameters. Figure 6.71 shows that (t_h) and (d_{min}) have relatively wider

ranges, indicating greater flexibility in their tuning to adapt to different traffic conditions. In contrast, (λ) remains tightly clustered around low values, suggesting that this parameter is more constrained to ensure stability in the model's response.

Furthermore, Figure 6.72 shows that all optimized parameters follow discrete distributions, implying that the parameter tuning converges to specific values rather than a continuous range. This suggests that certain parameter settings are more favorable for achieving stable and reliable control behavior under varying highway conditions. The narrow clustering of (λ) shows that consistent system dynamics were maintained, while the broader range of (t_h) and (d_{min}) indicates that time headway and minimum distance must be more adaptable to handling fluctuations in traffic flow.

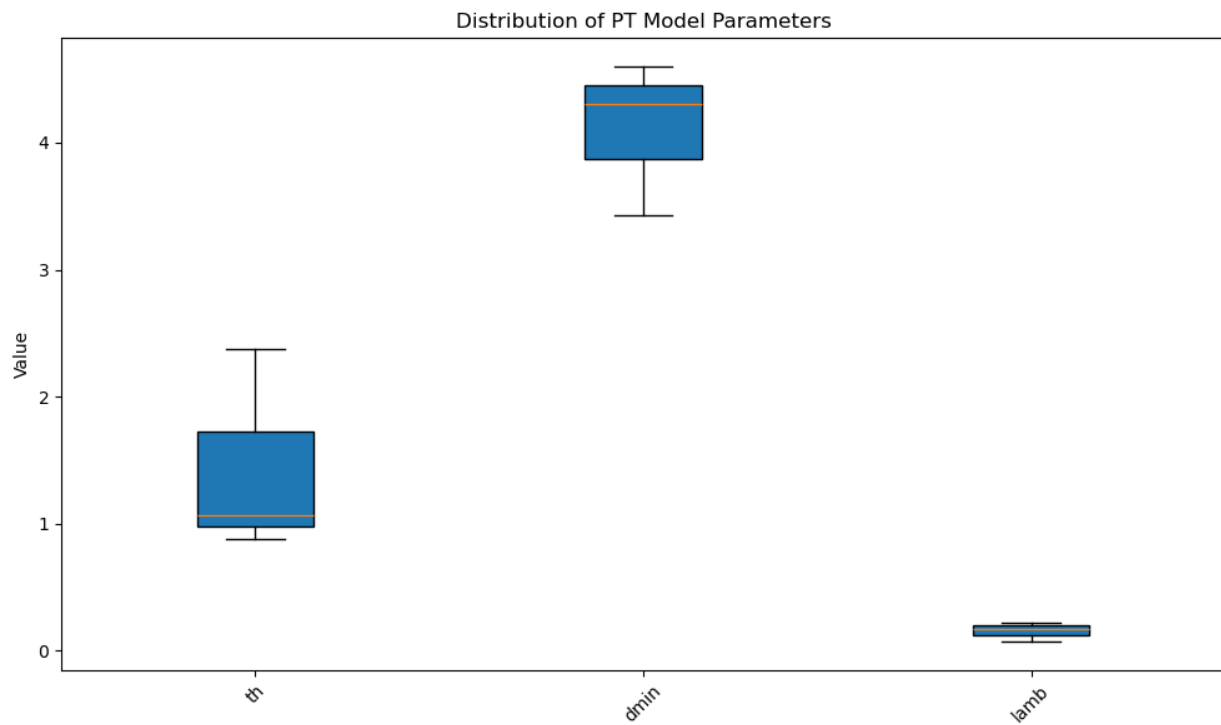


Figure 6.71: Parameter ranges for CTH in I90/94.

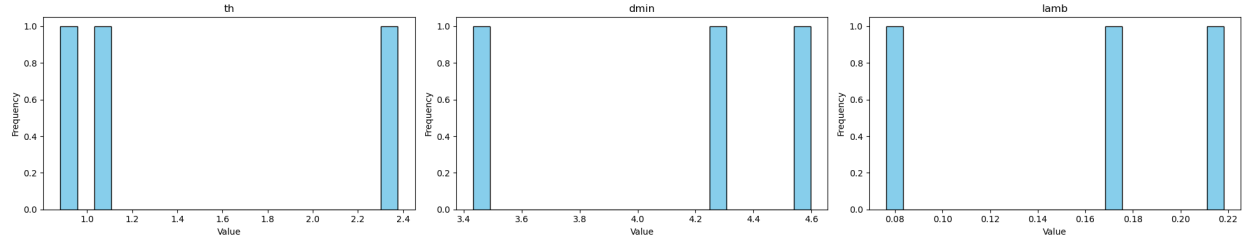


Figure 6.72: Parameter histogram for CTH in I90/94.

6.2.6 CTH Phoenix Simulated Results

The simulated results for the CTH model in the Phoenix dataset are presented in Figures 6.73, 6.74, 6.75, and 6.76. The simulated follower closely aligns with the calibrated position and speed of the target follower, as shown in Figures 6.73 and 6.76 for vehicles 13 and 2 in run 9NS. However, noticeable speed deviations are observed for vehicles 31 and 2 in run 9ES, as illustrated in Figures 6.74 and 6.75. These deviations suggest that certain factors, such as acceleration responsiveness or varying traffic conditions, may have influenced the model's performance in maintaining a consistent speed.

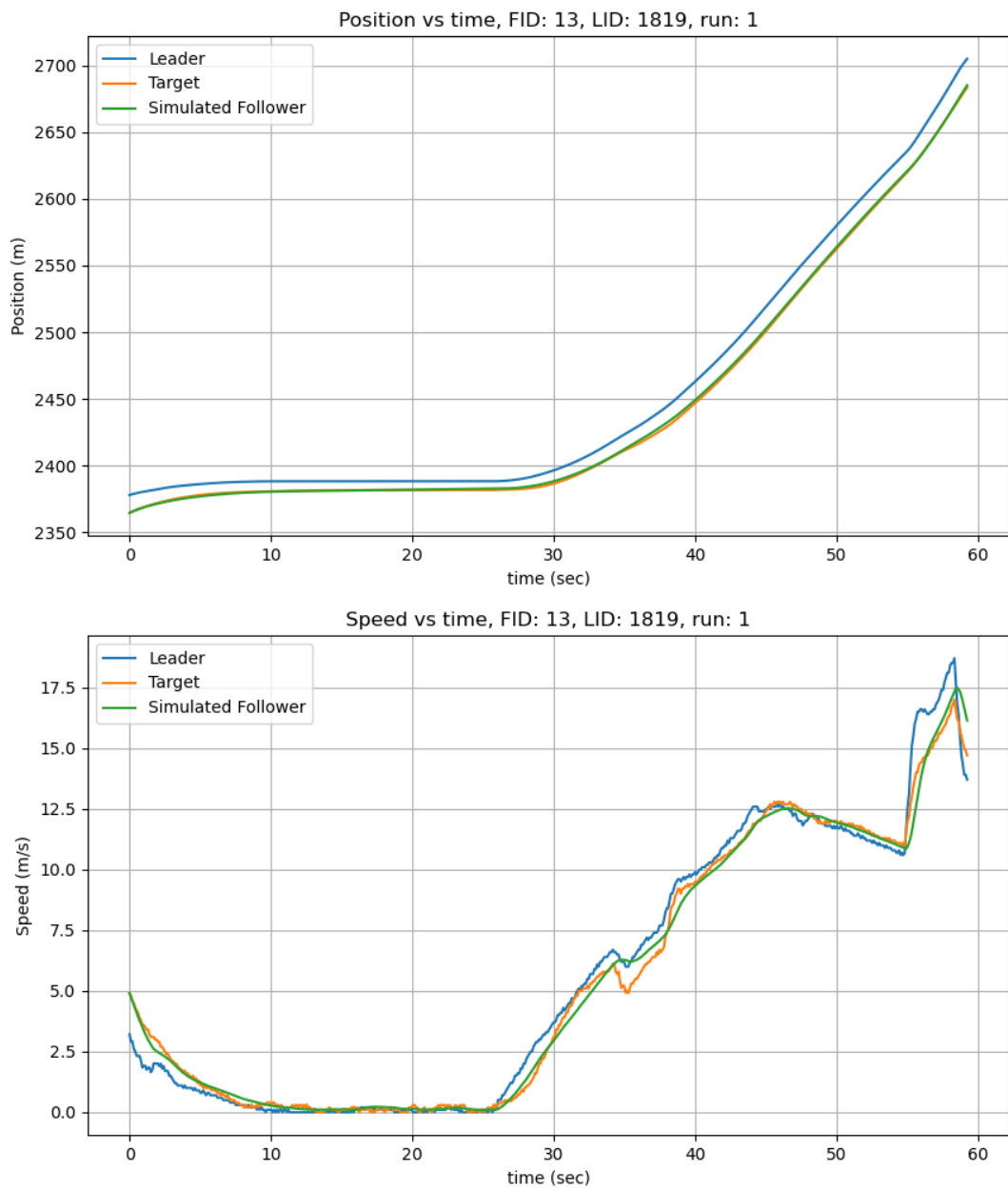


Figure 6.73: Position and speed for CTH for vehicle 13 in Phoenix data H1A3 run 6.

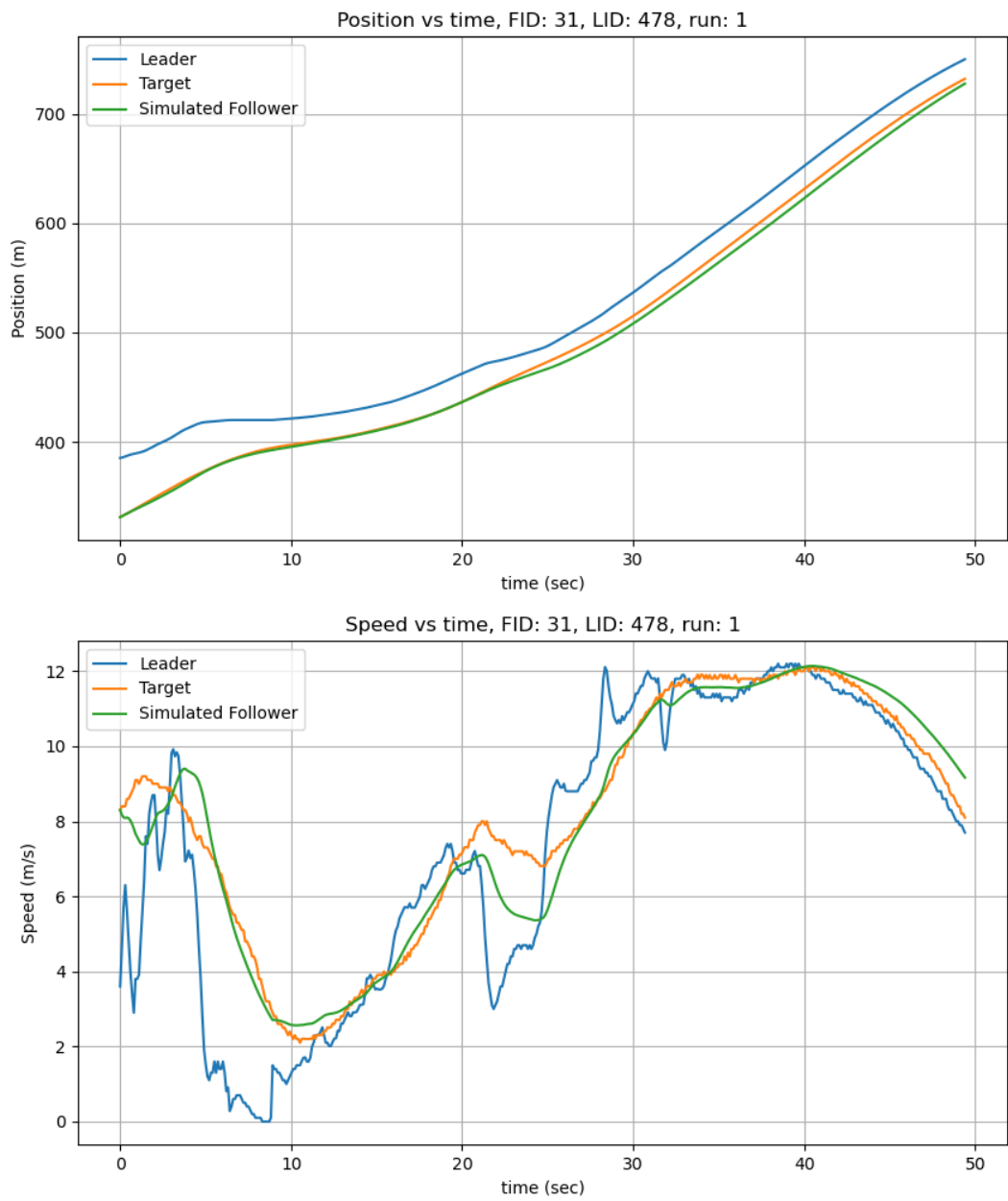


Figure 6.74: Position and speed for CTH for vehicle 31 in Phoenix data H1A3 run 1.

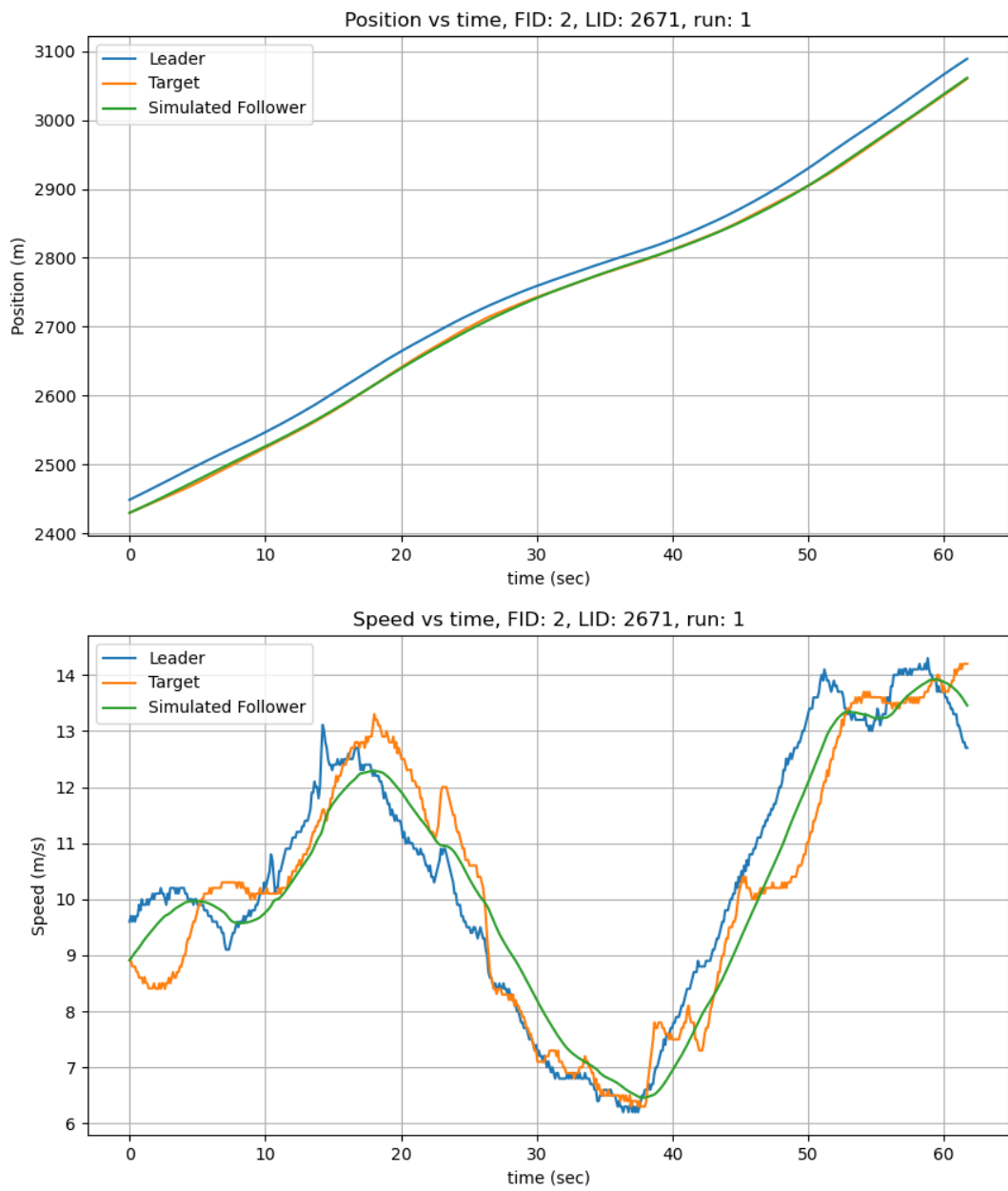


Figure 6.75: Position and speed for CTH for vehicle 2 in Phoenix data H1A3 run 9 ES.

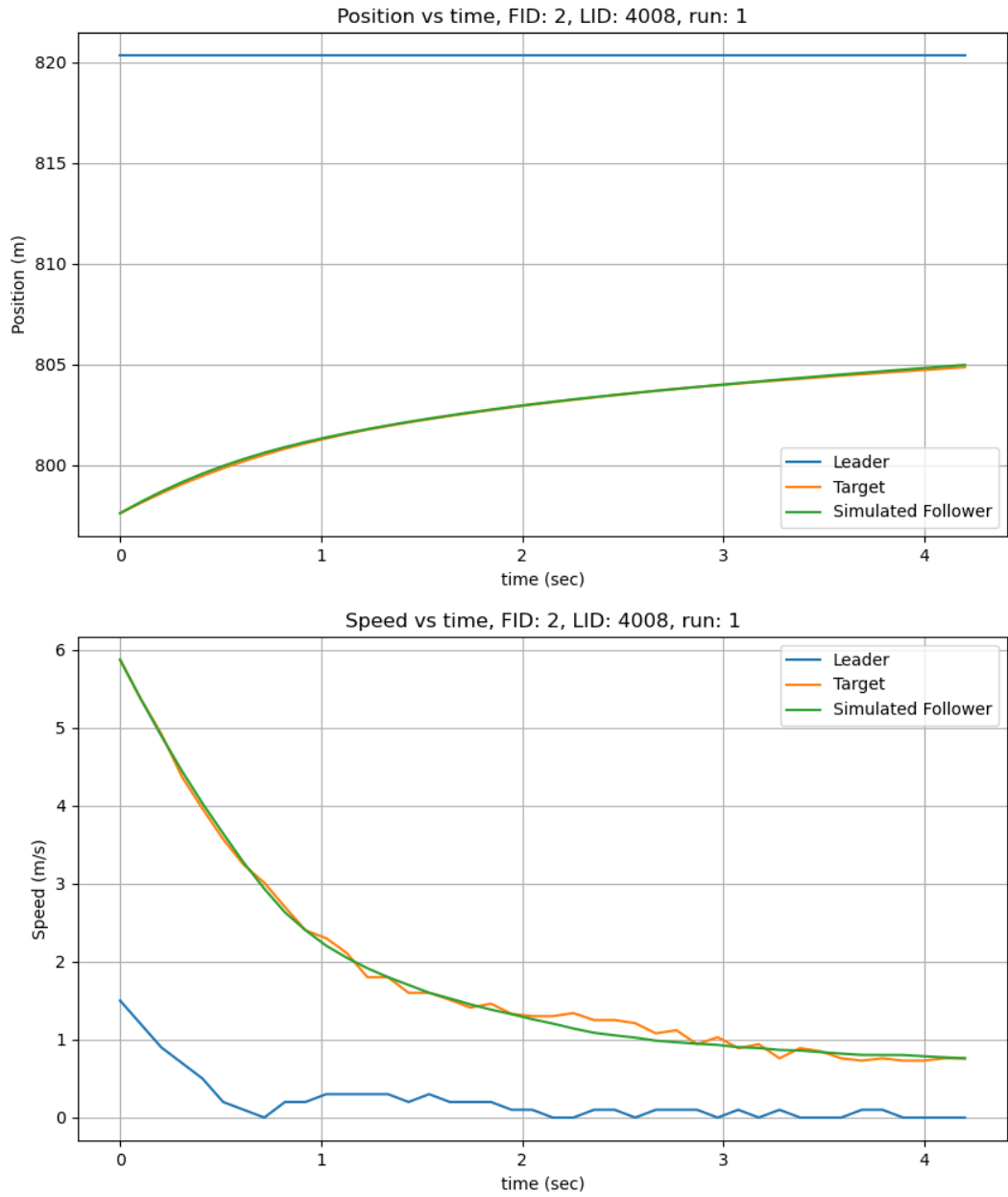


Figure 6.76: Position and speed for CTH for vehicle 2 in Phoenix data H1A3 run 9 NS.

The optimized parameter ranges for the CTH model in the Phoenix dataset illustrate variations across parameters. As shown in Figure 6.77, (d_{min}) shows a relatively wider range compared to

(t_h) , indicating flexible tuning parameters. In contrast, the (λ) values remain tightly clustered, suggesting minimal variations in controlling fluctuating behavior and ensuring system stability.

Figure 6.78 clearly shows a bimodal distribution for both (t_h) and (d_{min}) , implying that certain values are consistently favored during calibration. This strongly indicates the presence of distinct driving conditions or vehicle behaviors leading to the model selecting preferred parameter values over others. The narrow spread of (λ) maintains smooth acceleration adjustments and prevents excessive fluctuations in speed. These findings highlight the importance of adaptive tuning for (t_h) and (d_{min}) , while (λ) remains a relatively stable control parameter across different scenarios.

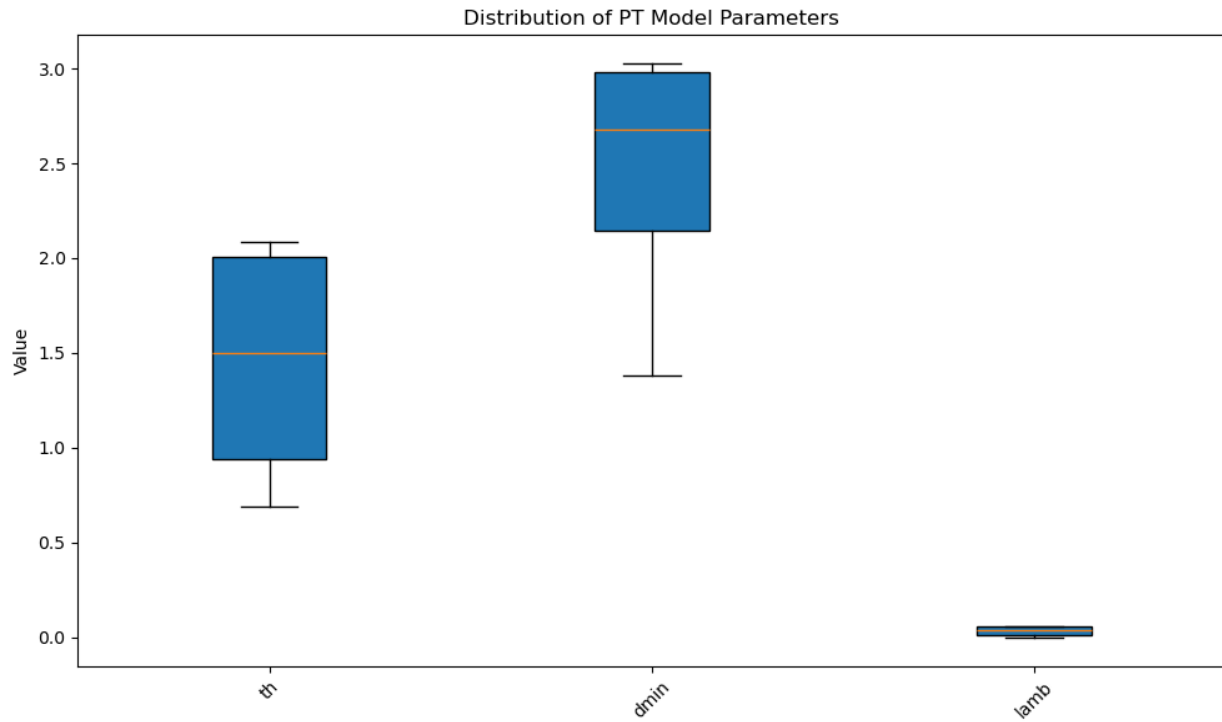


Figure 6.77: Parameter ranges for CTH in Phoenix.

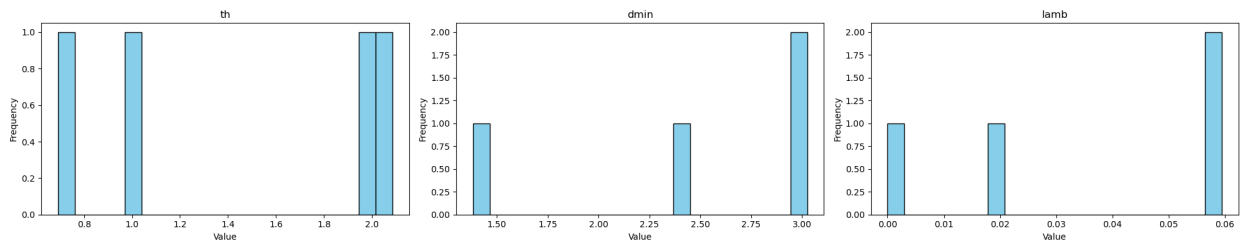


Figure 6.78: Parameter histogram for CTH in Phoenix.

6.2.7 TFS I294 Simulated Results

For Traffic Flow Stability policy (TFS), the simulated results for I294 are presented in Figures [6.79](#), [6.80](#), [6.81](#), [6.82](#), [6.83](#), [6.84](#), [6.85](#), [6.86](#), [6.87](#), [6.88](#), [6.89](#), [6.90](#), [6.91](#), [6.92](#), [6.93](#), [6.94](#), [6.95](#), [6.96](#), [6.97](#), [6.98](#), [6.99](#), [6.100](#), [6.101](#), [6.102](#), [6.103](#) and [6.104](#). The TFS model emphasizes stabilizing the traffic flow of vehicles and the generated simulated follower has performed well aligning the simulated position and speed with the target follower with some deviations.

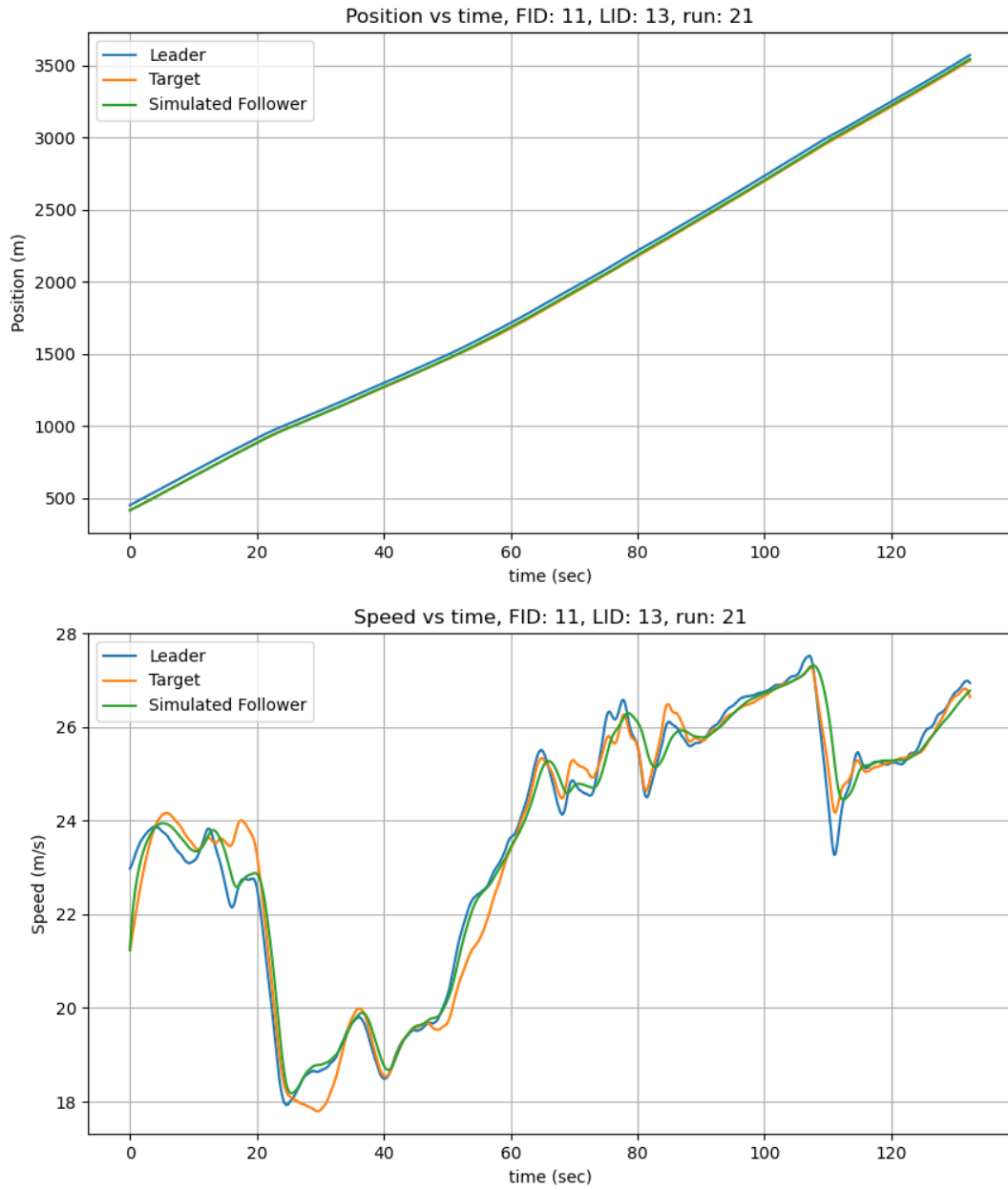


Figure 6.79: Position and speed for TFS for vehicle 11 in run 21 I294L1 dataset.

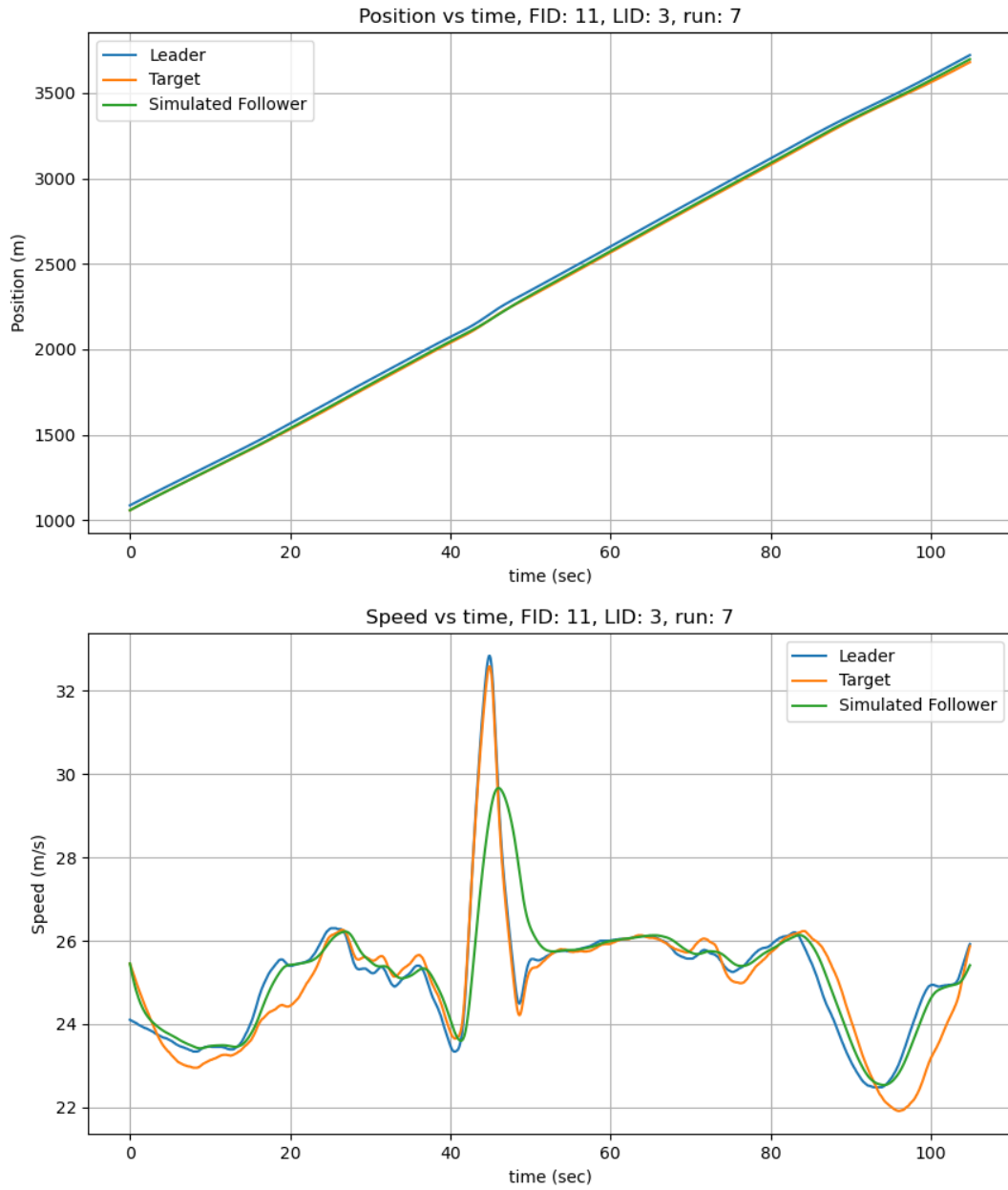


Figure 6.80: Position and speed for TFS for vehicle 11 in run 7 I294L1 dataset.

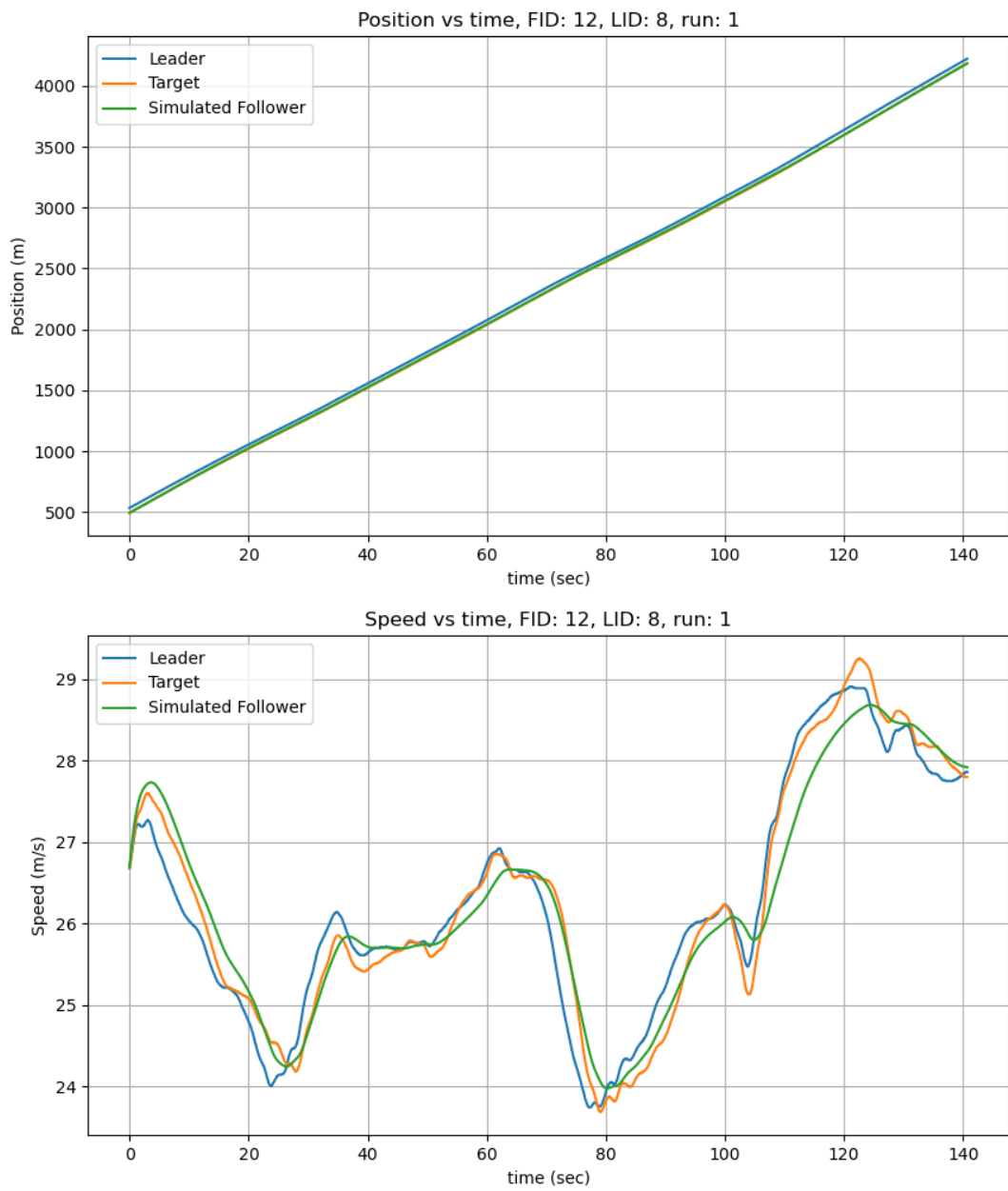


Figure 6.81: Position and speed for TFS for vehicle 12 in run 1 I294L1 dataset.

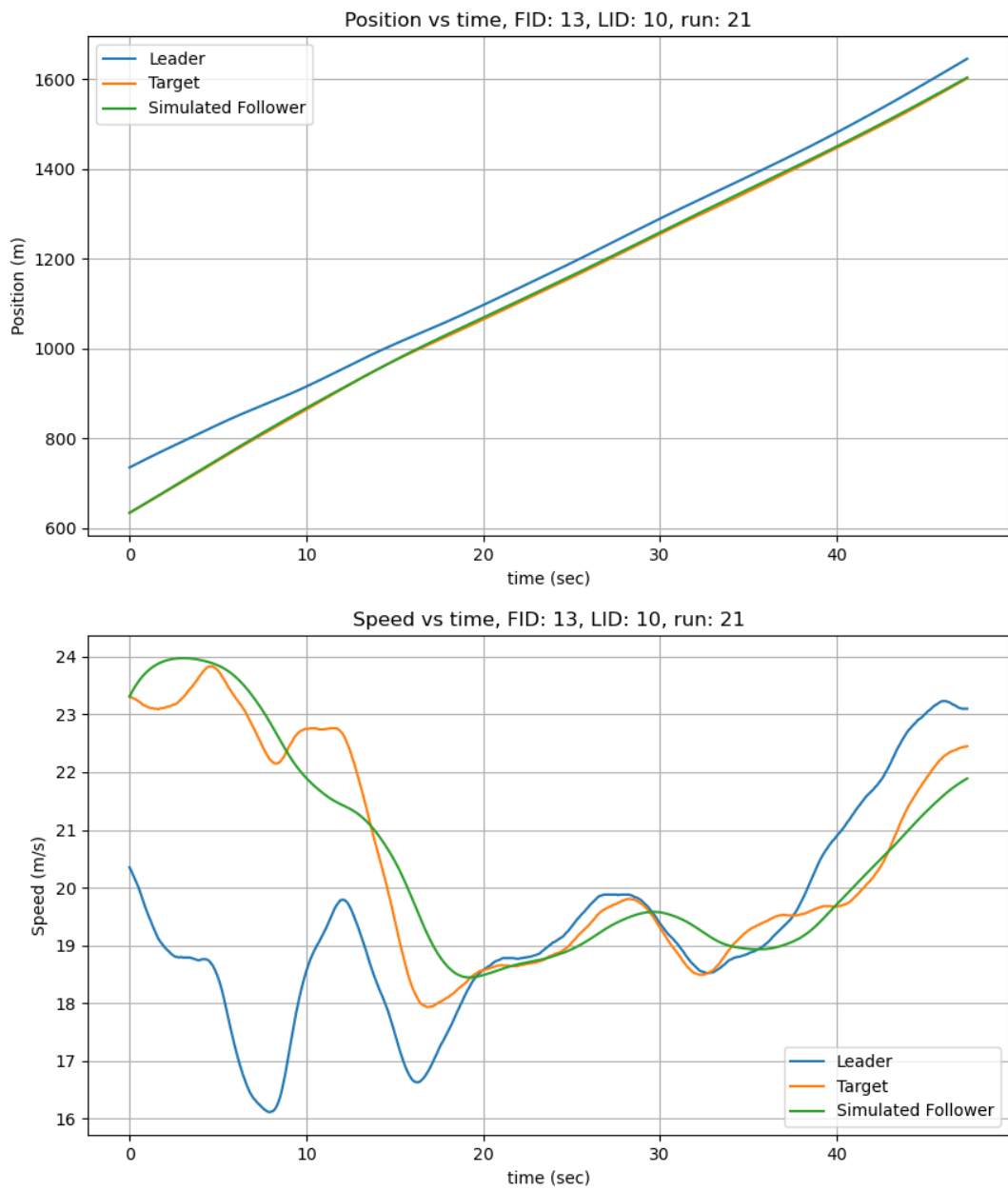


Figure 6.82: Position and speed for TFS for vehicle 13 in run 21 I294L1 dataset.

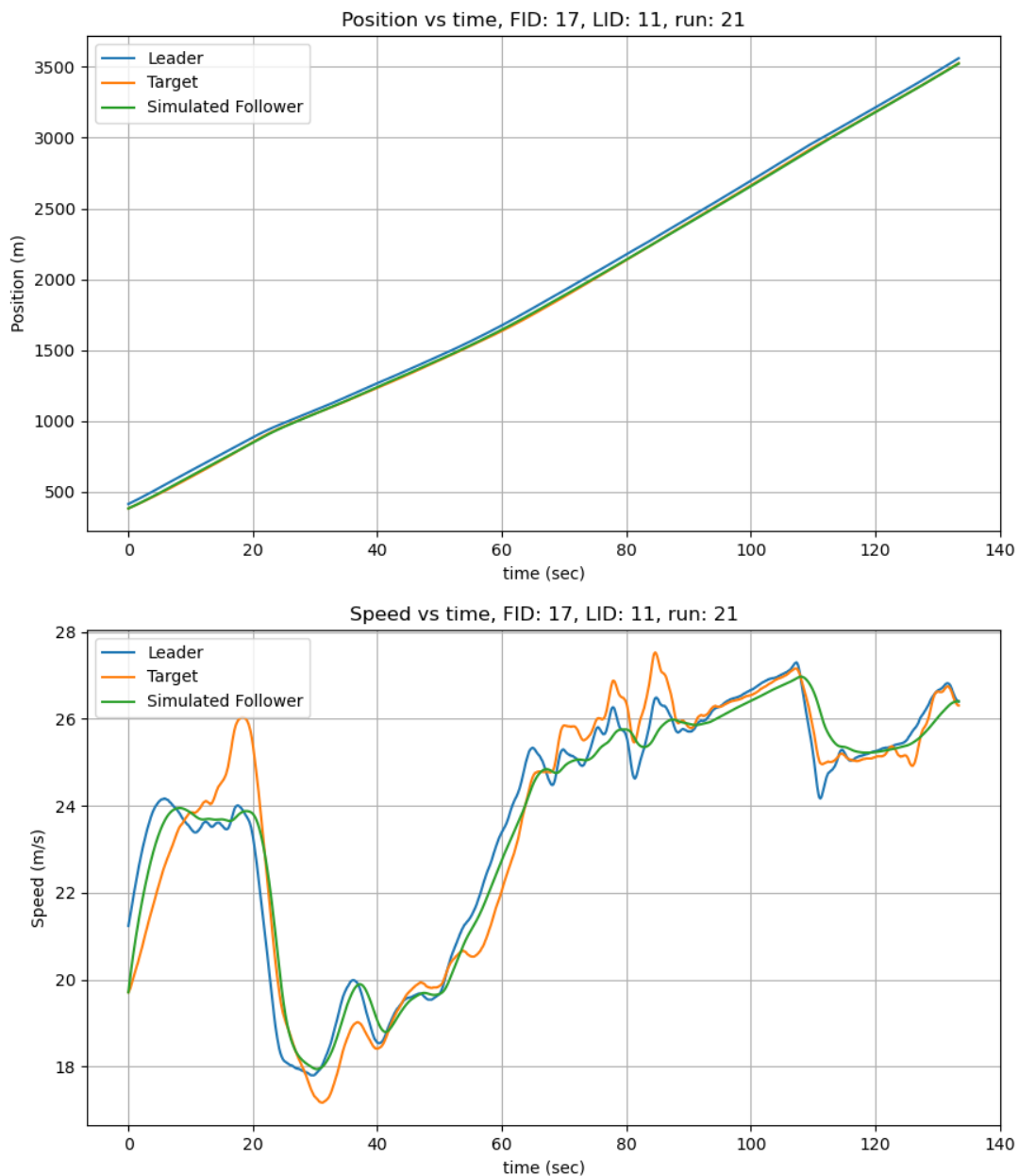


Figure 6.83: Position and speed for TFS for vehicle 17 in run 21 I294L1 dataset.

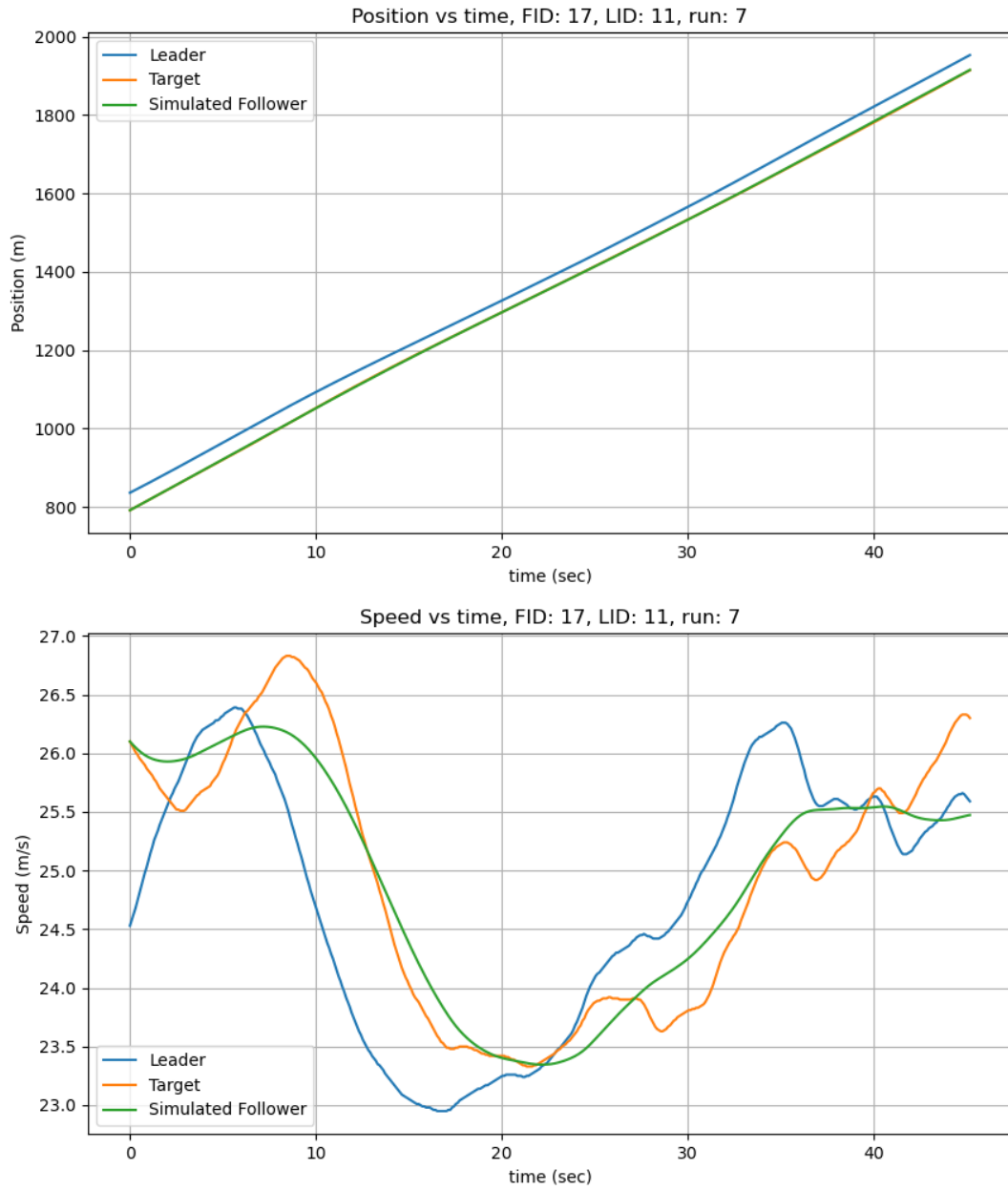


Figure 6.84: Position and speed for TFS for vehicle 17 in run 7 I294L1 dataset.

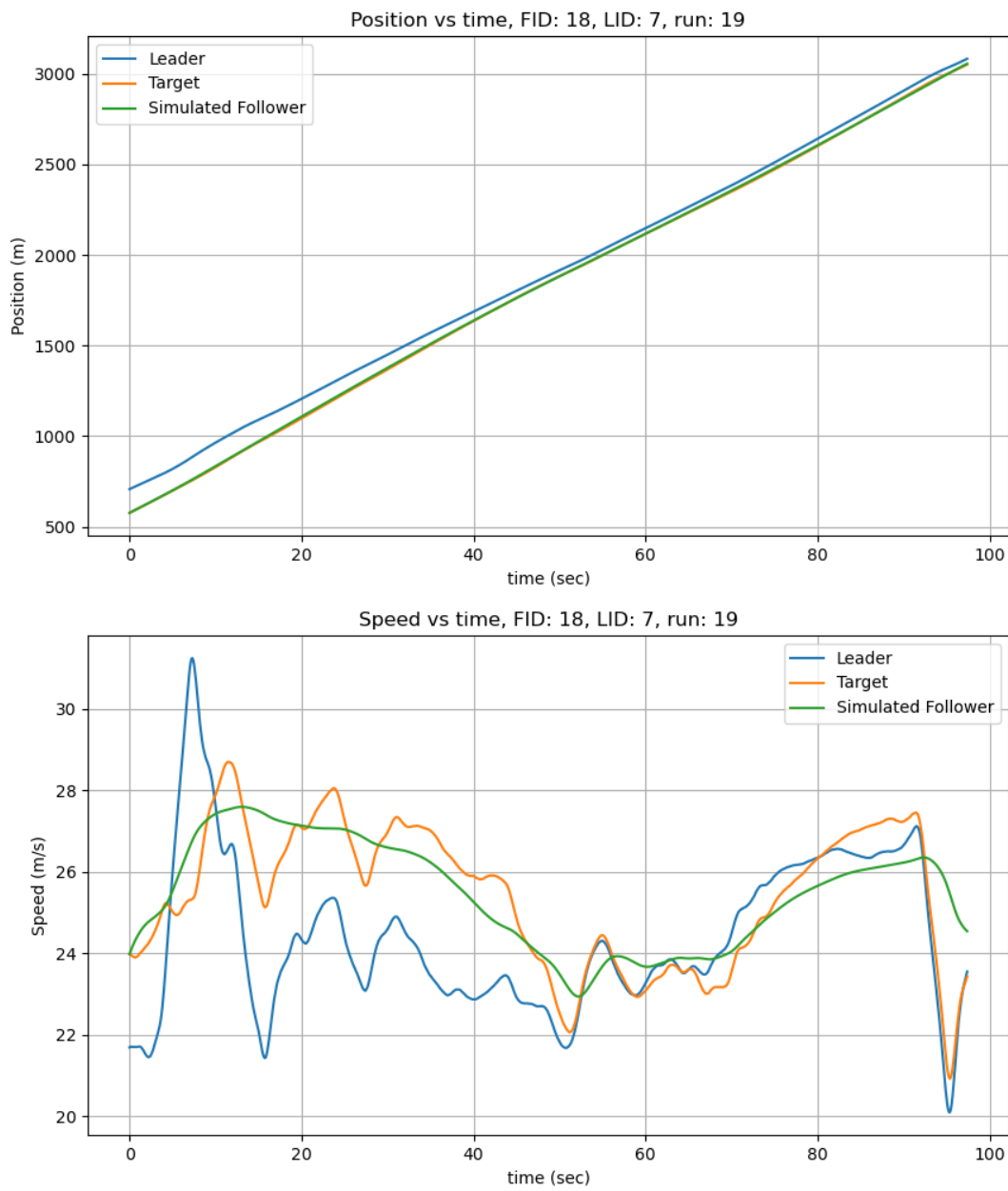


Figure 6.85: Position and speed for TFS for vehicle 18 in run 19 I294L1 dataset.

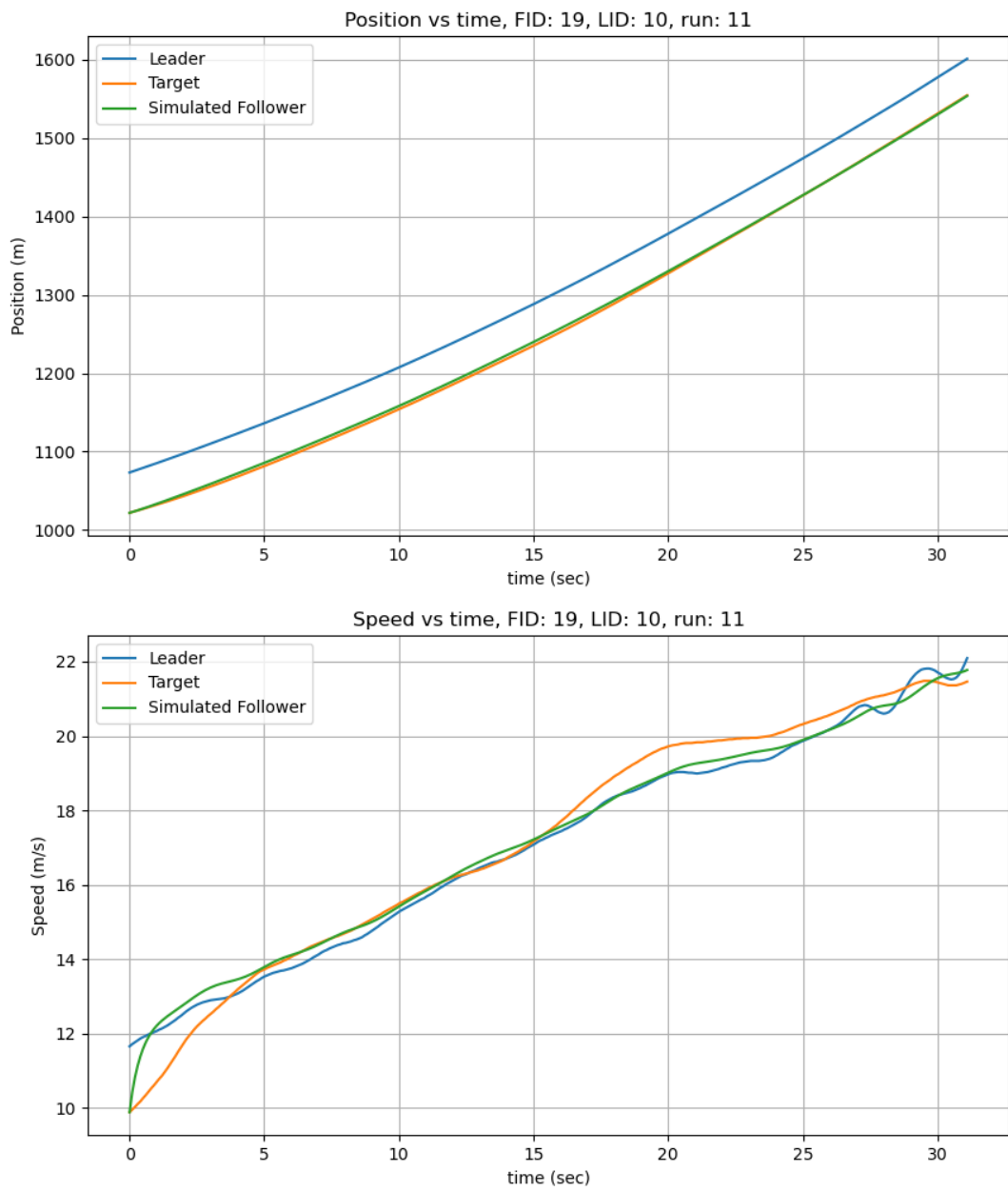


Figure 6.86: Position and speed for TFS for vehicle 19 in run 11 I294L1 dataset.

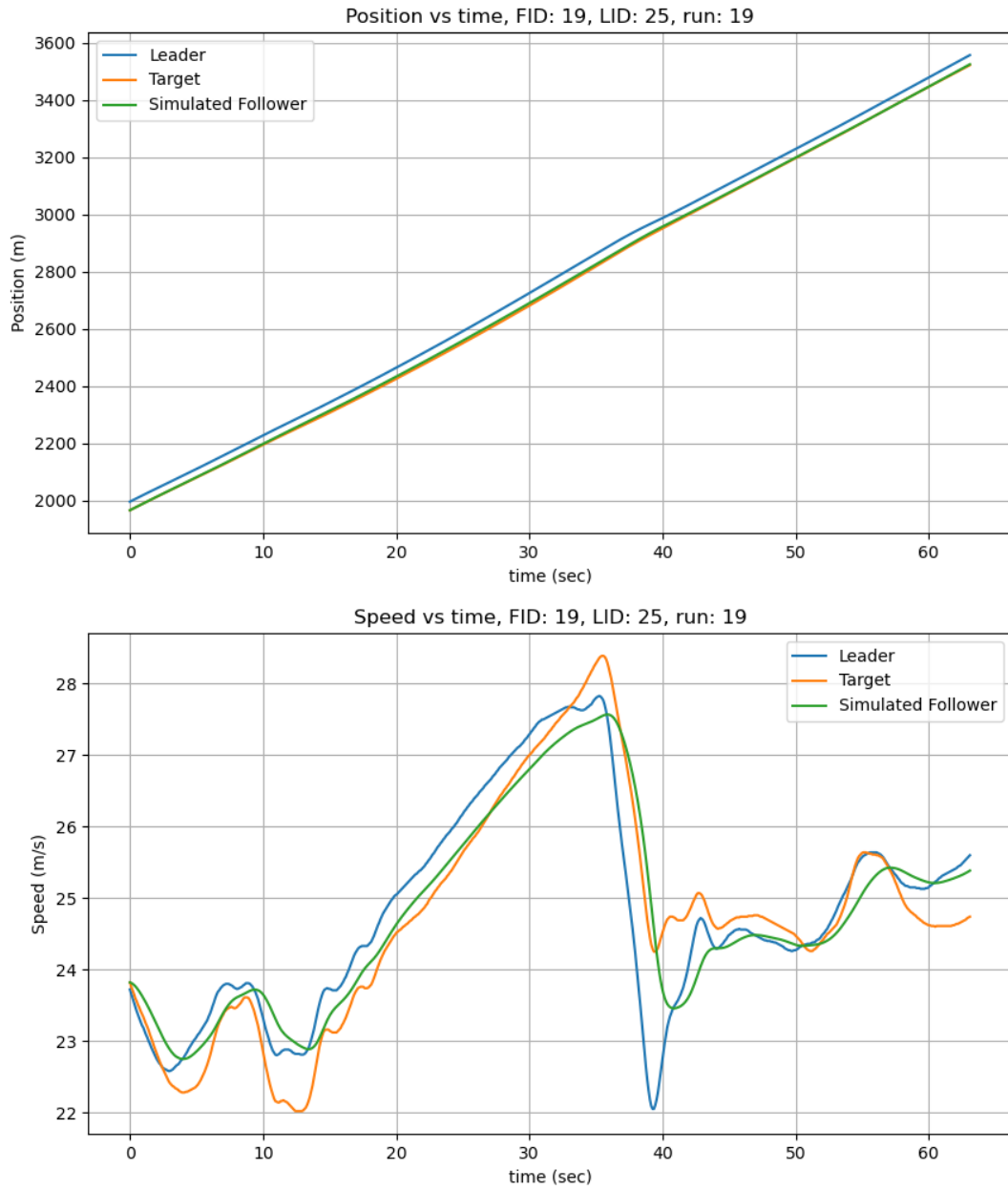


Figure 6.87: Position and speed for TFS for vehicle 19 in run 19 I294L1 dataset.

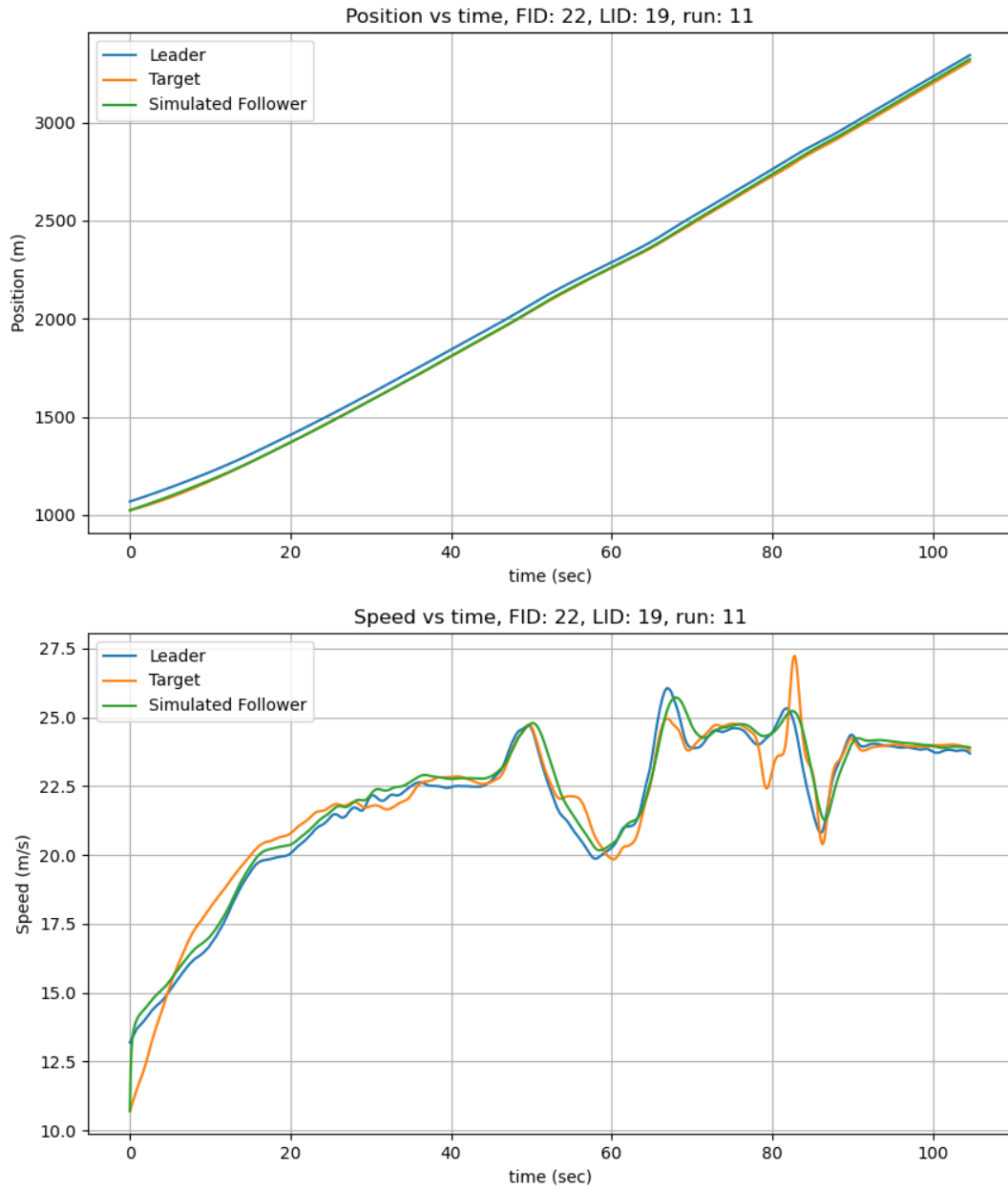


Figure 6.88: Position and speed for TFS for vehicle 22 in run 11 I294L1 dataset.

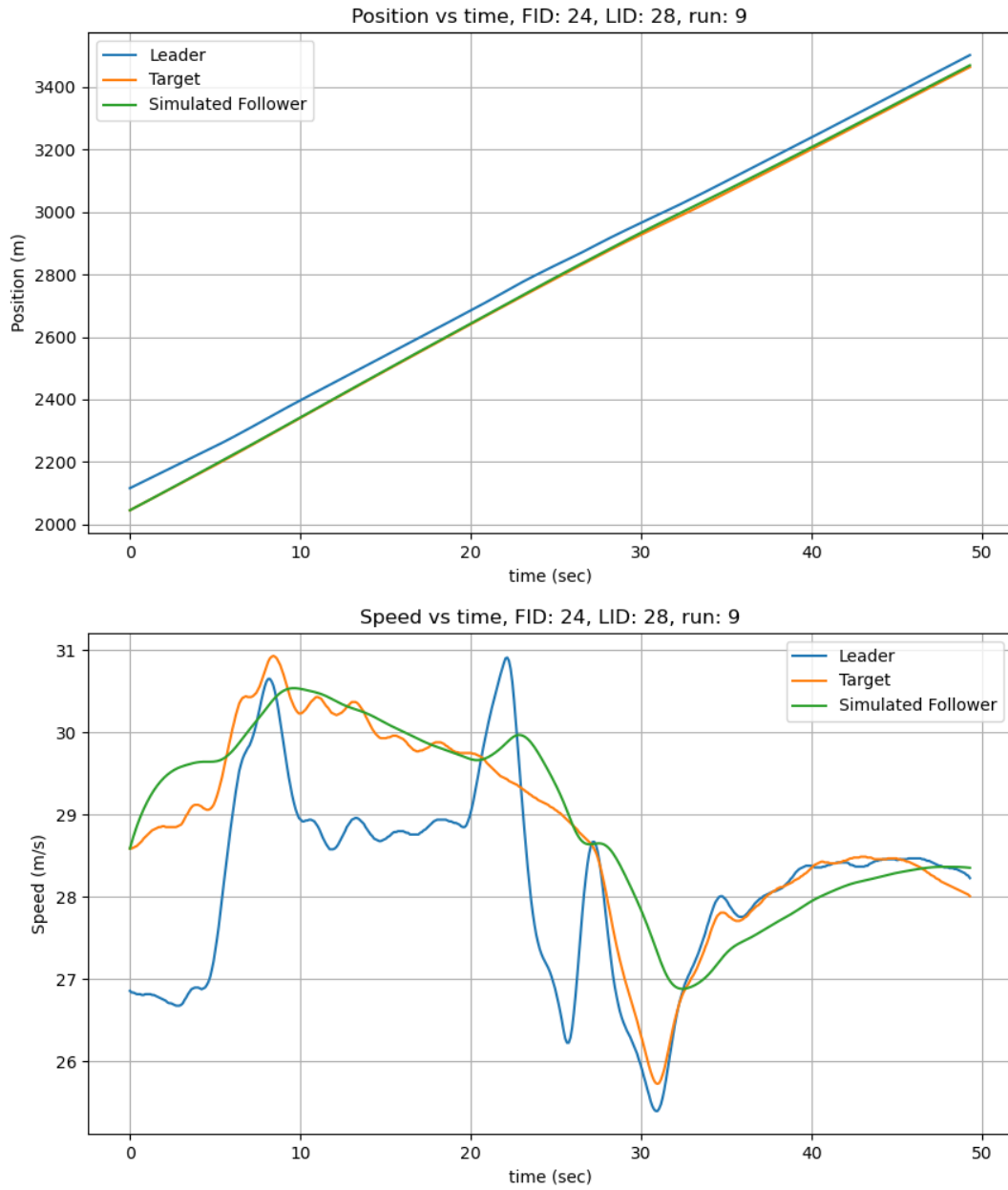


Figure 6.89: Position and speed for TFS for vehicle 24 in run 9 I294L1 dataset.

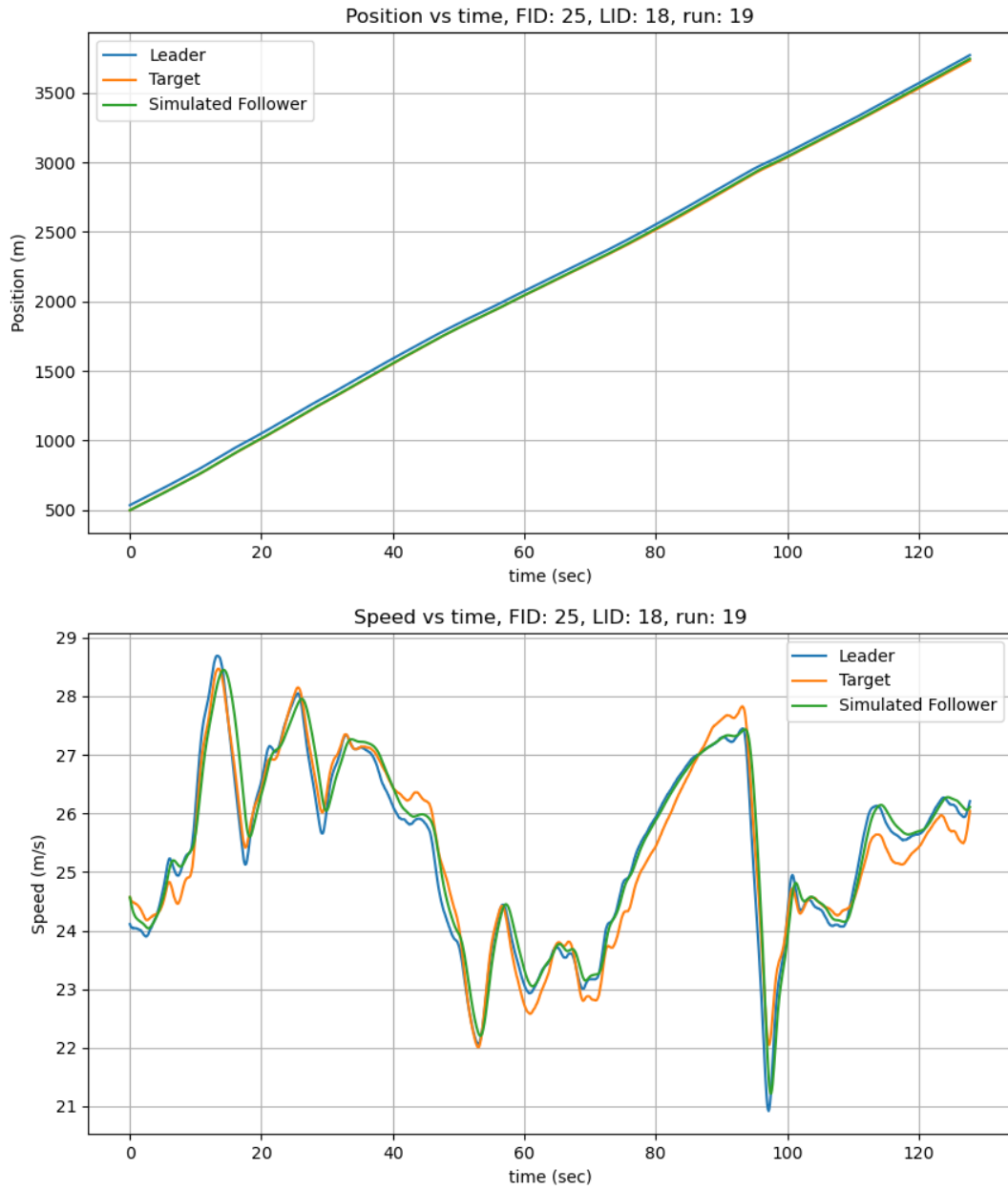


Figure 6.90: Position and speed for TFS for vehicle 25 in run 19 I294L1 dataset.

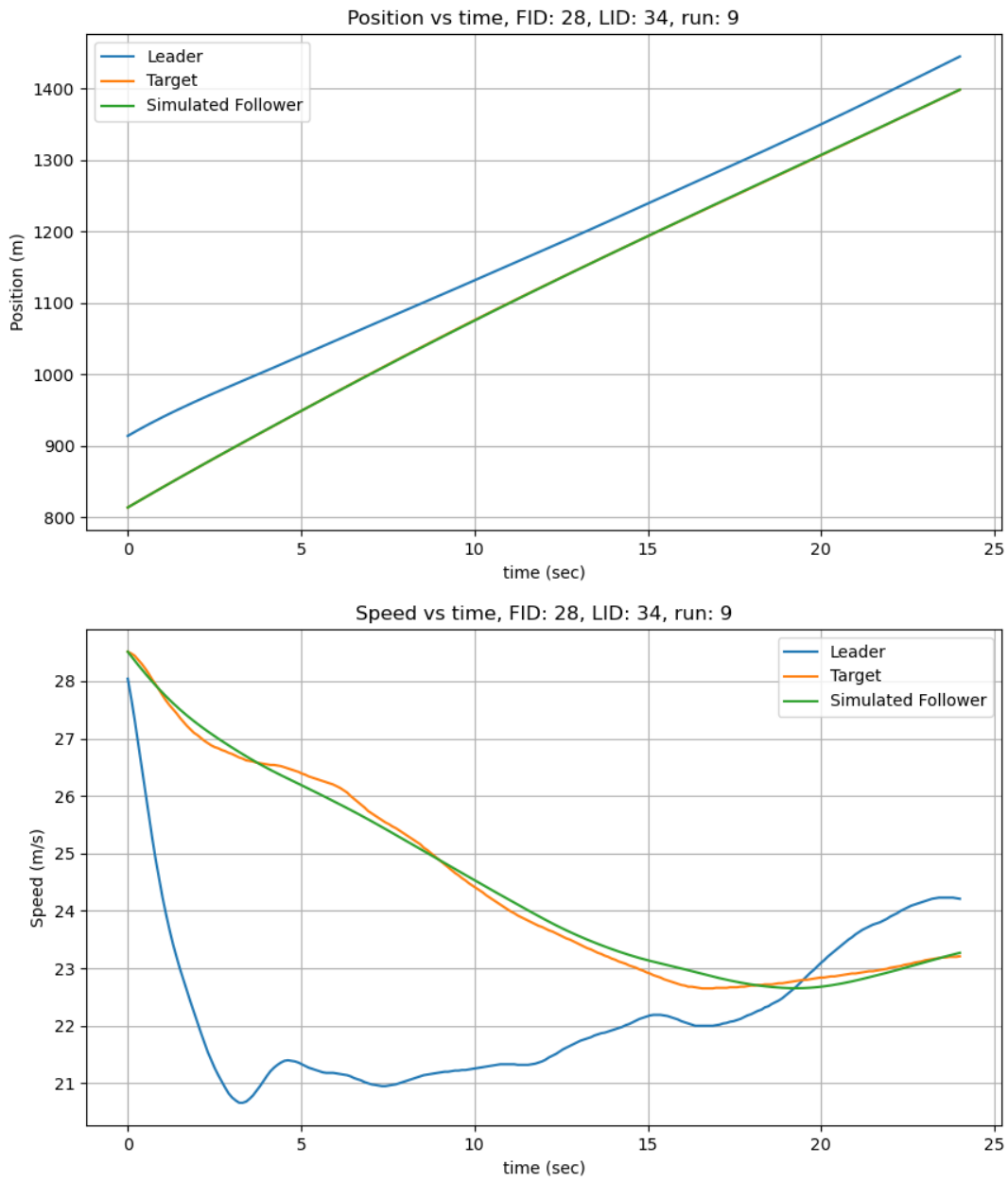


Figure 6.91: Position and speed for TFS for vehicle 28 in run 9 I294L1 dataset.

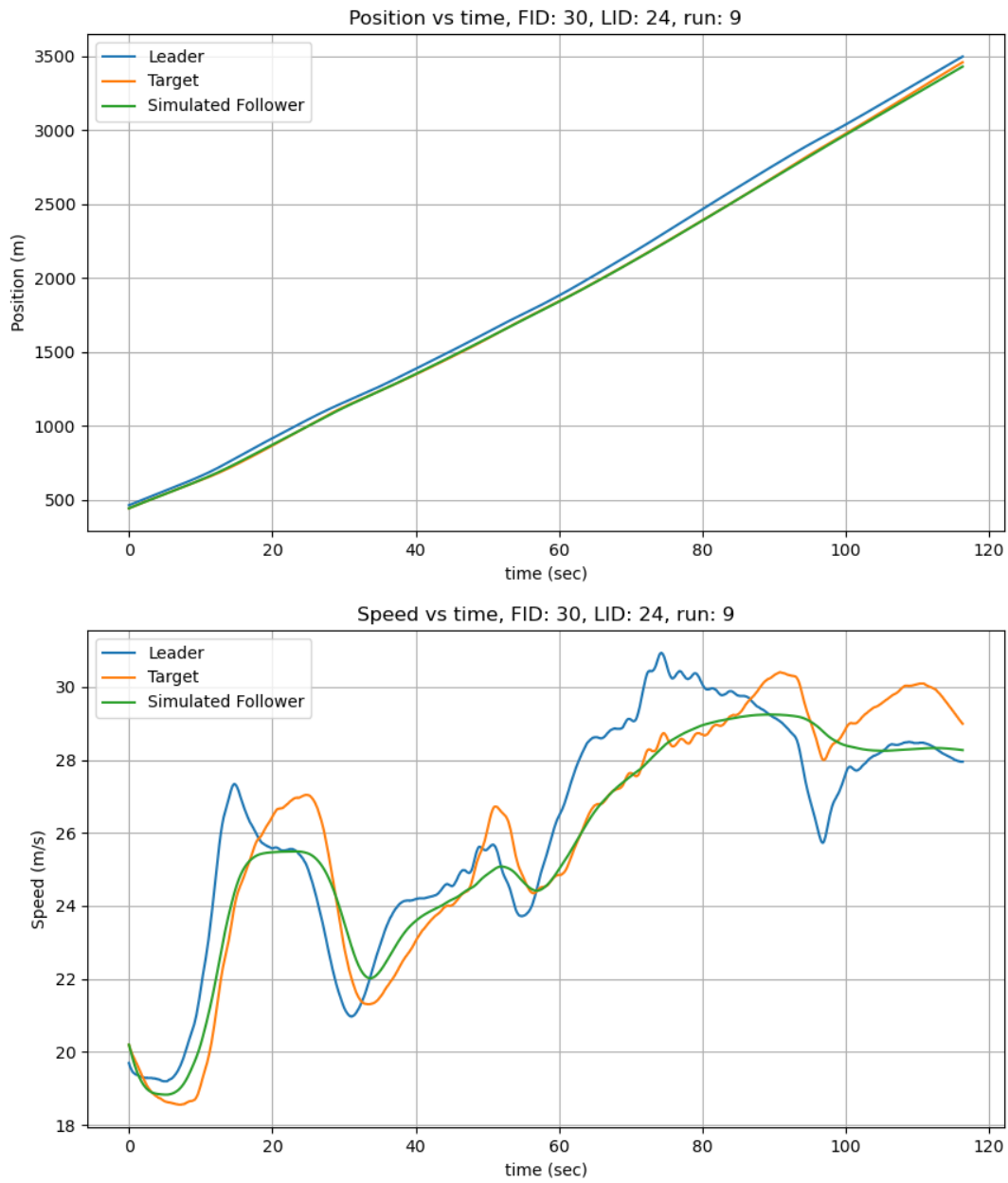


Figure 6.92: Position and speed for TFS for vehicle 30 in run 9 I294L1 dataset.

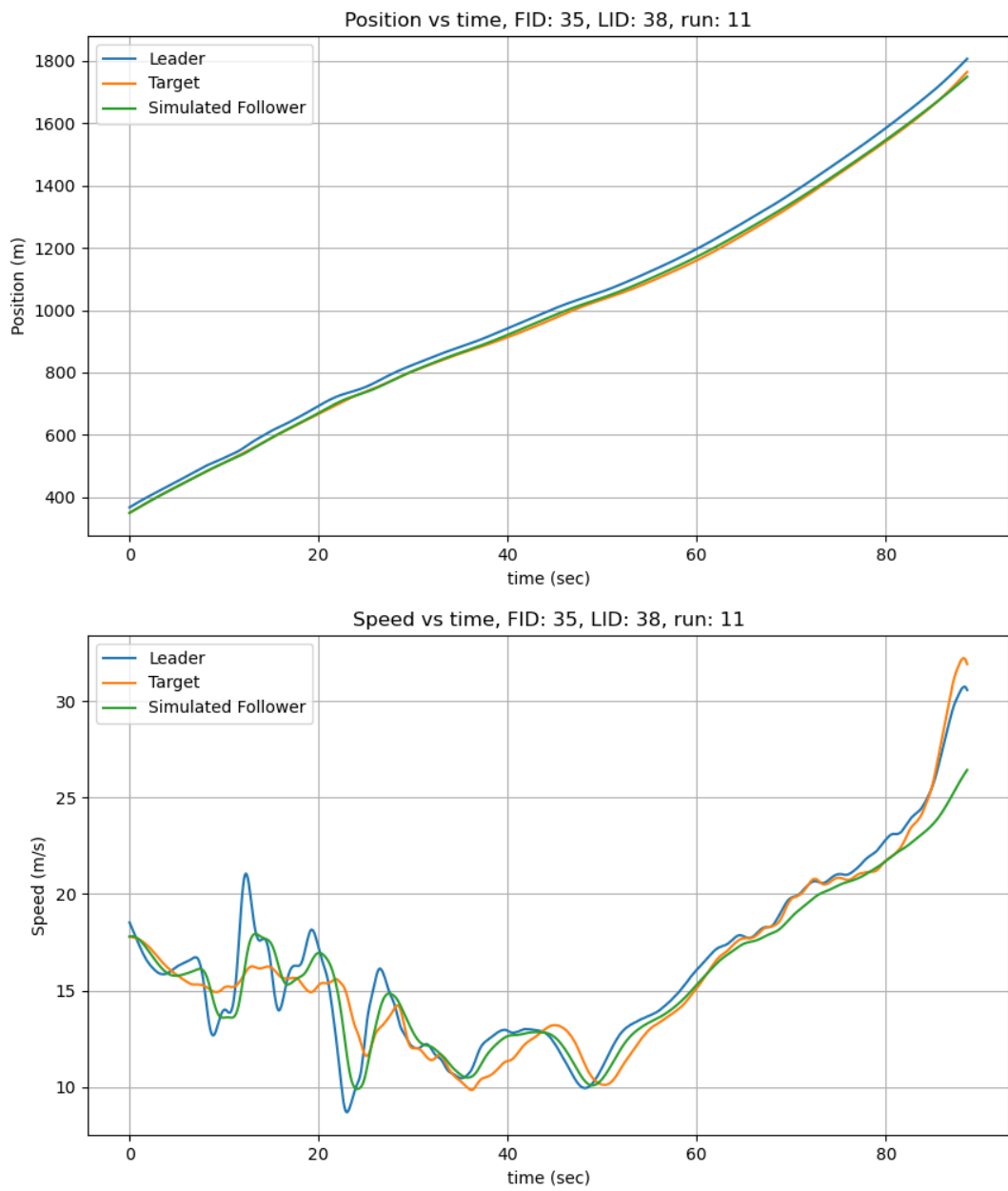


Figure 6.93: Position and speed for TFS for vehicle 35 in run 11 I294L1 dataset.

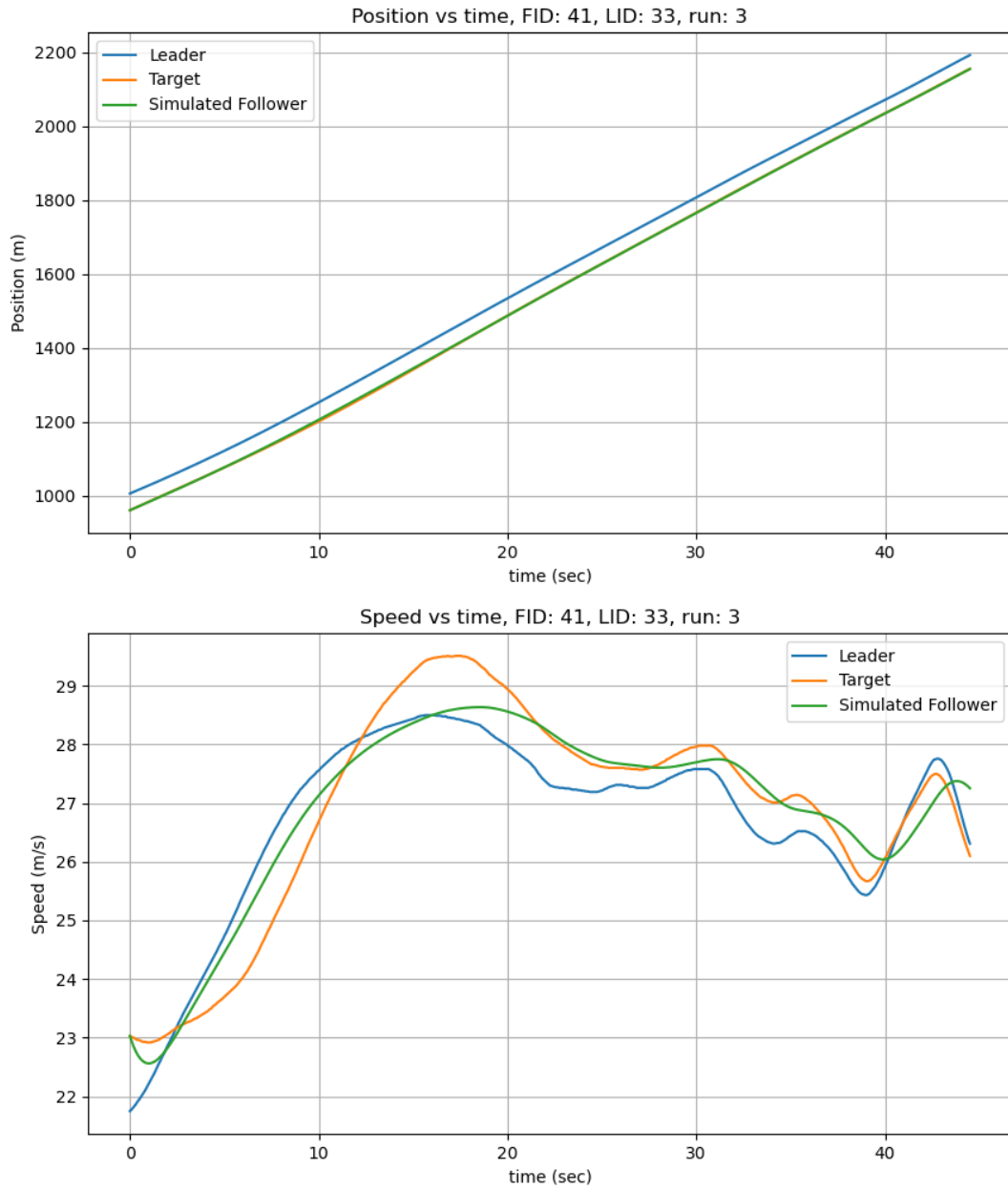


Figure 6.94: Position and speed for TFS for vehicle 41 in run 3 I294L1 dataset.

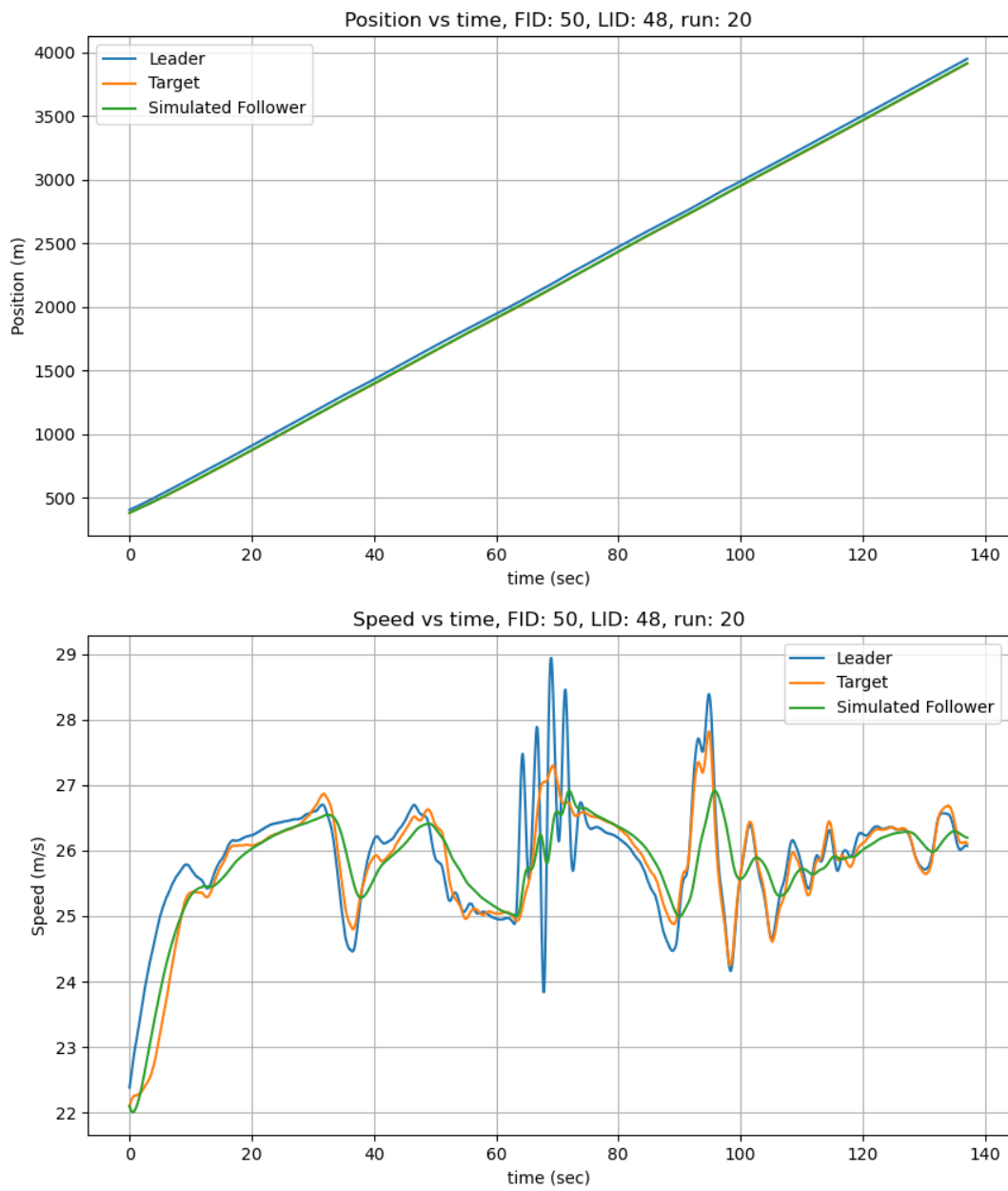


Figure 6.95: Position and speed for TFS for vehicle 50 in run 20 I294L1 dataset.

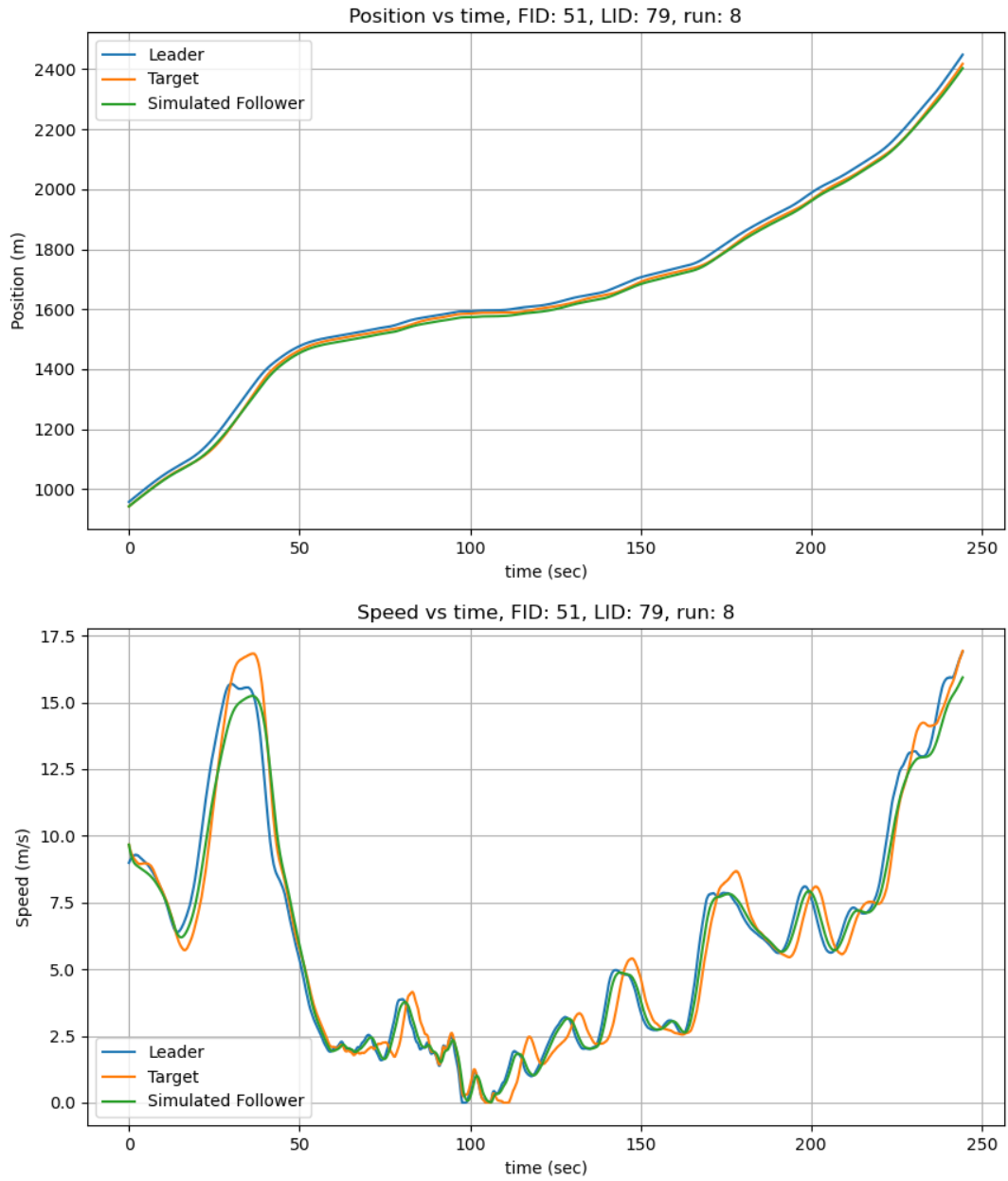


Figure 6.96: Position and speed for TFS for vehicle 51 in run 8 I294L1 dataset.

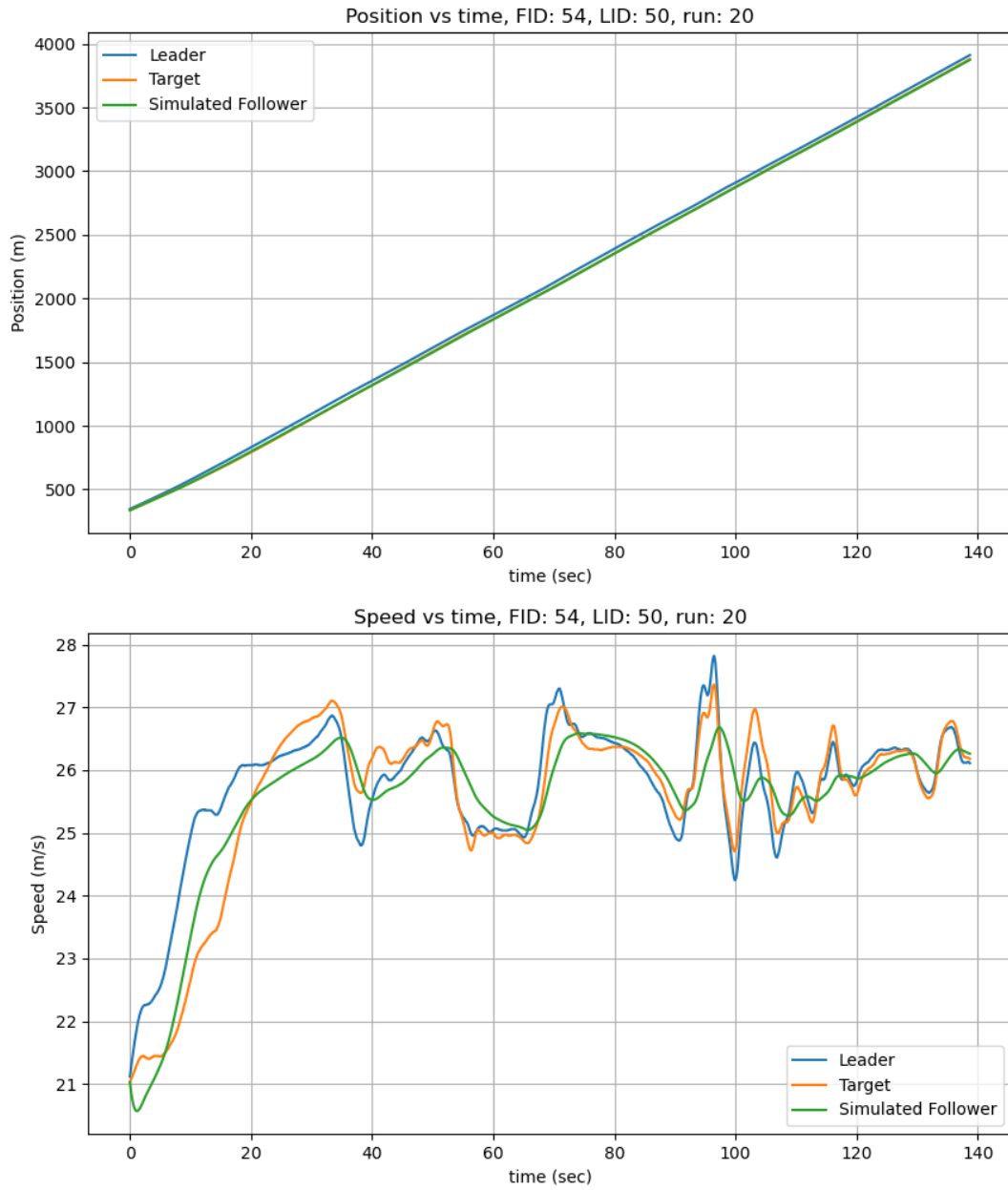


Figure 6.97: Position and speed for TFS for vehicle 54 in run 20 I294L1 dataset.

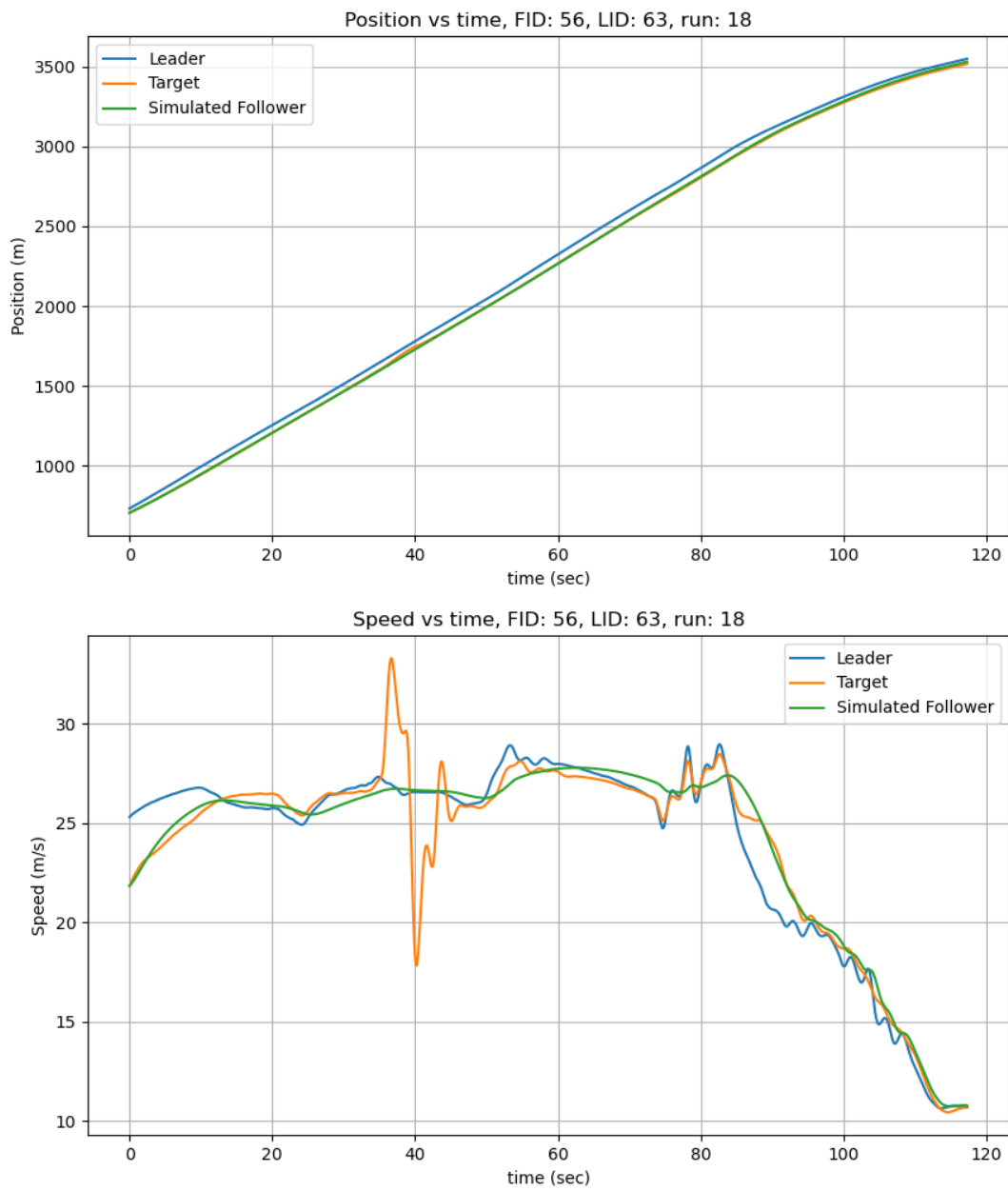


Figure 6.98: Position and speed for TFS for vehicle 56 in run 18 I294L1 dataset.

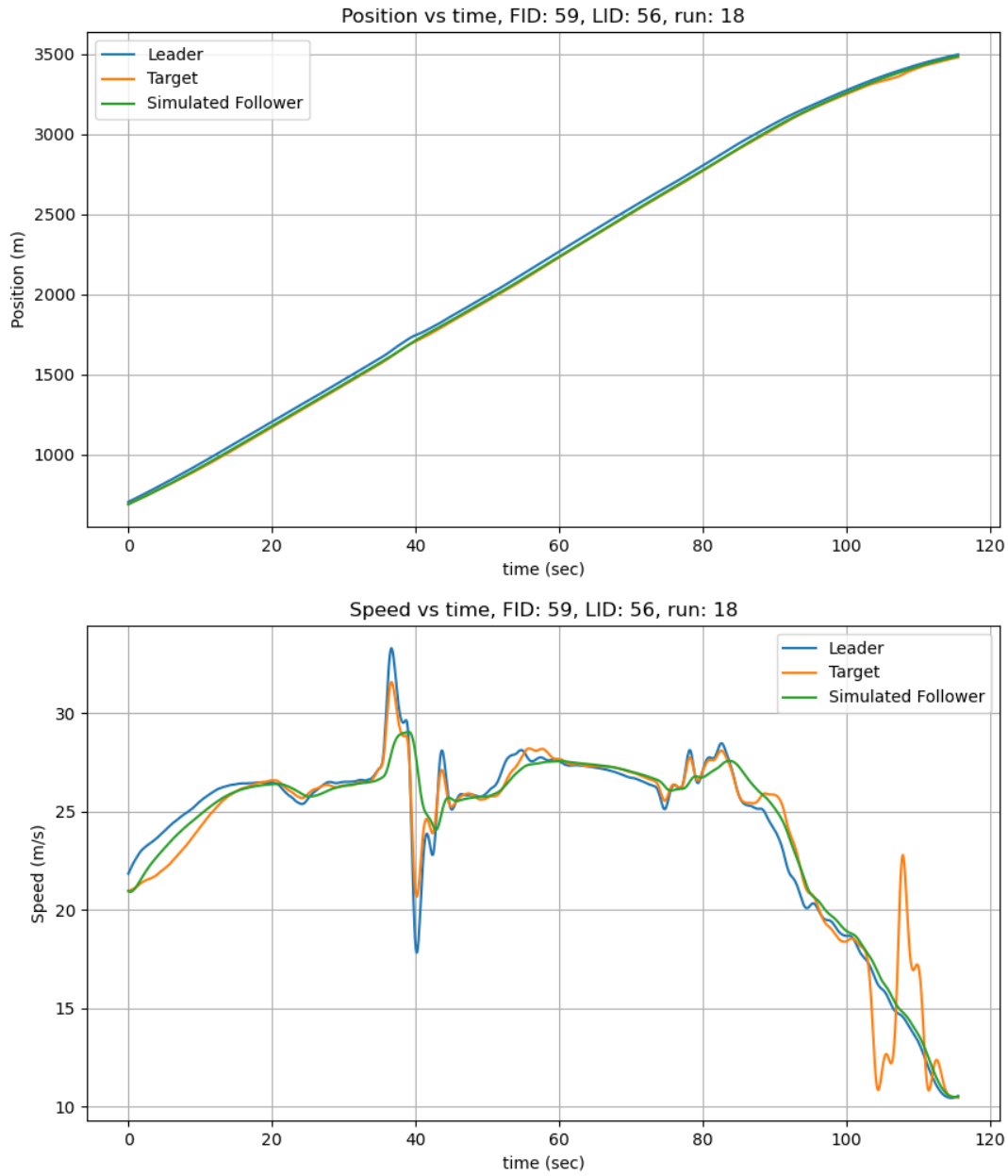


Figure 6.99: Position and speed for TFS for vehicle 59 in run 18 I294L1 dataset.

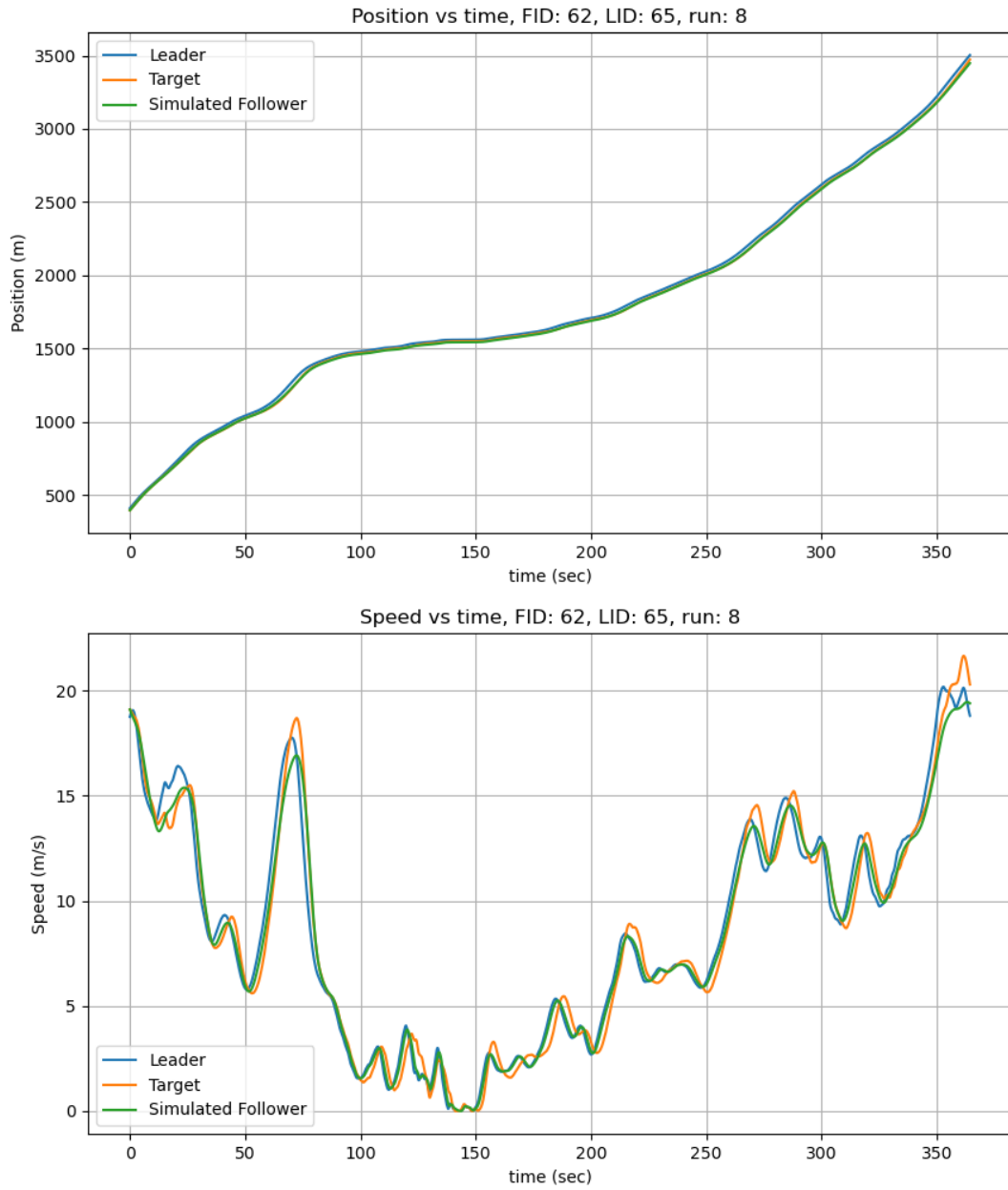


Figure 6.100: Position and speed for TFS for vehicle 62 in run 8 I294L1 dataset.

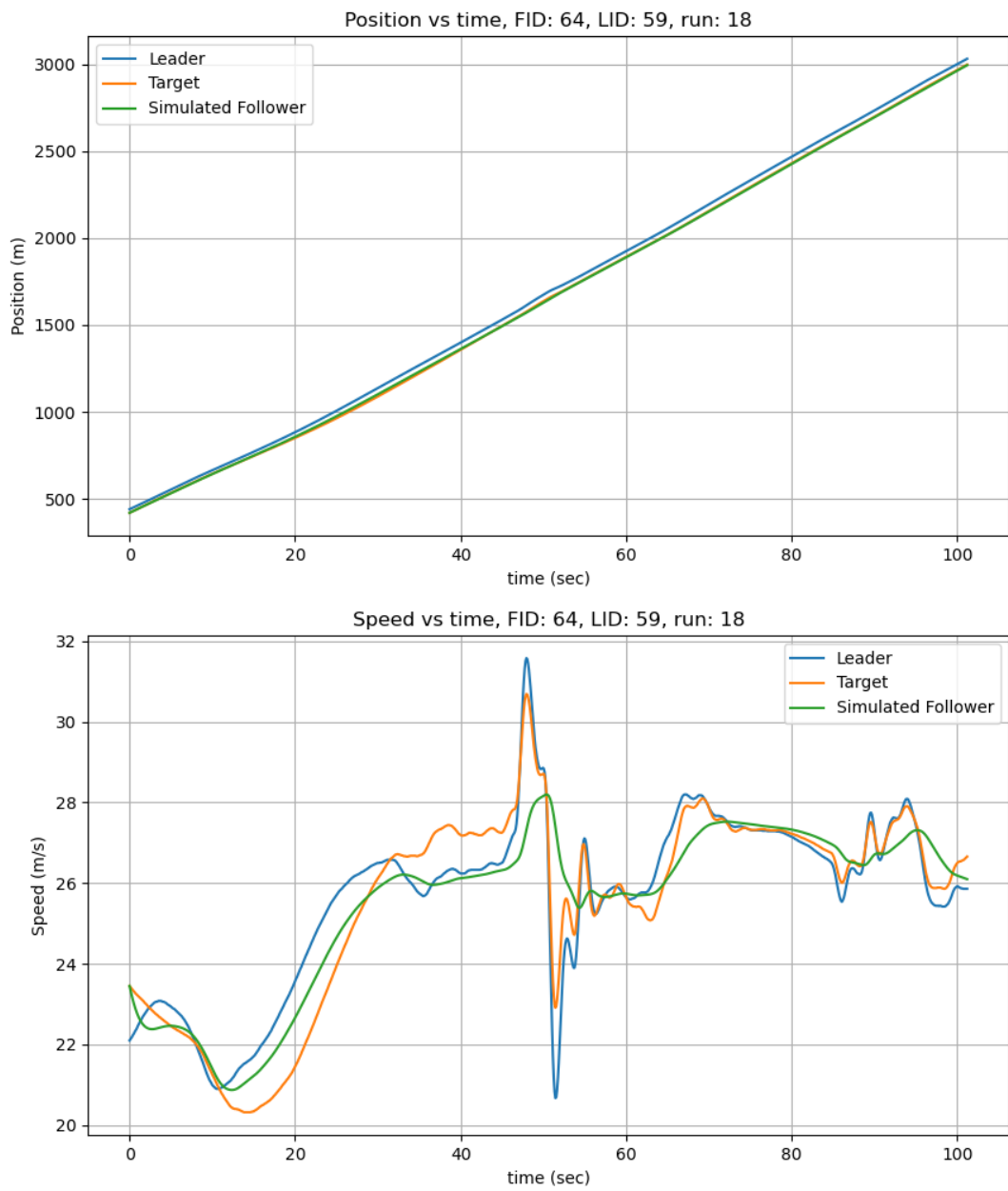


Figure 6.101: Position and speed for TFS for vehicle 64 in run 18 I294L1 dataset.

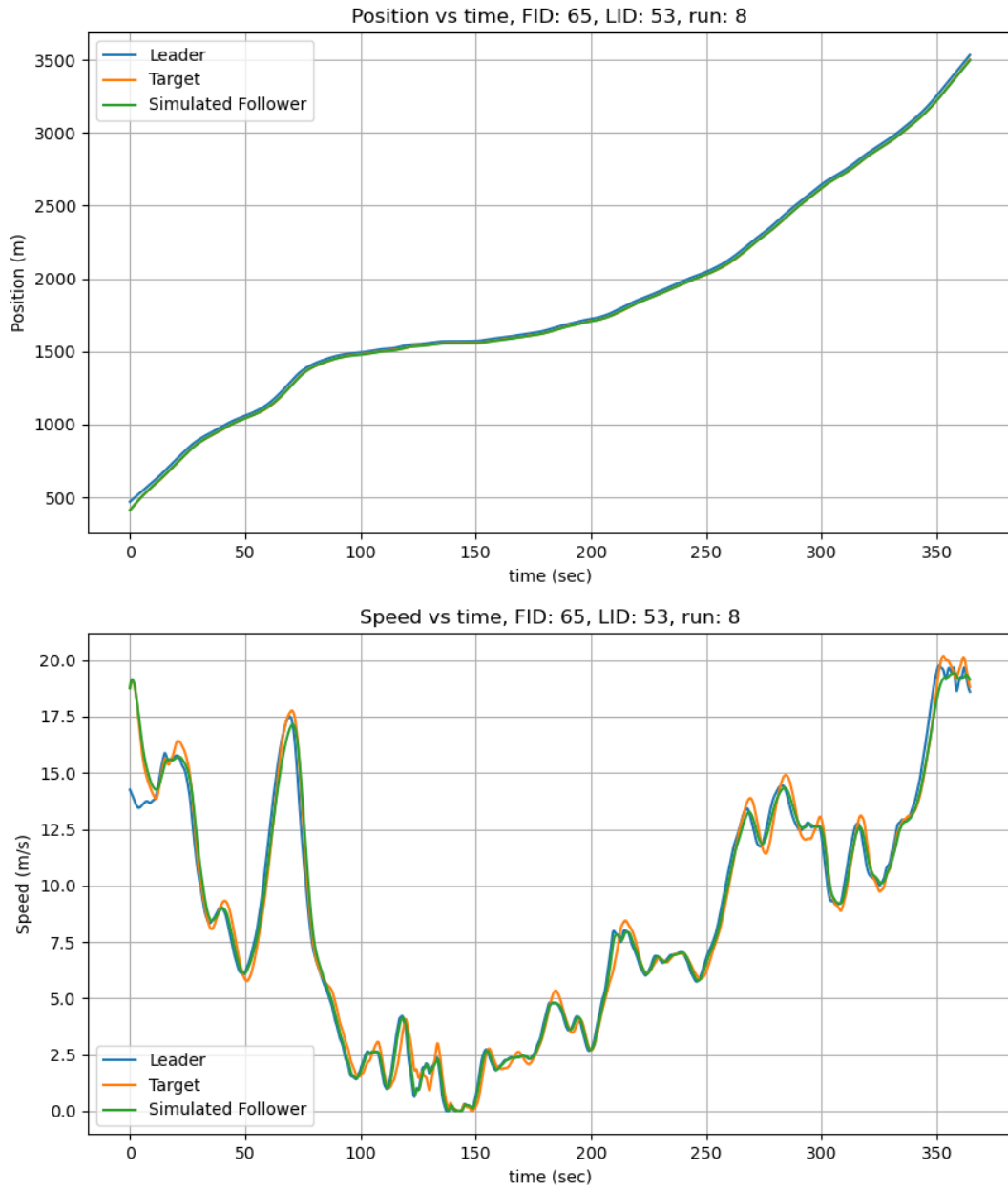


Figure 6.102: Position and speed for TFS for vehicle 65 in run 8 I294L1 dataset.

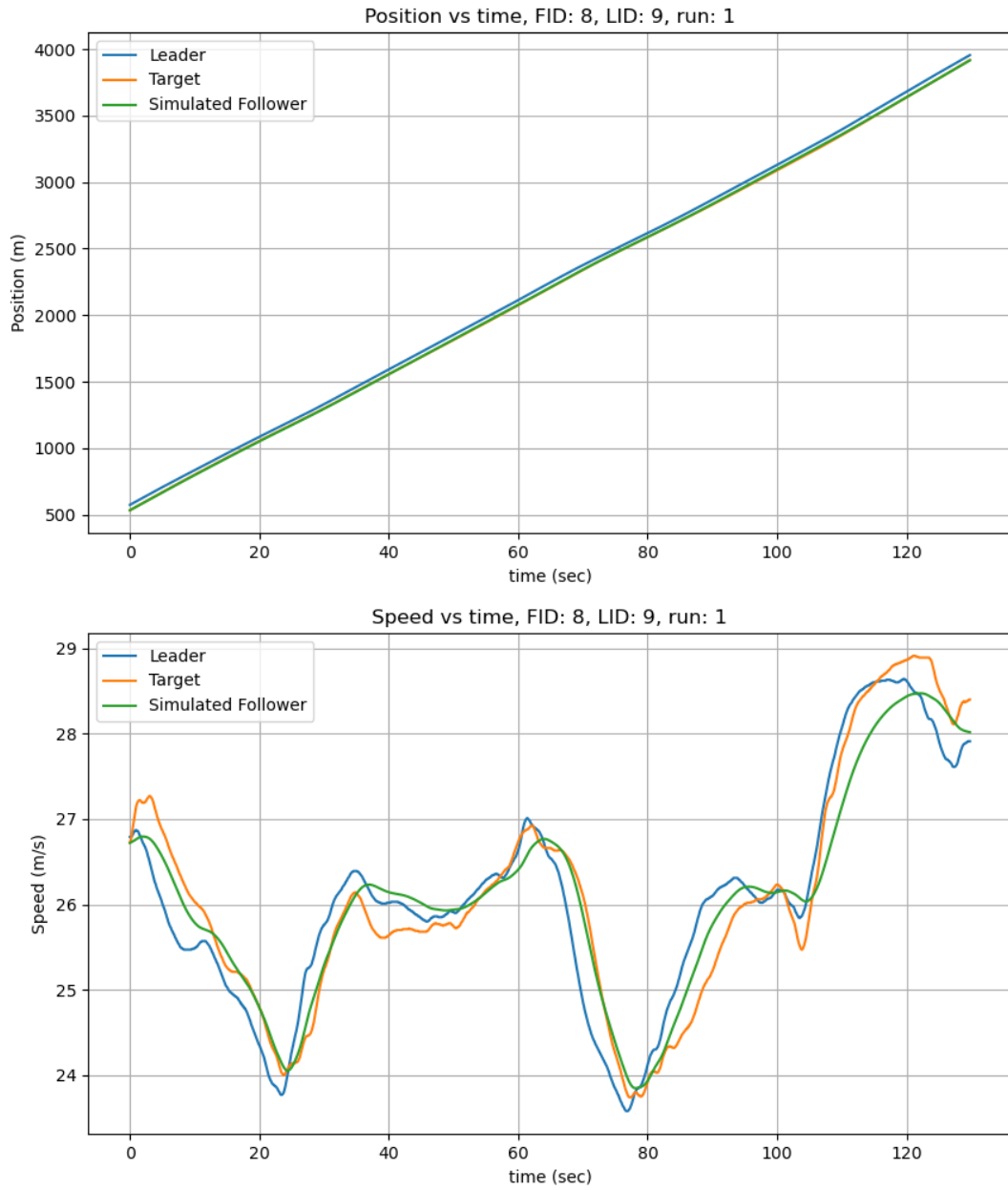


Figure 6.103: Position and speed for TFS for vehicle 8 in run 1 I294L1 dataset.

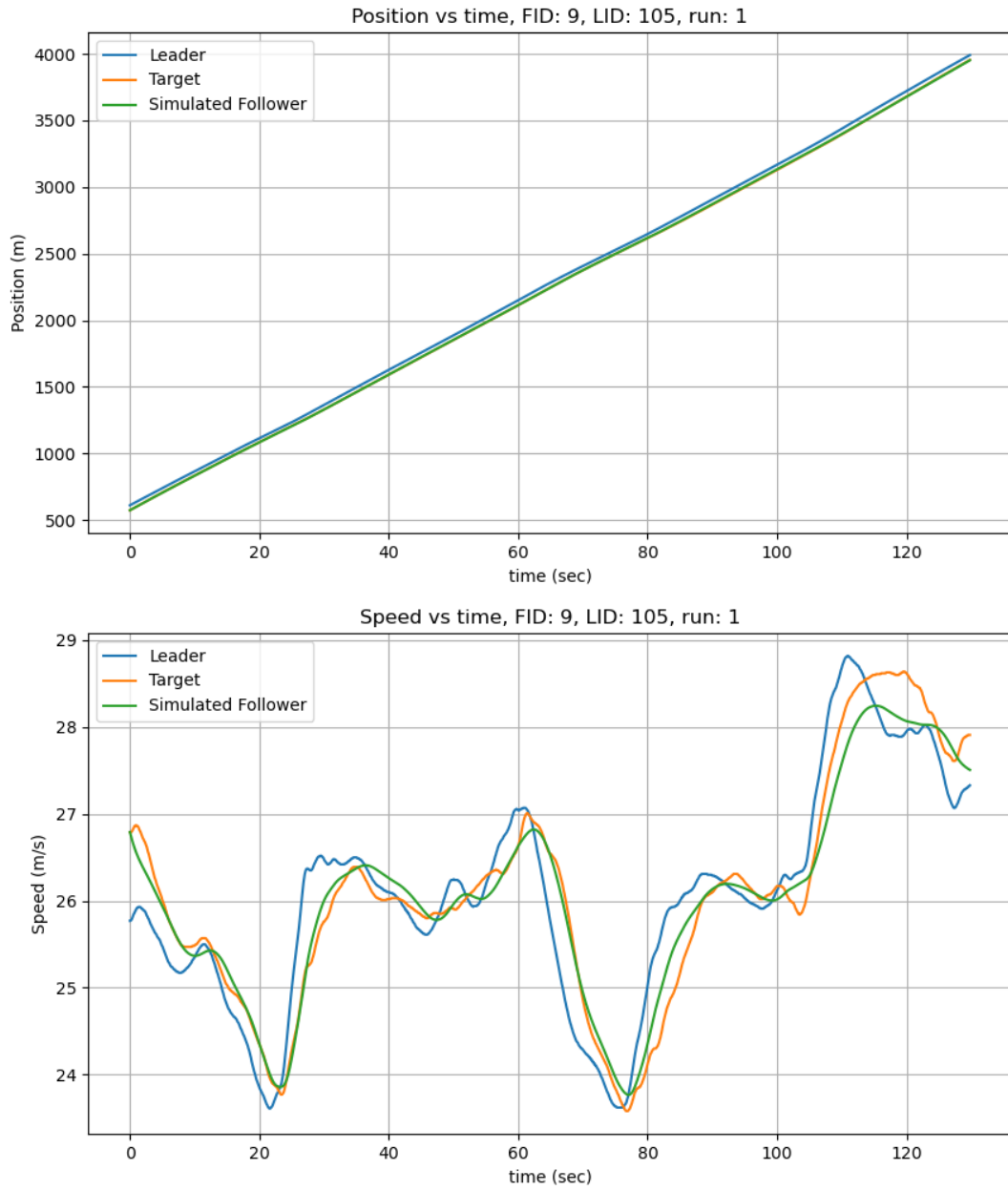


Figure 6.104: Position and speed for TFS for vehicle 9 in run 1 I294L1 dataset.

The optimized parameter ranges for the TFS model in the I294 dataset shows variability across different parameters, as shown in Figure 6.105. The (v_f) had the largest range,

indicating significant variations in free-flow speed due to changing traffic conditions and driving behaviors. In contrast, (ρ_m) and (λ) remain tightly clustered, suggesting that these parameters have maintained consistency during the calibration process.

Figure 6.106 illustrates the skewness of the parameter distributions. Specifically, (ρ_m) and (λ) are left-skewed, implying that lower values were more frequently selected during optimization, while (v_f) is skewed to the right, indicating that higher values were more frequently selected, reflecting varying traffic flow speeds and free-flow conditions in the dataset.

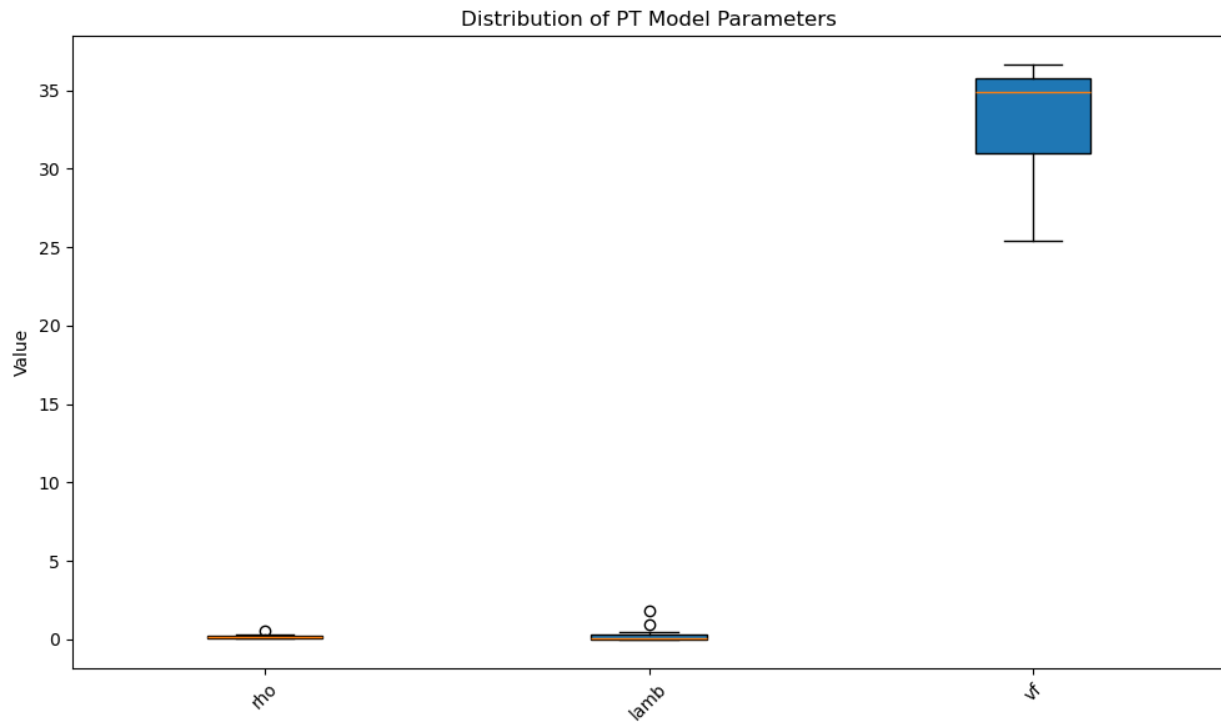


Figure 6.105: Parameter ranges for TFS in I294L1 dataset.

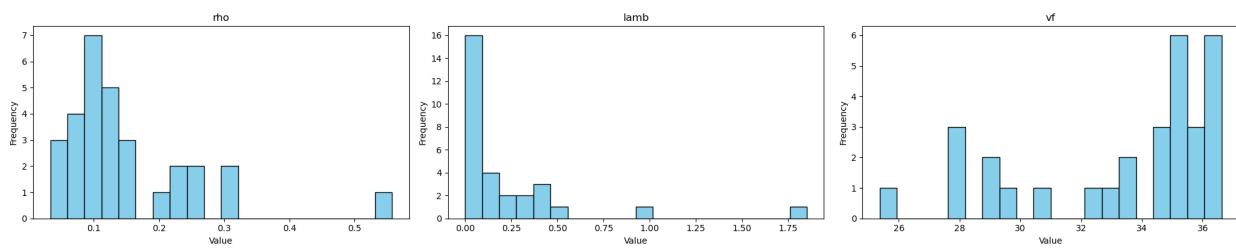


Figure 6.106: Parameter histogram for TFS in I294L1 dataset.

6.2.8 TFS I90/94 Simulated Results

The simulated results for TFS model in the I90/94 dataset are presented in Figures [6.107](#), [6.108](#), and [6.109](#) using the TFS model. For vehicle 5366 and 195, it can be determined that the controller can track the position with minimum speed pattern deviations shown in Figures [6.107](#) and [6.108](#). However, there is a minor deviation with speed patterns for vehicle 286 shown in Figure [6.109](#) although the simulated position closely aligns with the target position.

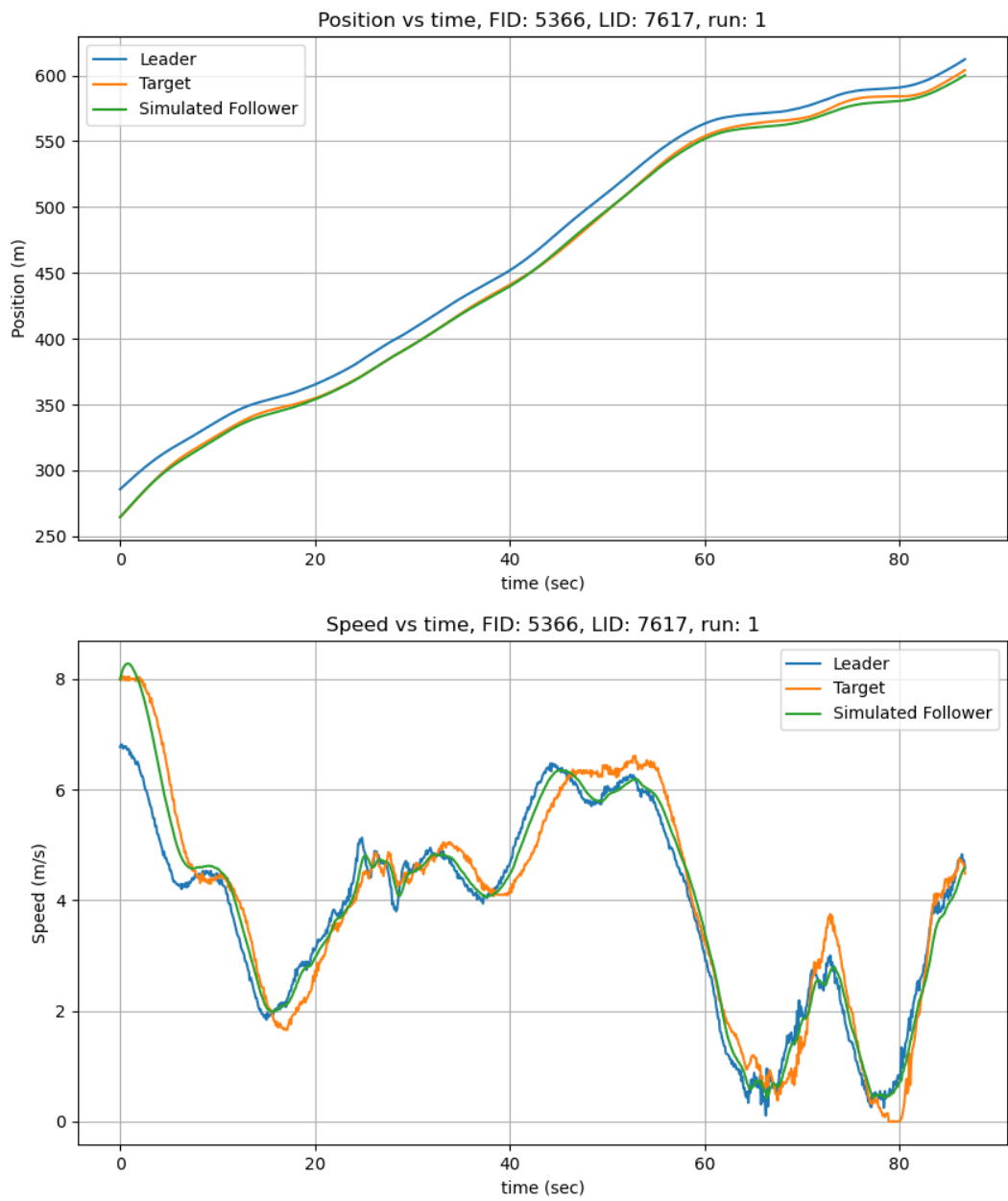


Figure 6.107: Position and speed for TFS for vehicle 5366 in I90/94 dataset.

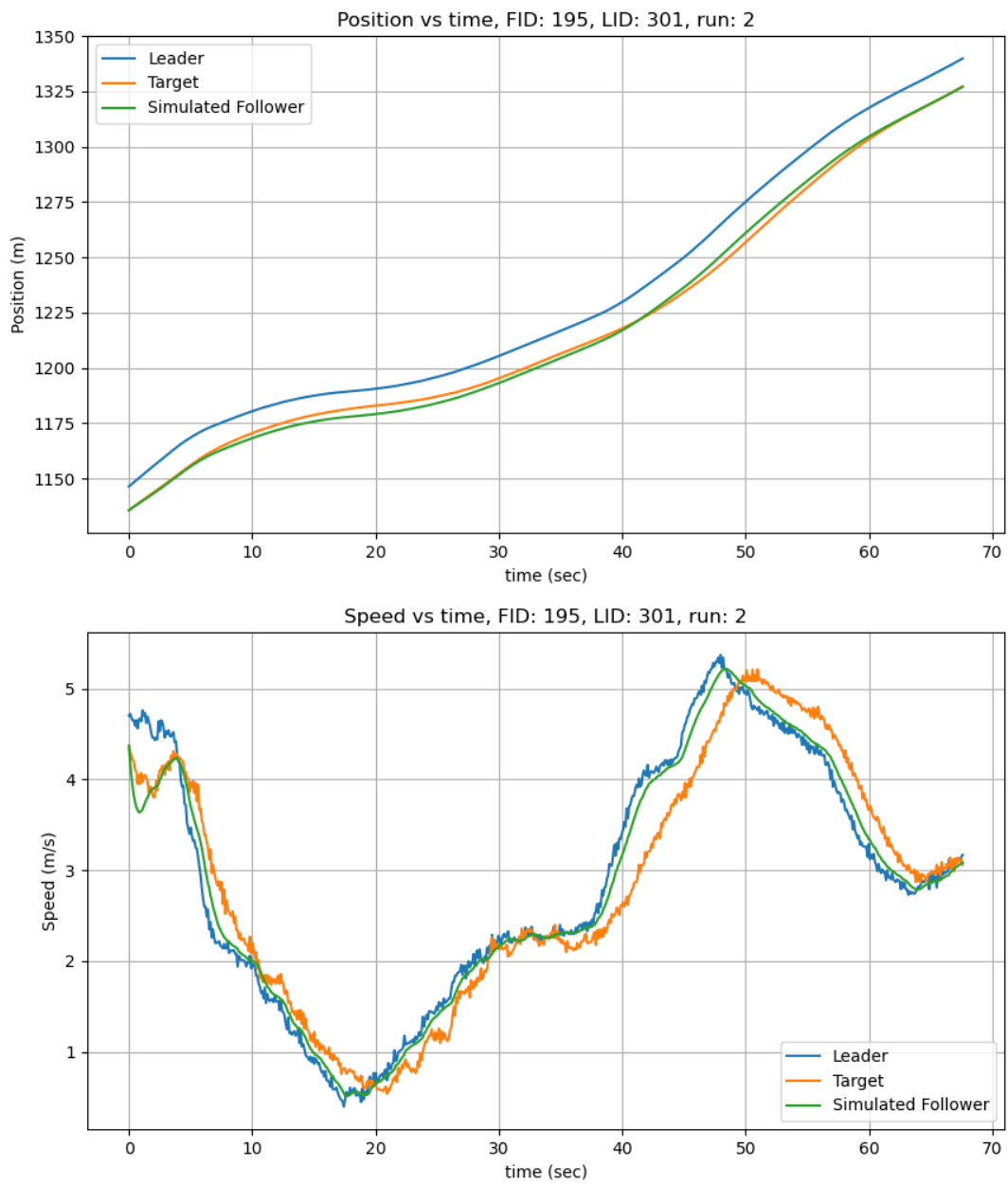


Figure 6.108: Position and speed for TFS for vehicle 195 in I90/94 dataset.

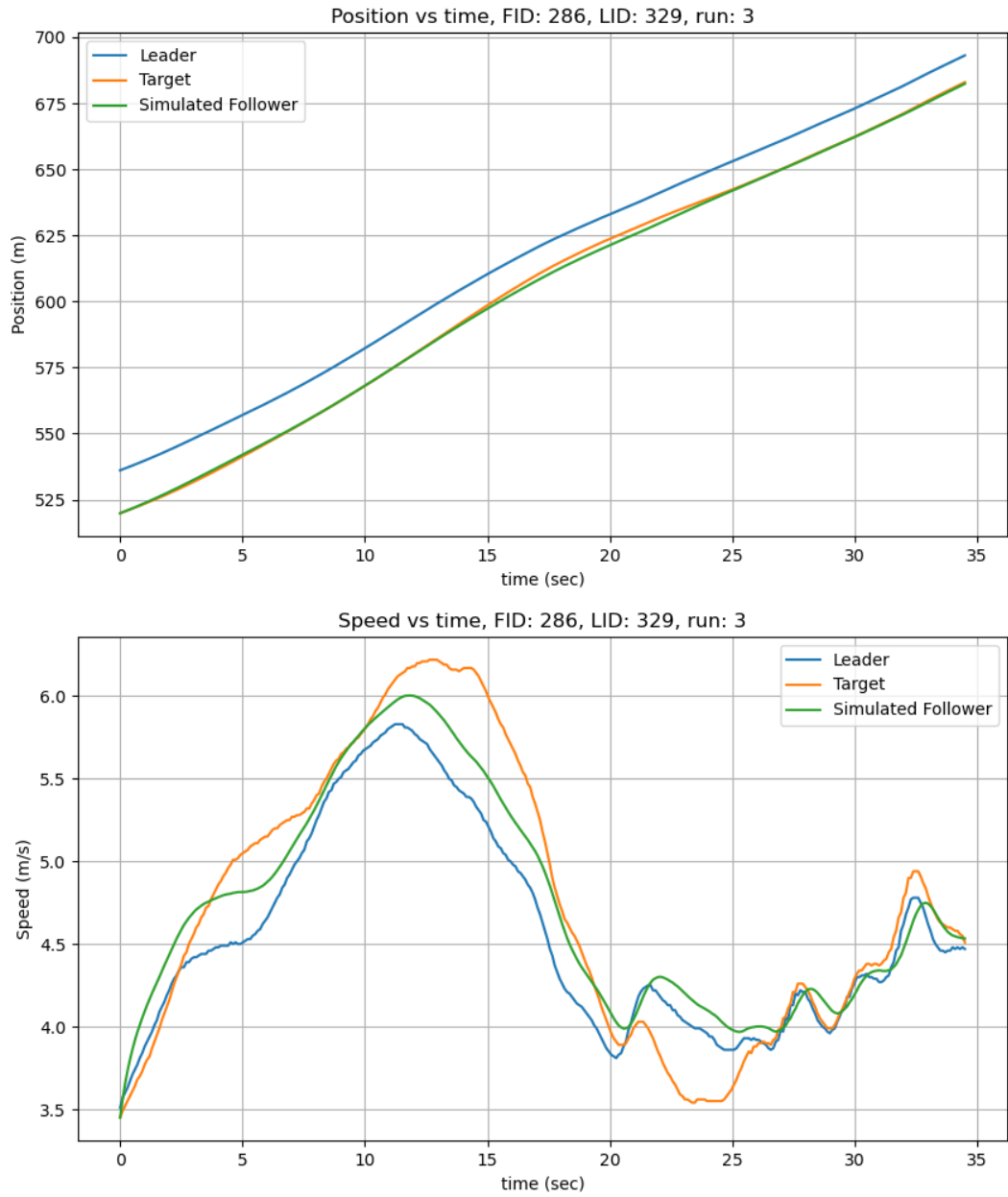


Figure 6.109: Position and speed for TFS for vehicle 286 in I90/94 dataset.

The optimized parameter ranges for the TFS model in the I90/94 dataset, as shown in Figure 6.110, indicate small variations across parameters. While (v_f) has the highest range, the

numeric values remain tightly clustered, suggesting a consistent free-flow speed across different calibration instances. Similarly, (ρ_m) and (λ) maintain low ranges with minimal variation, indicating that traffic flow sensitivity and stability adjustments are relatively uniform across different traffic scenarios.

Figure 6.111 illustrates that the optimized parameters follow discrete distributions, with values concentrated at specific numeric points rather than being continuously spread out. This pattern suggests that the model favors specific parameter values during optimization, potentially due to traffic dynamics constraints in the dataset. The consistent clustering of (ρ_m) and (λ) stabilizes flow fluctuations, while the narrow distribution of (v_f) suggests the vehicle maintaining appropriate free-flow speed.

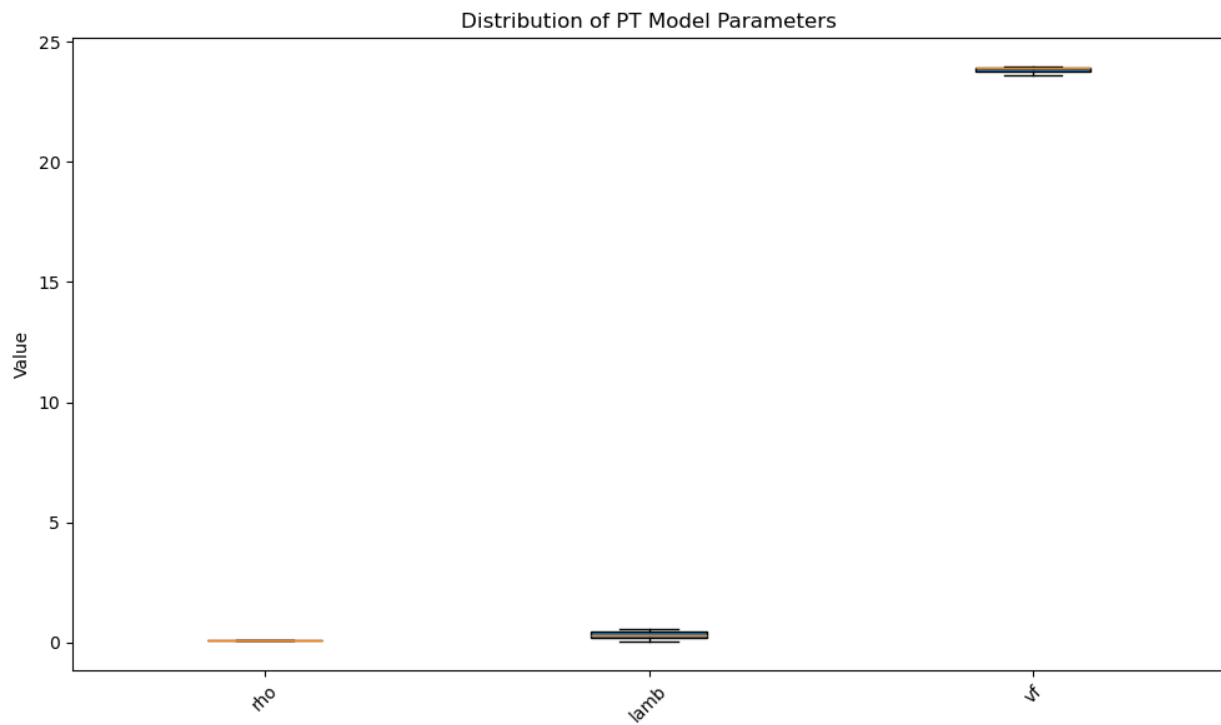


Figure 6.110: Parameter ranges for TFS in I90/94.

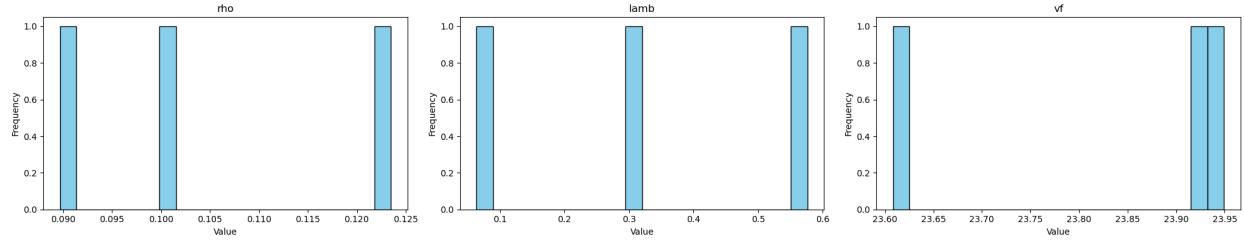


Figure 6.111: Parameter histogram for TFS in I90/94.

6.2.9 TFS Phoenix Simulated Results

The simulated results for the TFS model in the Phoenix dataset are presented in Figures 6.112, 6.113, 6.114, and 6.115. The simulated follower closely aligns with the calibrated position and speed of the target follower, as shown in Figures 6.112 and 6.115 for vehicles 13 and 2 in run 9NS. However, noticeable speed deviations are observed for vehicles 31 and 2 in run 9ES, as illustrated in Figures 6.113 and 6.114.

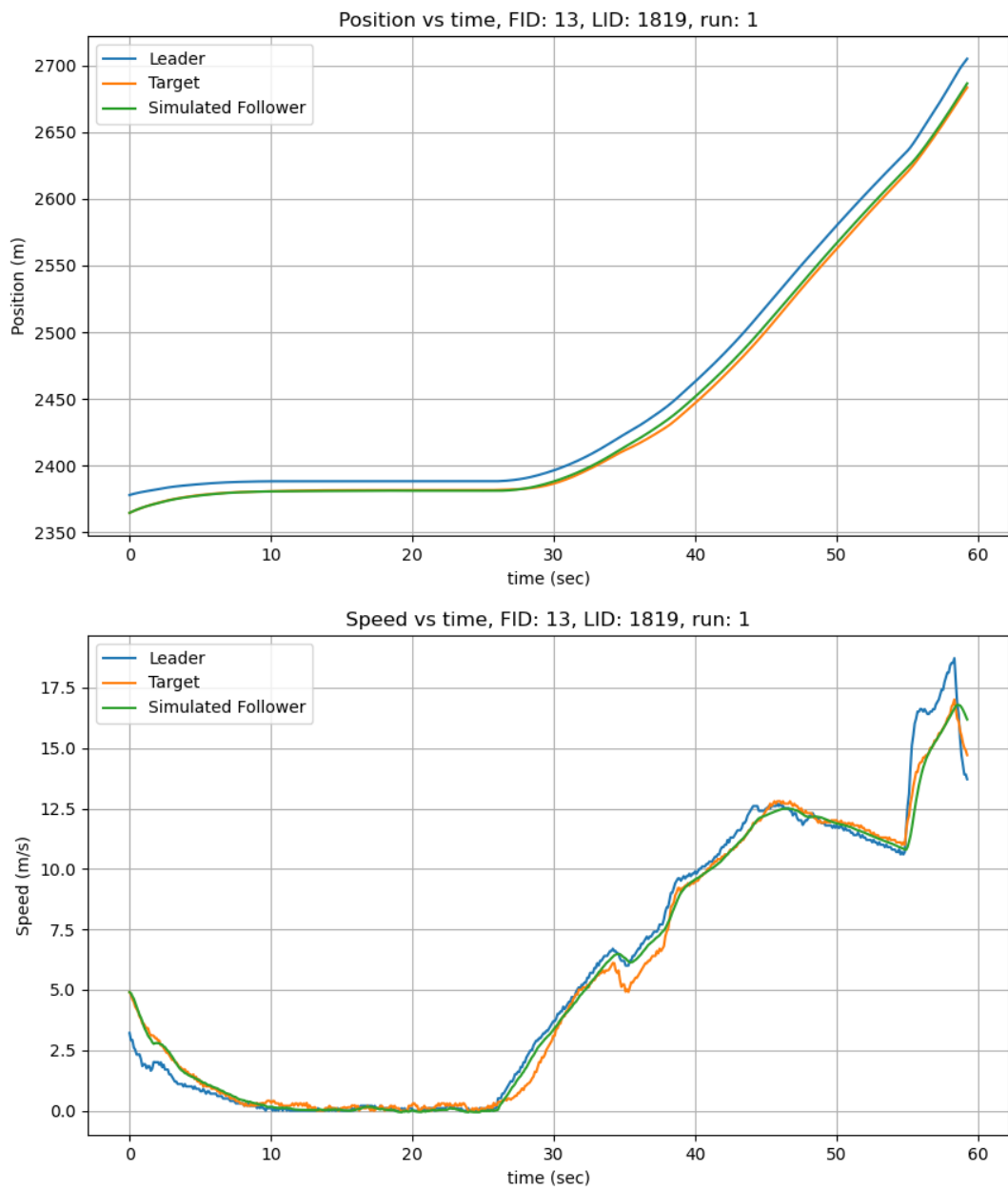


Figure 6.112: Position and speed for TFS for vehicle 13 in Phoenix data H1A3 run 6.

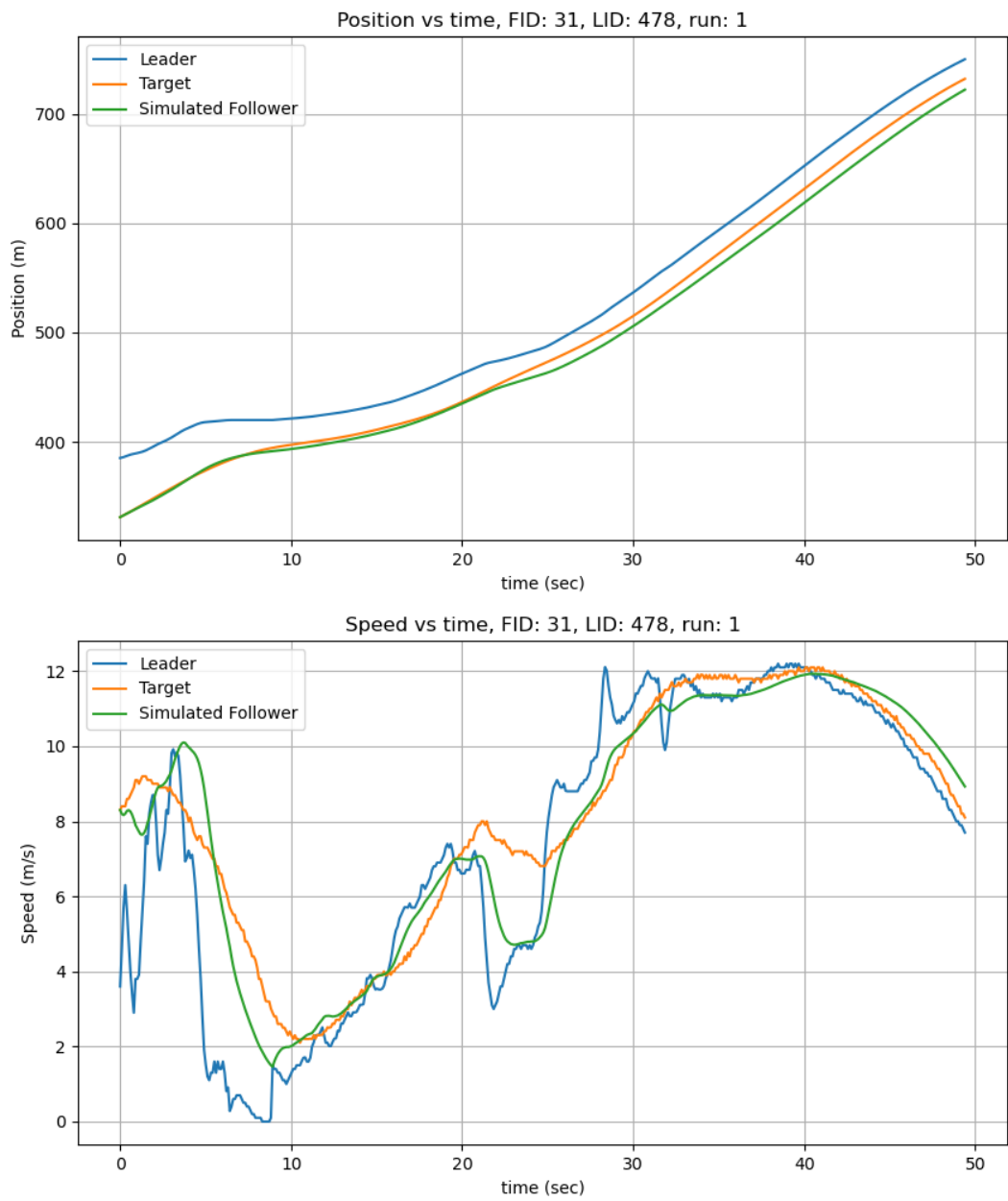


Figure 6.113: Position and speed for TFS for vehicle 31 in Phoenix data H1A3 run 1.

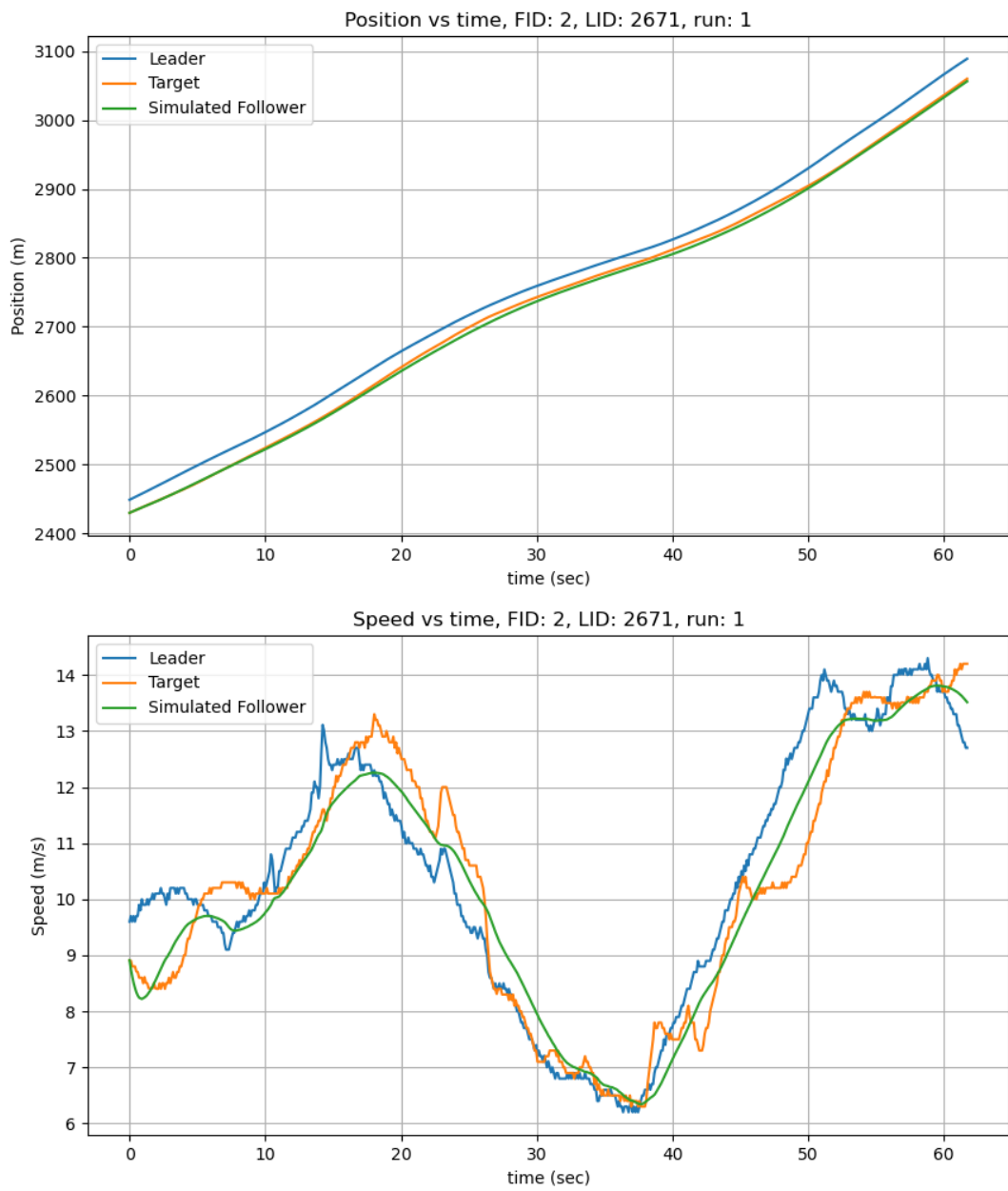


Figure 6.114: Position and speed for TFS for vehicle 2 in Phoenix data H1A3 run 9 ES.

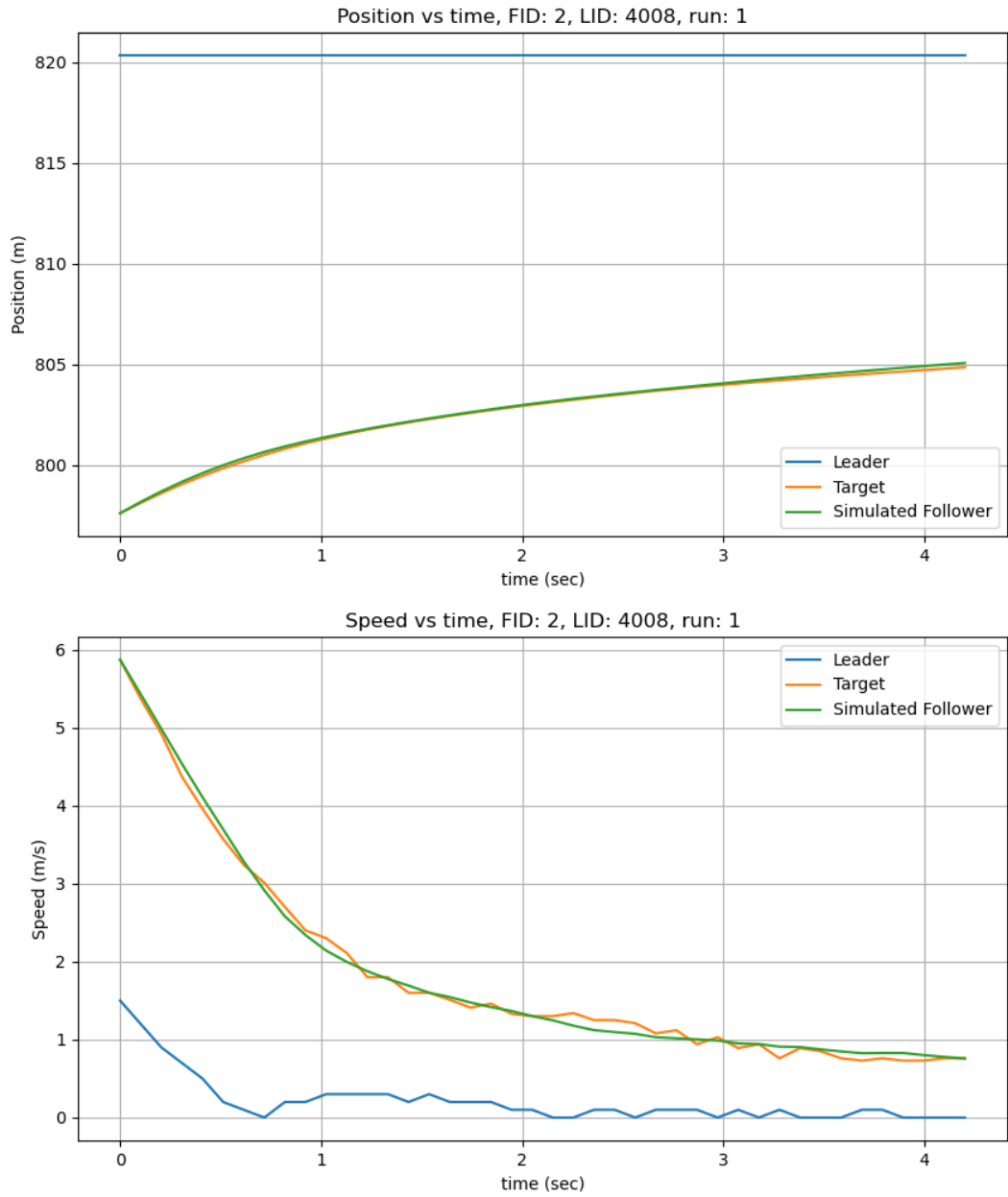


Figure 6.115: Position and speed for TFS for vehicle 2 in Phoenix data H1A3 run 9 NS.

The optimized parameter ranges for the TFS model in the Phoenix dataset, as shown in Figure 6.116, indicate minimal variability across parameters. The free-flow speed (v_f) remains

highly consistent, with values tightly clustered around a high range, suggesting a uniform traffic flow behavior in the dataset. Similarly, (ρ_m) and (λ) has minimal variation, indicating that traffic density sensitivity and stability adjustments remain relatively consistent across different calibration runs.

Figure 6.117 shows that the optimized parameters follow discrete distributions, with values concentrated at specific numeric points rather than being continuously spread. This pattern suggests that the TFS model consistently selects specific parameter values during calibration. The narrow clustering of (ρ_m) and (λ) suggests that their roles in regulating flow stability remain uniform, maintaining consistent traffic dynamics.

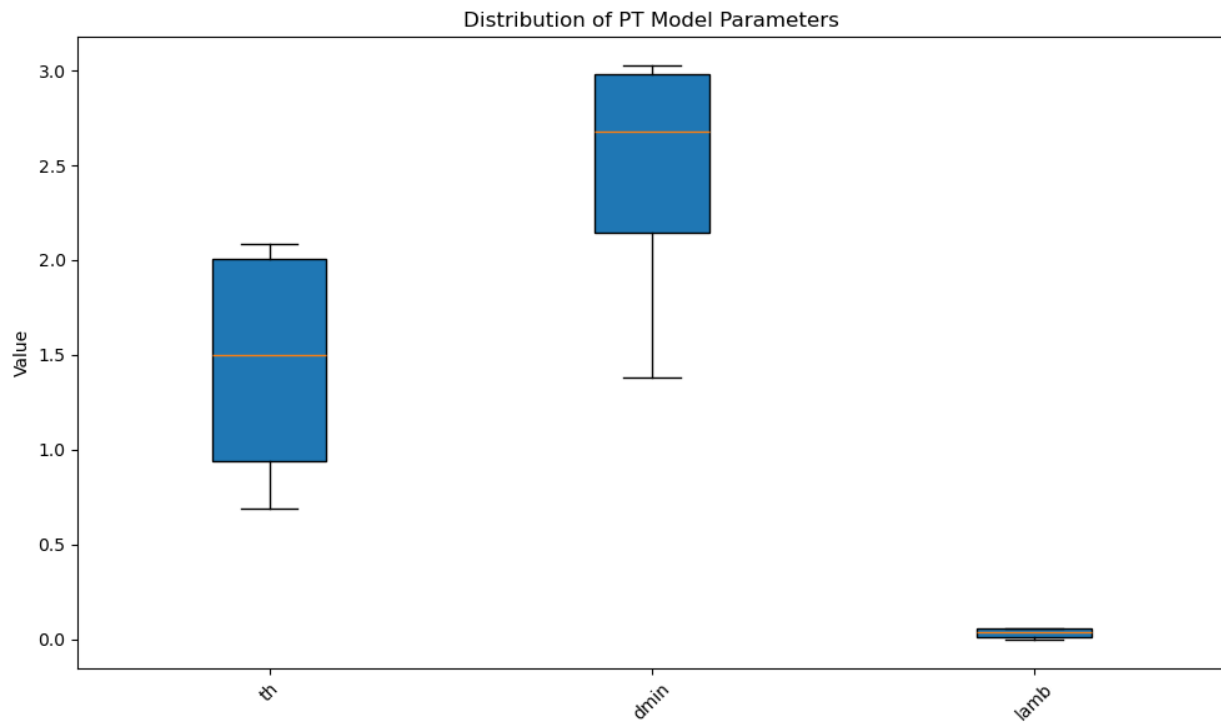


Figure 6.116: Parameter ranges for TFS in Phoenix.

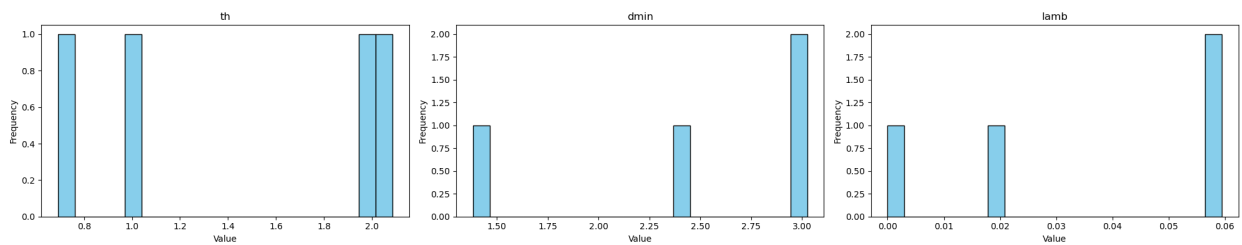


Figure 6.117: Parameter histogram for TFS in Phoenix.

6.2.10 CSF I294 Simulated Results

For Constant Safety Factor policy (CSF), the simulated results for I294 are presented in Figures [6.118](#), [6.119](#), [6.120](#), [6.121](#), [6.122](#), [6.123](#), [6.124](#), [6.125](#), [6.126](#), [6.127](#), [6.128](#), [6.129](#), [6.130](#), [6.131](#), [6.132](#), [6.133](#), [6.133](#), [6.134](#), [6.135](#), [6.136](#), [6.137](#), [6.138](#), [6.139](#), [6.140](#), [6.141](#), [6.142](#), and [6.143](#). The CSF model adjusts the trajectories by taking into safety parameters such as the safety factor (K), braking coefficient (γ), and safety distance (d_{min}) to closely align the simulated position and speed with the target position and speed. Overall, the simulated position strongly aligns with the target position despite some speed variations.

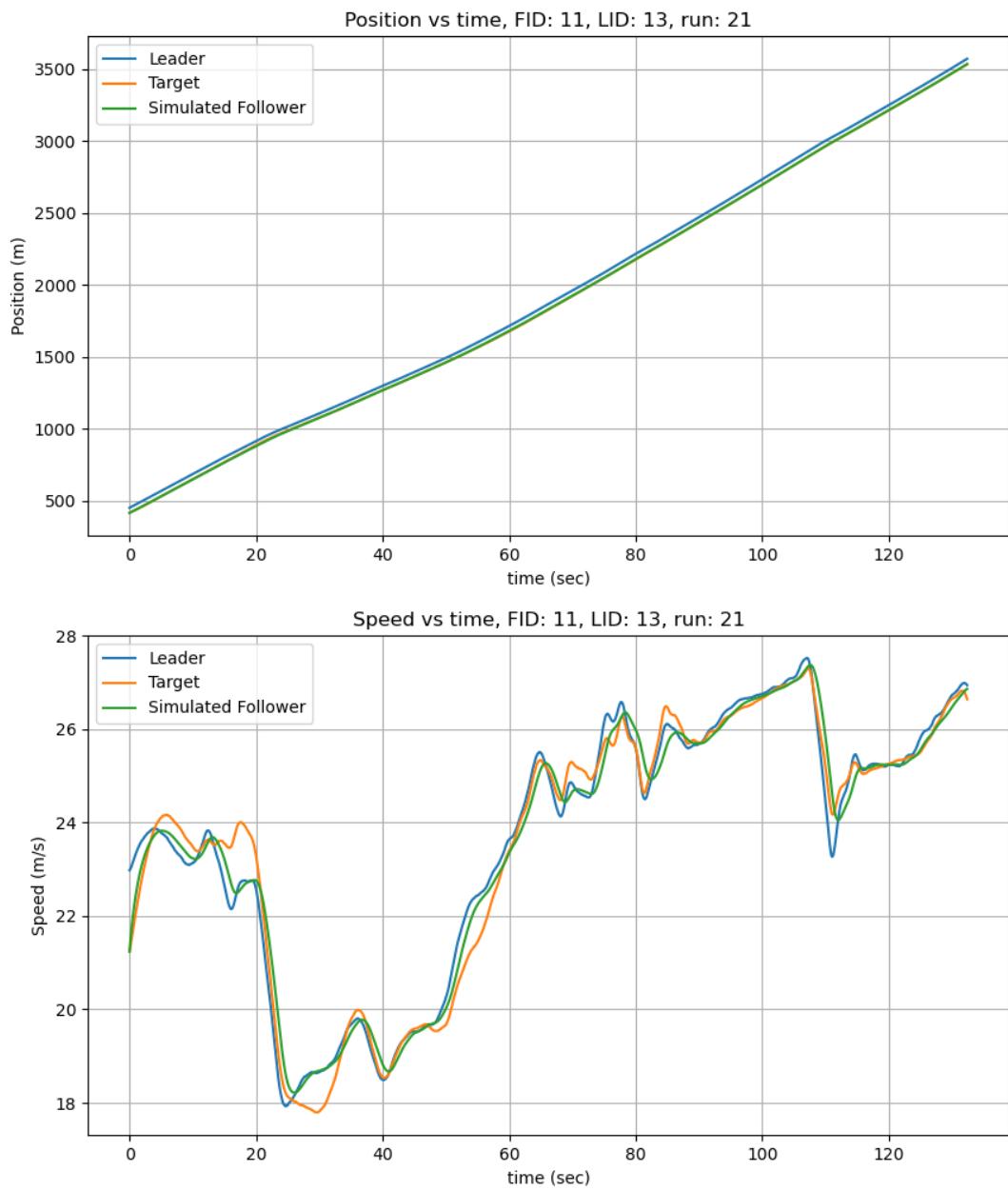


Figure 6.118: Position and speed for CSF for vehicle 11 in run 21 I294L1 dataset.

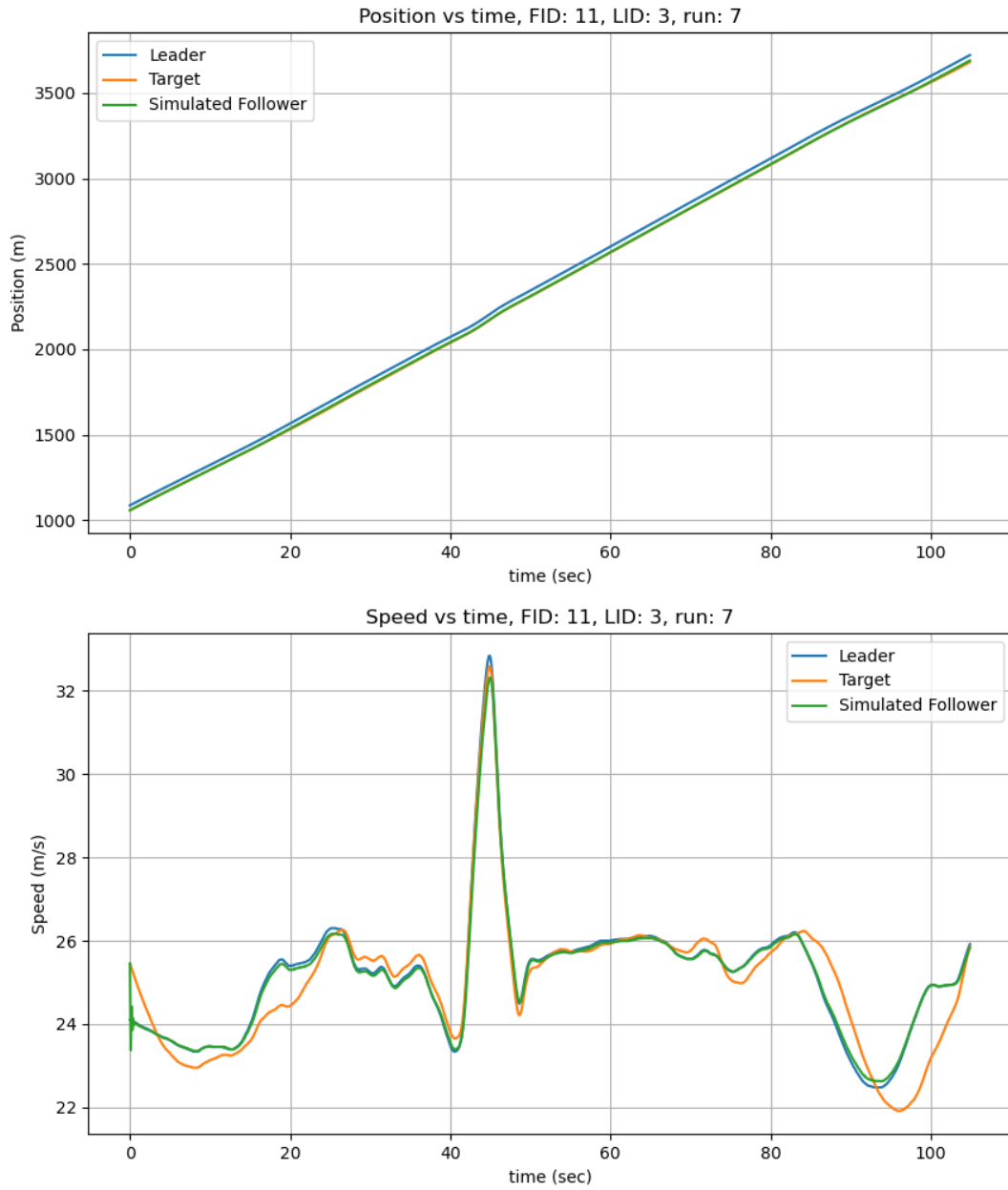


Figure 6.119: Position and speed for CSF for vehicle 11 in run 7 I294L1 dataset.

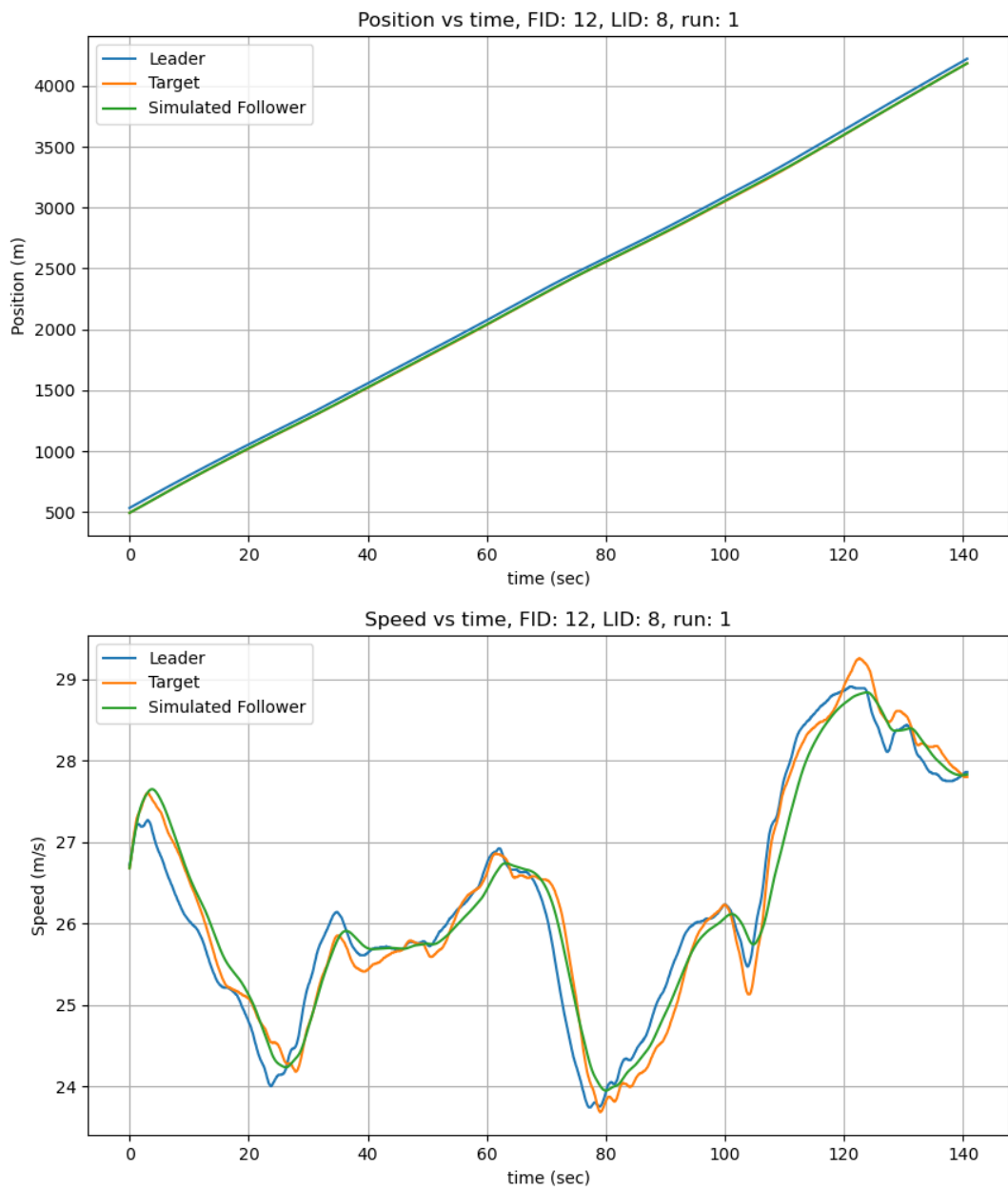


Figure 6.120: Position and speed for CSF for vehicle 12 in run 1 I294L1 dataset.

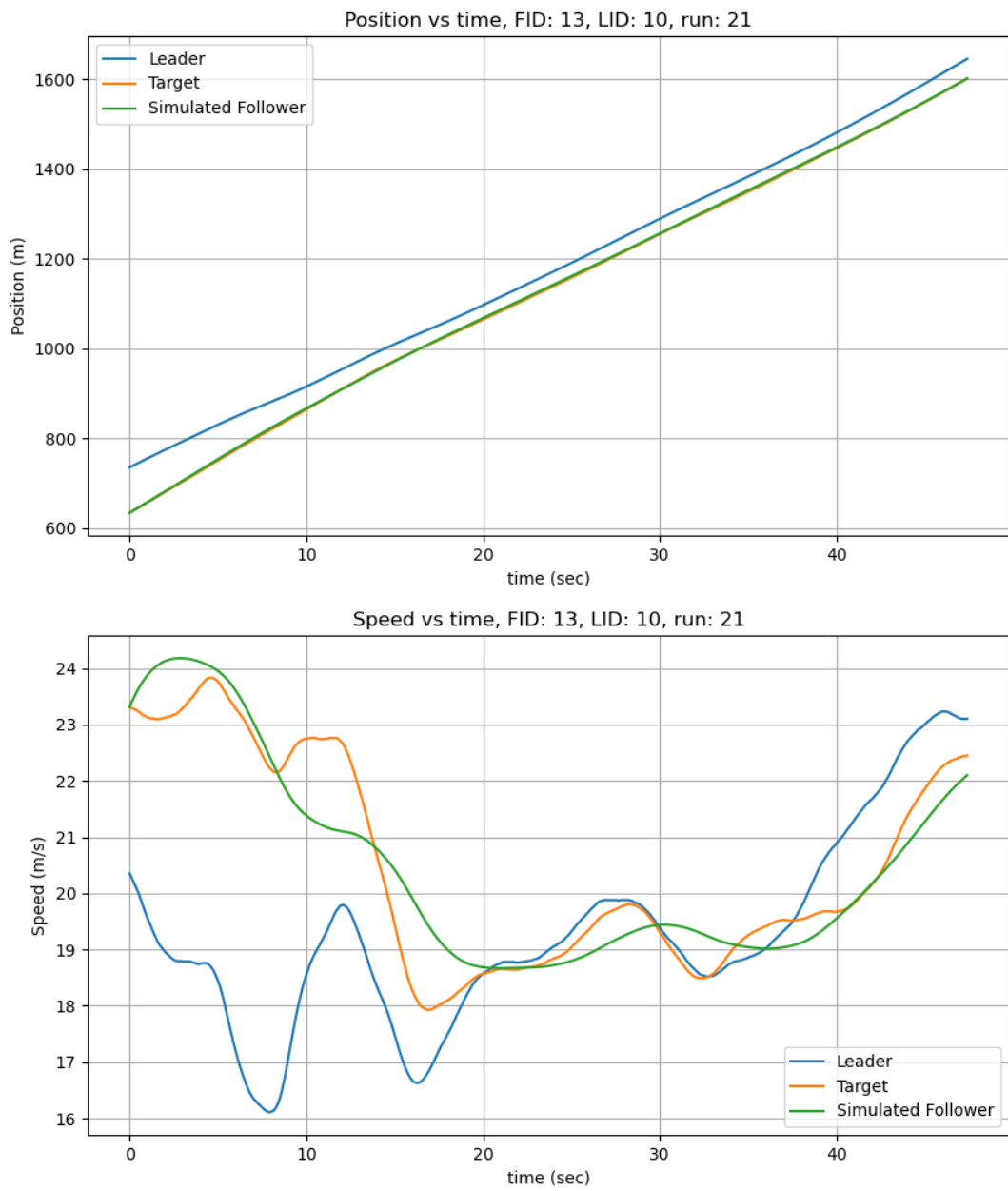


Figure 6.121: Position and speed for CSF for vehicle 13 in run 21 I294L1 dataset.

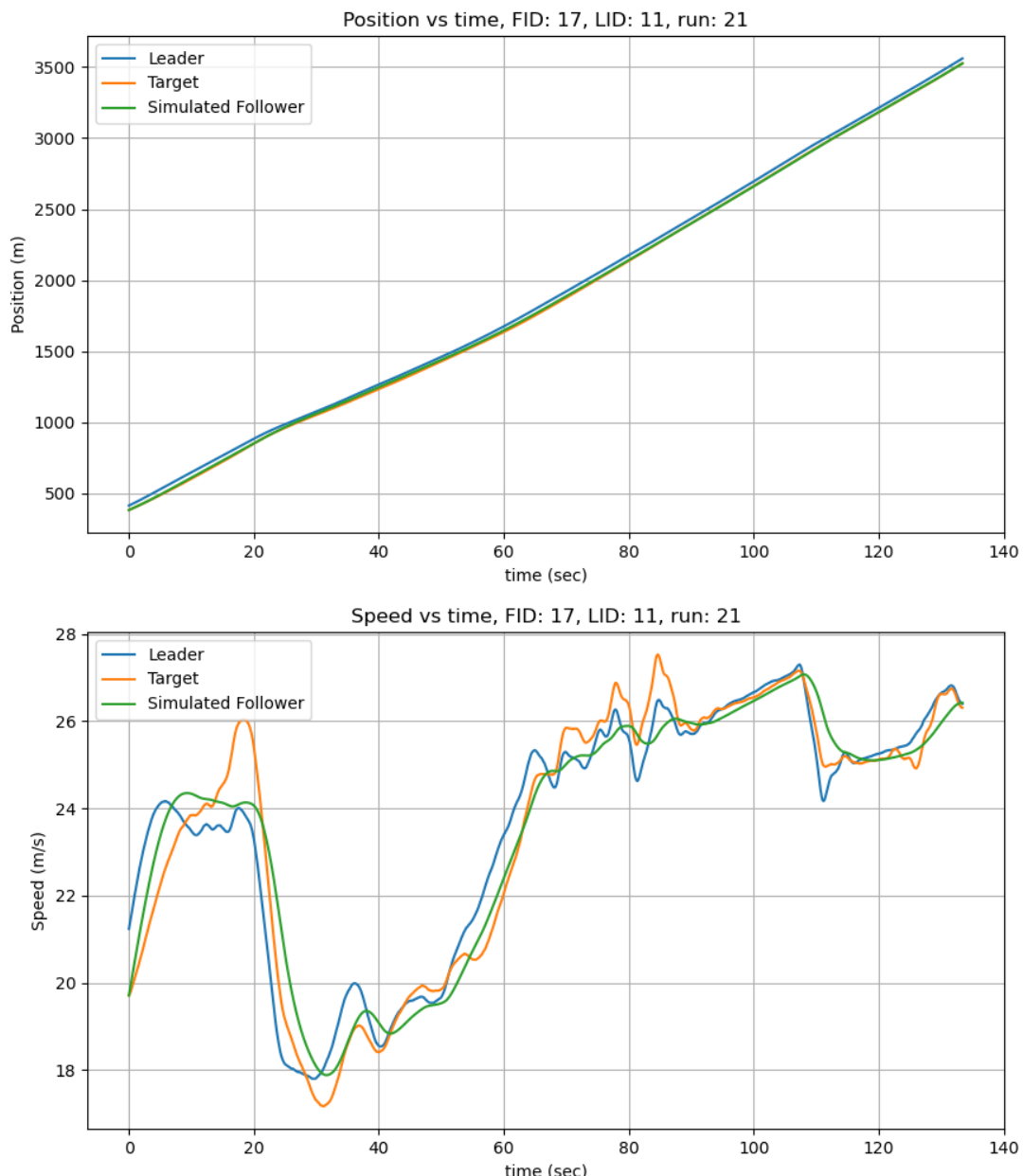


Figure 6.122: Position and speed for CSF for vehicle 17 in run 21 I294L1 dataset.

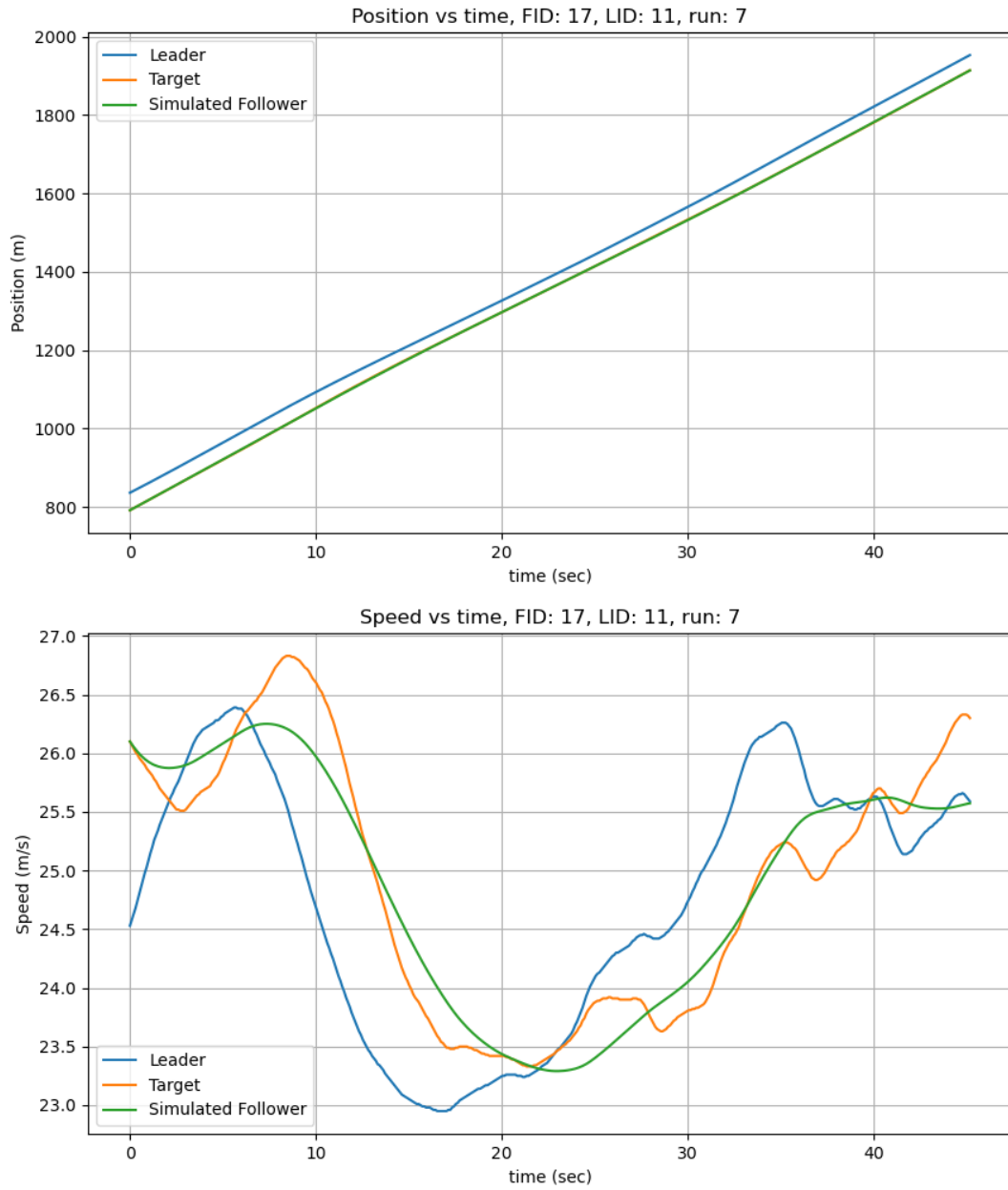


Figure 6.123: Position and speed for CSF for vehicle 17 in run 7 I294L1 dataset.

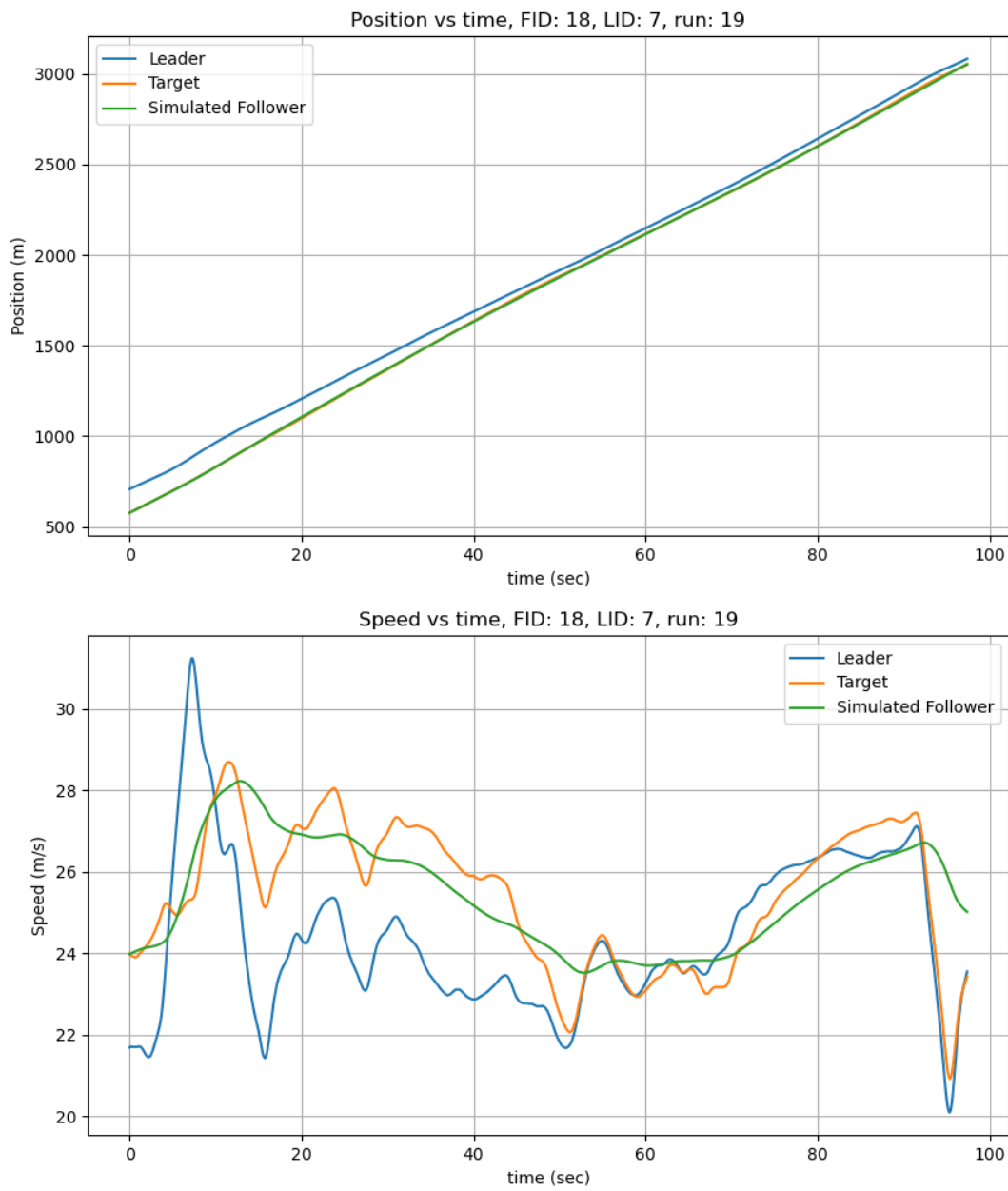


Figure 6.124: Position and speed for CSF for vehicle 18 in run 19 I294L1 dataset.

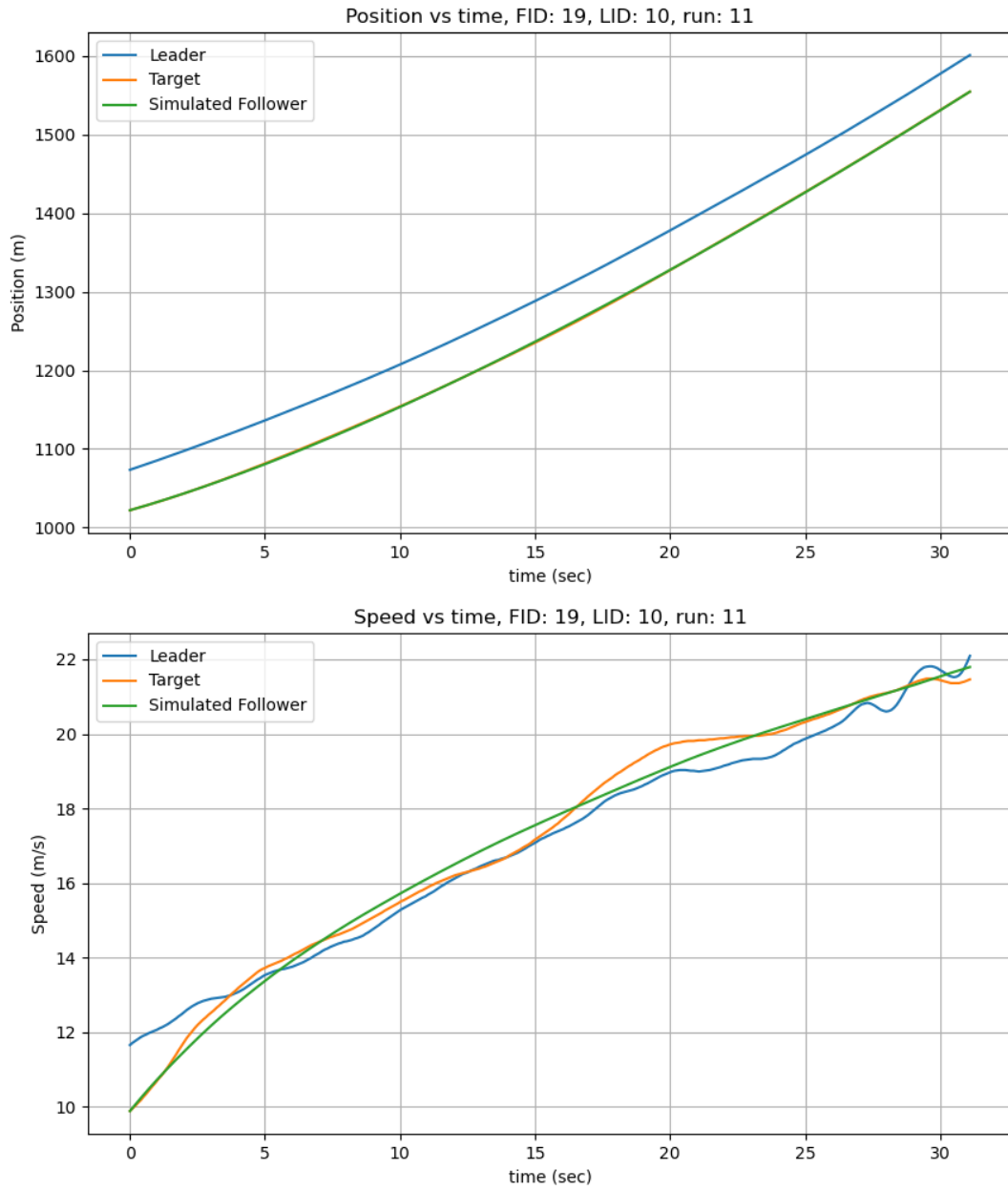


Figure 6.125: Position and speed for CSF for vehicle 19 in run 11 I294L1 dataset.

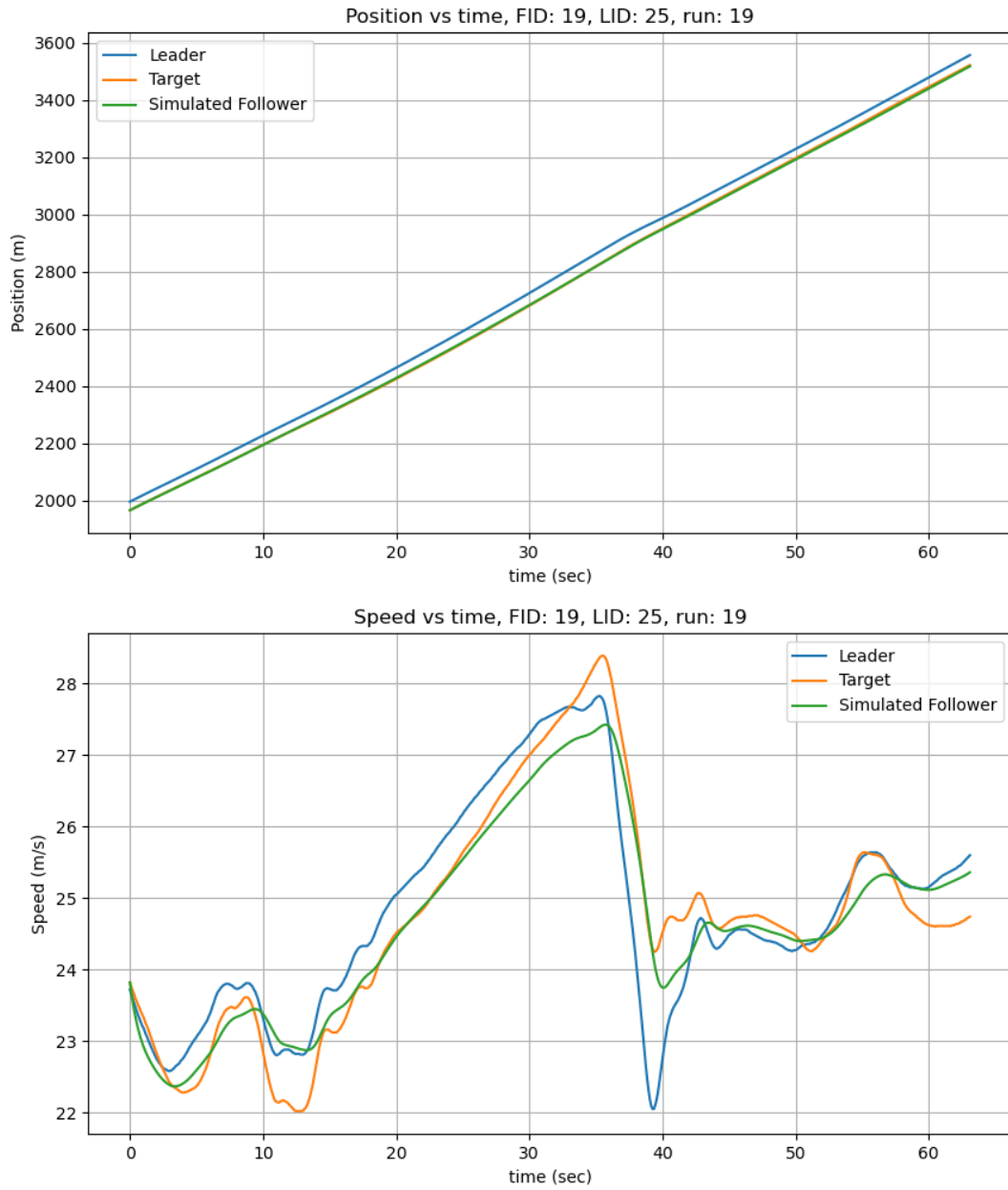


Figure 6.126: Position and speed for CSF for vehicle 19 in run 19 I294L1 dataset.

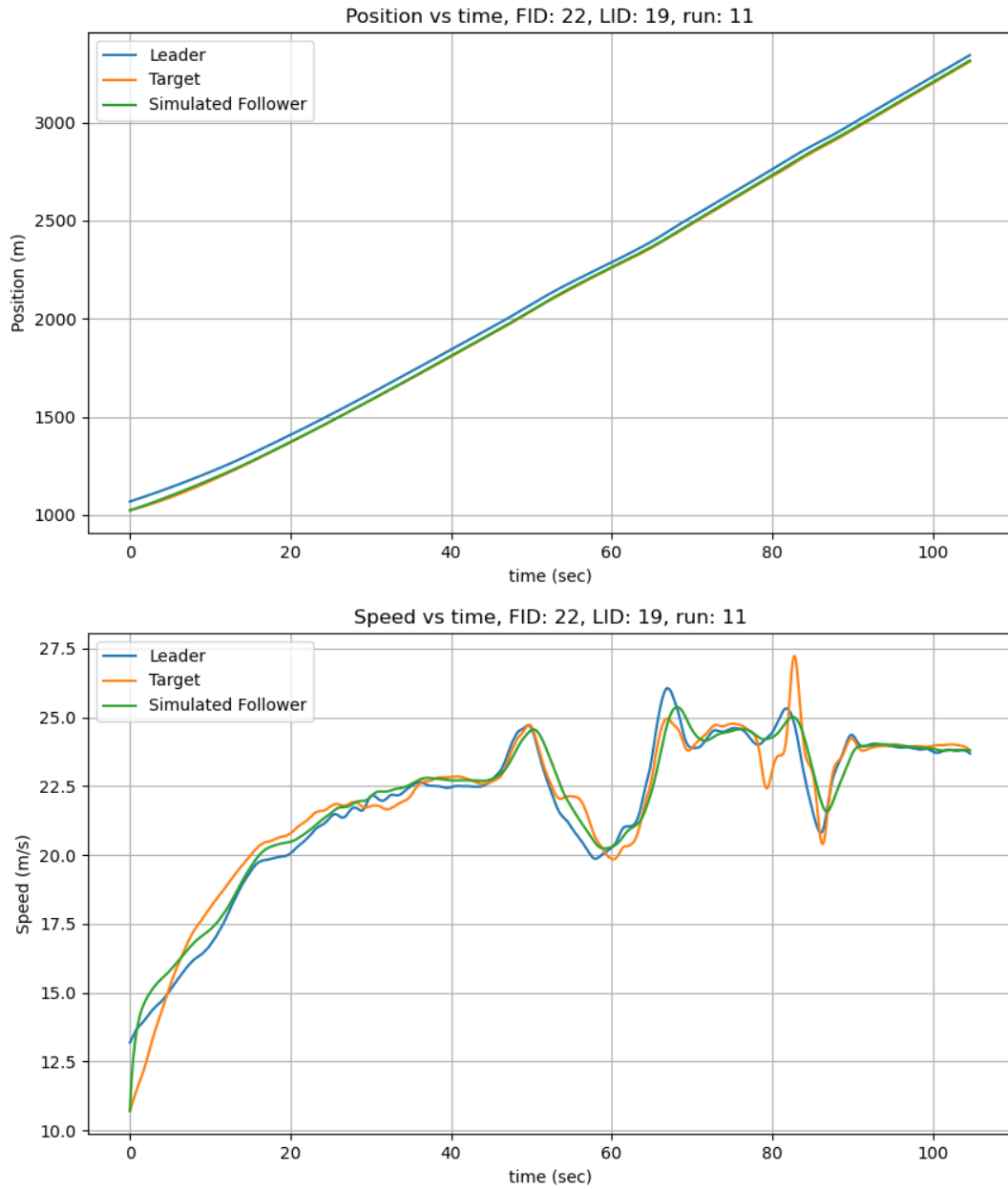


Figure 6.127: Position and speed for CSF for vehicle 22 in run 11 I294L1 dataset.

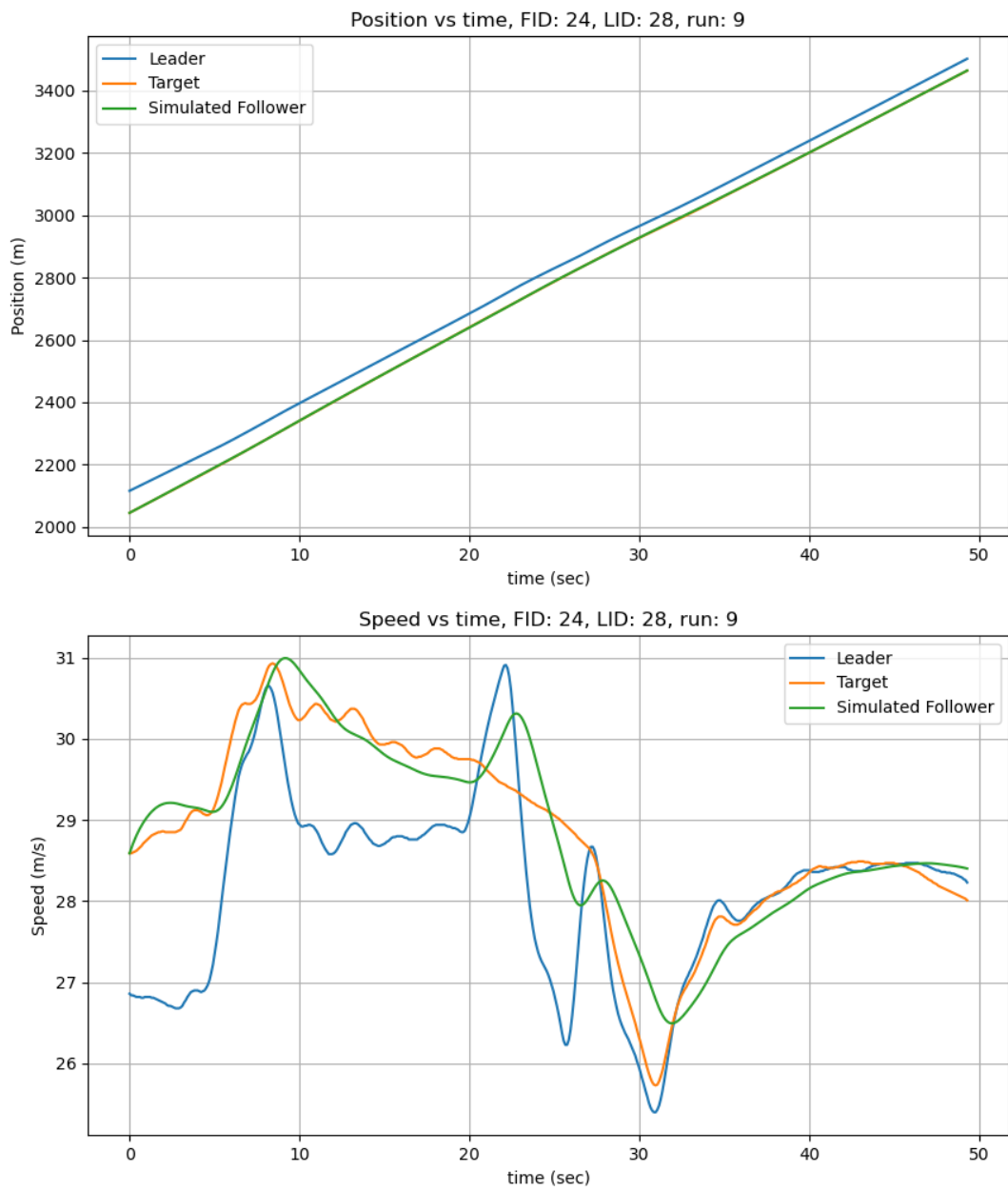


Figure 6.128: Position and speed for CSF for vehicle 24 in run 9 I294L1 dataset.

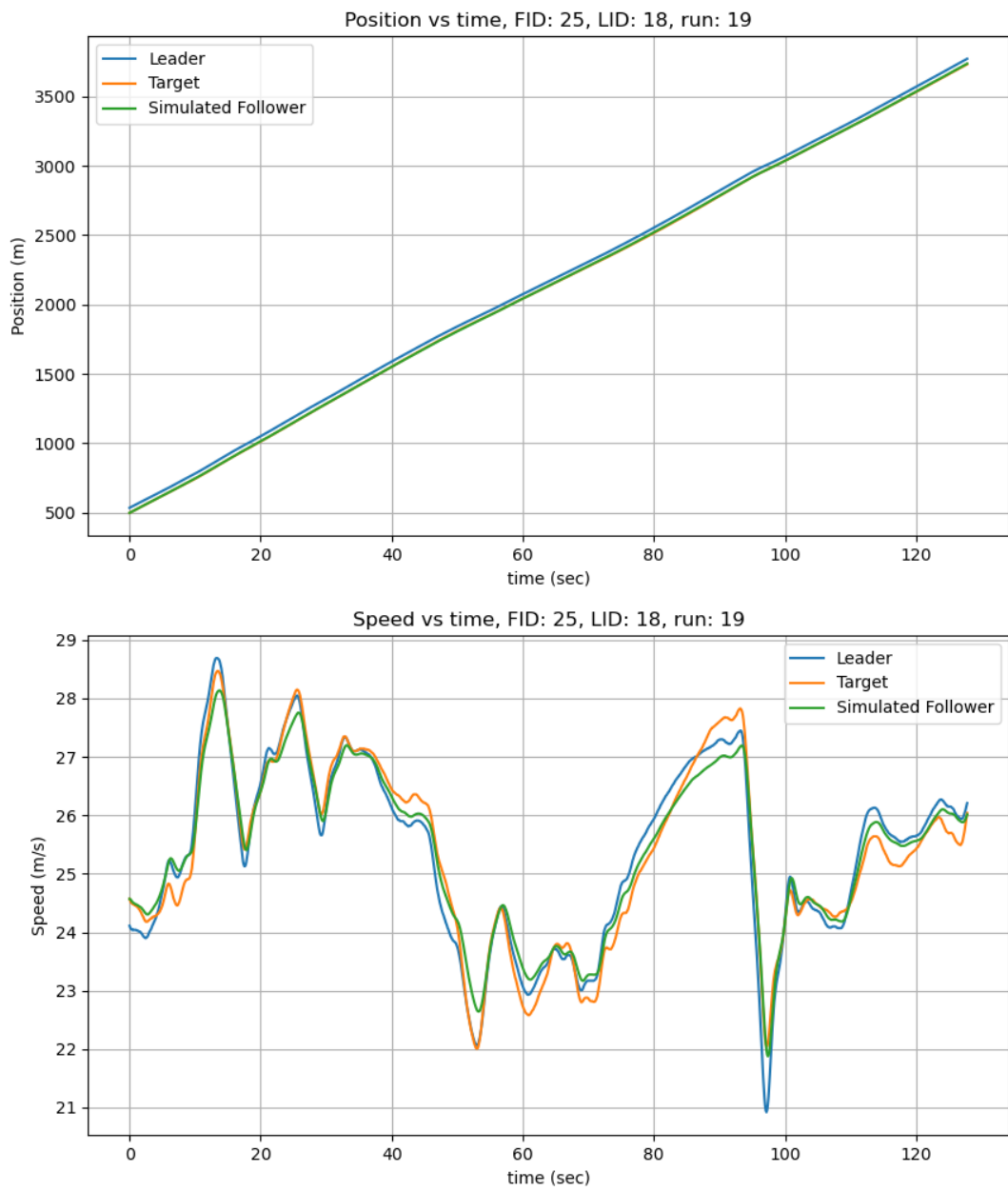


Figure 6.129: Position and speed for CSF for vehicle 25 in run 19 I294L1 dataset.

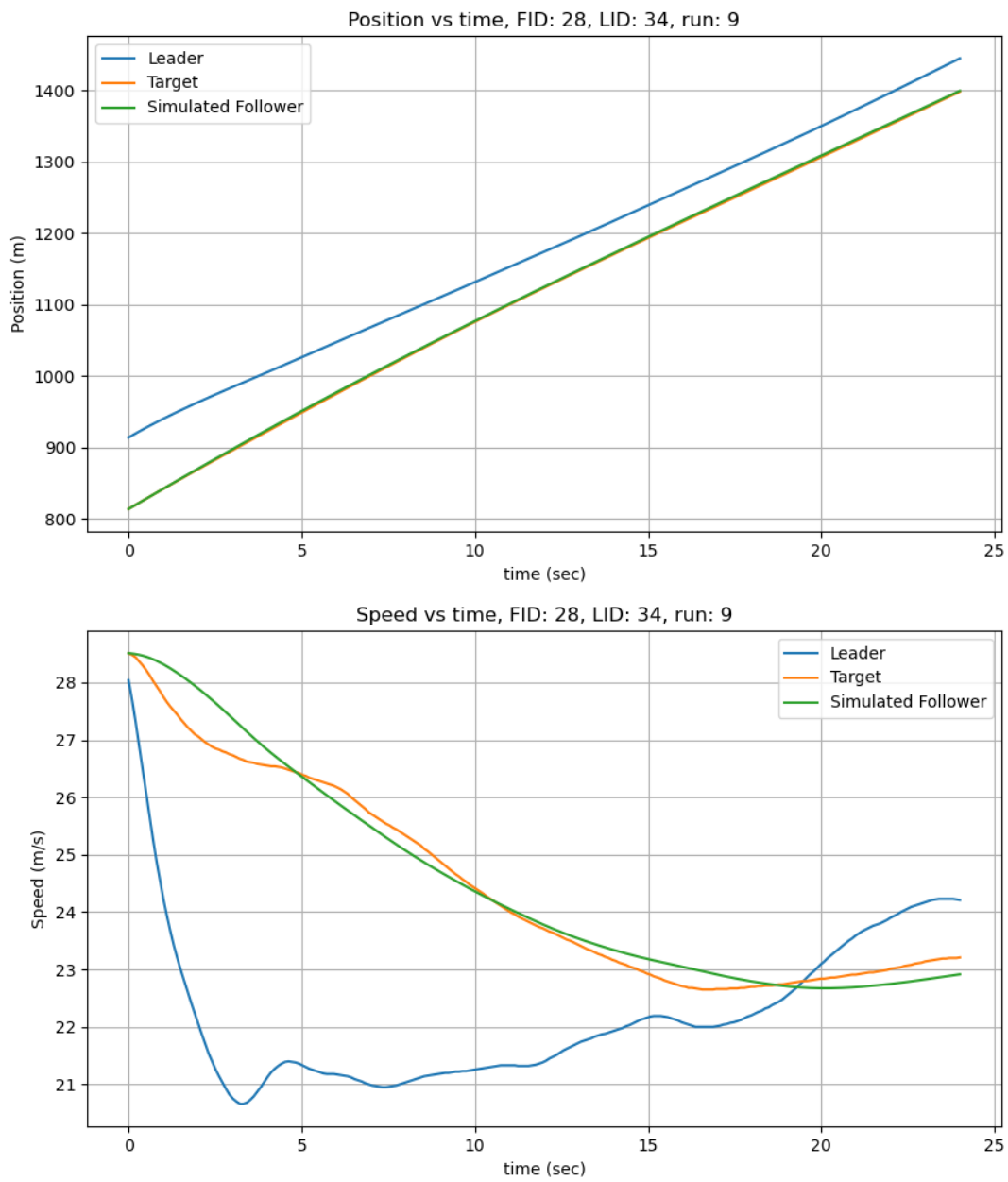


Figure 6.130: Position and speed for CSF for vehicle 28 in run 9 I294L1 dataset.

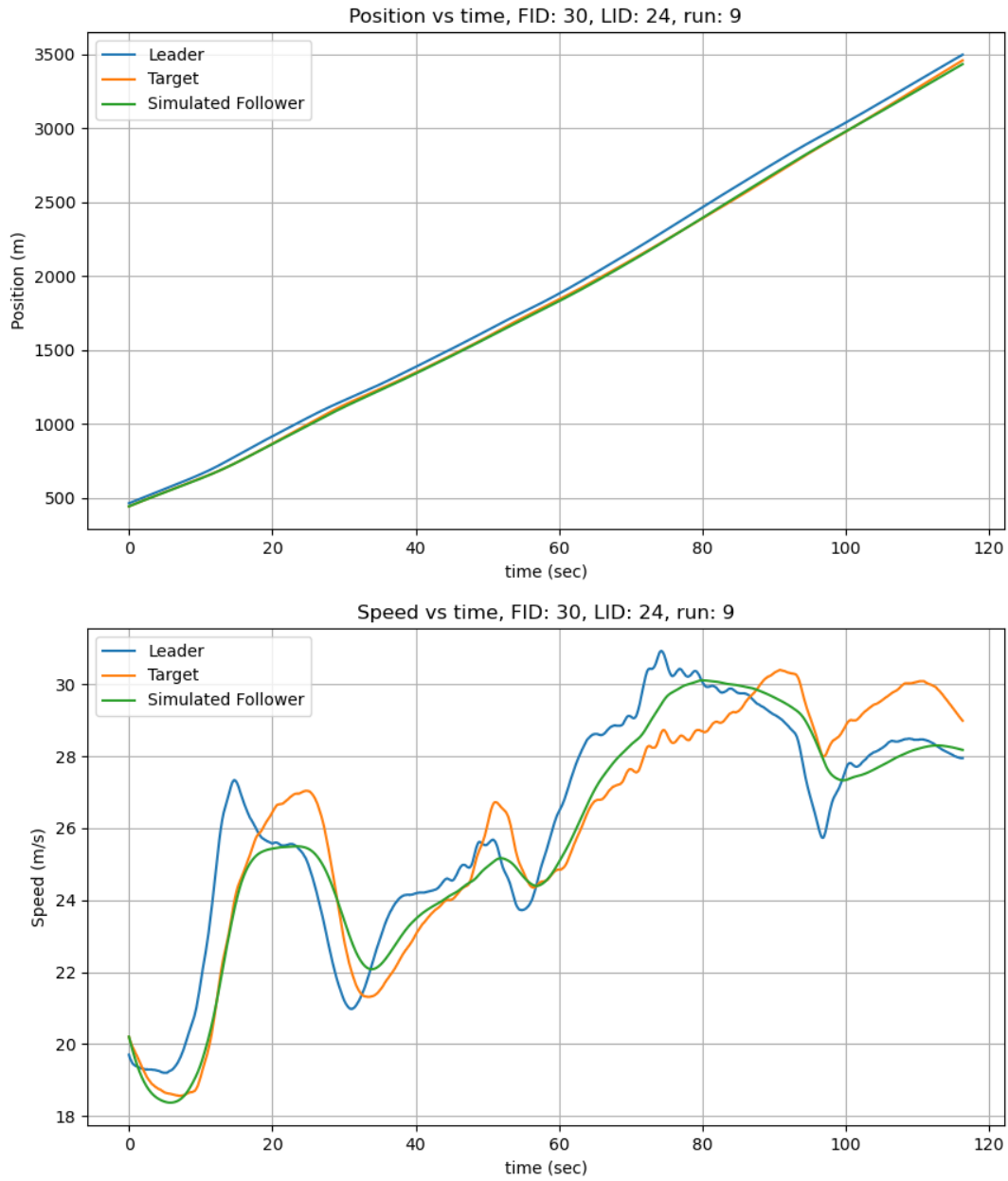


Figure 6.131: Position and speed for CSF for vehicle 30 in run 9 I294L1 dataset.

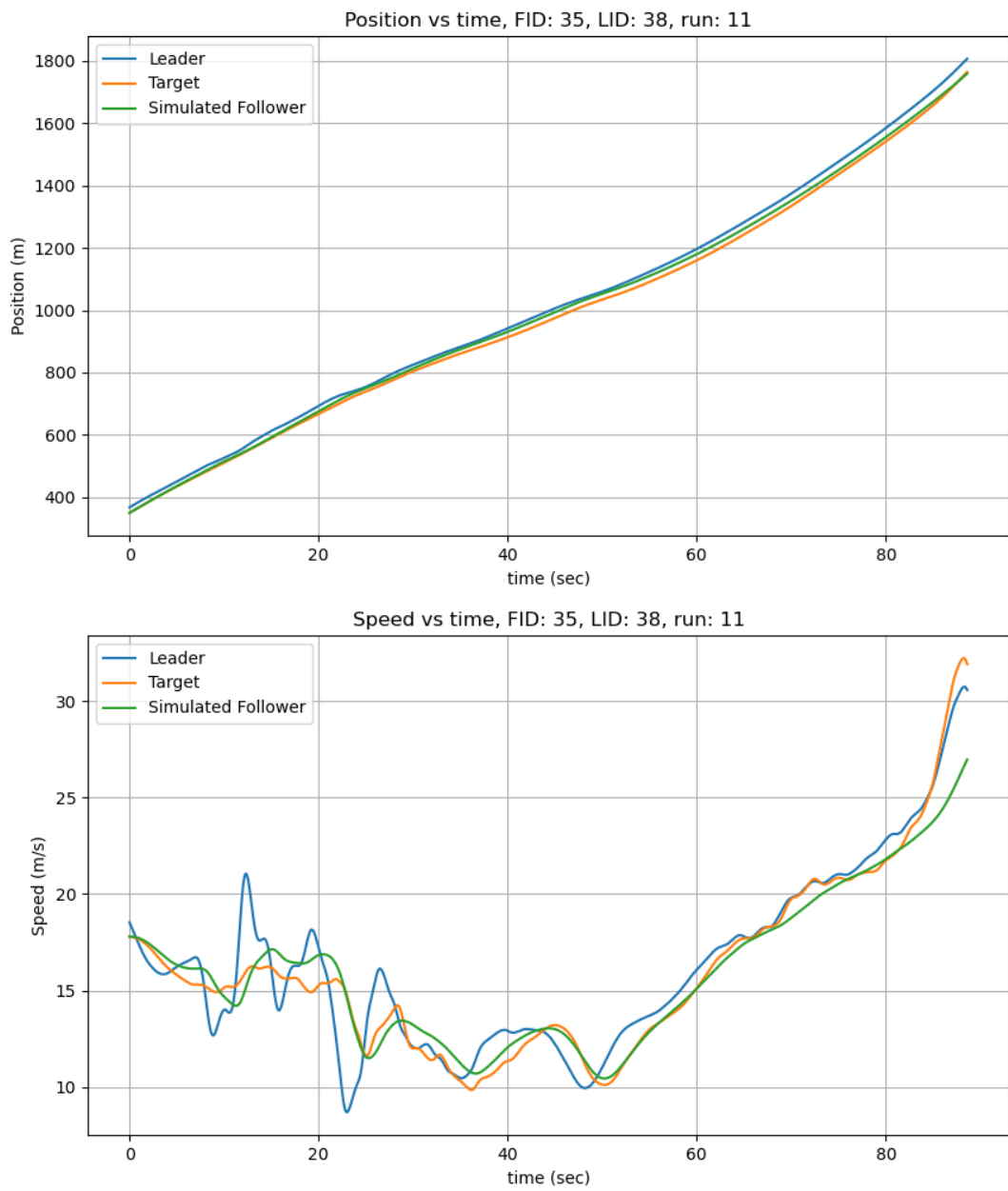


Figure 6.132: Position and speed for CSF for vehicle 35 in run 11 I294L1 dataset.

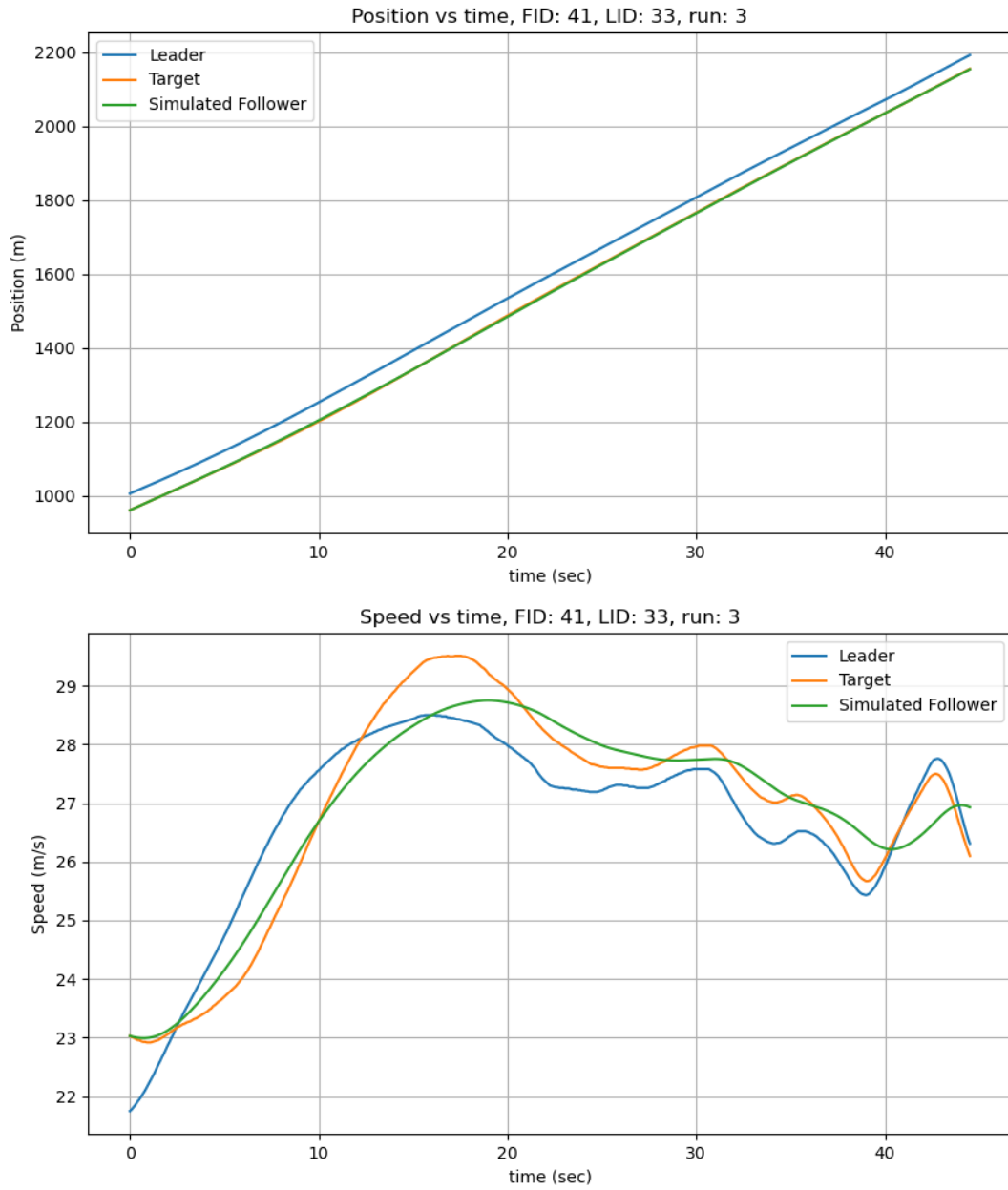


Figure 6.133: Position and speed for CSF for vehicle 41 in run 3 I294L1 dataset.

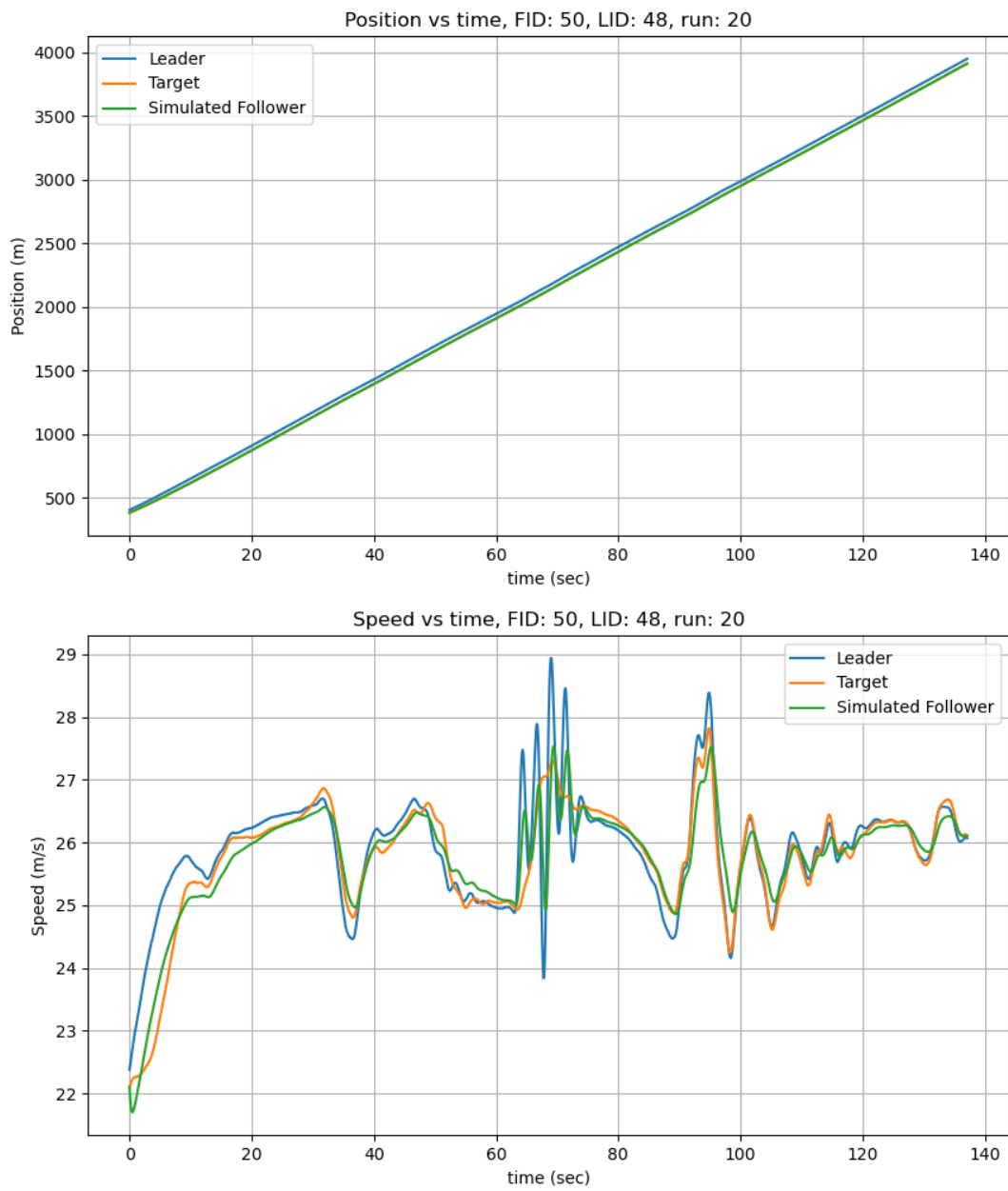


Figure 6.134: Position and speed for CSF for vehicle 50 in run 20 I294L1 dataset.

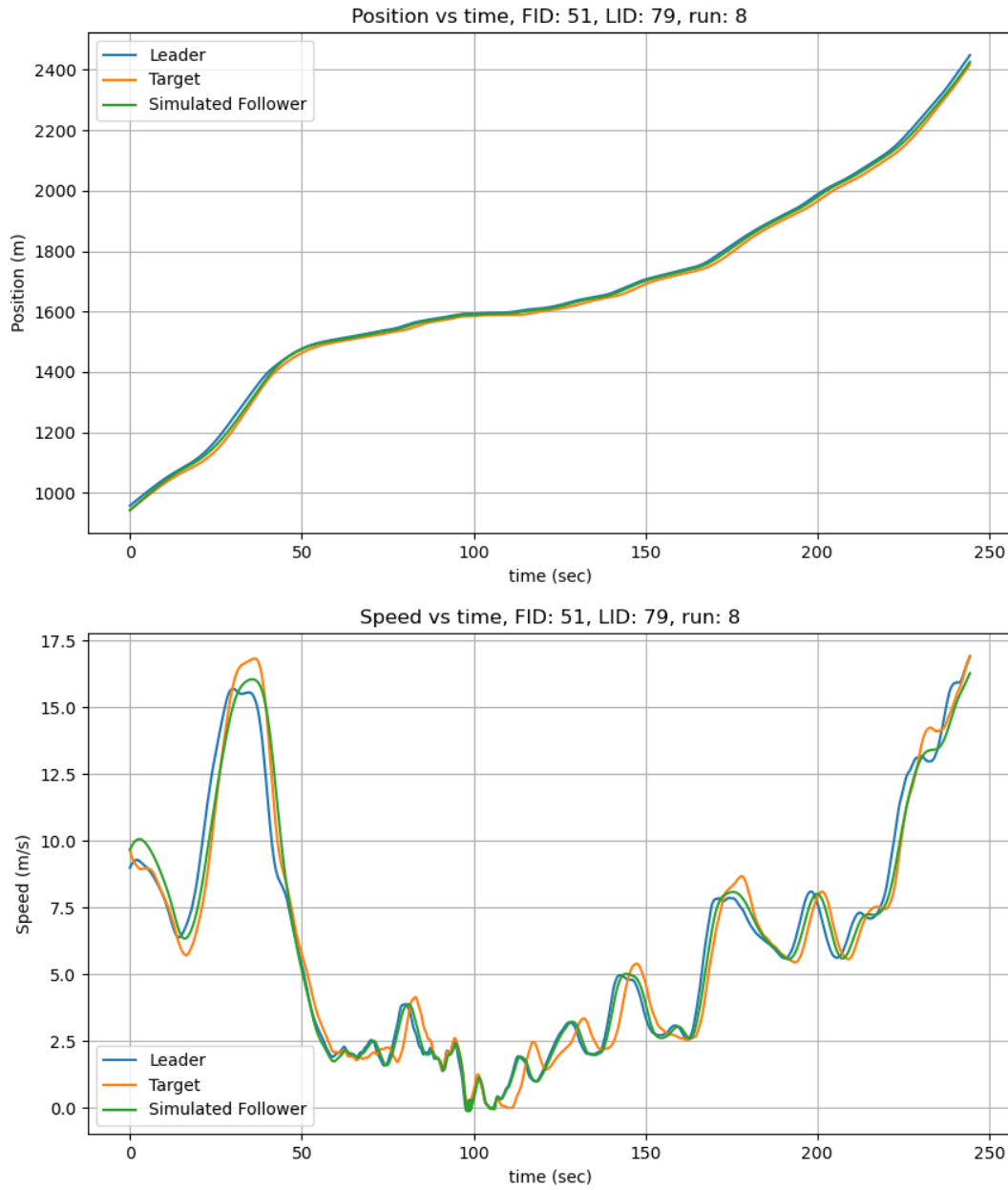


Figure 6.135: Position and speed for CSF for vehicle 51 in run 8 I294L1 dataset.

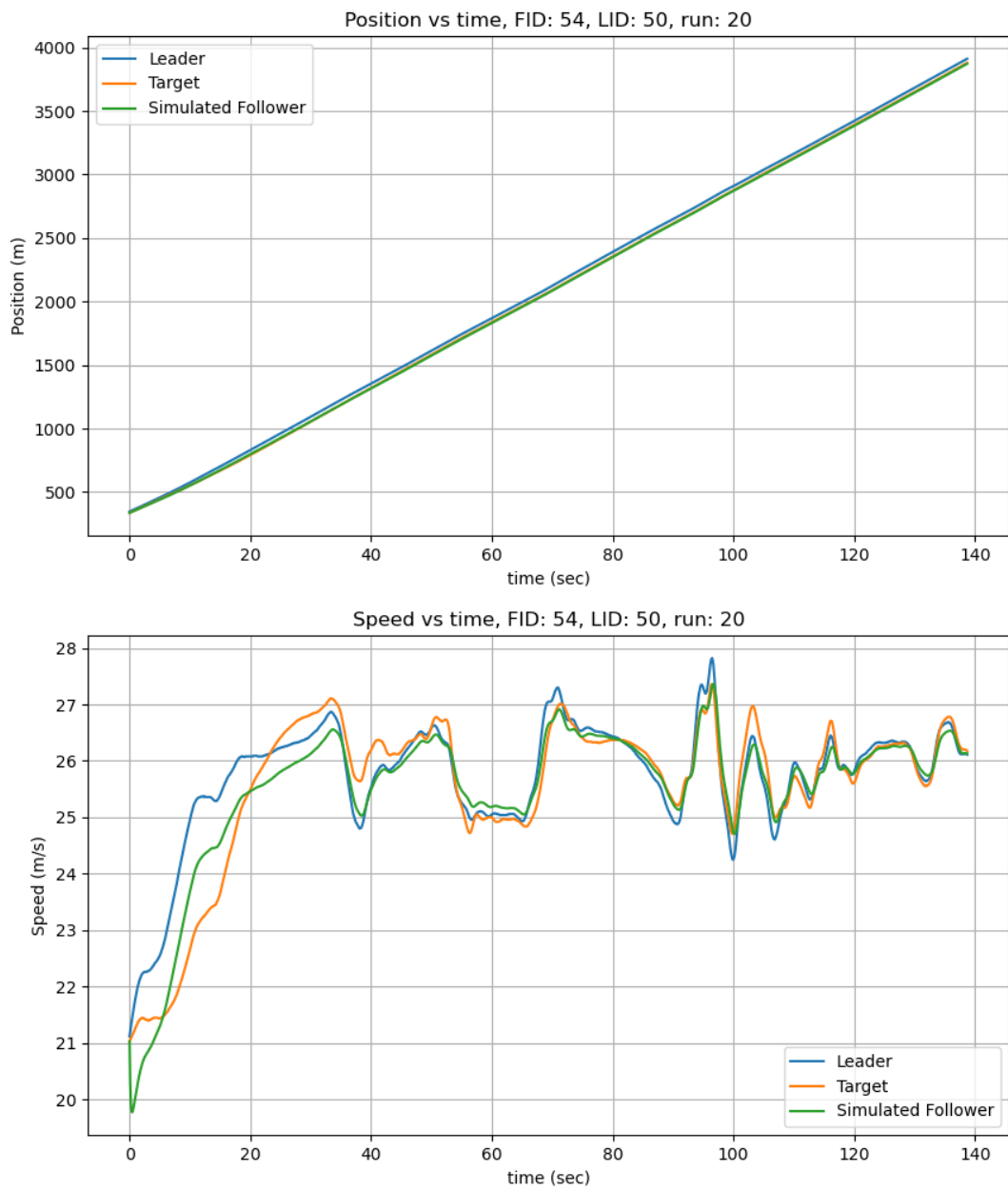


Figure 6.136: Position and speed for CSF for vehicle 54 in run 20 I294L1 dataset.

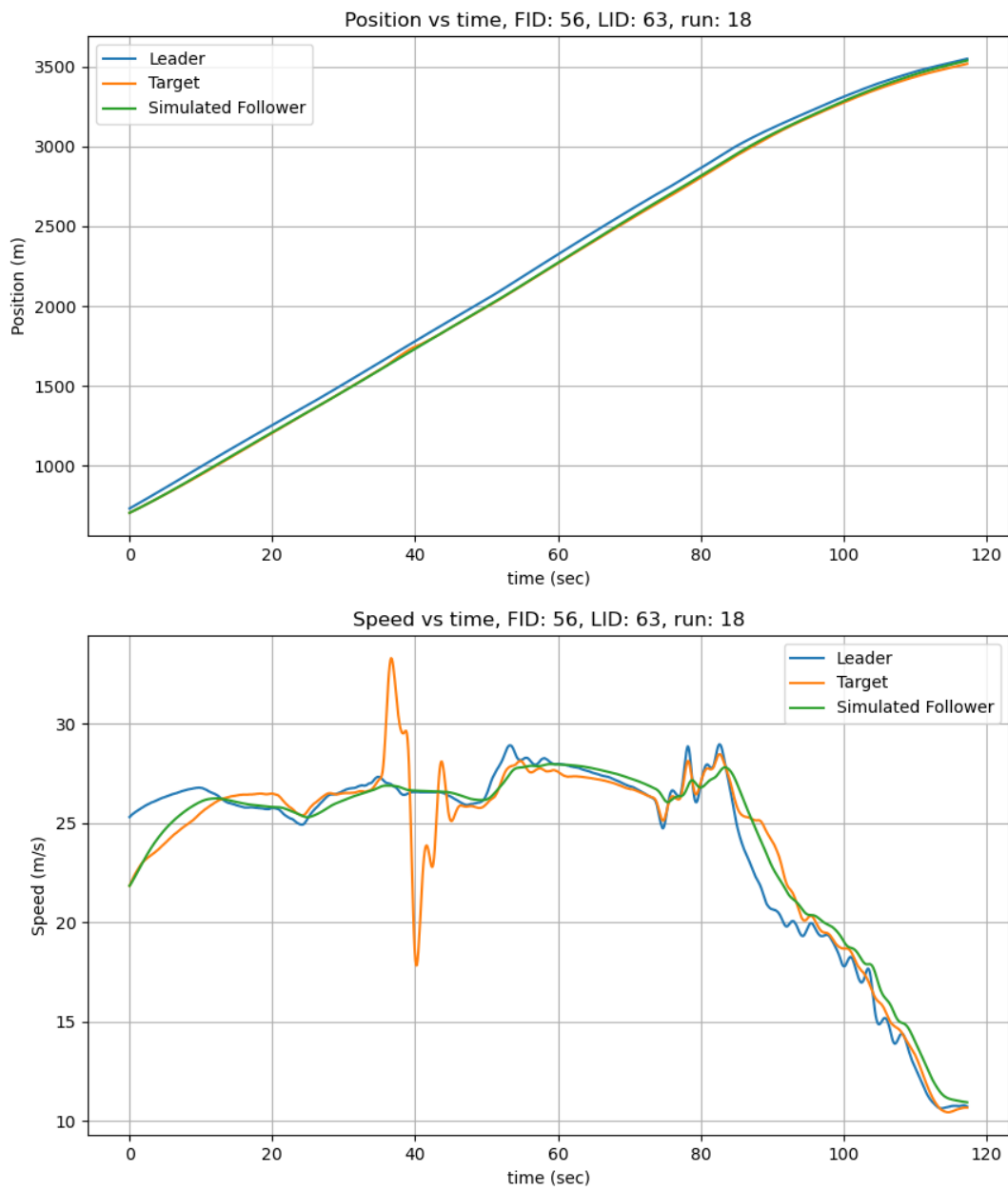


Figure 6.137: Position and speed for CSF for vehicle 56 in run 18 I294L1 dataset.

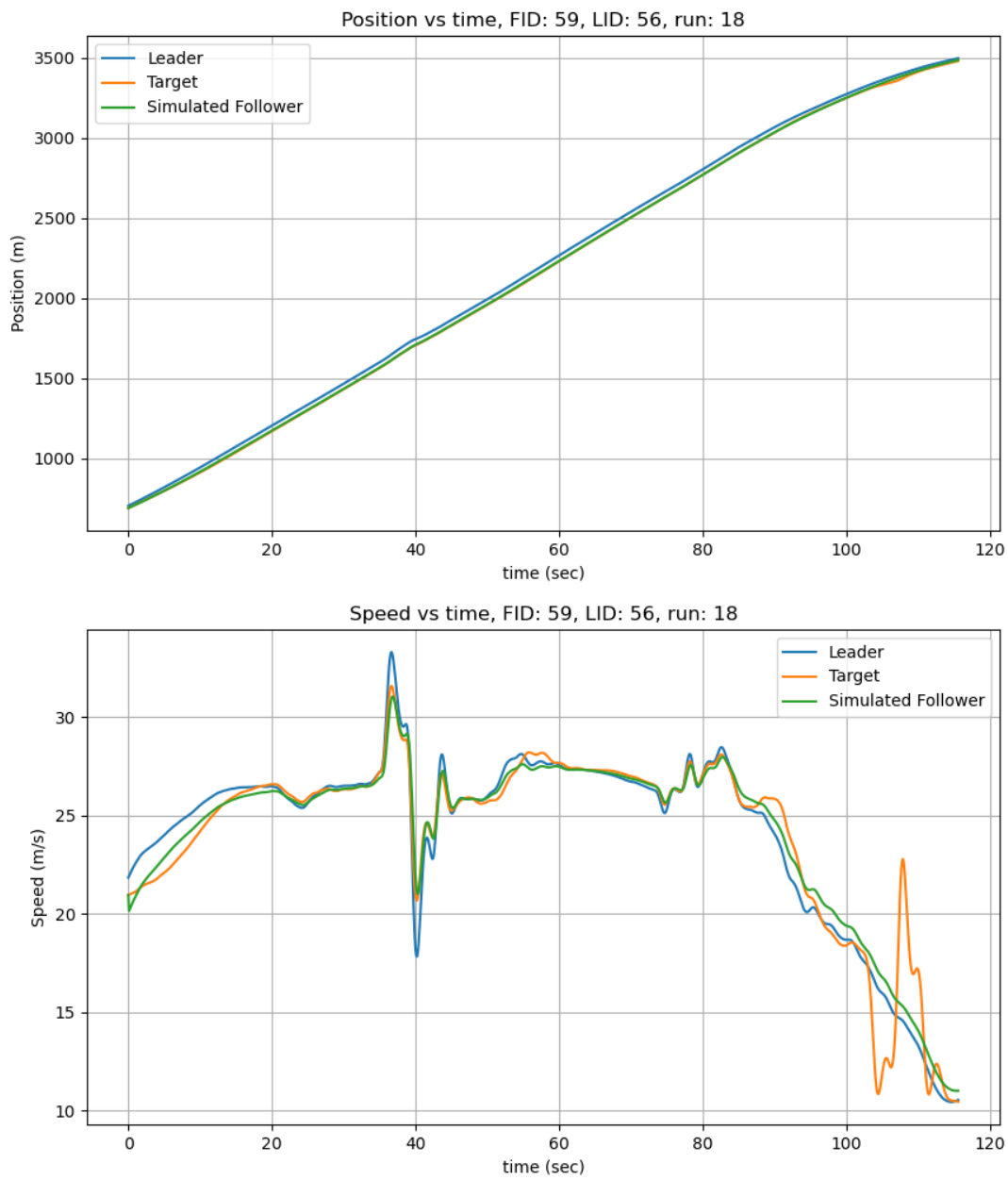


Figure 6.138: Position and speed for CSF for vehicle 59 in run 18 I294L1 dataset.

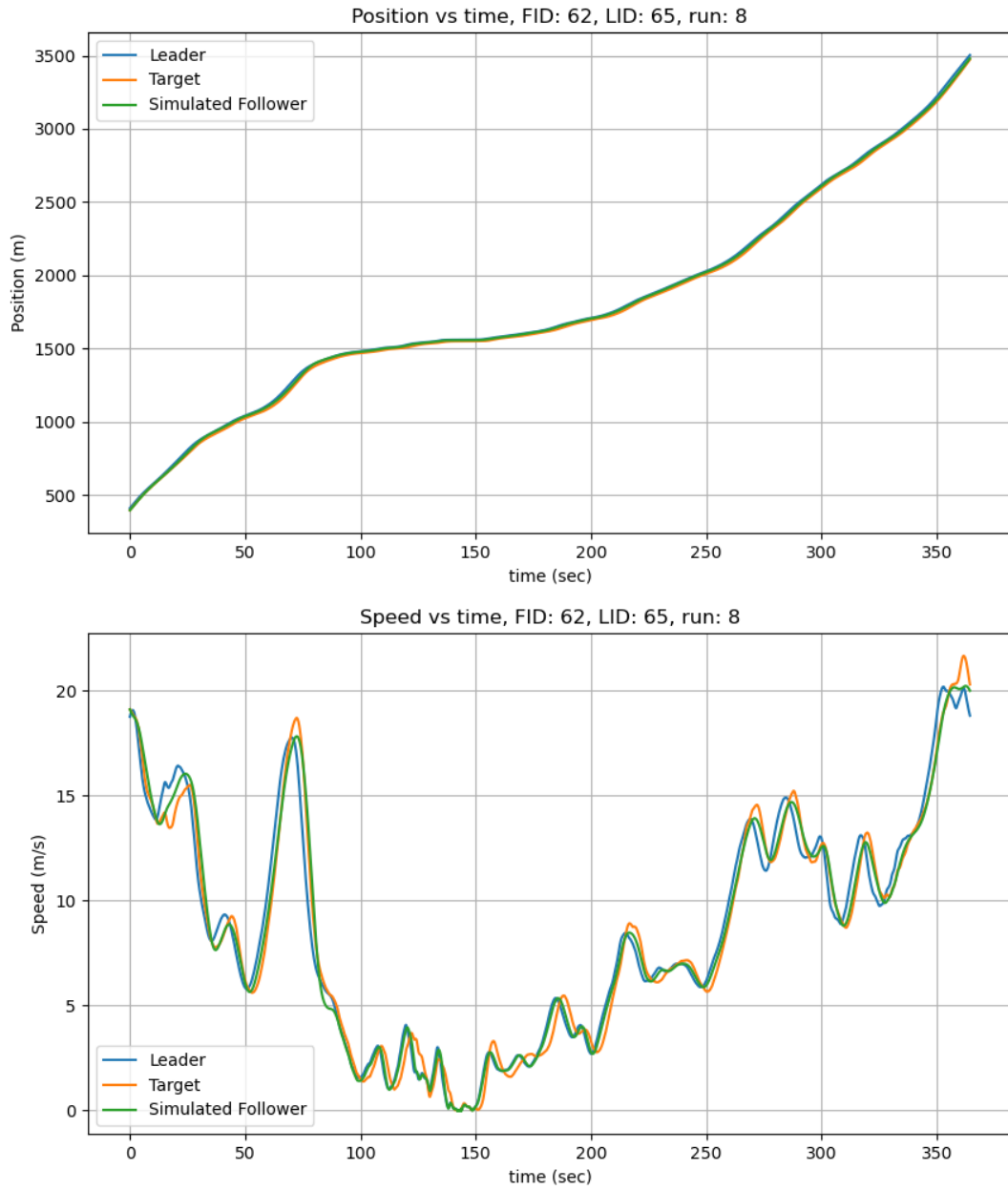


Figure 6.139: Position and speed for CSF for vehicle 62 in run 8 I294L1 dataset.

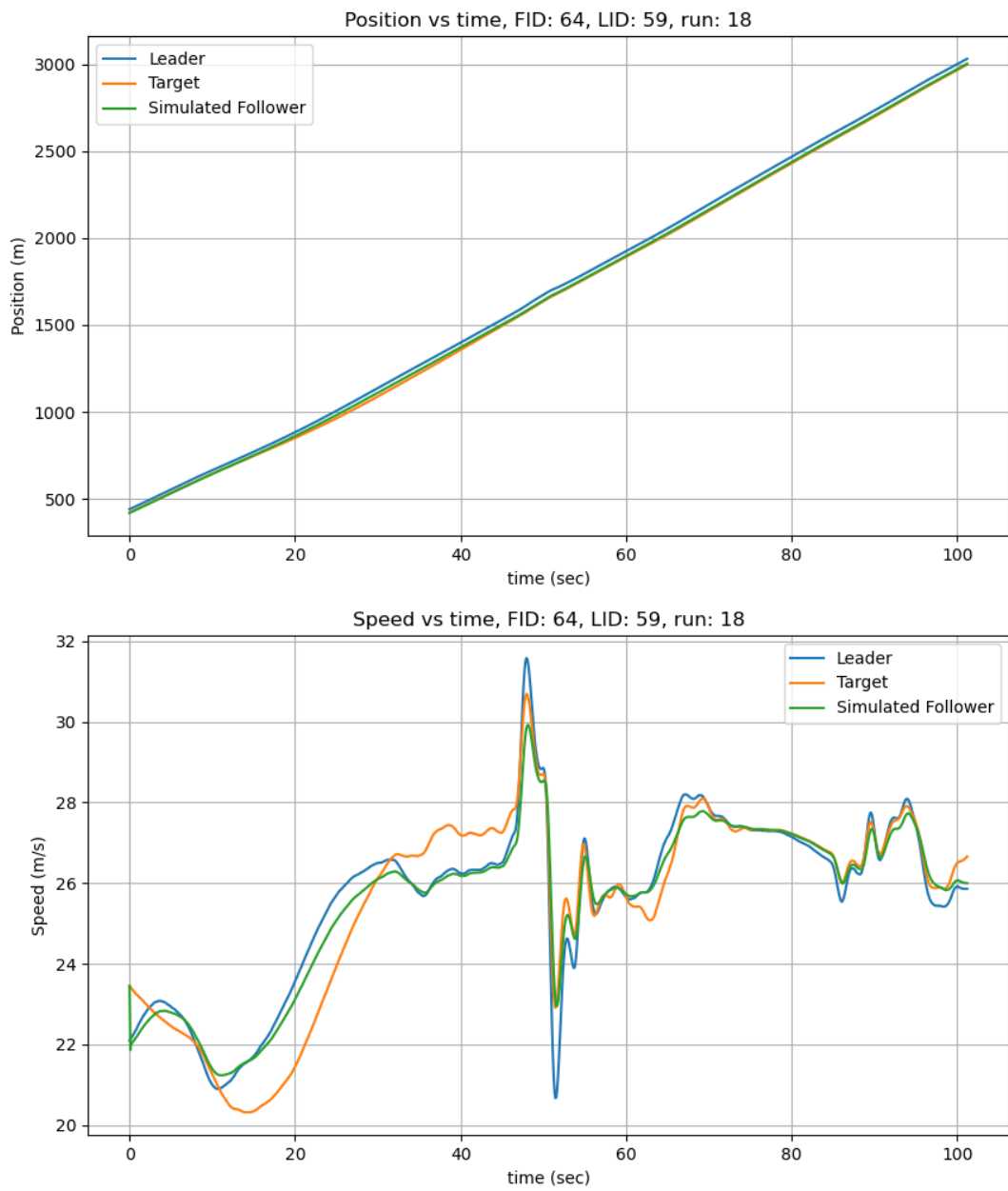


Figure 6.140: Position and speed for CSF for vehicle 64 in run 18 I294L1 dataset.

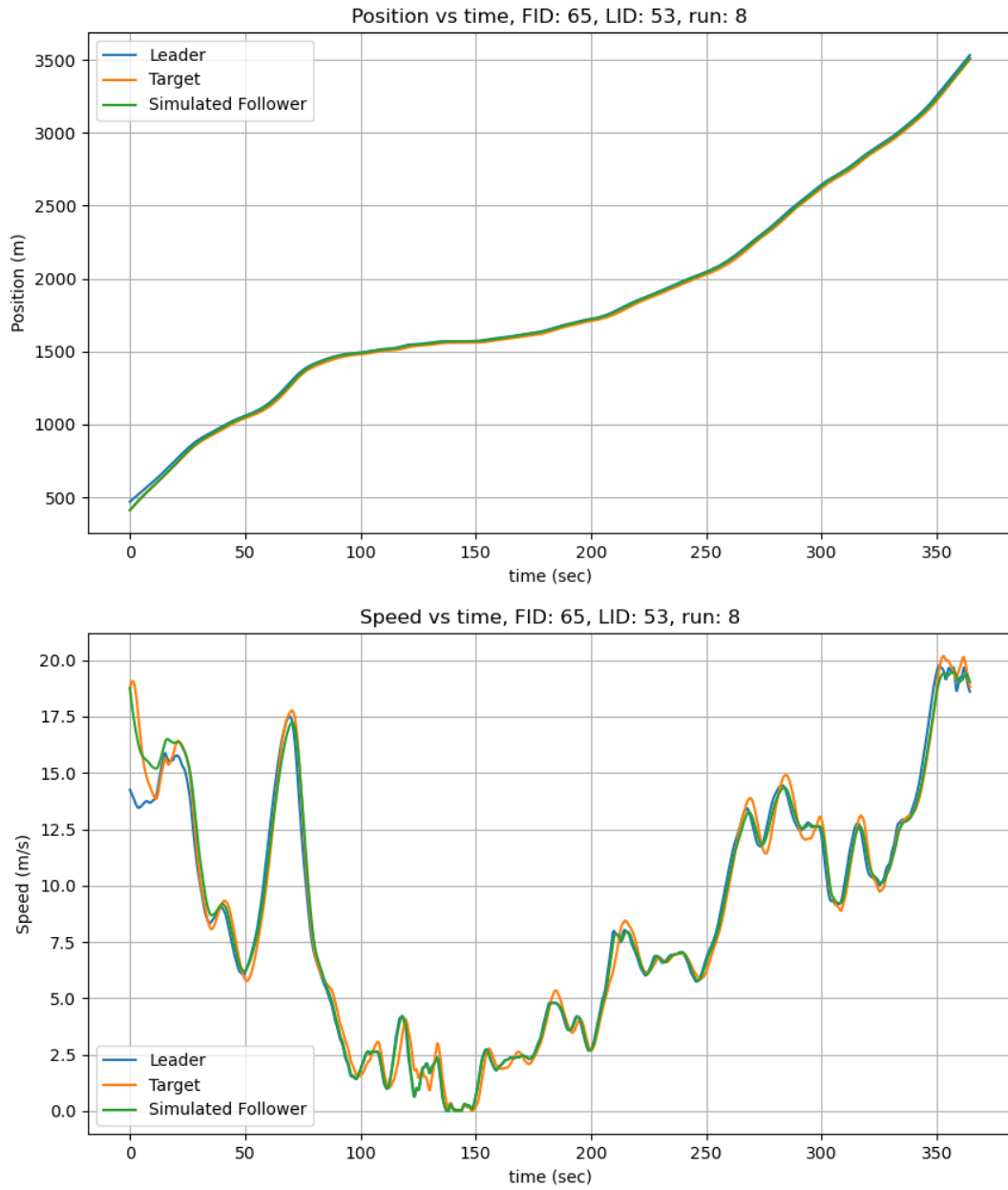


Figure 6.141: Position and speed for CSF for vehicle 65 in run 8 I294L1 dataset.

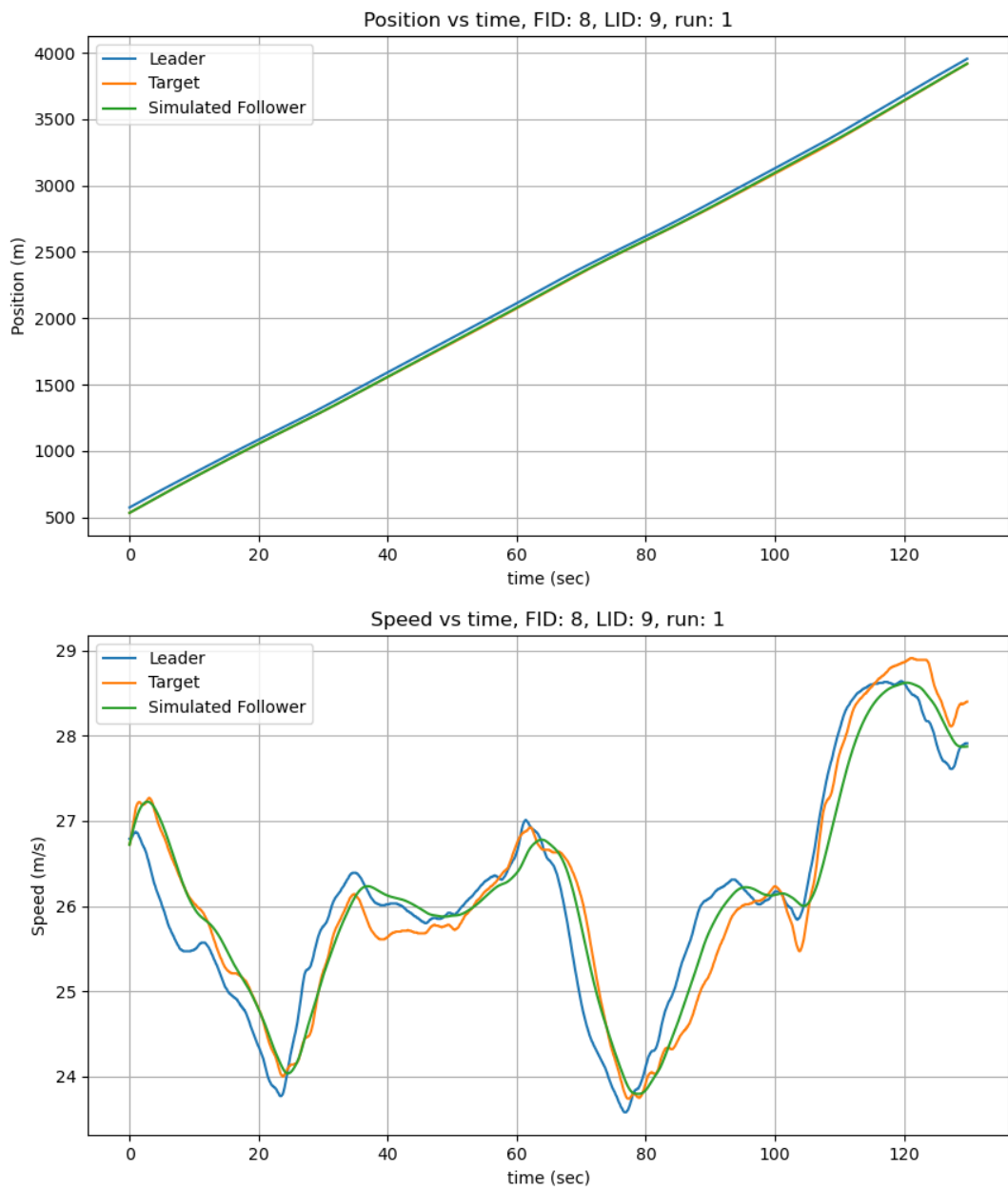


Figure 6.142: Position and speed for CSF for vehicle 8 in run 1 I294L1 dataset.

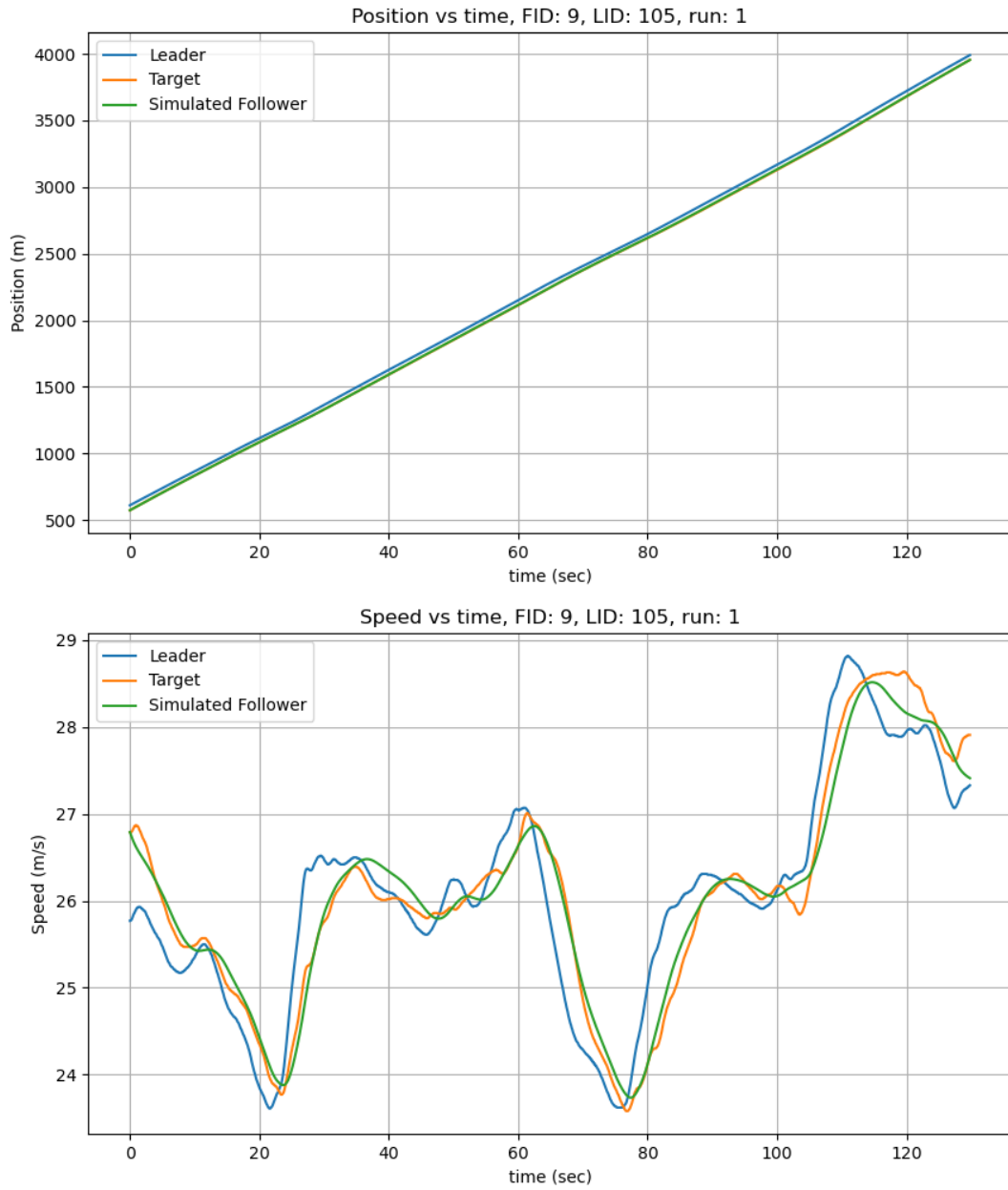


Figure 6.143: Position and speed for CSF for vehicle 9 in run 1 I294L1 dataset.

The optimized parameter ranges for the CSF model in the I294 dataset, as illustrated in Figure 6.144, shows significant variability across parameters. The parameter (d_{min}) has

the highest degree of variability, with a broad range, indicating that the minimum desired spacing fluctuates based on different traffic conditions. Conversely, (K) , (λ) , and (γ) has relatively narrower distributions. However, multiple outliers have been shown, suggesting that in certain calibration cases, the optimization process deviated from the primary values chosen.

Figure 6.145 shows that the distribution of (λ) is skewed to the right, with lower values appearing more frequently, indicating that most optimized solutions favor smaller stability coefficients. Similarly, the majority of (γ) values are concentrated near zero, implying that braking adjustments were not applied aggressively in the optimization process. Additionally, the multi-modal distributions observed for (d_{min}) and (K) suggest that multiple distinct parameter groupings exist, due to safety adjustments in response to varied traffic conditions.

The outliers in (K) , (λ) , and (γ) suggests occasional extreme parameter values, which may be the result of unusual traffic flow dynamics or specific cases where it was necessary for the TFS model to apply more aggressive control actions to maintain stability and safety. It is indicative that the outlier numeric values had to be used in response of the vehicle trying to adjust the unusual traffic condition to ensure safety in driving.

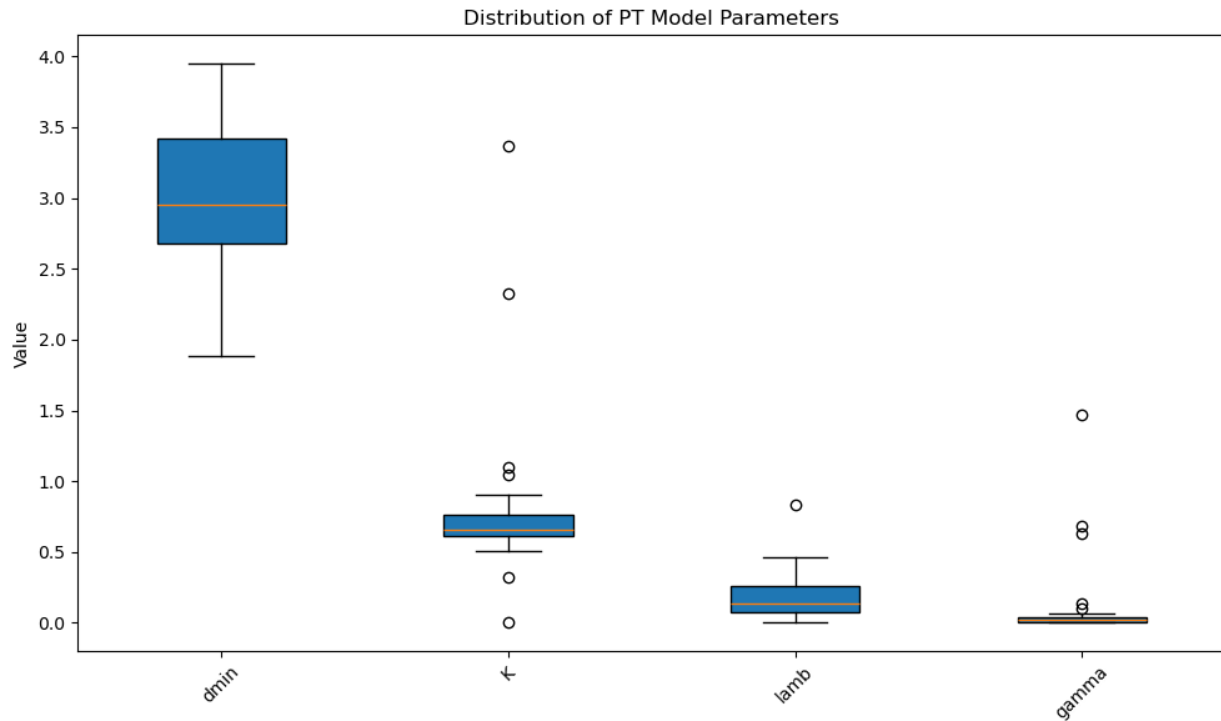


Figure 6.144: Parameter ranges for CSF in I294L1 dataset.

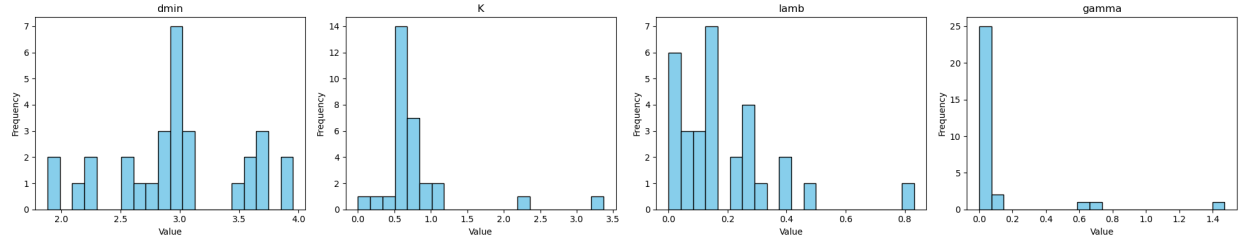


Figure 6.145: Parameter histogram for CSF in I294L1 dataset.

6.2.11 CSF I90/94 Simulated Results

The simulated results for I90/94 are presented in Figures 6.146 6.147, and 6.148 using the CSF Policy. For vehicle 5366 and 195, it can be determined that the controller can track the position with minimum speed pattern deviations shown in Figures 6.146 and 6.147. However, there is a minor deviation with speed patterns for vehicle 286 shown in Figure 6.148 although the simulated position closely aligns with the target position.

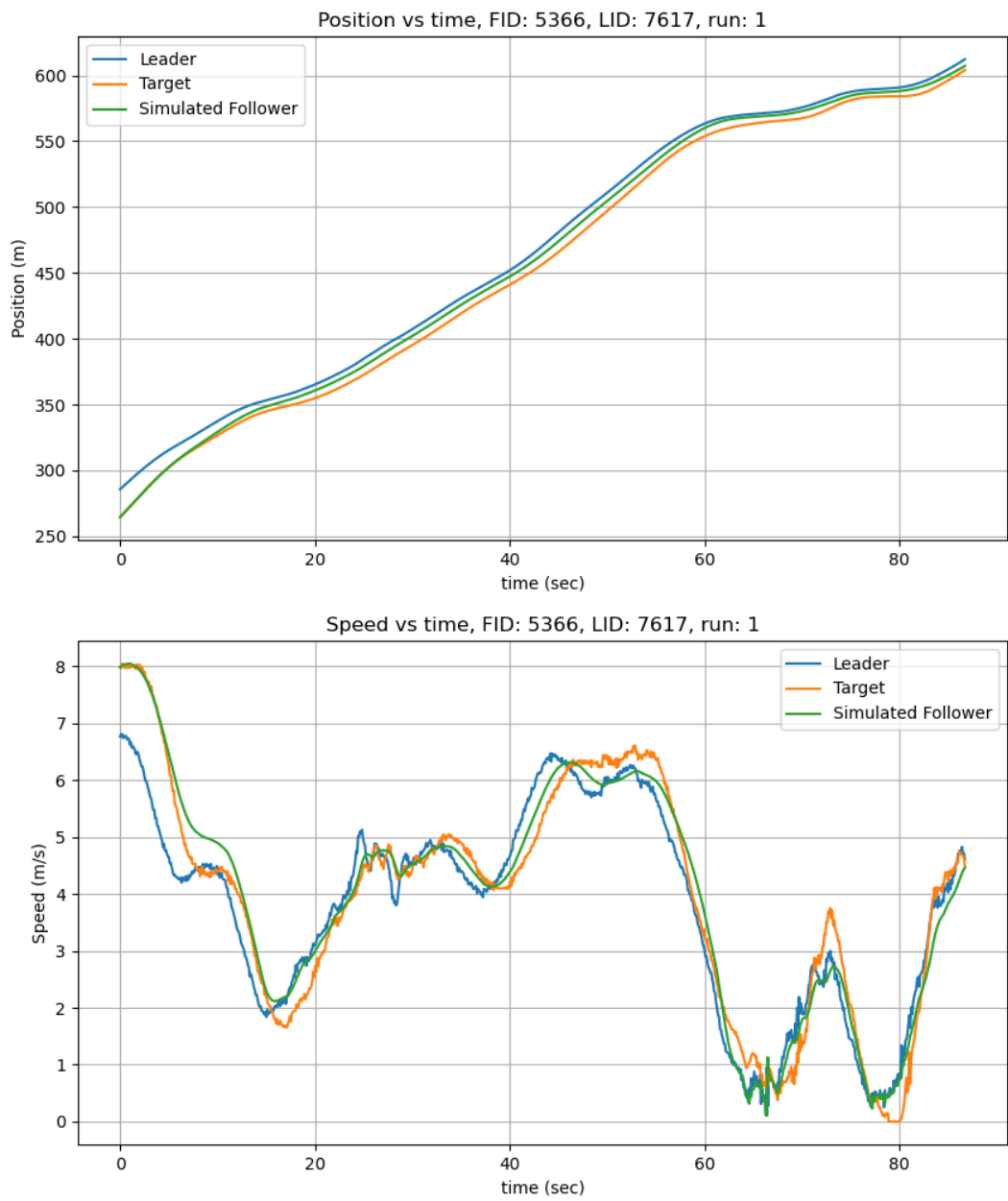


Figure 6.146: Position and speed for CSF for vehicle 5366 in I90/94 dataset.

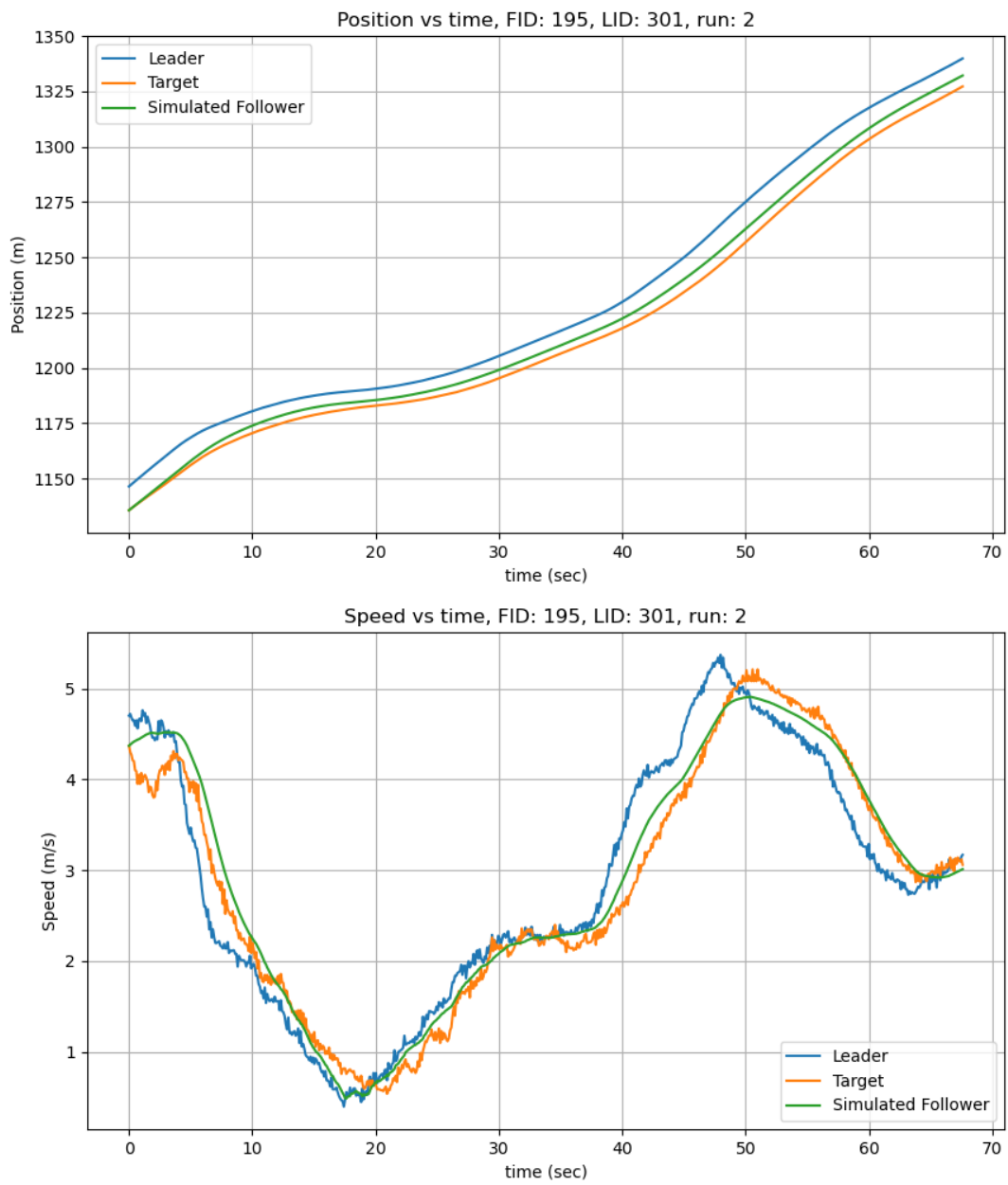


Figure 6.147: Position and speed for CSF for vehicle 195 in I90/94 dataset.

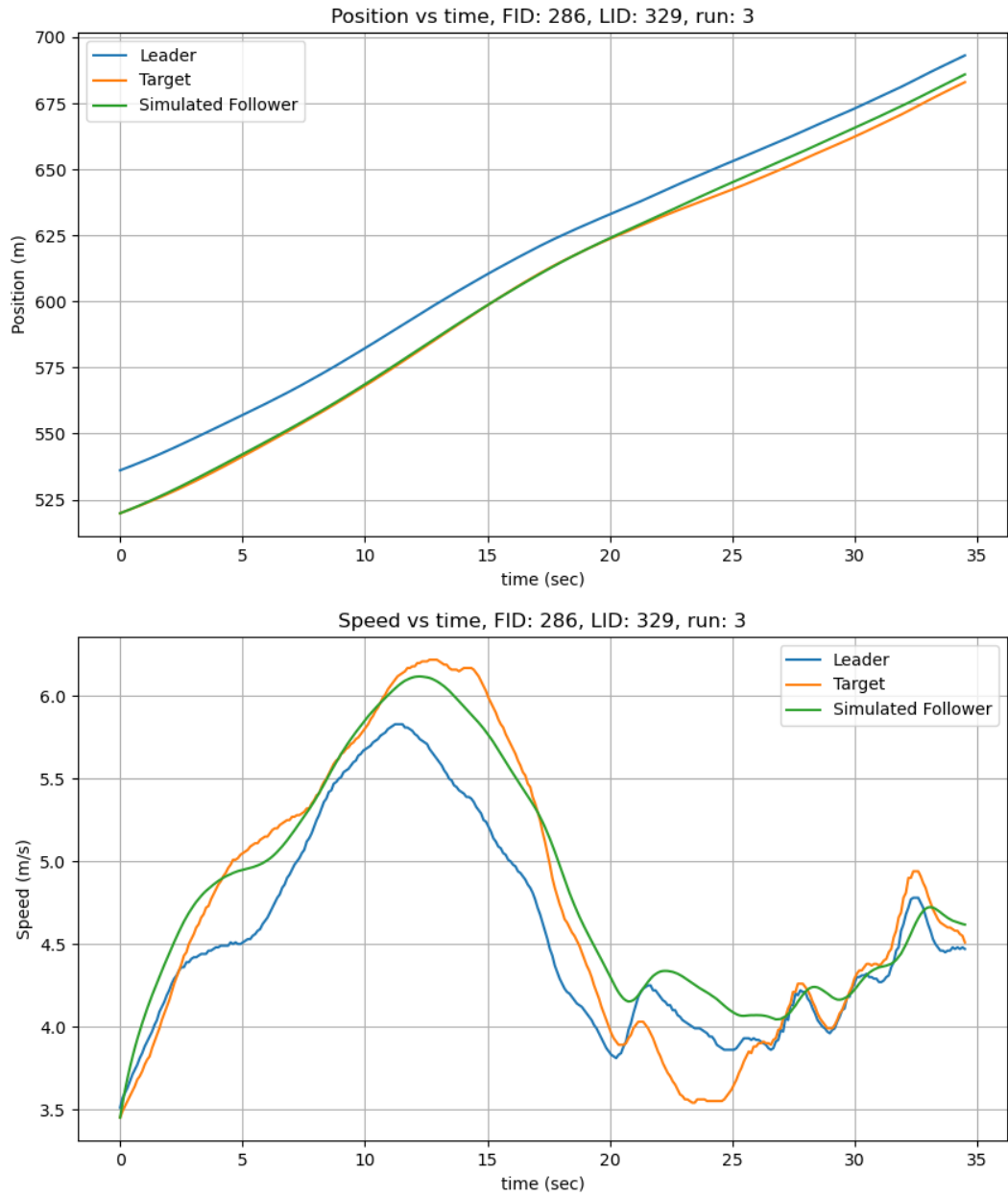


Figure 6.148: Position and speed for CSF for vehicle 286 in I90/94 dataset.

The optimized parameter ranges for the CSF model in the I90/94 dataset, as depicted in Figure 6.149, show limited variation across most parameters. The parameter (d_{min}) shows

the widest range, evidently showing the CSF policy's emphasis on maintaining safe following distances under varying traffic conditions. Conversely, the parameters (K), (λ), and (γ) remain tightly clustered, suggesting that the control gains and braking adjustments are more consistent across different scenarios.

Figure 6.150 shows that the optimized parameters follow discrete distributions, with values concentrated at specific numerical points rather than being continuously spread out. The tight clustering of (K) and (λ) indicates that the model consistently stabilizes around particular parameter values, minimizing fluctuations in vehicle behavior. Similarly, (γ) is clustered near the value zero, suggesting that braking was not applied too aggressively. Thus, smoother deceleration patterns were shown rather than abrupt braking maneuvers.

There were no outlier values during calibration which suggests that the optimization process consistently converged to a well-defined solution space, ensuring the model's reliability in maintaining stable vehicle behavior. However, the broader spread in (d_{min}) indicates greater adaptability in determining safe spacing based on external traffic conditions.

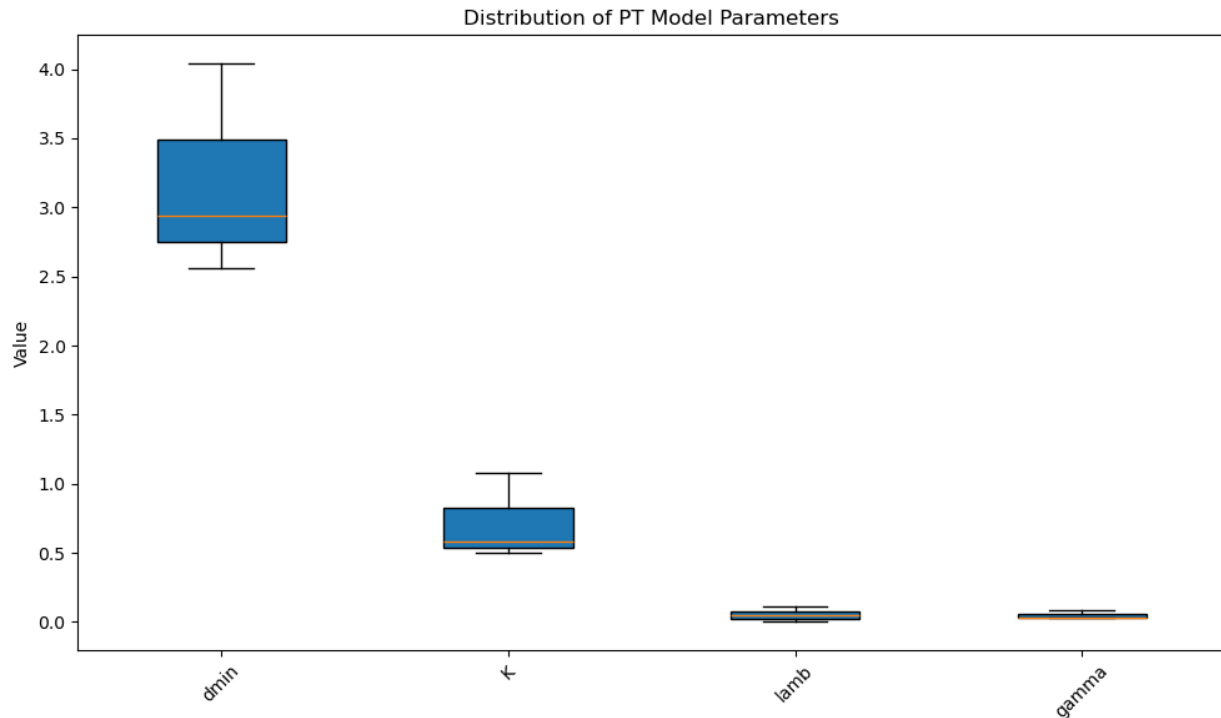


Figure 6.149: Parameter ranges for CSF in I90/94.

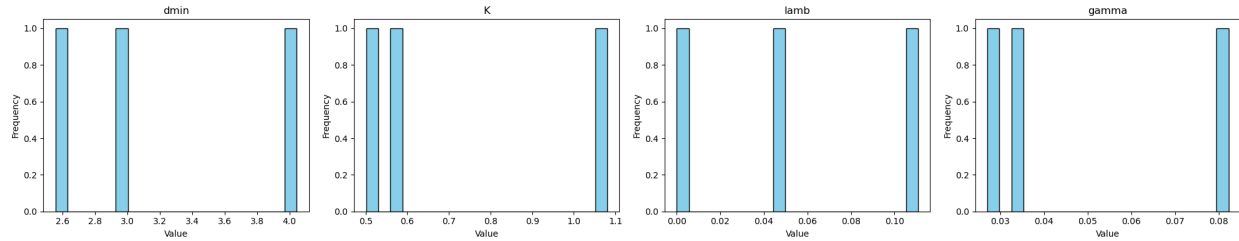


Figure 6.150: Parameter histogram for CSF in I90/94.

6.2.12 CSF Phoenix Simulated Results

The simulated results for the CSF model in the Phoenix dataset are presented in Figures 6.151, 6.152, 6.153, and 6.154. The simulated follower closely aligns with the calibrated position and speed of the target follower, as shown in Figures 6.151 and 6.154 for vehicles 13 and 2 in run 9NS. However, noticeable speed deviations are observed for vehicles 31 and 2 in run 9ES, as illustrated in Figures 6.152 and 6.153.

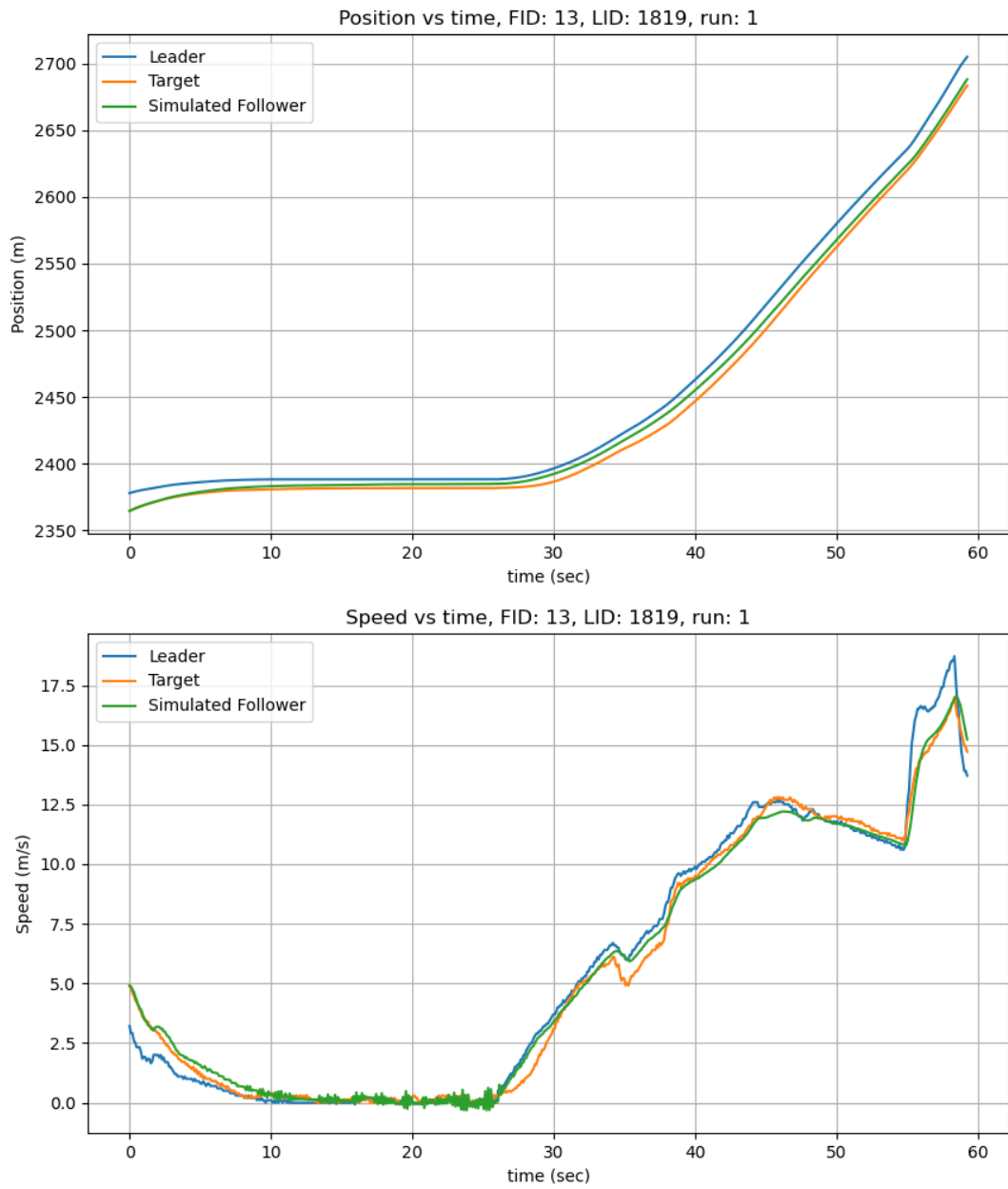


Figure 6.151: Position and speed for CSF for vehicle 13 in Phoenix data H1A3 run 6.

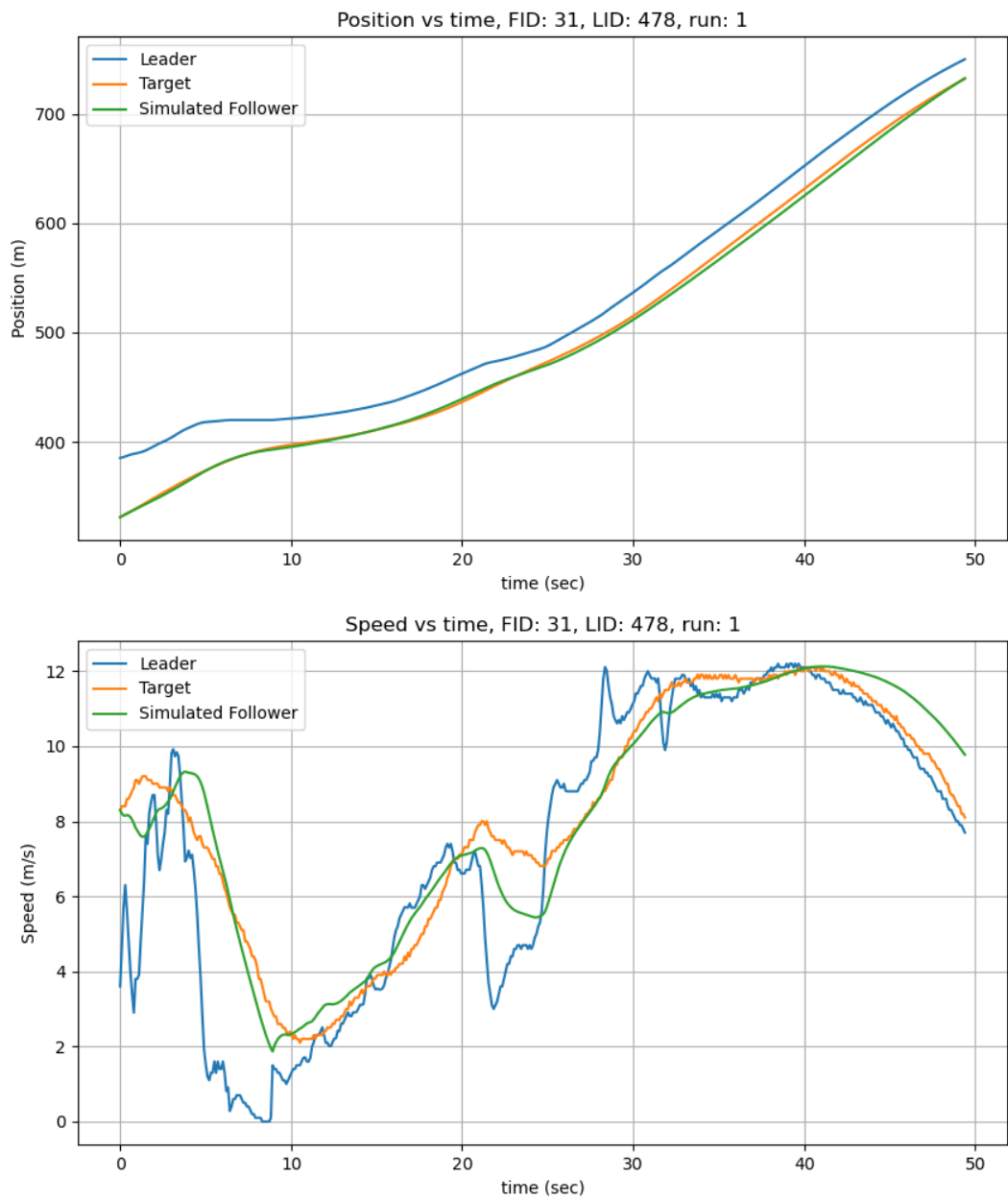


Figure 6.152: Position and speed for CSF for vehicle 31 in Phoenix data H1A3 run 1.

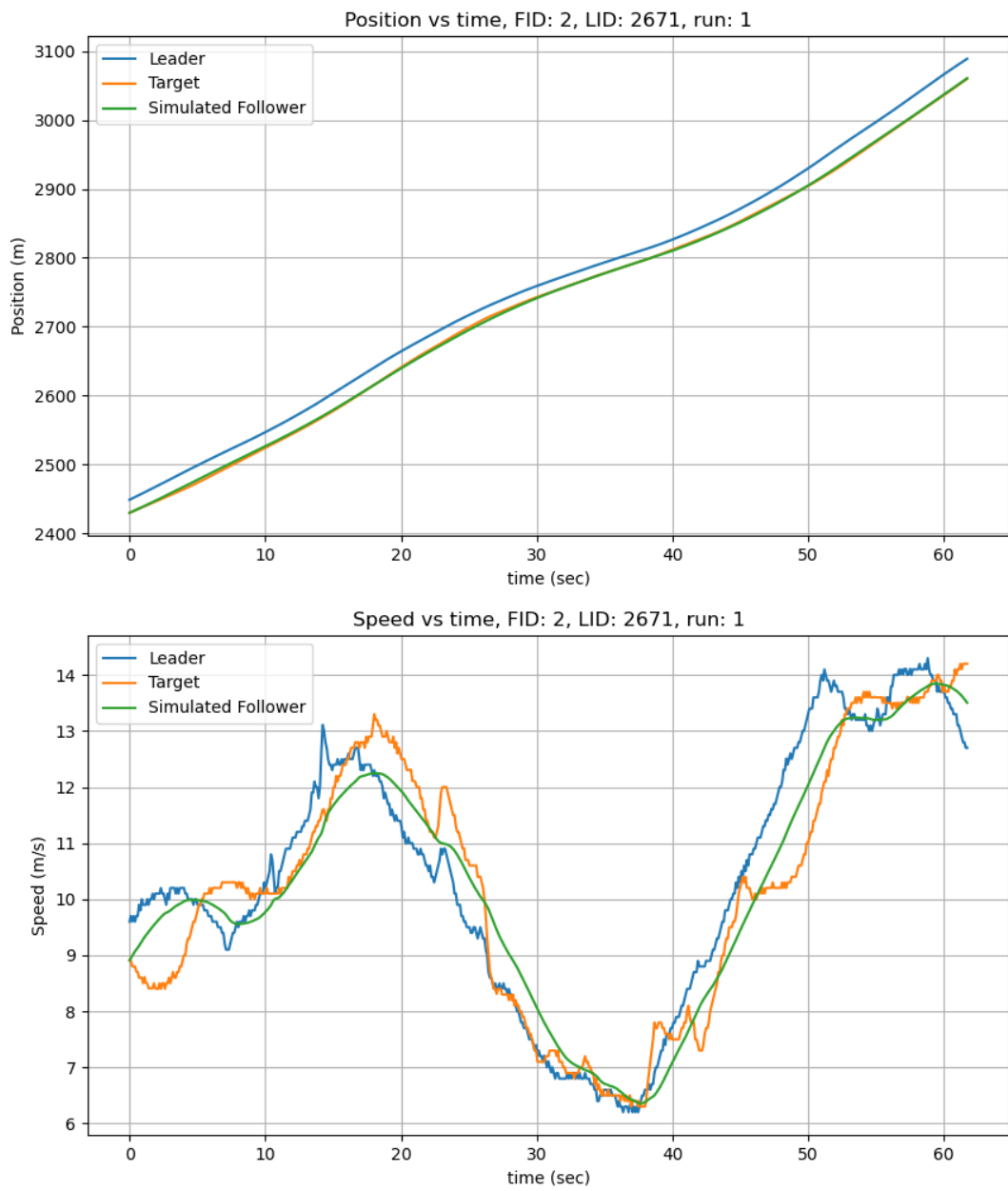


Figure 6.153: Position and speed for CSF for vehicle 2 in Phoenix data H1A3 run 9 ES.

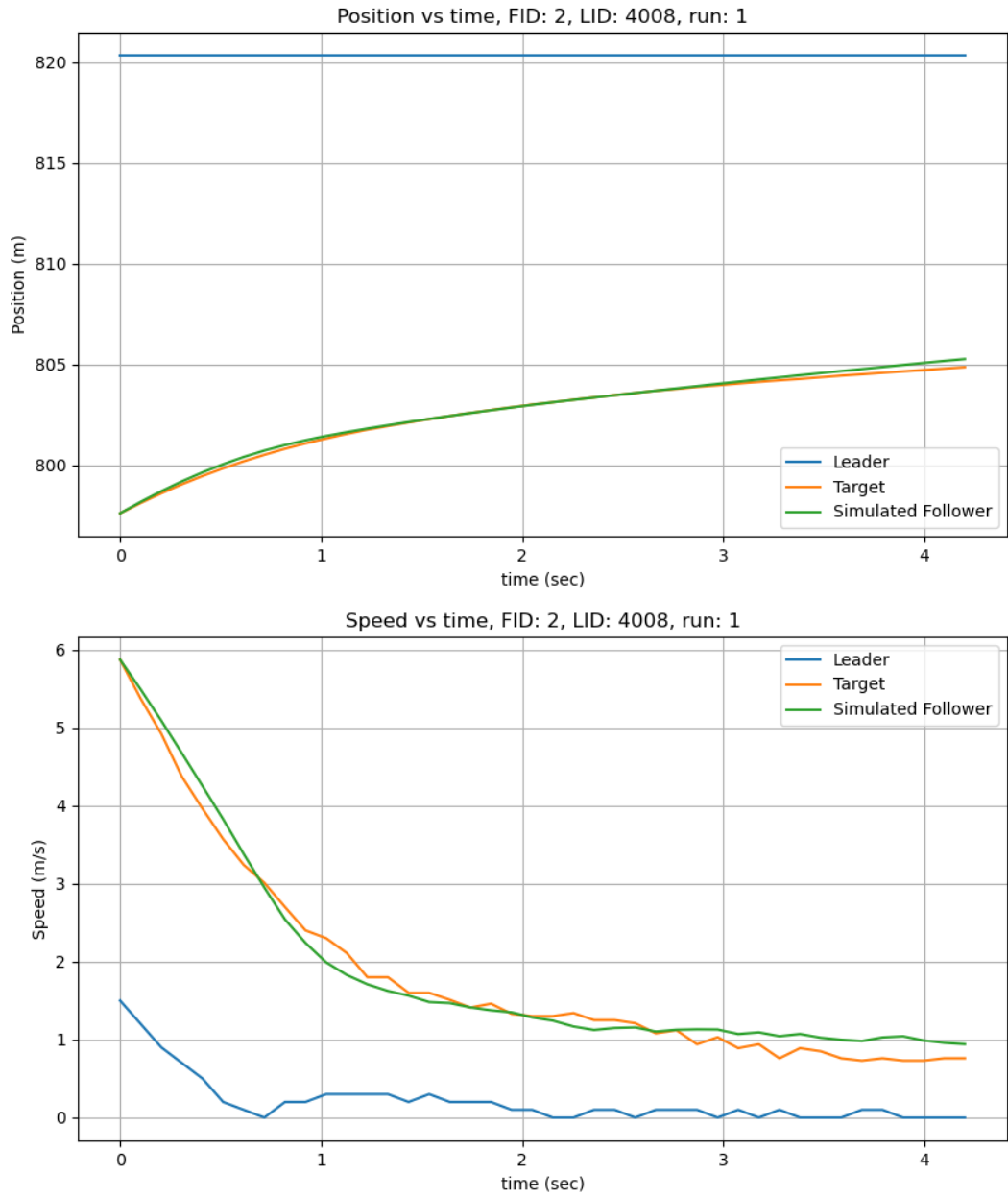


Figure 6.154: Position and speed for CSF for vehicle 2 in Phoenix data H1A3 run 9 NS.

The optimized parameter ranges for the CSF policy in the Phoenix dataset are presented in Figure 6.155, showing variations across different parameters. The parameter (K) exhibits

the widest range, suggesting greater adaptability in control response under varying traffic conditions. The parameter (d_{min}) also shows a relatively wide range, indicating that safe following distances are more flexible just like the parameter (K).

In contrast, the parameters (λ) and (γ) remain tightly clustered, suggesting consistent values across different calibration scenarios. An outlier value is observed in (d_{min}), indicating a result where the optimized parameter deviates from the general range calibrated. Figure 6.156 illustrates that the parameters follow discrete distributions, with values concentrated at specific points rather than being continuously spread out. This suggests that the optimization process consistently favors certain parameter values.

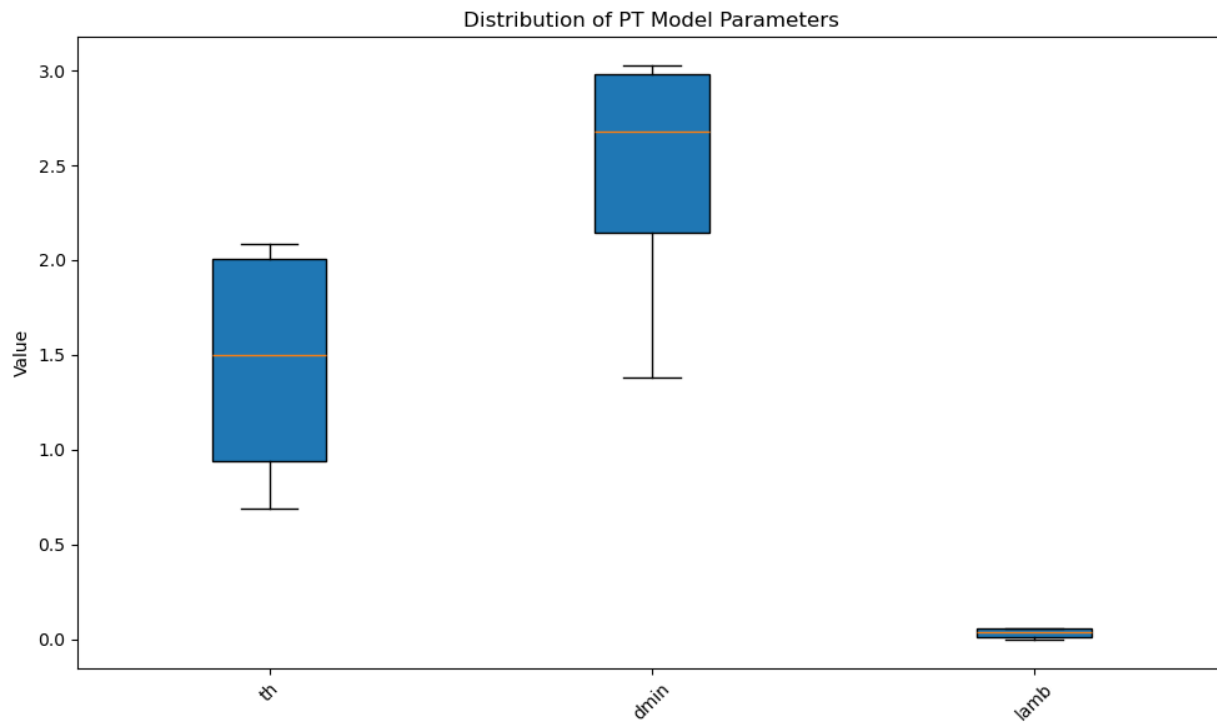


Figure 6.155: Parameter ranges for CSF in Phoenix.

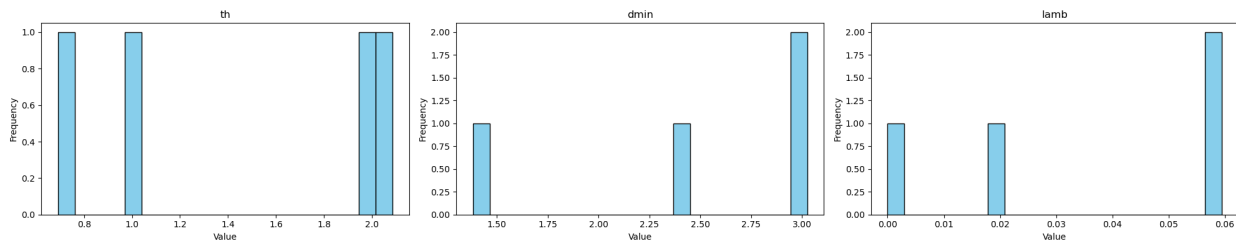


Figure 6.156: Parameter histogram for CSF in Phoenix.

6.2.13 IDM I294 Simulated Results

For Intelligent Driver Model (IDM), the simulated results for I294 are presented in Figures [6.157](#), [6.158](#), [6.159](#), [6.160](#), [6.161](#), [6.162](#), [6.163](#), [6.164](#), [6.165](#), [6.166](#), [6.167](#), [6.168](#), [6.169](#), [6.170](#), [6.171](#), [6.172](#), [6.172](#), [6.173](#), [6.174](#), [6.175](#), [6.176](#), [6.177](#), [6.178](#), [6.179](#), [6.180](#), [6.181](#), and [6.182](#). The IDM calibrates the trajectories by finding the most optimal parameter such as the max acceleration (a), desired speed (v_0), safe distance (s_0), time headway (T), and comfort deceleration value (b) for braking. Overall, the simulated position strongly aligns with the target position despite some speed variations.

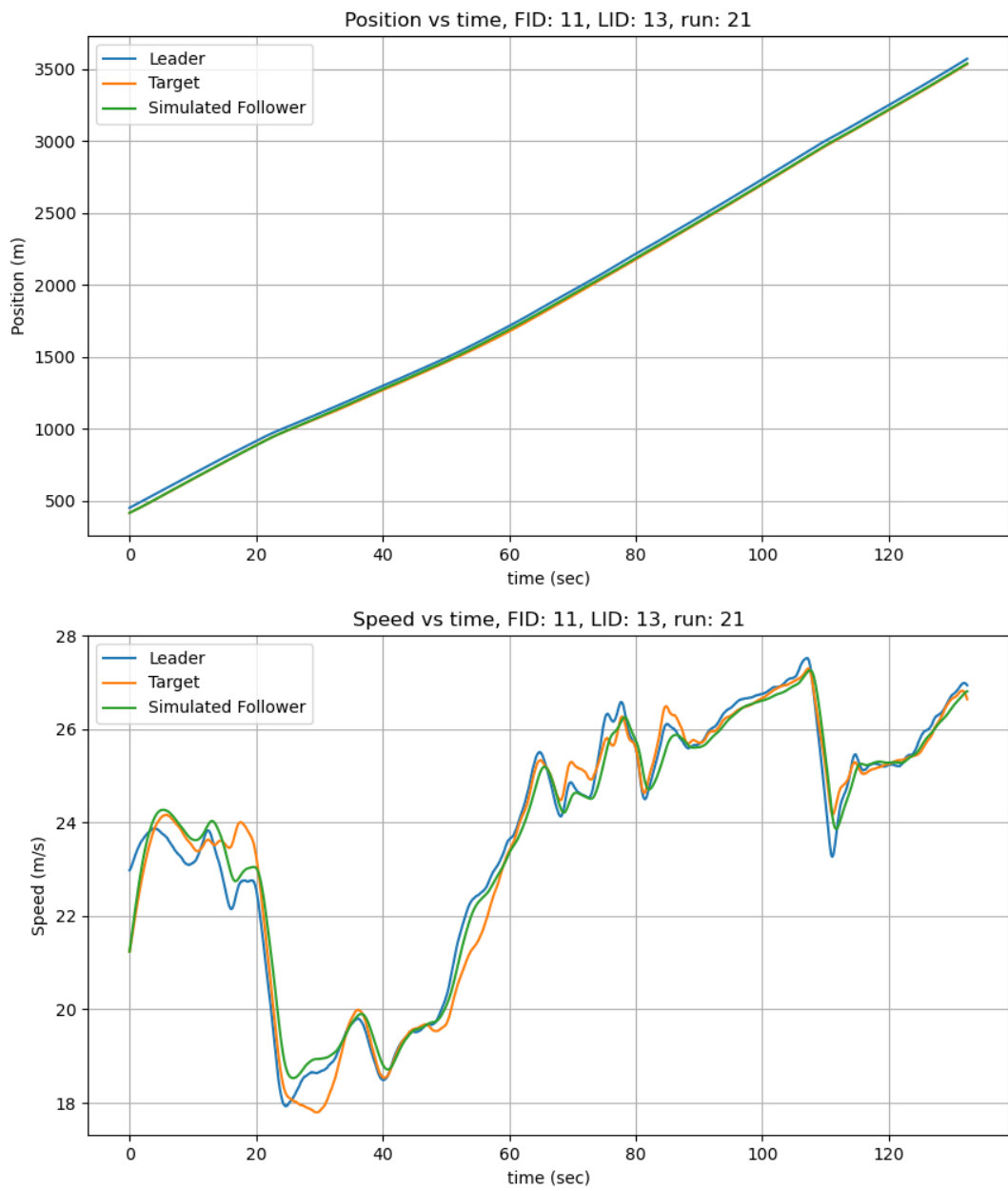


Figure 6.157: Position and speed for IDM for vehicle 11 in run 21 I294L1 dataset.

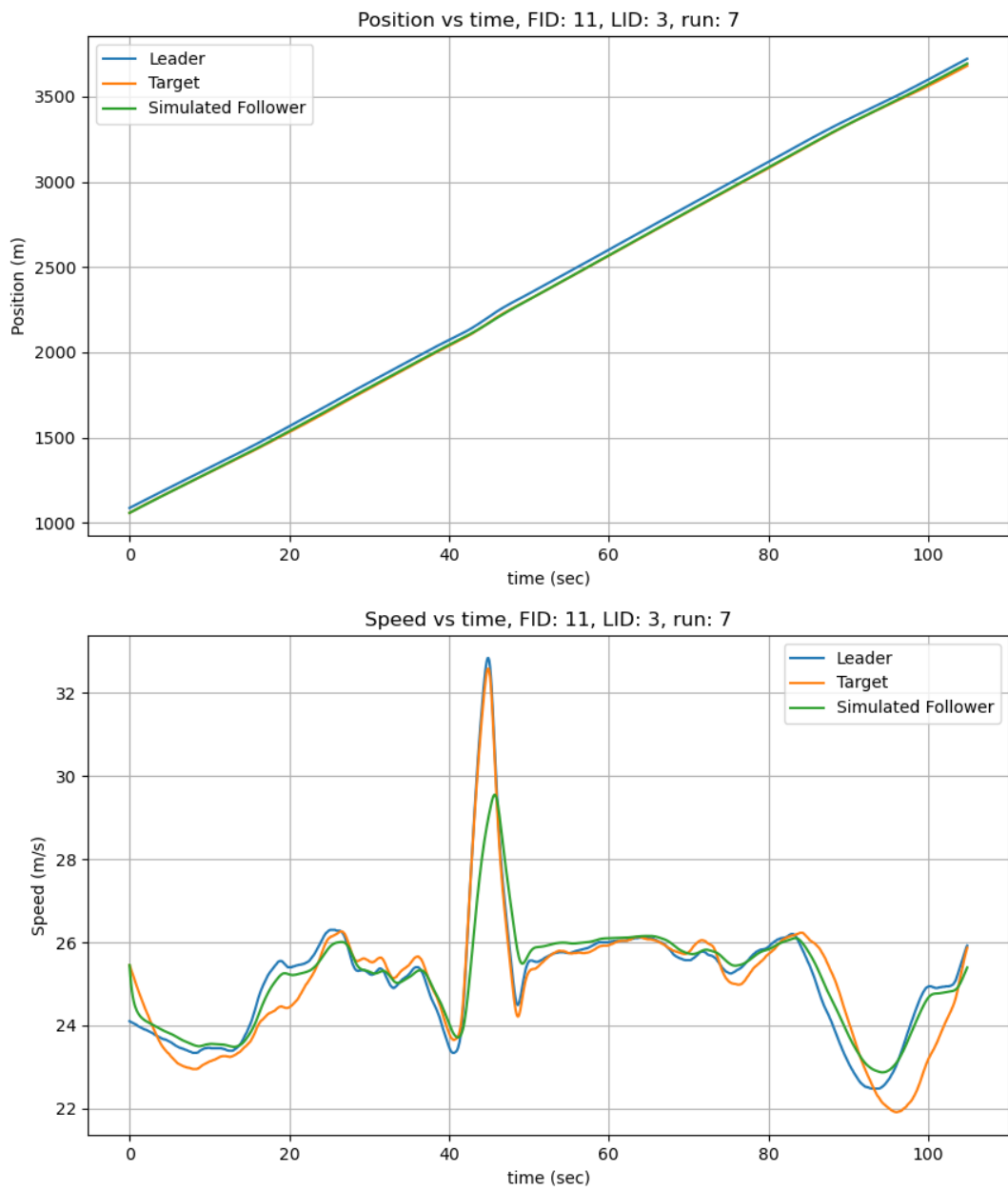


Figure 6.158: Position and speed for IDM for vehicle 11 in run 7 I294L1 dataset.

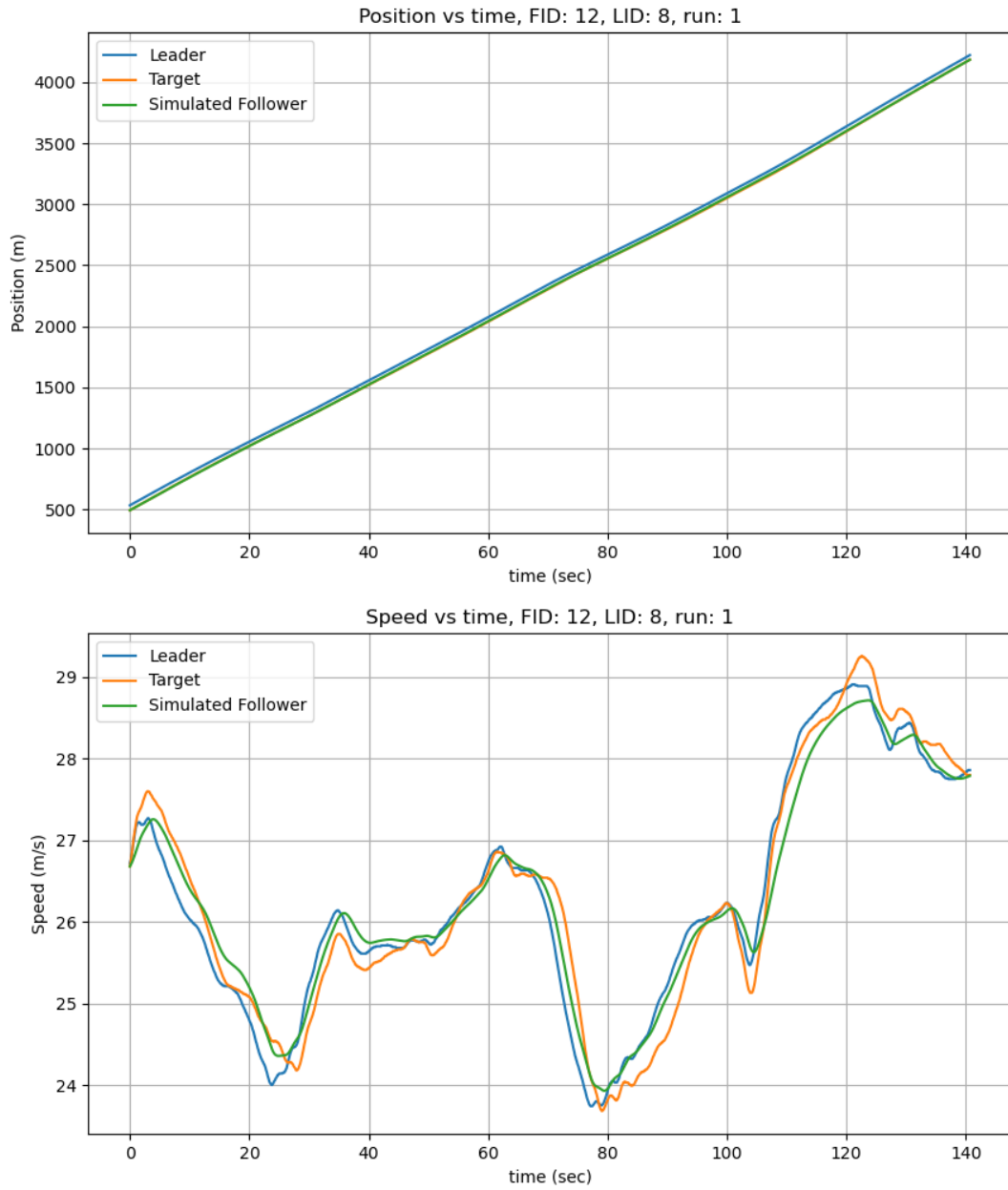


Figure 6.159: Position and speed for IDM for vehicle 12 in run 1 I294L1 dataset.

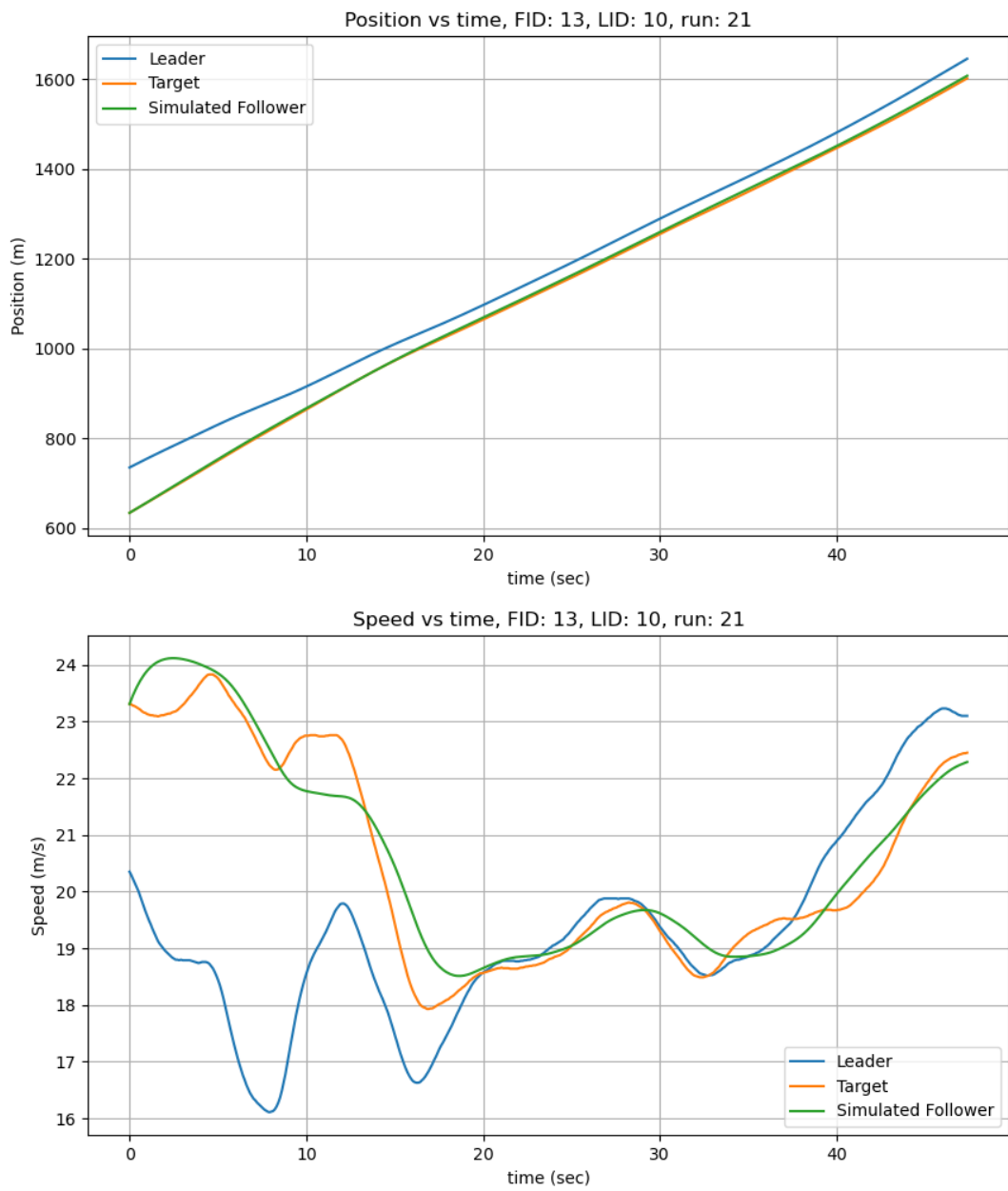


Figure 6.160: Position and speed for IDM for vehicle 13 in run 21 I294L1 dataset.

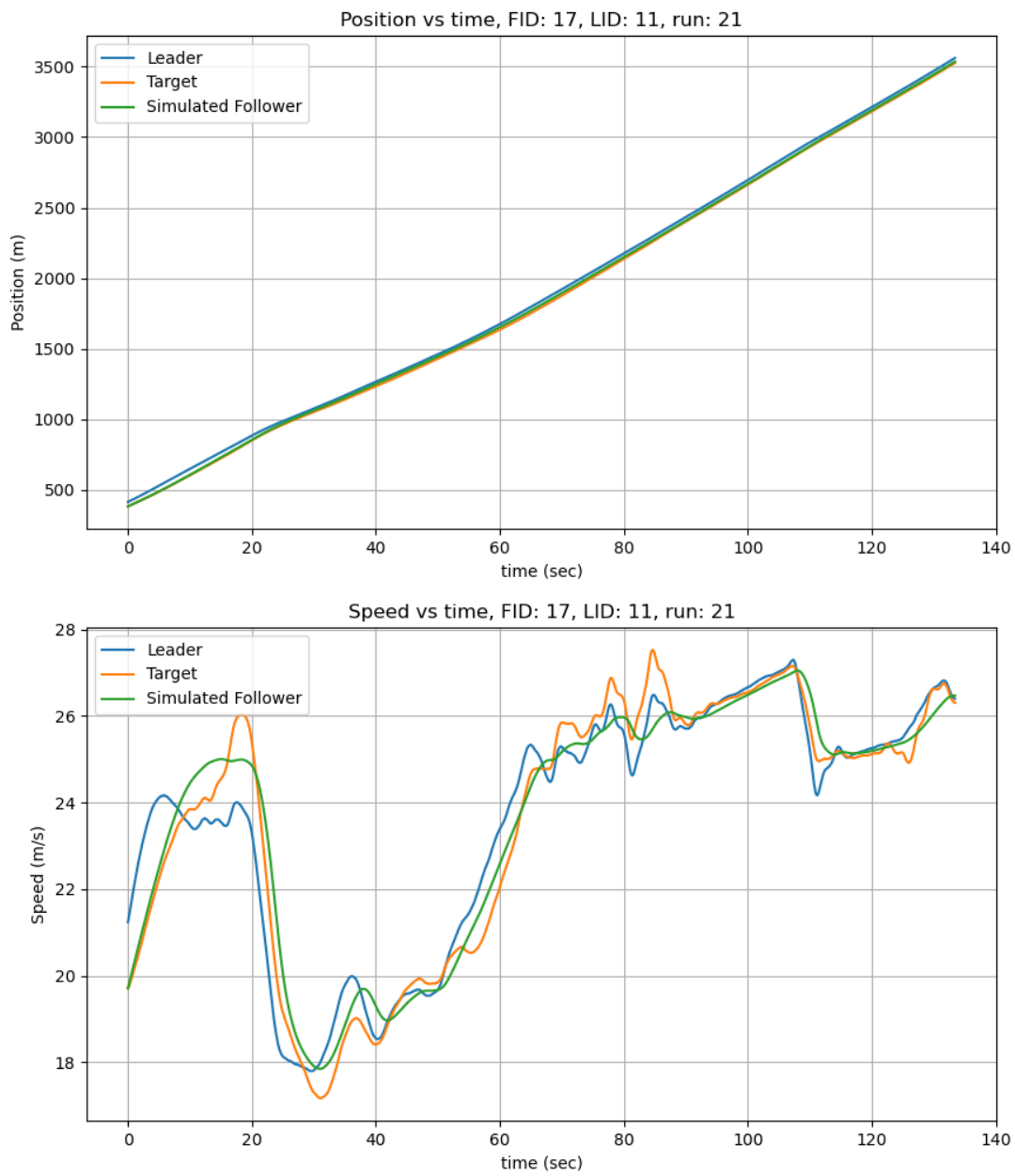


Figure 6.161: Position and speed for IDM for vehicle 17 in run 21 I294L1 dataset.

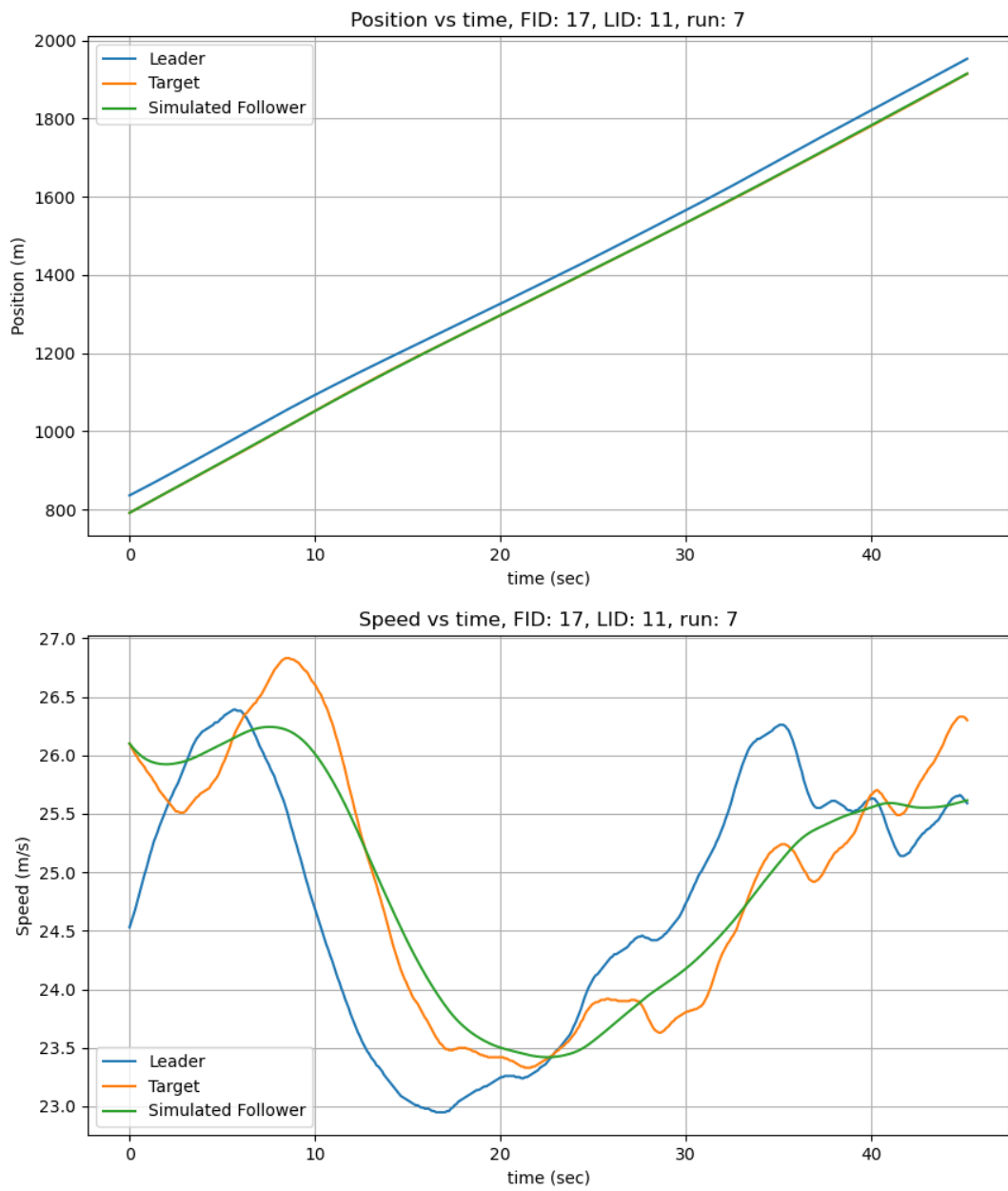


Figure 6.162: Position and speed for IDM for vehicle 17 in run 7 I294L1 dataset.

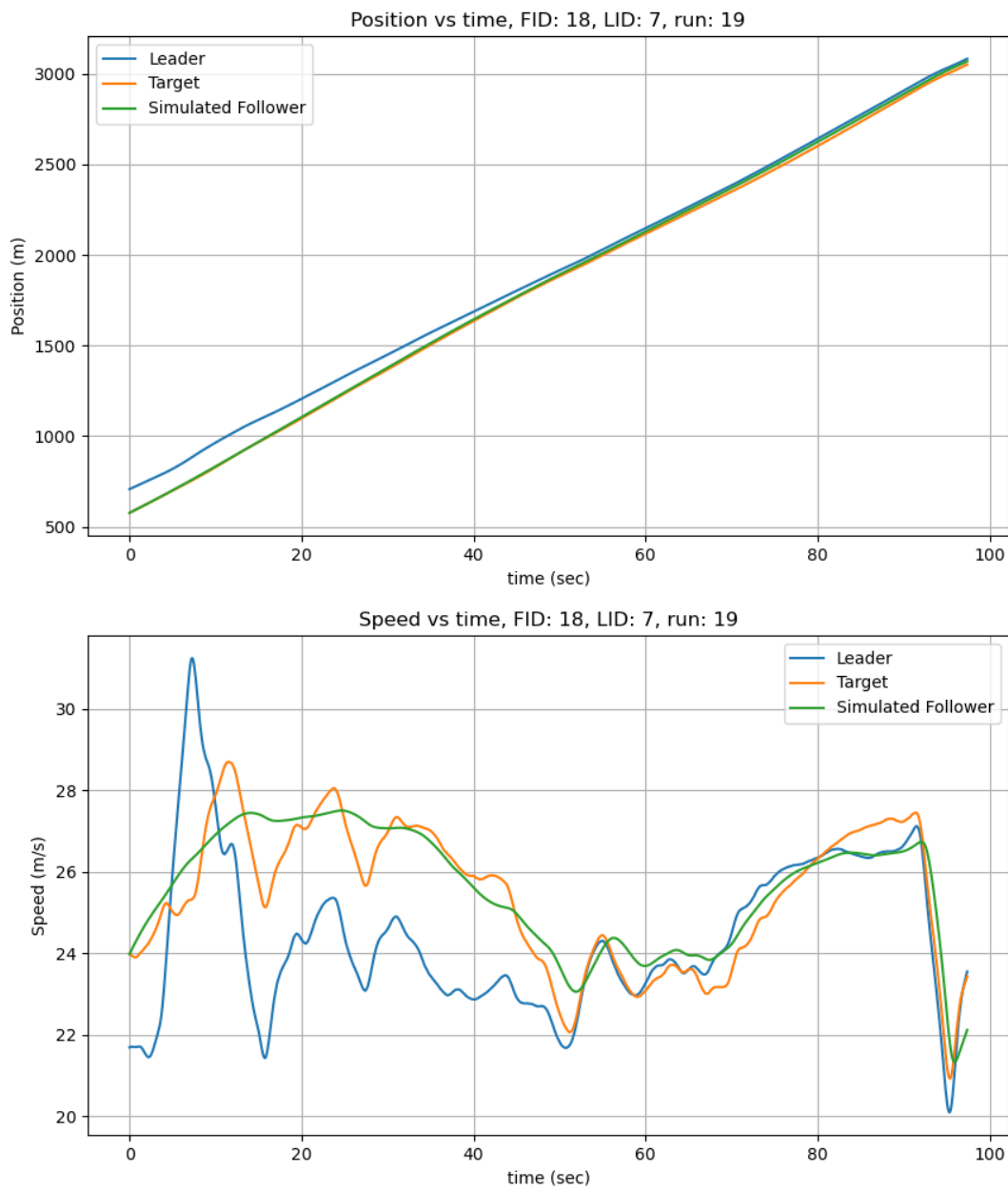


Figure 6.163: Position and speed for IDM for vehicle 18 in run 19 I294L1 dataset.

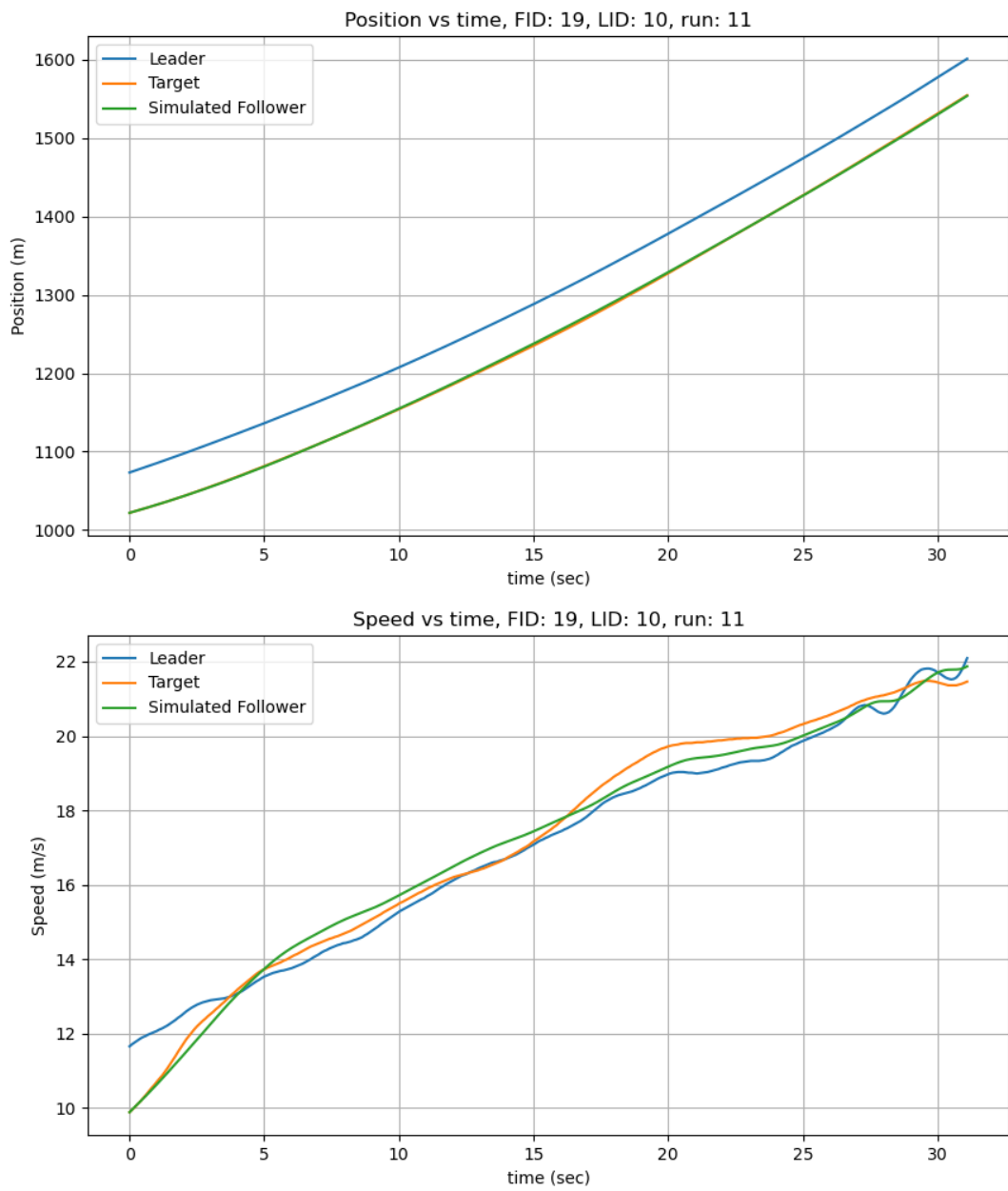


Figure 6.164: Position and speed for IDM for vehicle 19 in run 11 I294L1 dataset.

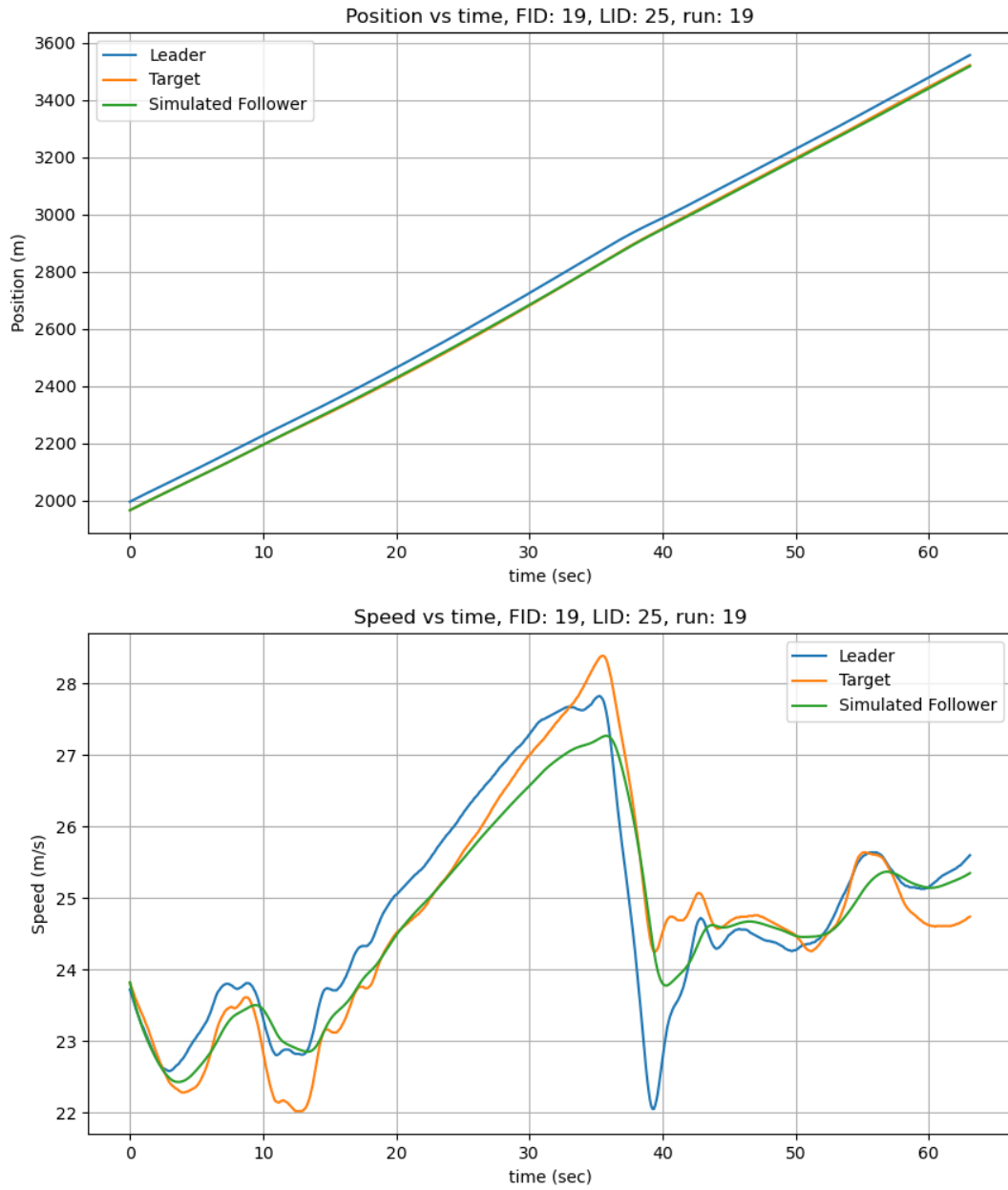


Figure 6.165: Position and speed for IDM for vehicle 19 in run 19 I294L1 dataset.

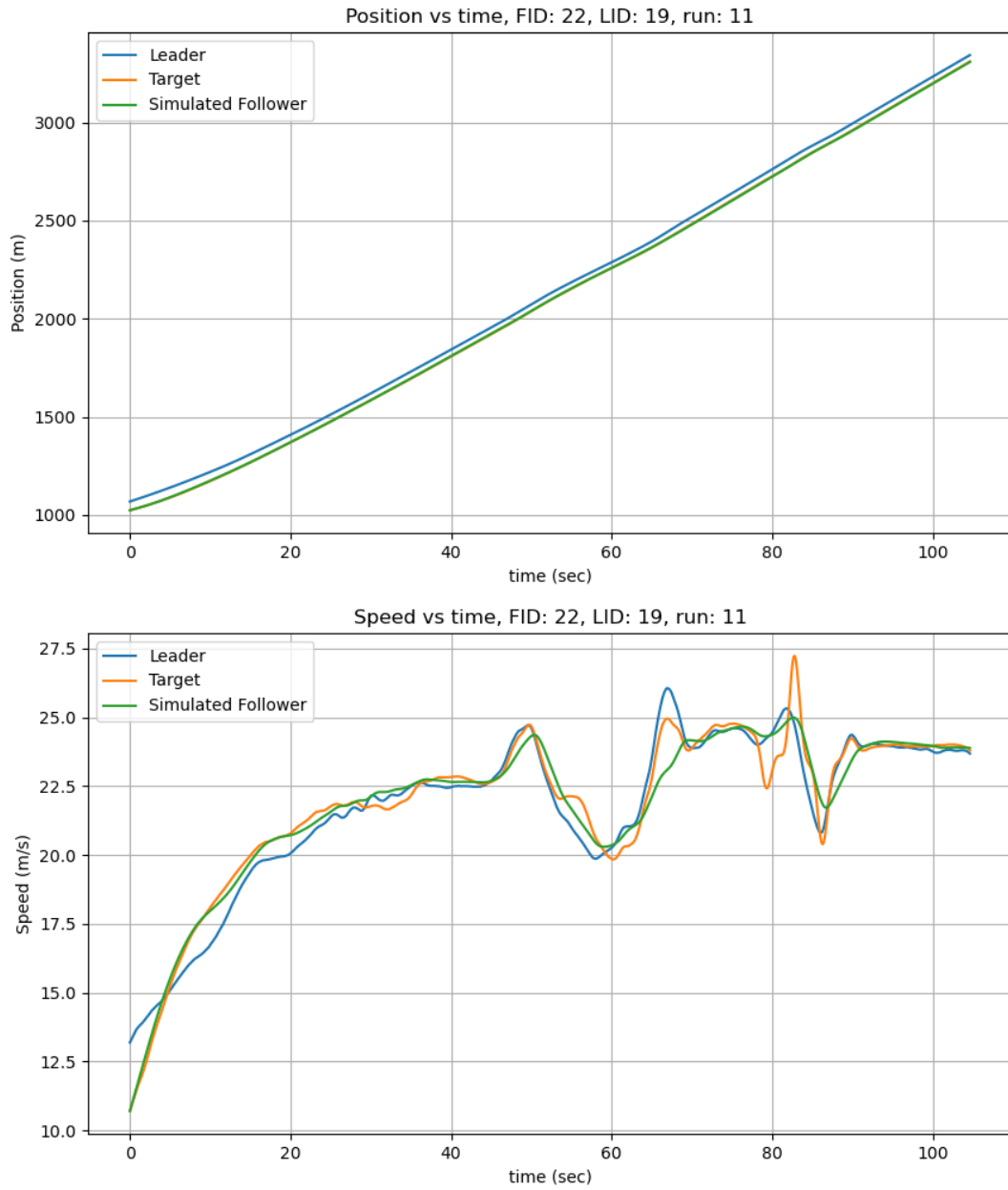


Figure 6.166: Position and speed for IDM for vehicle 22 in run 11 I294L1 dataset.

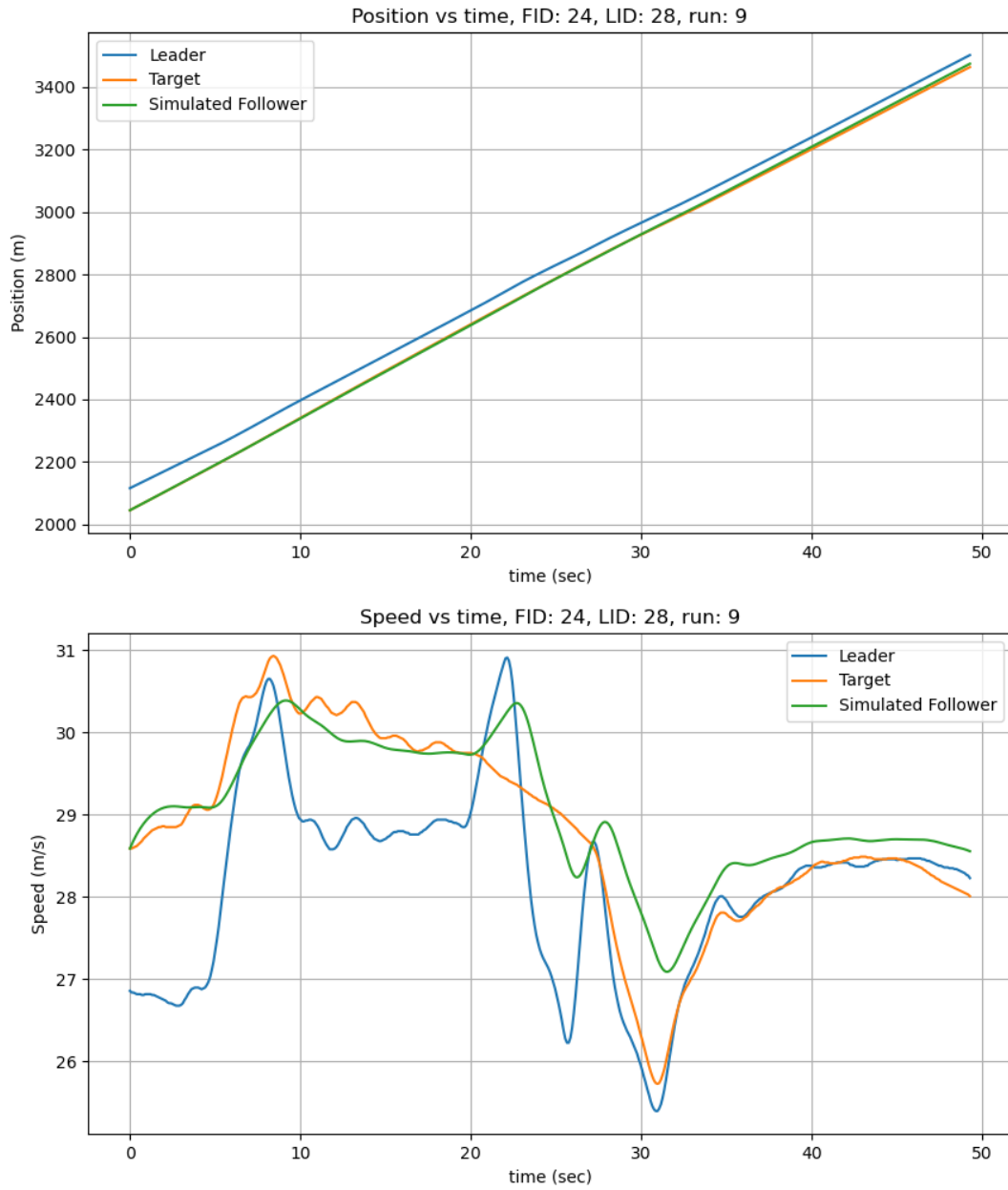


Figure 6.167: Position and speed for IDM for vehicle 24 in run 9 I294L1 dataset.

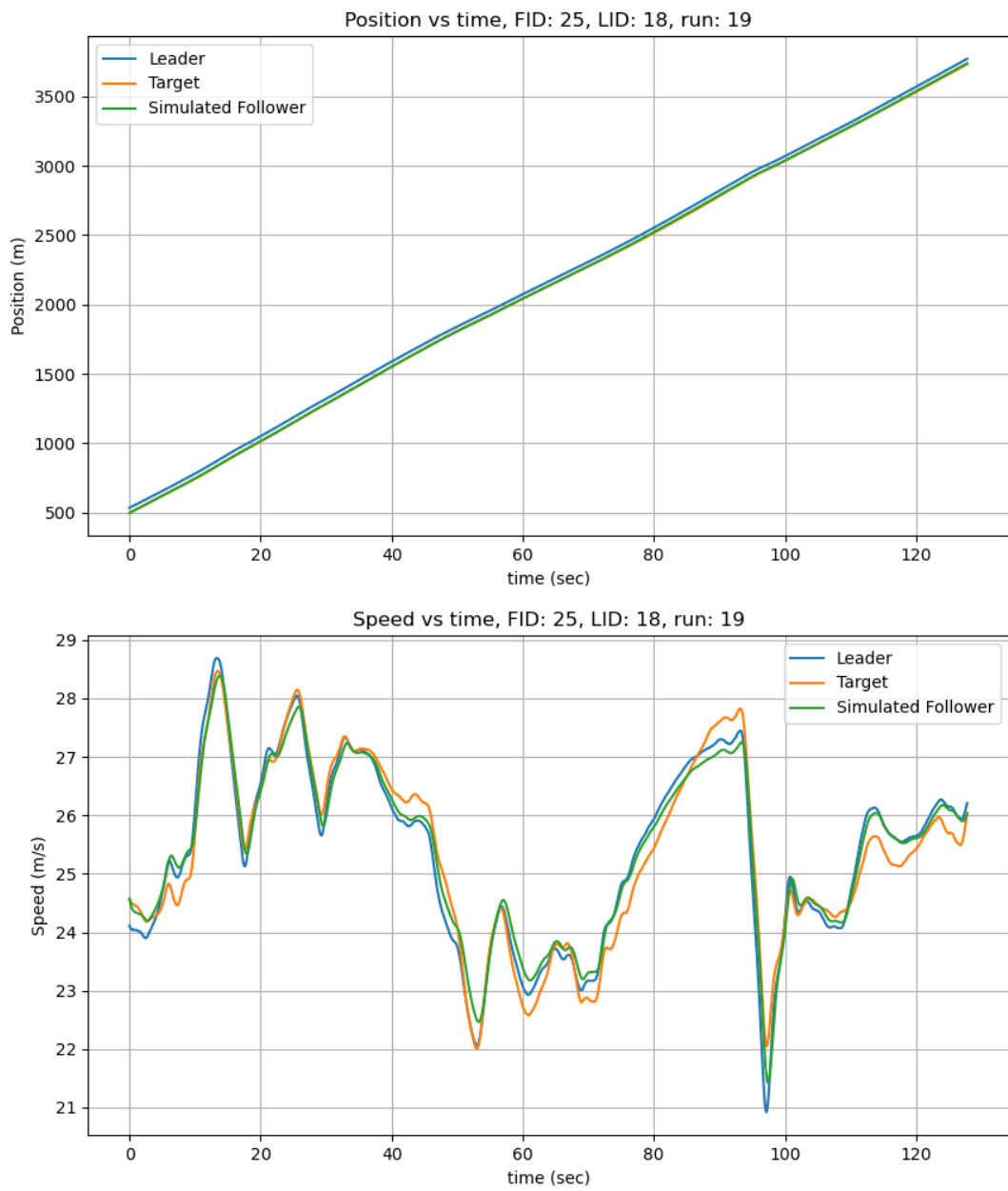


Figure 6.168: Position and speed for IDM for vehicle 25 in run 19 I294L1 dataset.

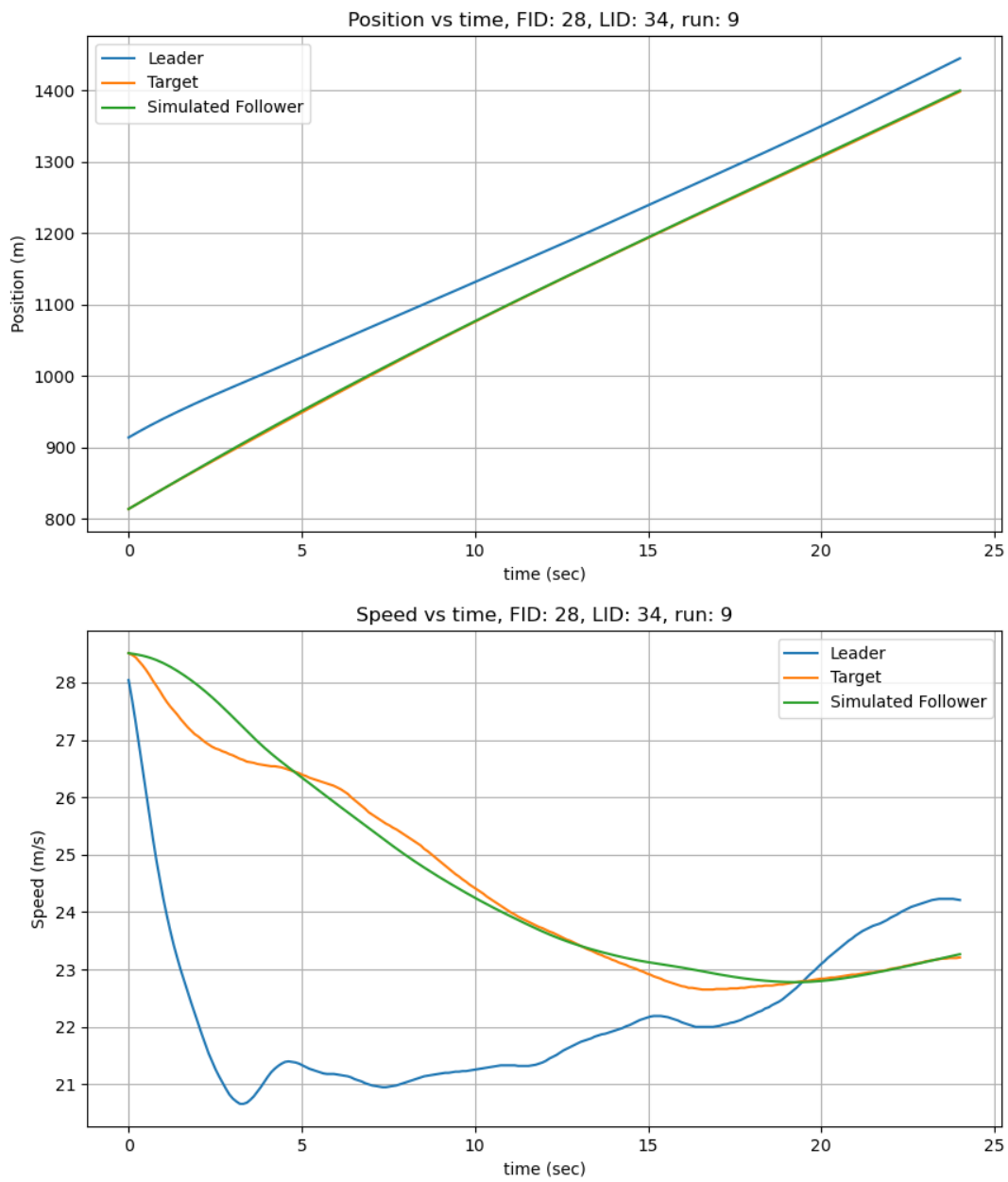


Figure 6.169: Position and speed for IDM for vehicle 28 in run 9 I294L1 dataset.

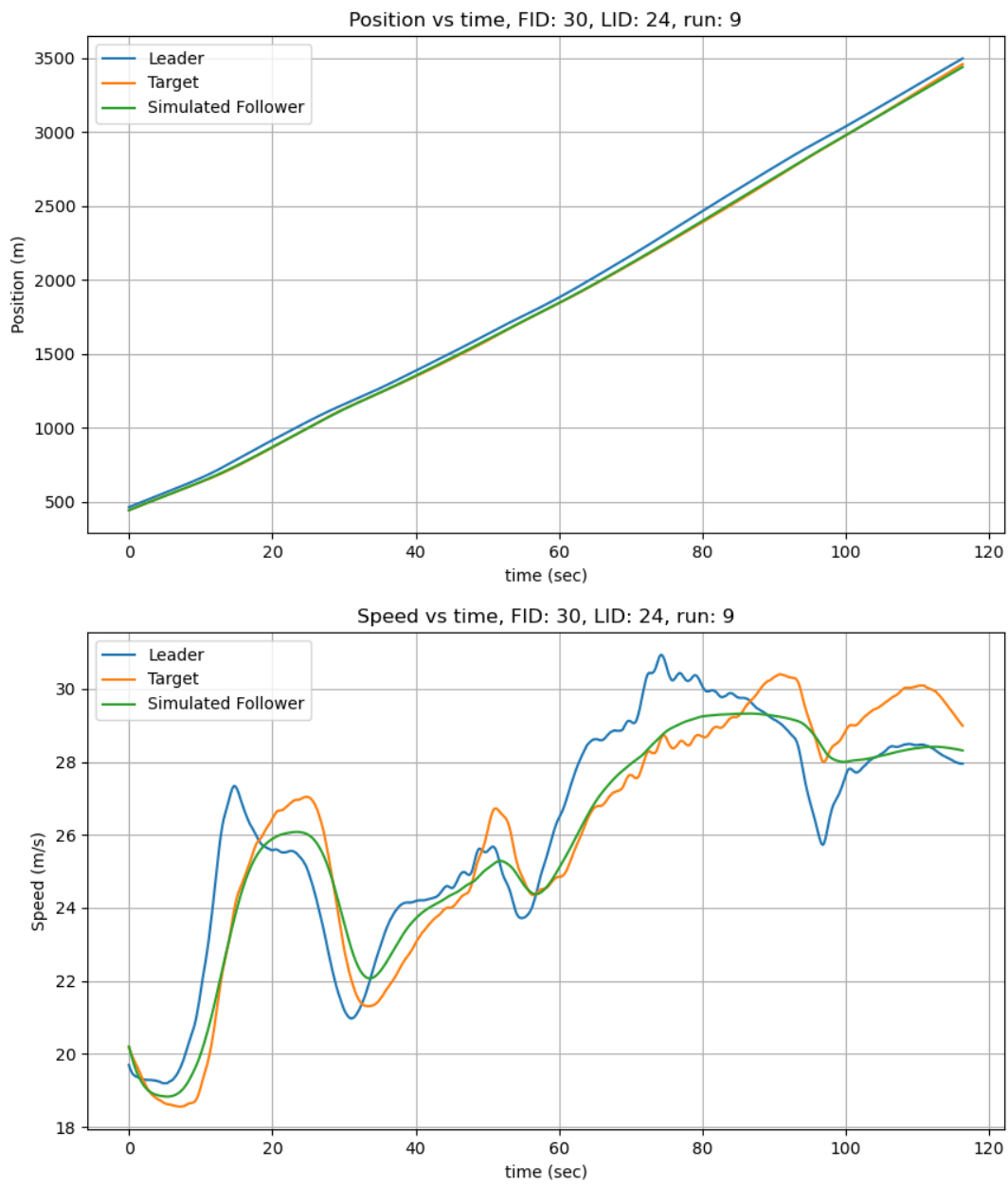


Figure 6.170: Position and speed for IDM for vehicle 30 in run 9 I294L1 dataset.

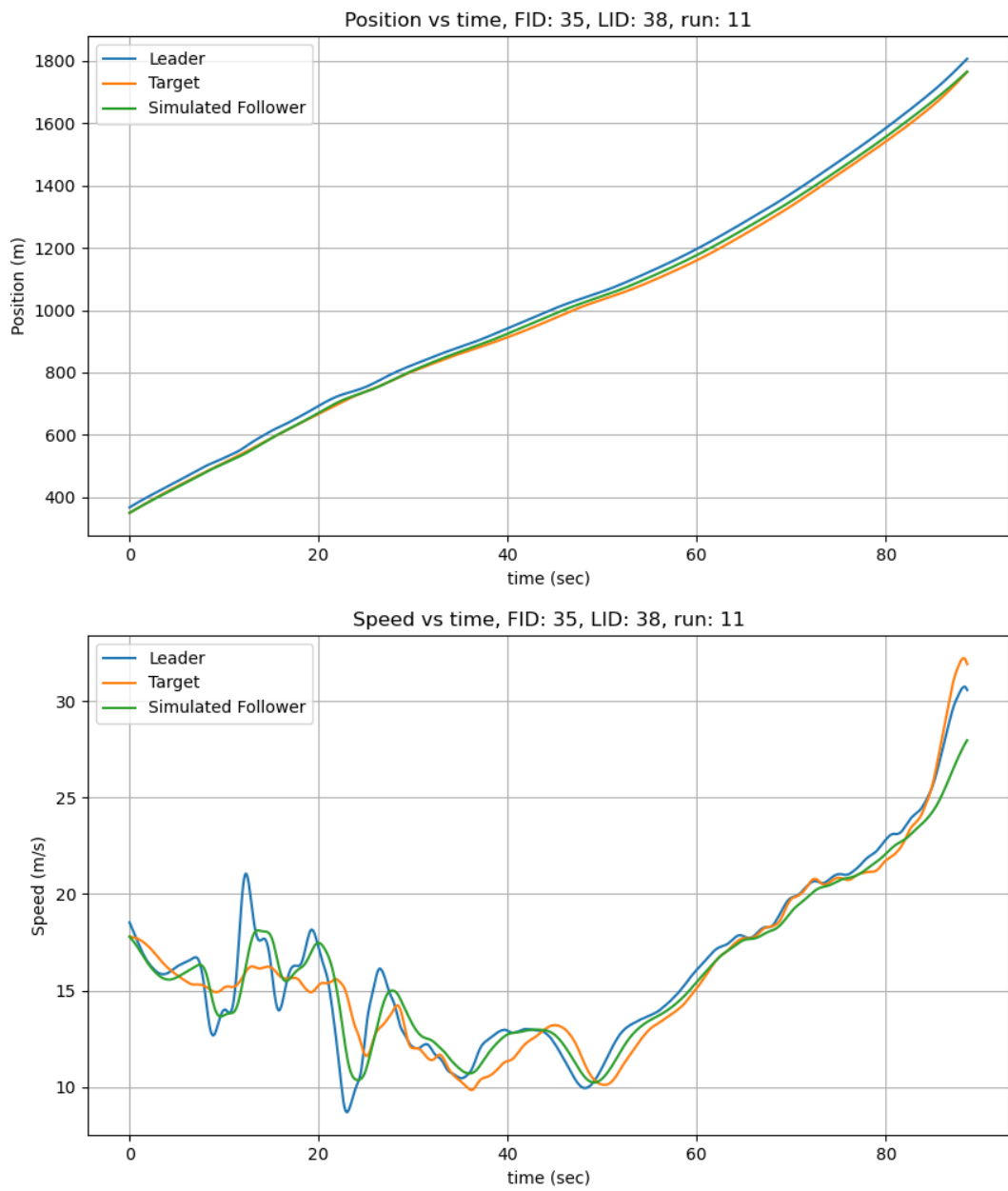


Figure 6.171: Position and speed for IDM for vehicle 35 in run 11 I294L1 dataset.

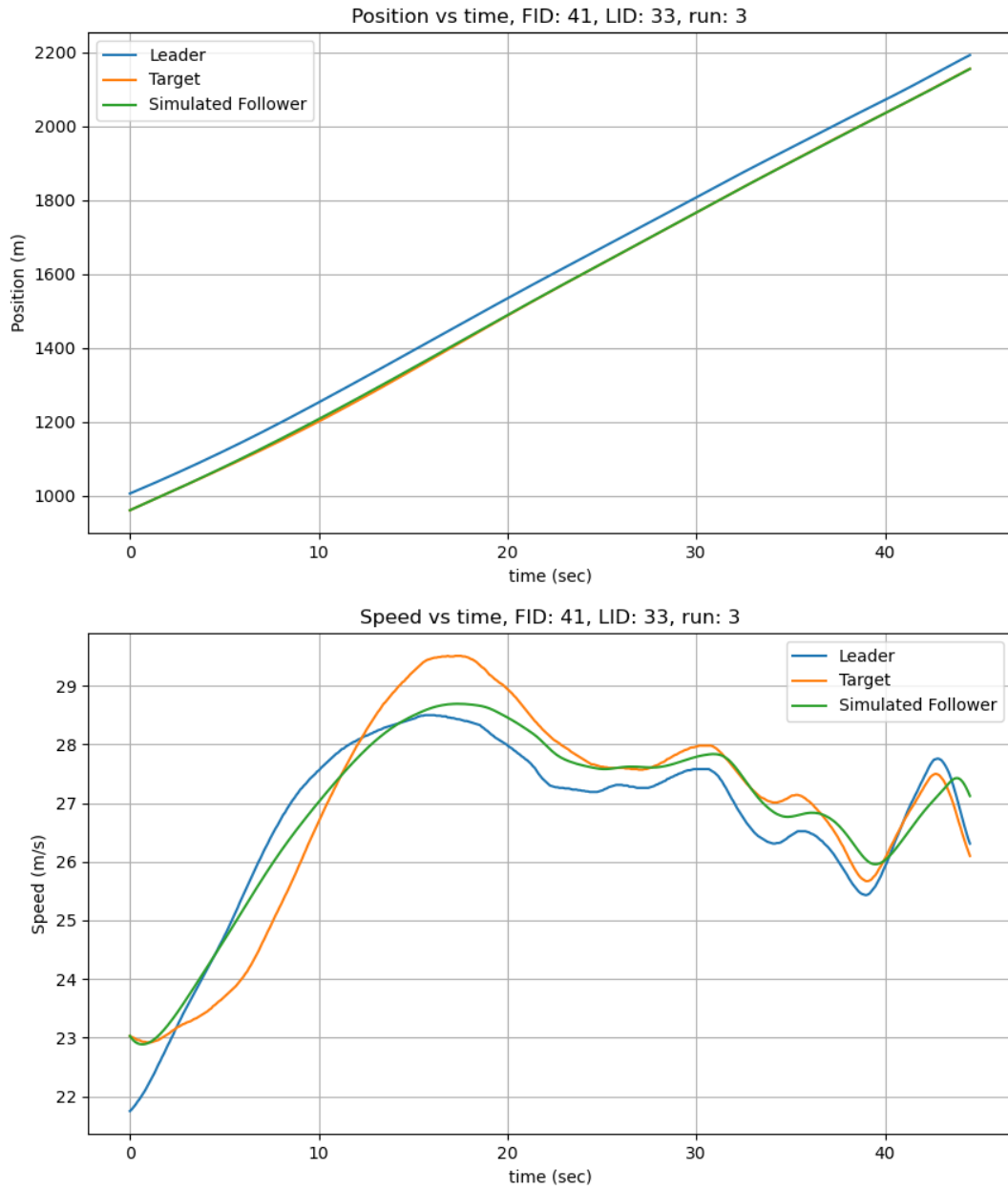


Figure 6.172: Position and speed for IDM for vehicle 41 in run 3 I294L1 dataset.

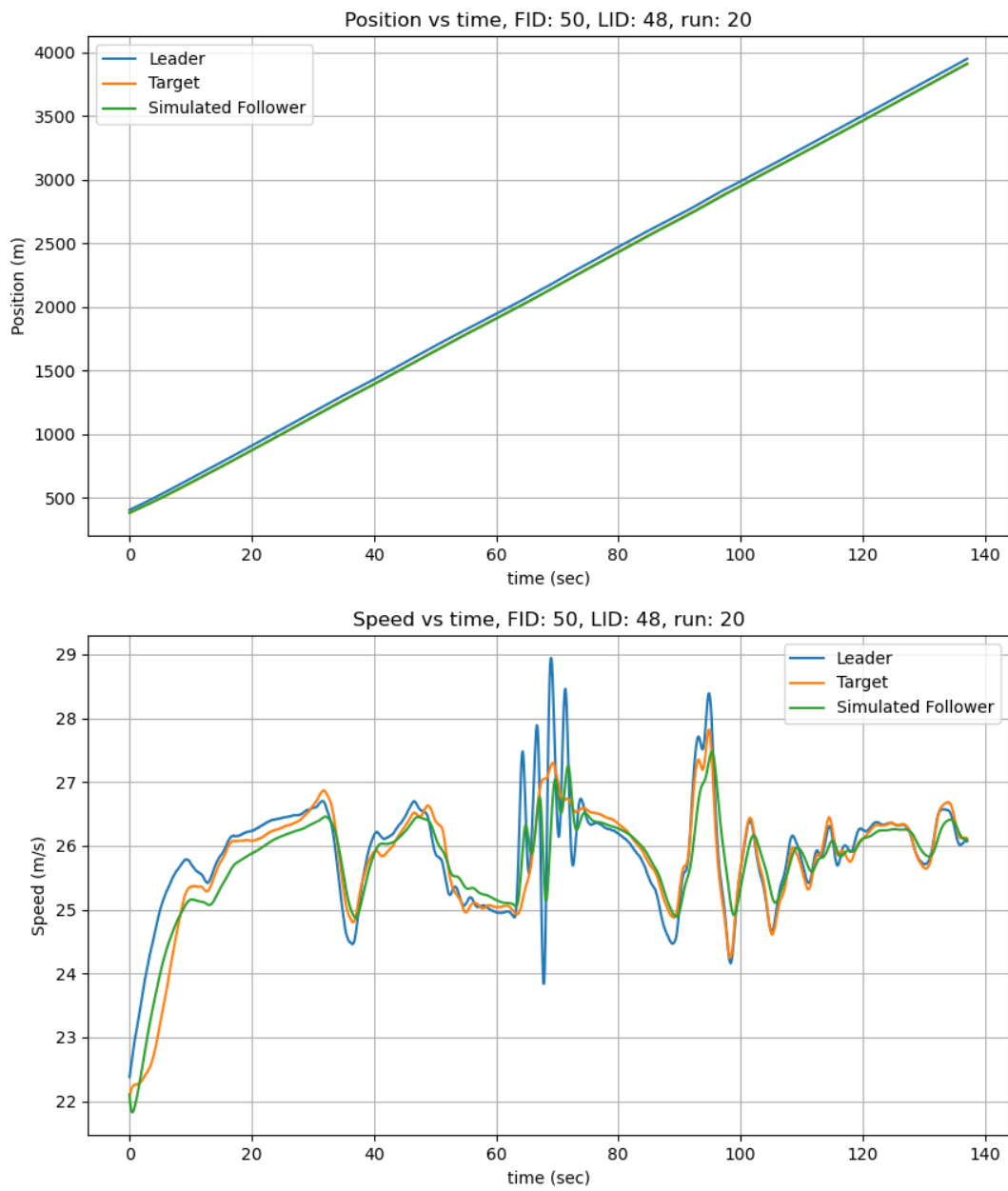


Figure 6.173: Position and speed for IDM for vehicle 50 in run 20 I294L1 dataset.

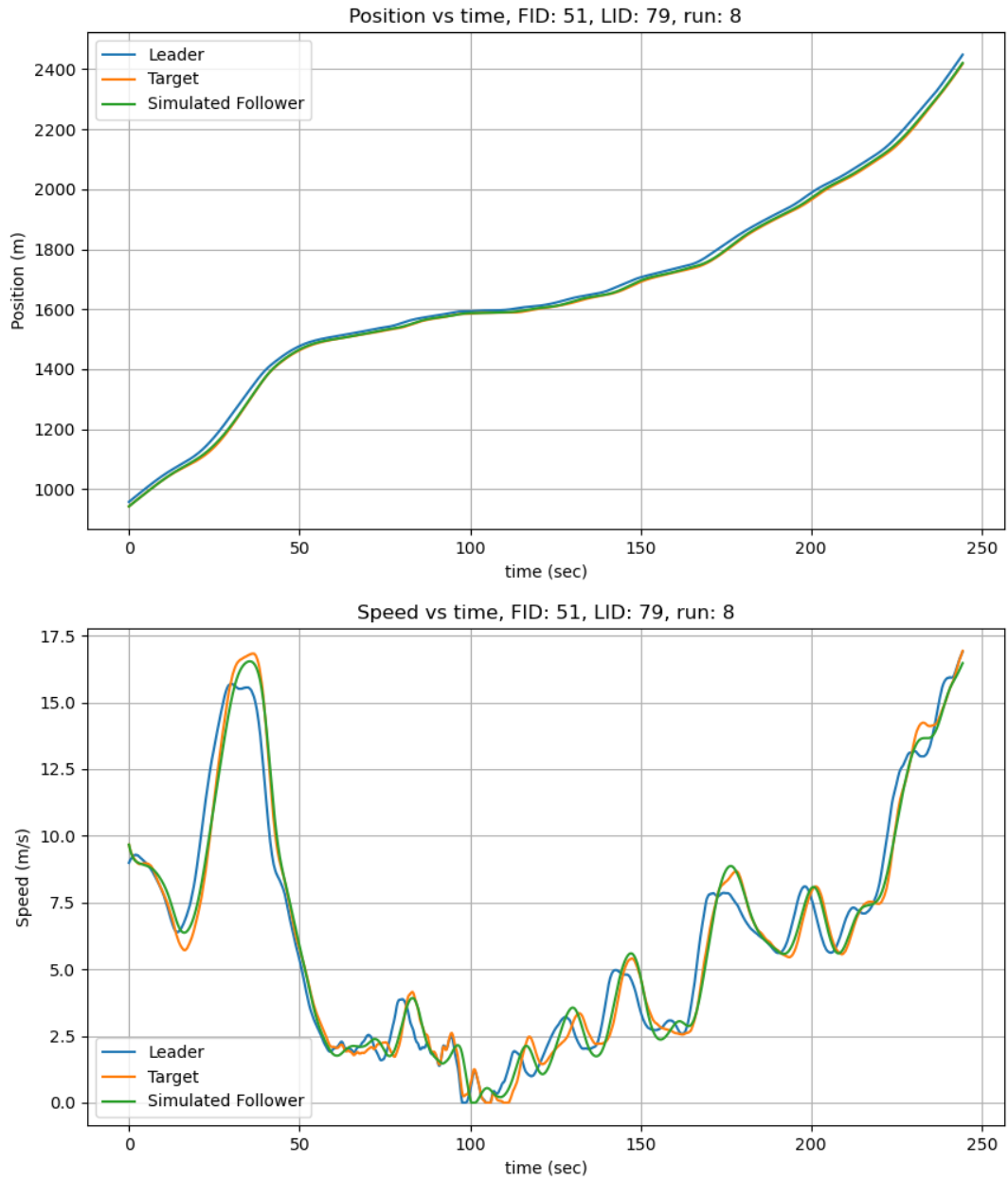


Figure 6.174: Position and speed for IDM for vehicle 51 in run 8 I294L1 dataset.

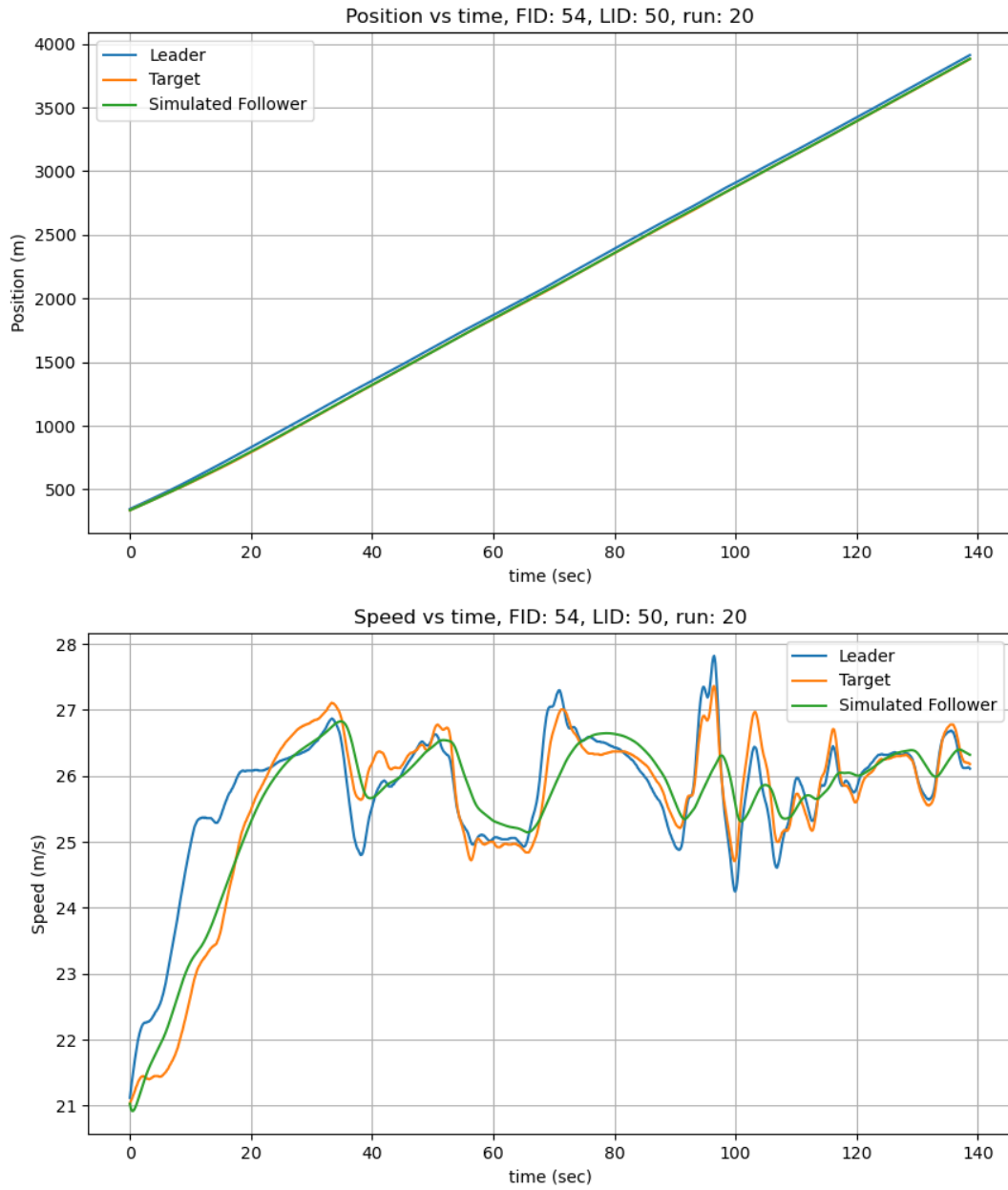


Figure 6.175: Position and speed for IDM for vehicle 54 in run 20 I294L1 dataset.

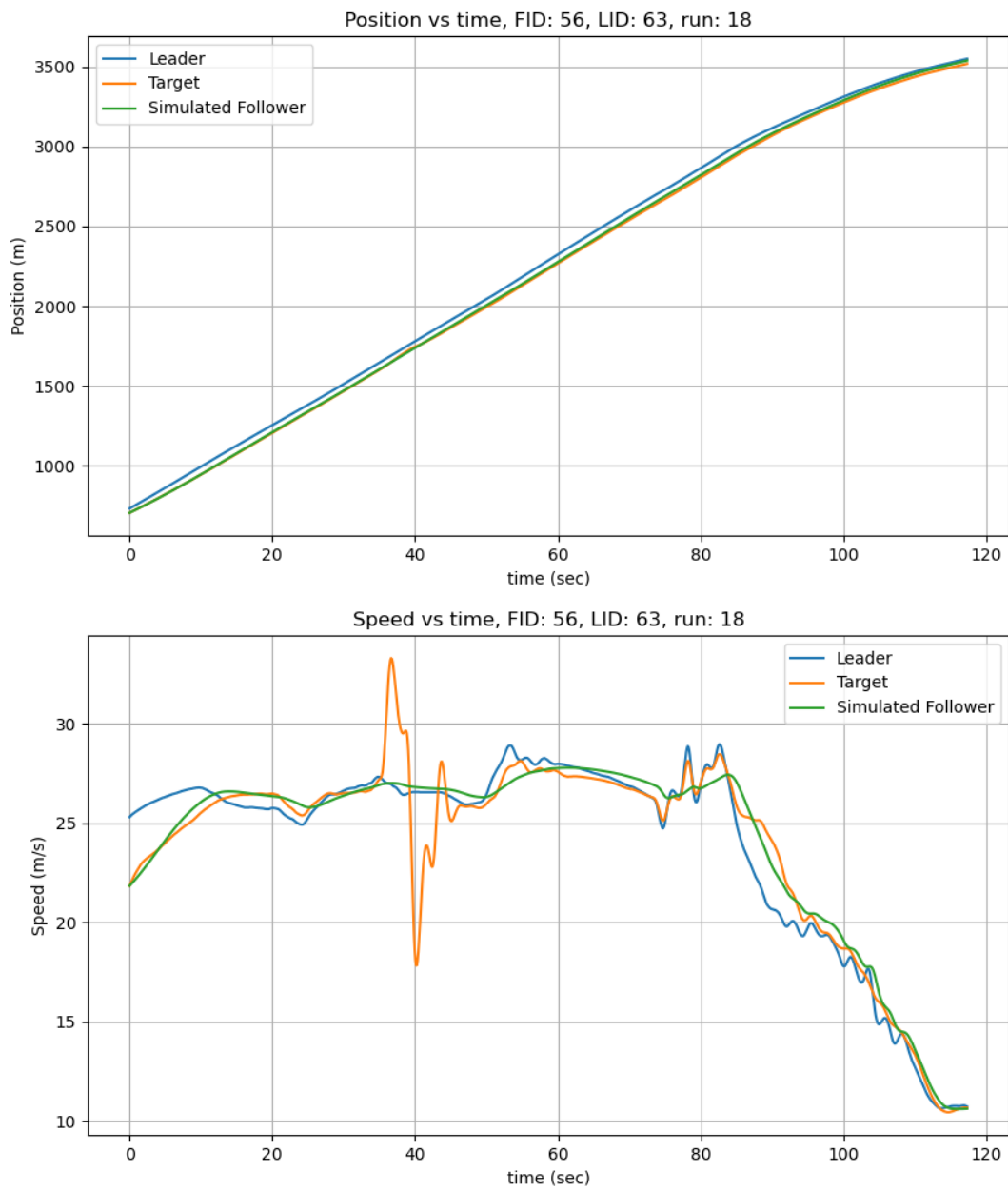


Figure 6.176: Position and speed for IDM for vehicle 56 in run 18 I294L1 dataset.

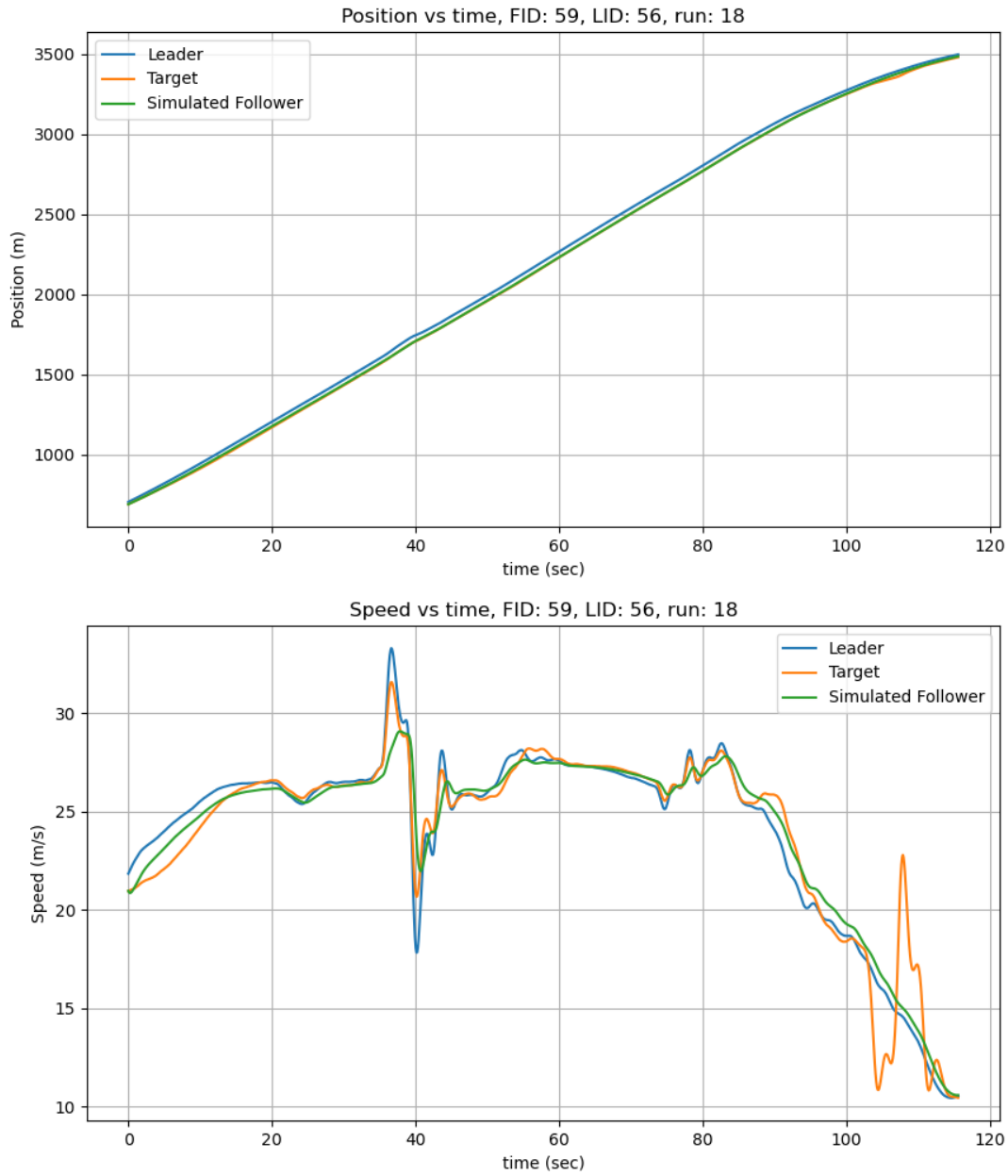


Figure 6.177: Position and speed for IDM for vehicle 59 in run 18 I294L1 dataset.

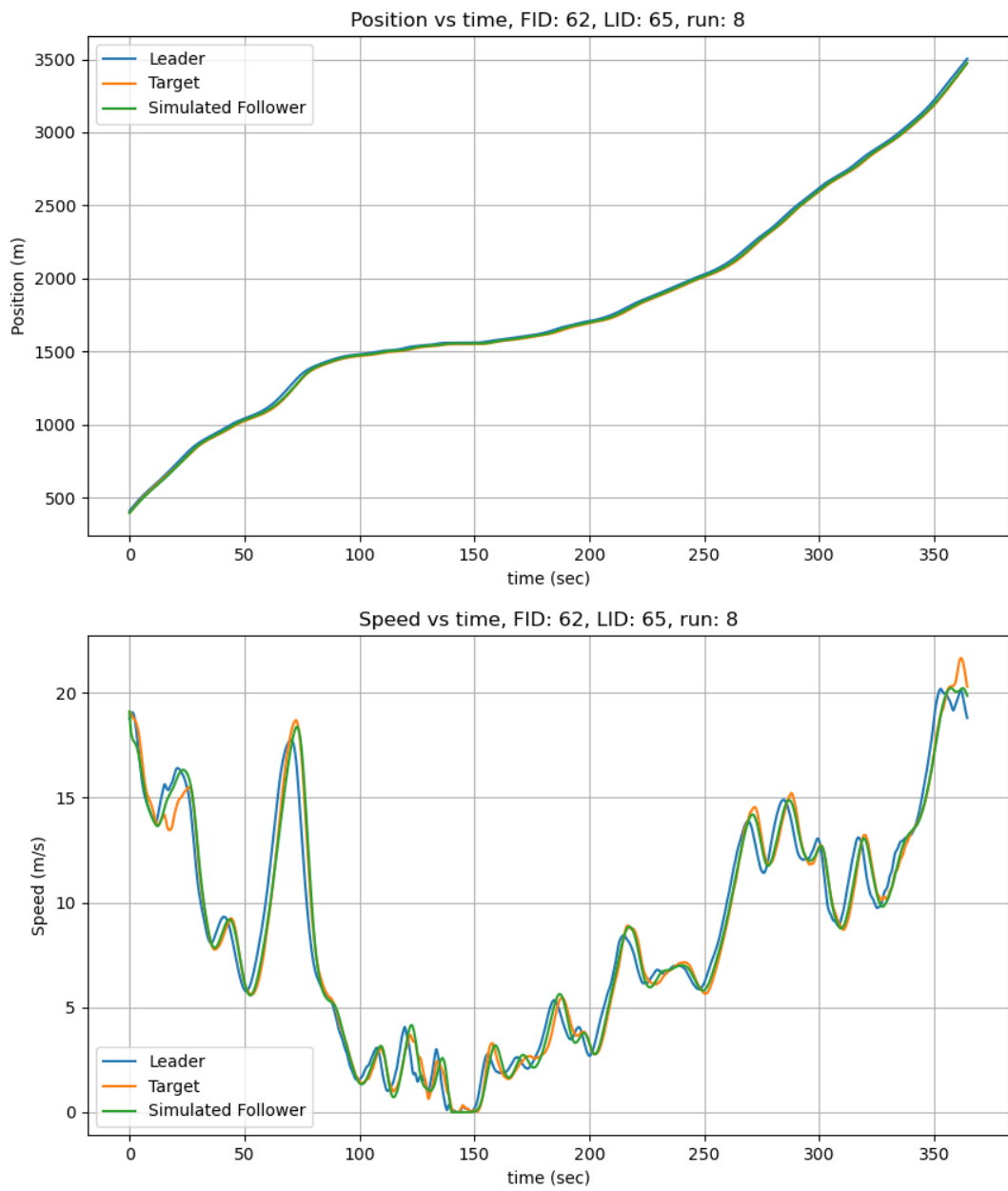


Figure 6.178: Position and speed for IDM for vehicle 62 in run 8 I294L1 dataset.

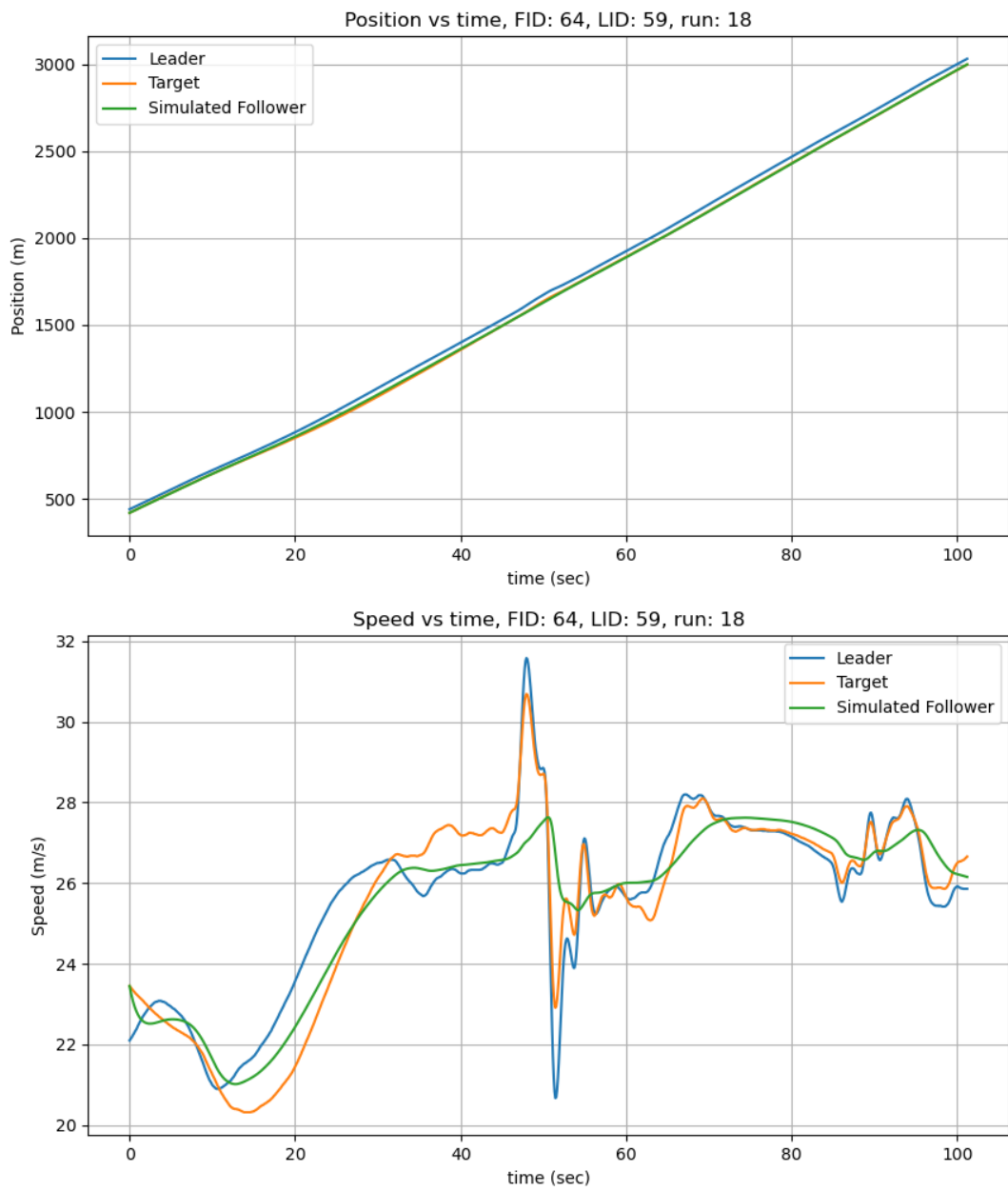


Figure 6.179: Position and speed for IDM for vehicle 64 in run 18 I294L1 dataset.

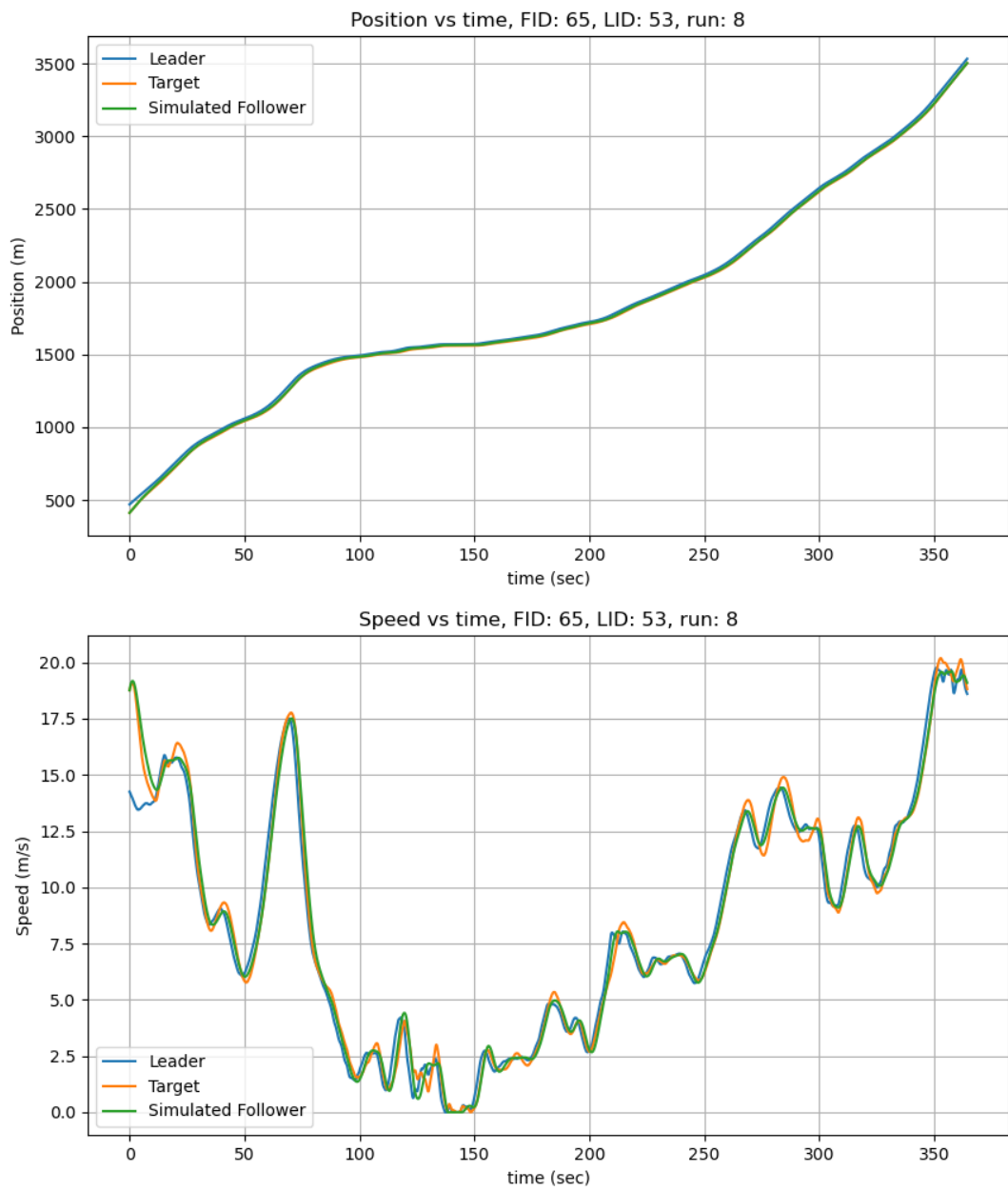


Figure 6.180: Position and speed for IDM for vehicle 65 in run 8 I294L1 dataset.

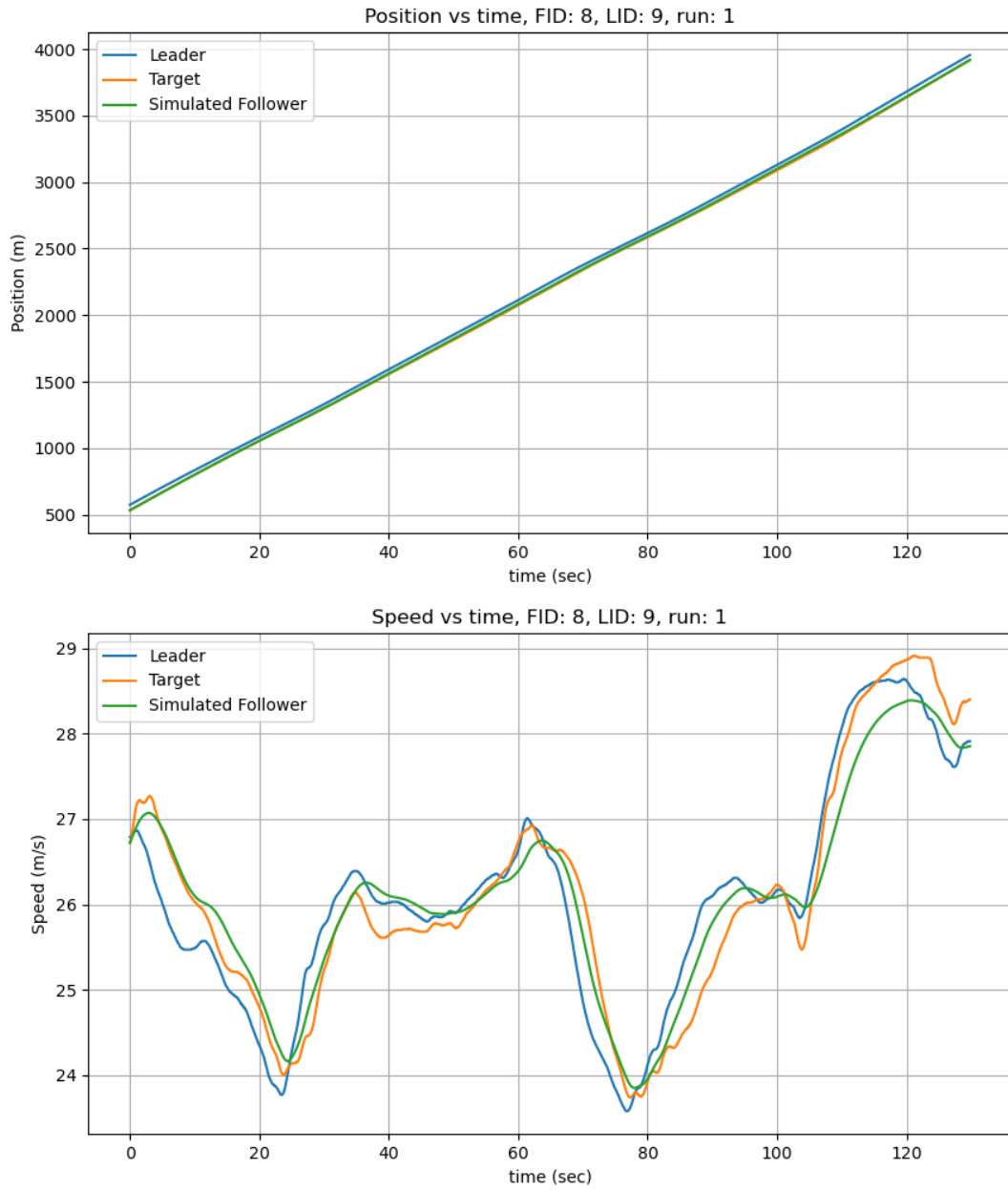


Figure 6.181: Position and speed for IDM for vehicle 8 in run 1 I294L1 dataset.

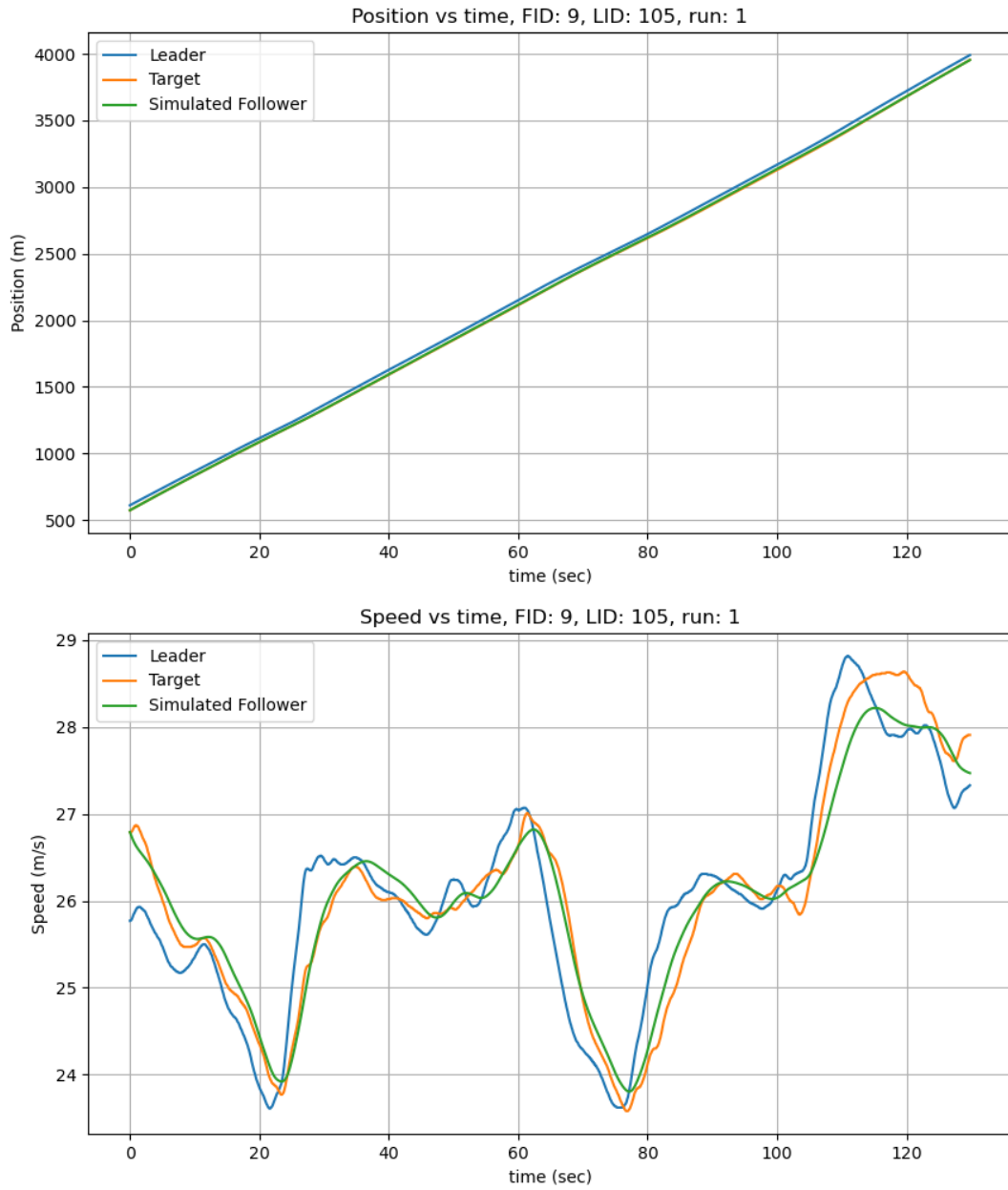


Figure 6.182: Position and speed for IDM for vehicle 9 in run 1 I294L1 dataset.

The optimized parameter ranges for the IDM model in the I294 dataset are presented in Figure 6.183, illustrating variability among different parameters. The desired speed (v_0)

exhibits the widest range, indicating that vehicles frequently operate at a relatively higher free-flow speed while maintaining safe following distances while driving in the highway.

Conversely, the parameters maximum acceleration (a_{max}), time headway (T), and comfortable deceleration (b) remain tightly clustered at the calibrated ranges, implying that the system requires minimal abrupt adjustments to ensure stability in traffic flow. The safe distance between vehicles (s_0) also shows moderate variability, indicating some adaptation in stopping distances based on different driving behaviors.

Furthermore, as illustrated in Figure 6.184, the optimized parameters follow multi-modal distributions, reflecting the diversity in driving behavior across different traffic conditions. This suggests that the calibration process effectively captures varying driving tendencies, from conservative to more aggressive driving styles, ensuring robust adaptation of the IDM model in real-world highway environments.

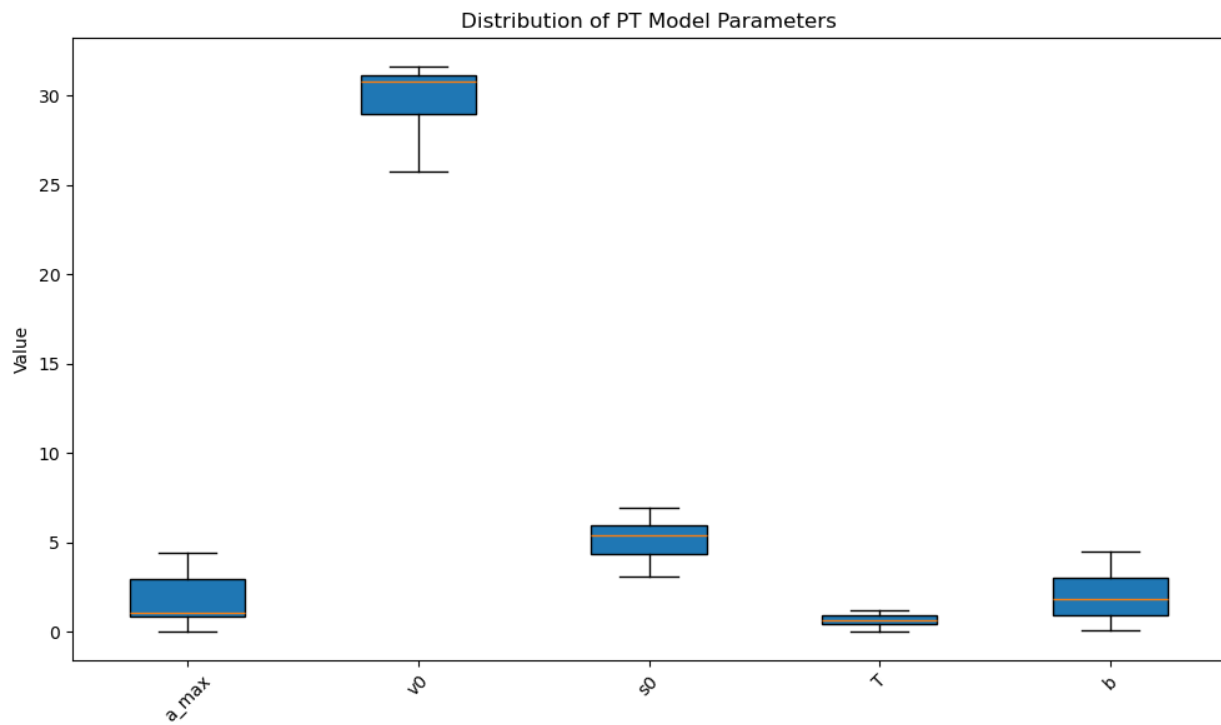


Figure 6.183: Parameter ranges for 04IDM in I294L1 dataset.

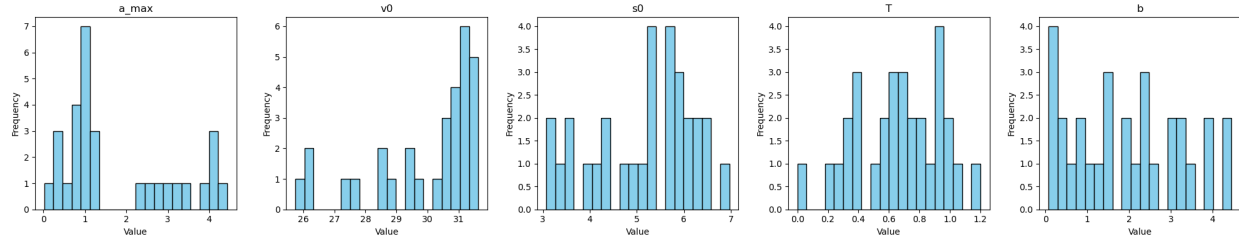


Figure 6.184: Parameter histogram for 04IDM in I294L1 dataset.

6.2.14 CSF I90/94 Simulated Results

The simulated results for I90/94 are presented in Figures 6.185 6.186, and 6.187 using IDM. For vehicle 5366 and 195, it can be determined that the controller can track the position with minimum speed pattern deviations shown in Figures 6.185 and 6.186. However, there is a minor deviation with speed patterns for vehicle 286 shown in Figure 6.187 although the simulated position closely aligns with the target position.

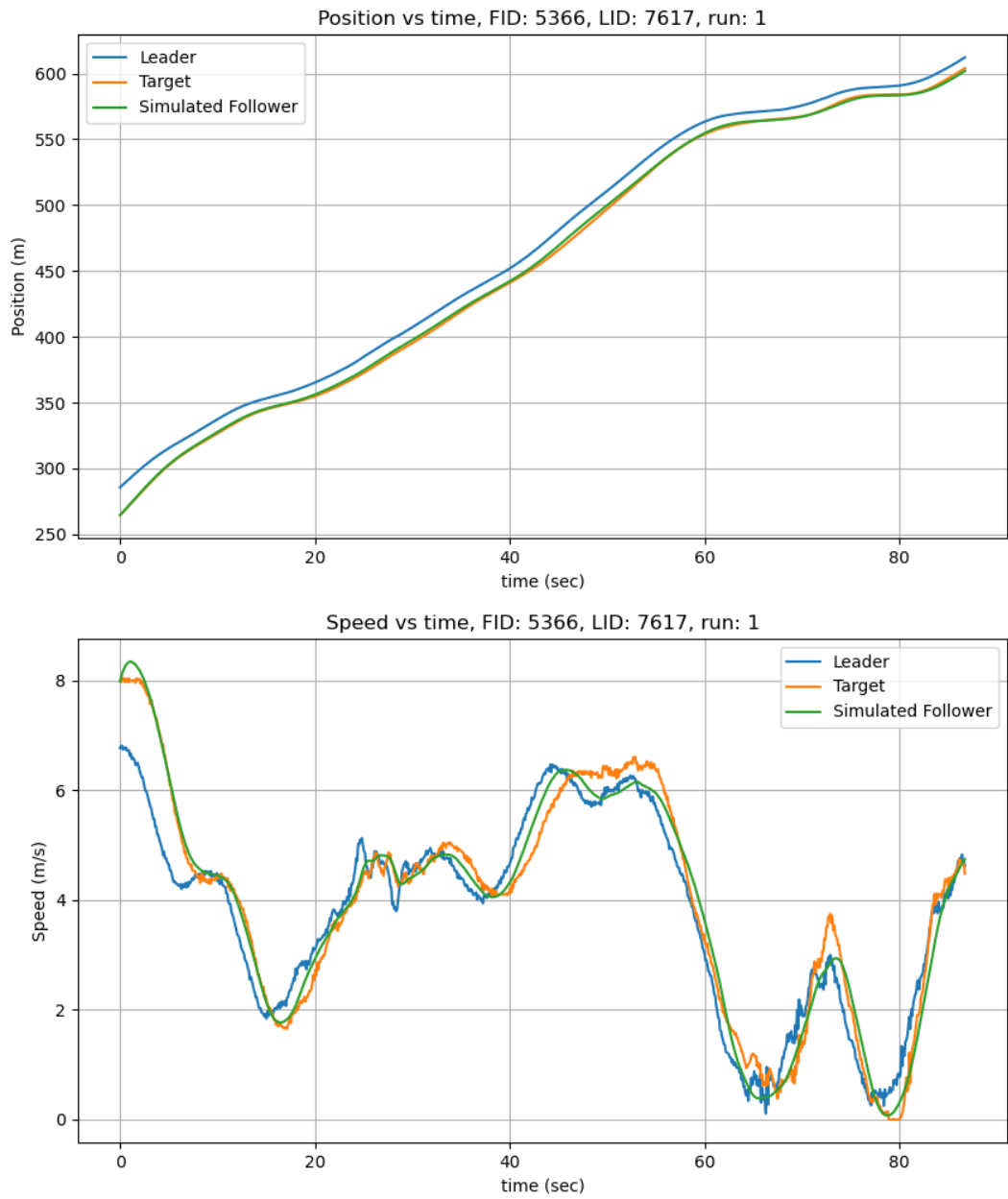


Figure 6.185: Position and speed for IDM for vehicle 5366 in I90/94 dataset.

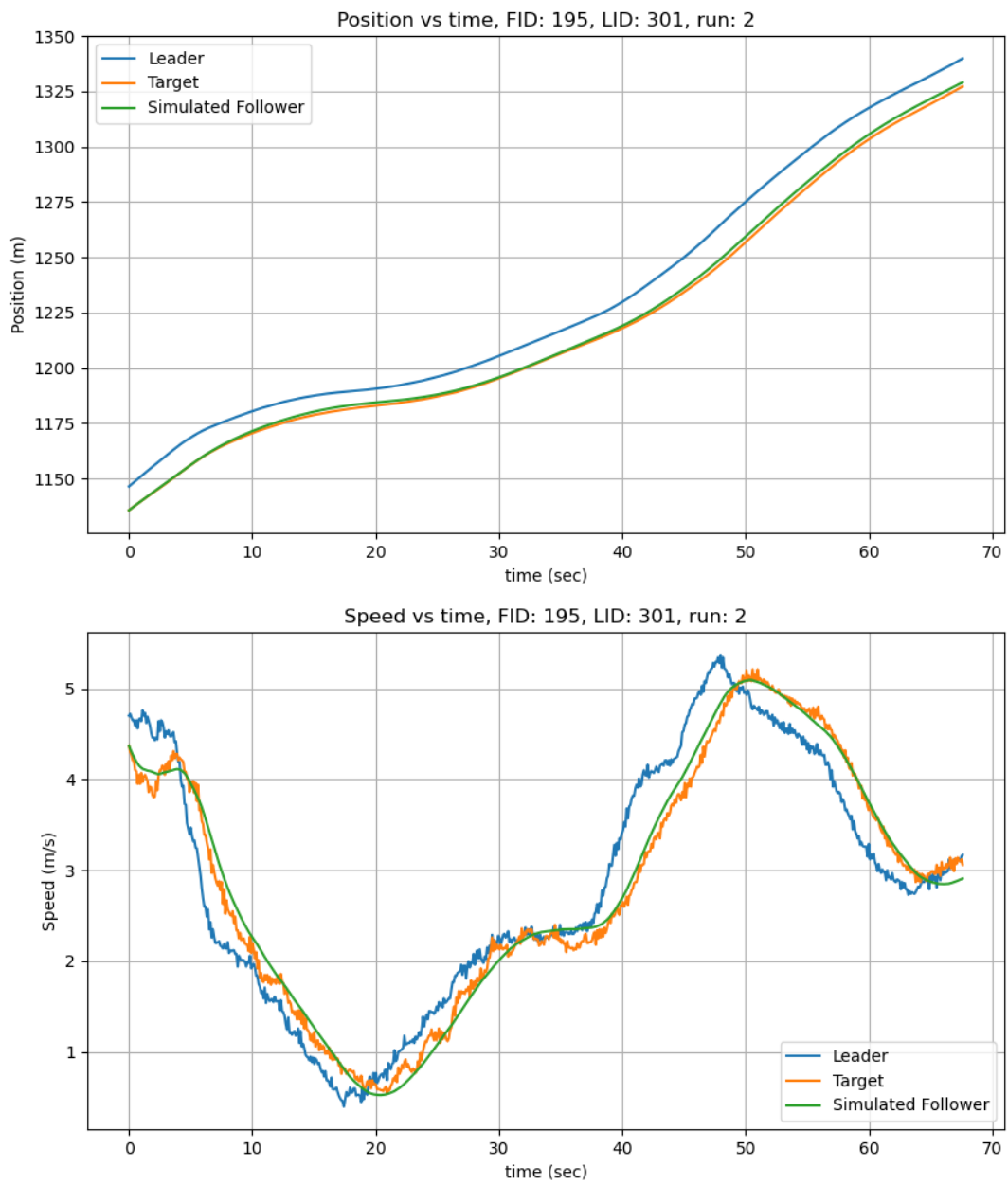


Figure 6.186: Position and speed for IDM for vehicle 195 in I90/94 dataset.

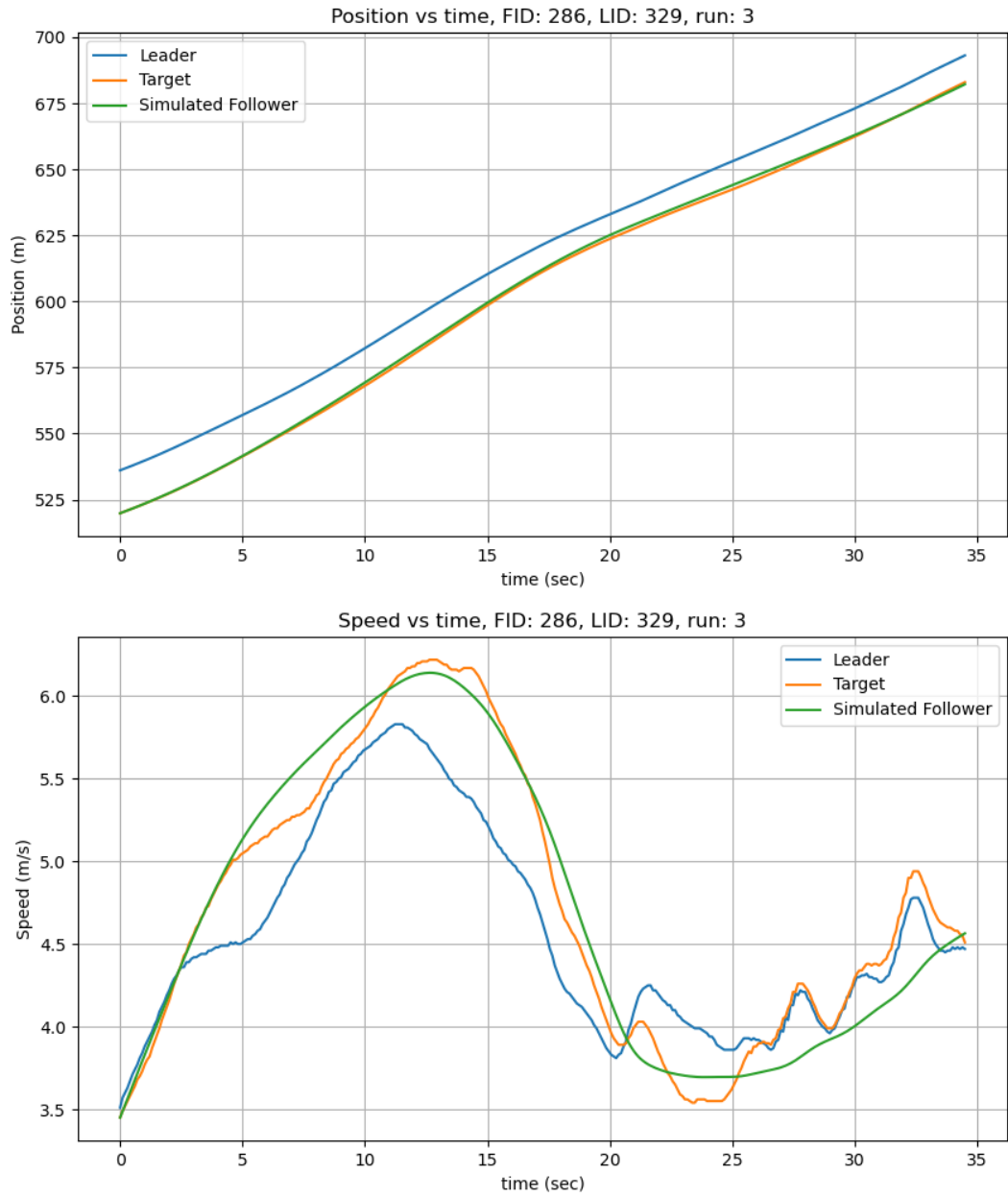


Figure 6.187: Position and speed for IDM for vehicle 286 in I90/94 dataset.

The optimized parameter ranges for IDM in the I90/94 dataset are illustrated in Figure 6.188, showing variations across different parameters. The desired speed (v_0) has the widest range,

suggesting that vehicles frequently travel at free-flow speed while maintaining a safe following distance. This indicates flexibility in speed adaptations.

In contrast, parameters such as the maximum acceleration (a_{max}), time headway (T), and comfortable deceleration (b) remain within a tighter range, implying consistent acceleration and braking behaviors with minimal sudden adjustments required for maintaining traffic stability. The safe distance between vehicles (s_0) also shows some variation, indicating variations in stopping distance.

Furthermore, as shown in Figure 6.189, the optimized parameters follow multi-modal distributions, suggesting varying driving behaviors across different traffic conditions. This variability of optimized parameters calibrated shows both conservative and aggressive driving behaviors replicating real-world driving patterns.

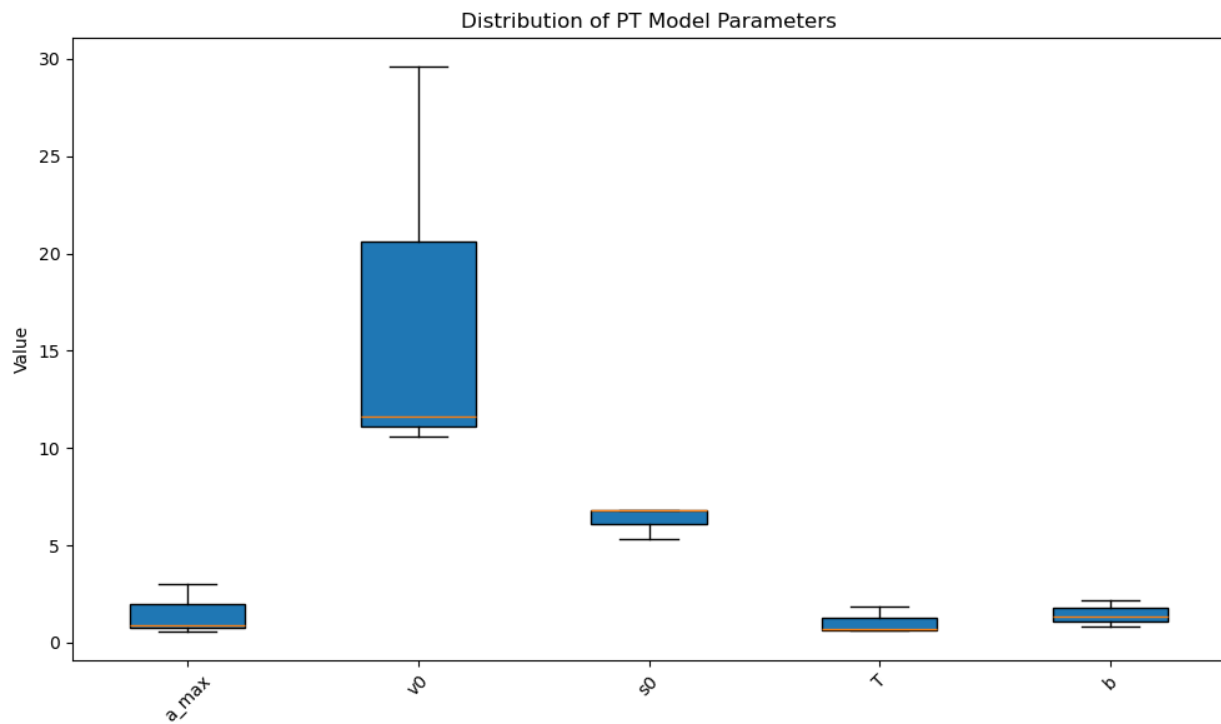


Figure 6.188: Parameter ranges for IDM in I90/94.

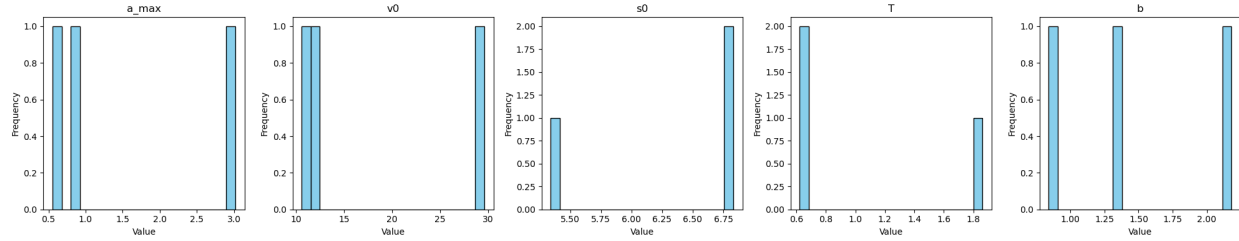


Figure 6.189: Parameter histogram for IDM in I90/94.

6.2.15 IDM Phoenix Simulated Results

The simulated results for the for IDM in the Phoenix dataset are presented in Figures 6.190, 6.191, 6.192, and 6.193. The simulated follower closely aligns with the calibrated position and speed of the target follower, as shown in Figures 6.190 and 6.193 for vehicles 13 and 2 in run 9NS. However, noticeable speed deviations are observed for vehicles 31 and 2 in run 9ES, as illustrated in Figures 6.191 and 6.192.

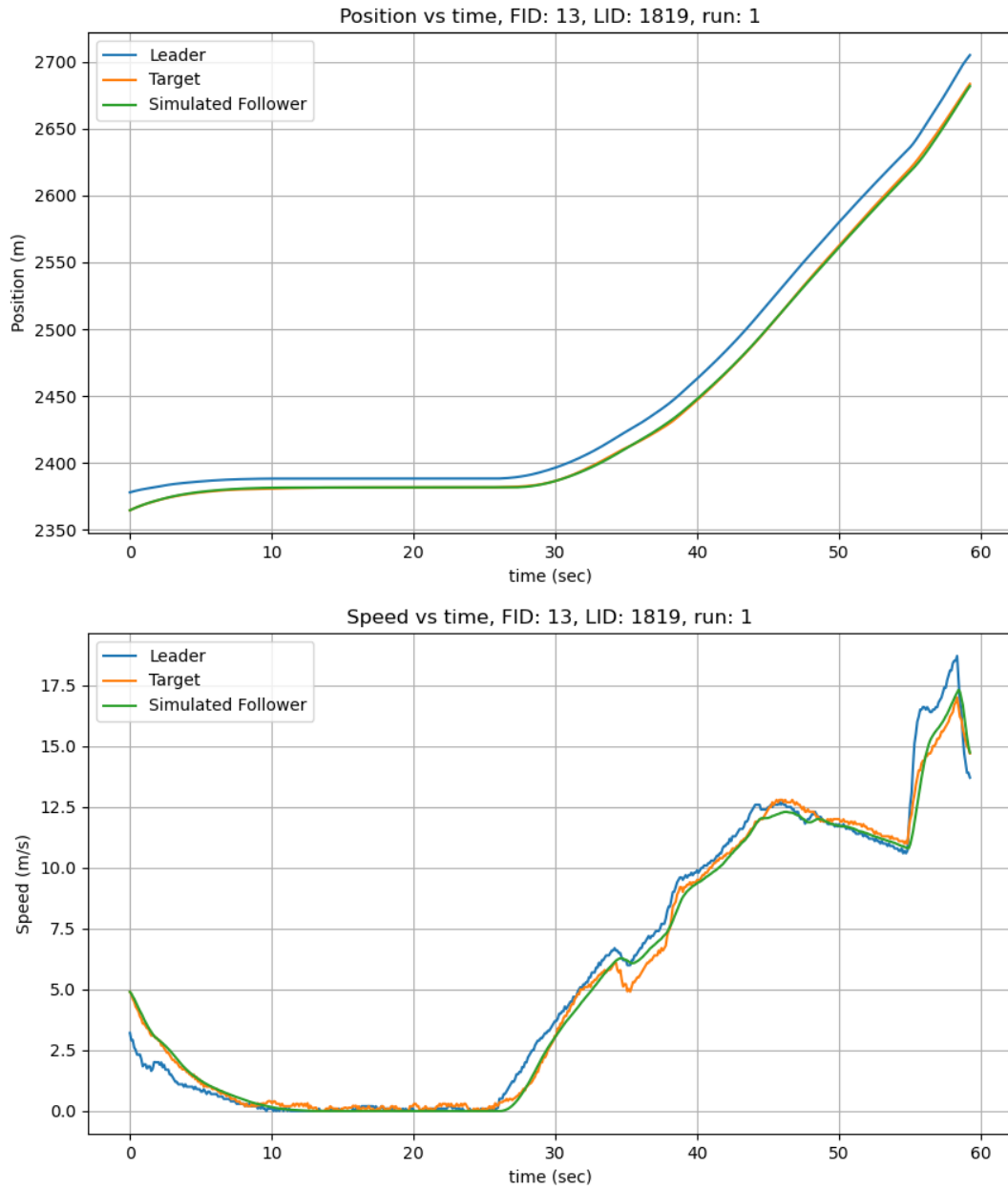


Figure 6.190: Position and speed for IDM for vehicle 13 in Phoenix data H1A3 run 6.

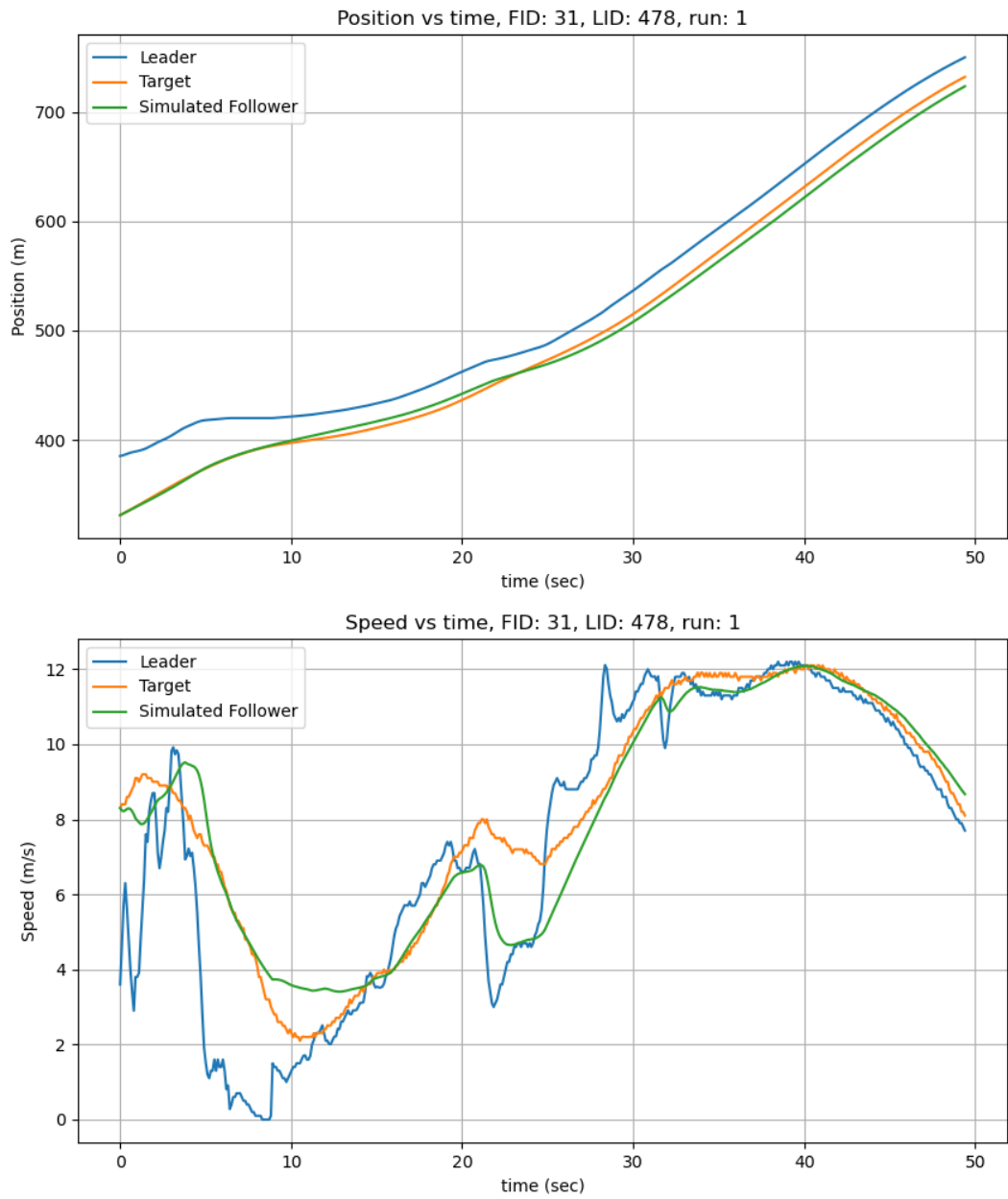


Figure 6.191: Position and speed for IDM for vehicle 31 in Phoenix data H1A3 run 1.

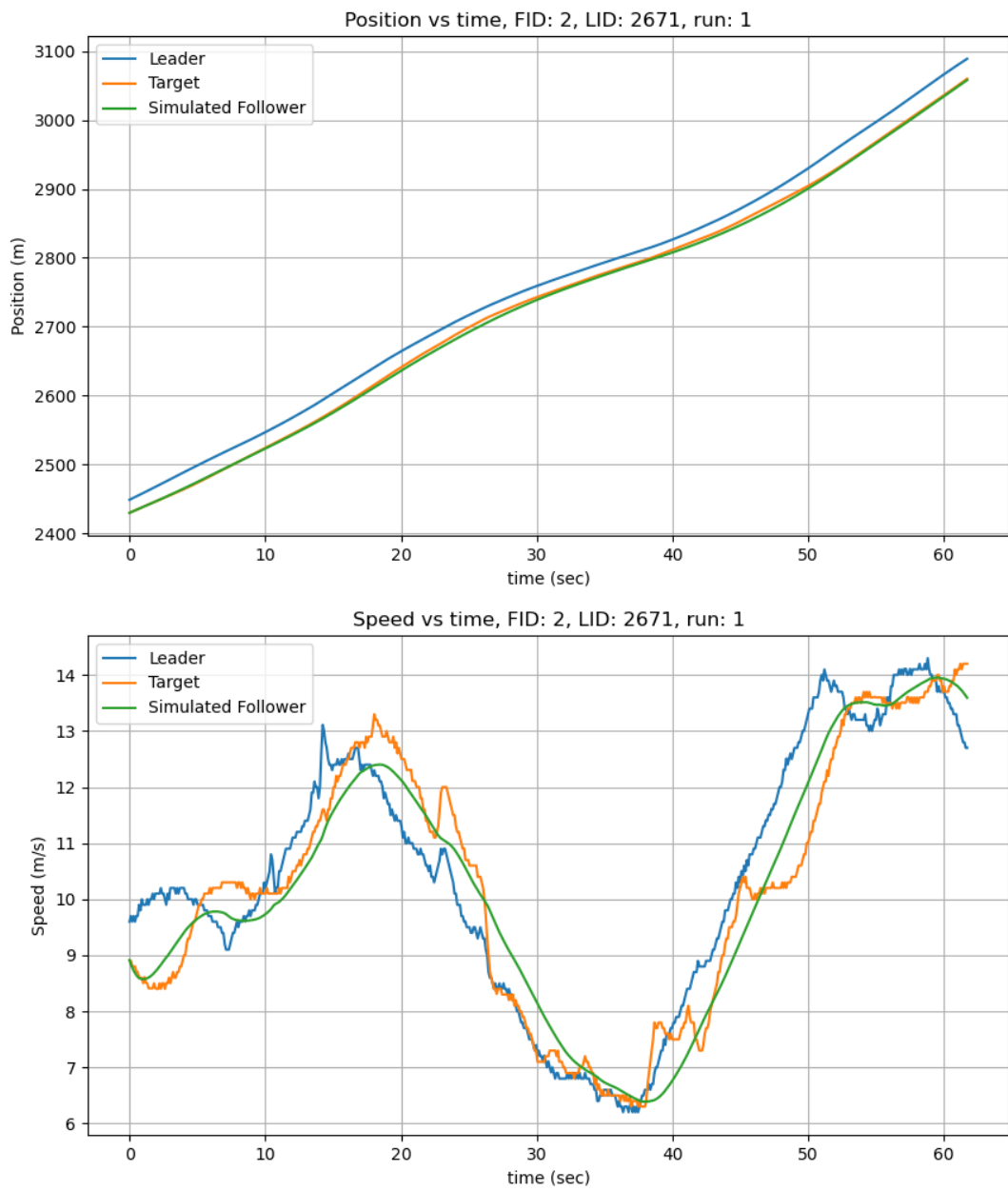


Figure 6.192: Position and speed for IDM for vehicle 2 in Phoenix data H1A3 run 9 ES.

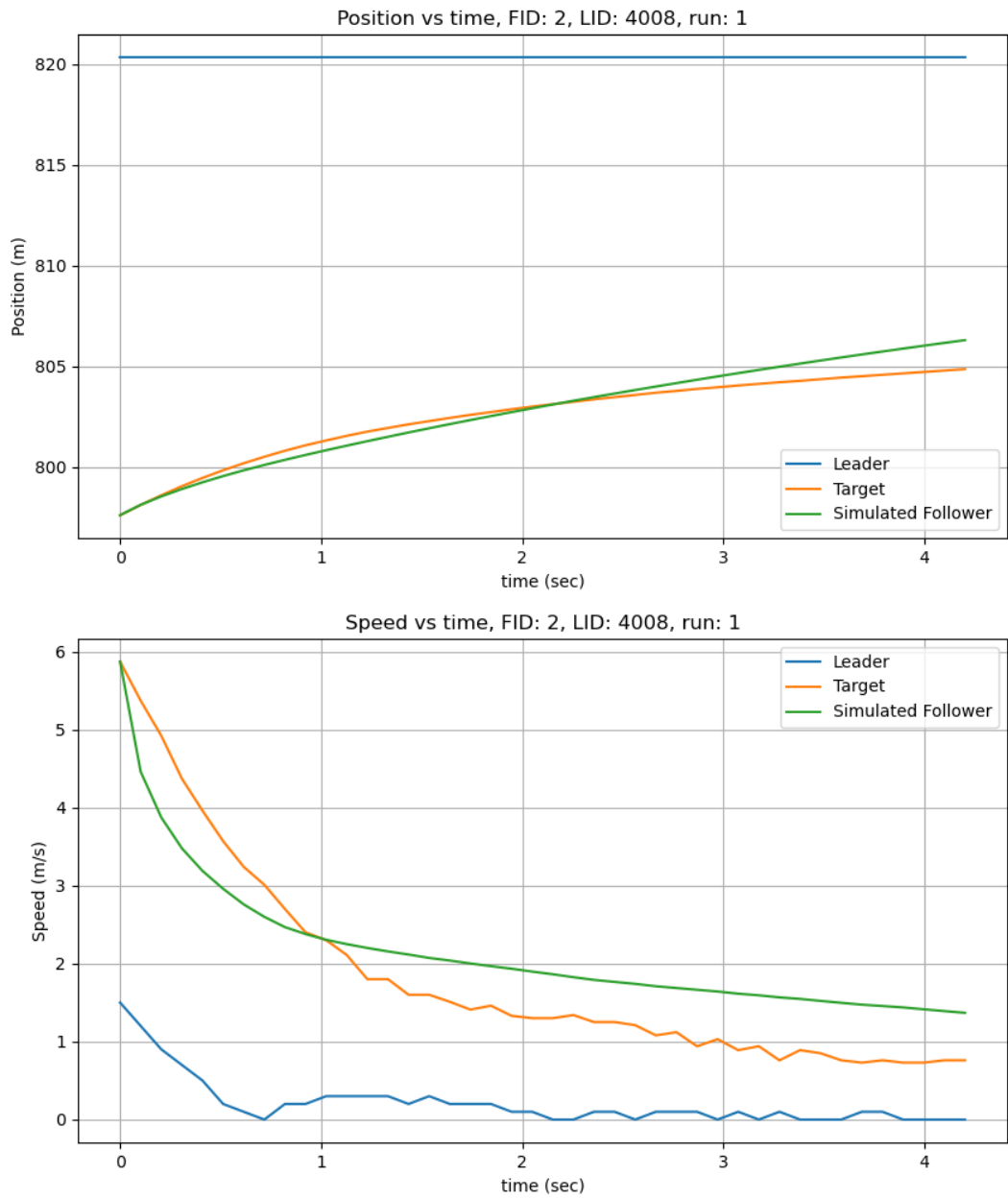


Figure 6.193: Position and speed for IDM for vehicle 2 in Phoenix data H1A3 run 9 NS.

The optimized parameter ranges for the Intelligent Driver Model (IDM) in the Phoenix dataset are presented in Figure 6.194, revealing notable variability across different parameters.

The desired speed (v_0) exhibits the largest variation, indicating that vehicles operate under diverse speed conditions, due to differences in driver behavior or fluctuating traffic conditions.

In contrast, the maximum acceleration (a_{\max}), time headway (T), and comfortable deceleration (b) remain within a more confined range. These results indicate that vehicles experience fewer abrupt acceleration and braking maneuvers, leading to more stable and safe car-following behavior. The safe distance between vehicles (s_0) is relatively small, strongly suggesting that vehicles maintain close following distances, due to high-density traffic scenarios in the dataset.

Additionally, some outliers are observed across multiple parameters during calibration, particularly in (s_0) and (b), suggesting that some vehicles had more aggressive or conservative driving behaviors. These outliers indicate that the vehicles had to adjust its control inputs in response to exceptional cases of unusually short headways or higher deceleration rates, deviating from the general traffic trend.

Figure 6.195 presents the distributions of the calibrated IDM parameters following multi-modal distributions. The distribution of (v_0) suggests distinct driving groups with varying speed values, while the acceleration and deceleration distributions indicate that most of the times, the vehicles adhere to a common driving pattern with minimal deviations. Multiple peaks of the calibrated parameters in the histograms shows the adaptability of IDM in replicating changing driving behaviors, ensuring a realistic representation of vehicle interactions within the Phoenix dataset.

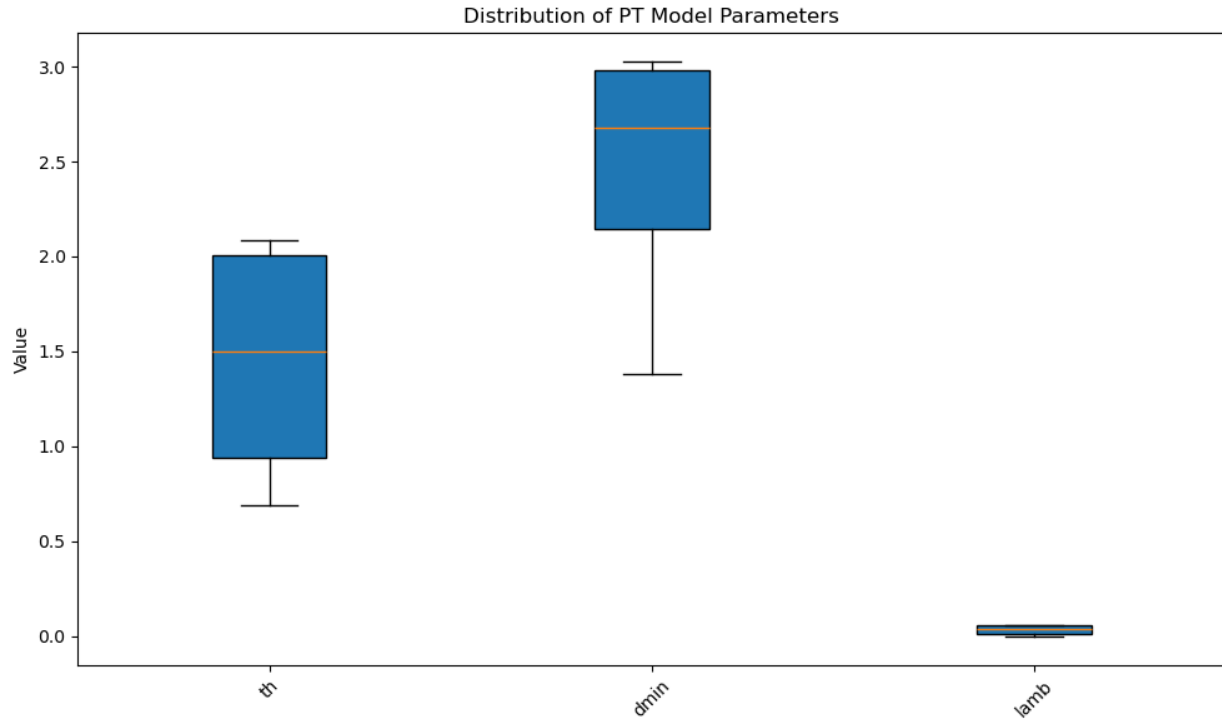


Figure 6.194: Parameter ranges for IDM in Phoenix.

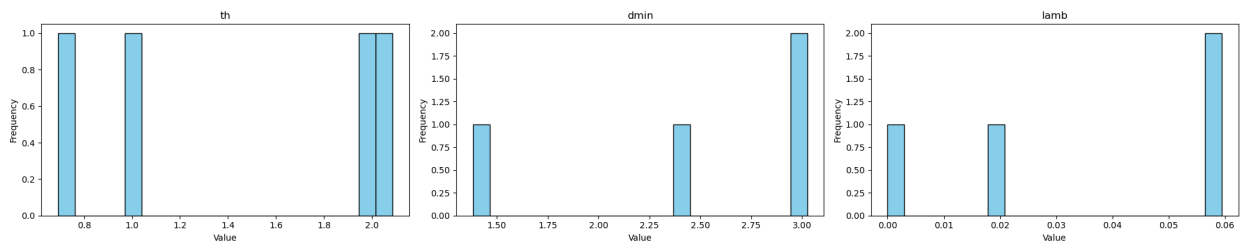


Figure 6.195: Parameter histogram for IDM in Phoenix.

6.3 Model Comparison

The control spacing policies were evaluated across the major highway datasets from I294, I90/94 and Phoenix. While the genetic algorithm calibrates the optimal parameters for each control spacing policy, the fitness function calculates the critical error metrics including the Mean Squared Error (MSE), Root Mean Squared Error (RMSE), Mean Absolute Error (MAE), Mean Absolute Percentage Error (MAPE), Normalized Root Mean Squared Error (NMSE), Sum of Squared Errors (SSE), and R^2 values to evaluate how well the model can align the simulated trajectories with the target trajectories. Results for each model in different highway datasets are shown in Table 6.7. The overall performance of the models across all

the highway datasets are presented in Table 6.8. These results implies that some control spacing policies may be suitable for varying traffic environments where other control spacing policies may be more appropriate for less fluctuating traffic environments.

Table 6.7: Performance comparison of different models on various datasets.

Model	Dataset	Error	MSE	RMSE	MAE	MAPE	NRMSE	SSE	R²
CSP	I294L1	494.344	0.473	0.604	0.435	3.359	0.066	49.174	0.902
CSP	I90/94	125.986	0.063	0.243	0.188	11.443	0.052	44.904	0.964
CSP	Phoenix	177.835	0.252	0.443	0.337	8.949	0.047	136.000	0.968
CTH	I294L1	514.590	0.527	0.639	0.457	3.805	0.069	48.538	0.894
CTH	I90/94	129.926	0.067	0.245	0.198	13.556	0.054	45.883	0.956
CTH	Phoenix	166.755	0.227	0.421	0.311	8.501	0.044	125.144	0.971
TFS	I294L1	526.597	0.493	0.619	0.428	3.845	0.063	55.824	0.911
TFS	I90/94	162.373	0.094	0.305	0.246	15.661	0.068	63.905	0.939
TFS	Phoenix	175.720	0.290	0.458	0.336	11.781	0.048	153.492	0.966
CSF	I294L1	495.446	0.417	0.566	0.400	3.897	0.058	42.474	0.929
CSF	I90/94	137.392	0.074	0.266	0.208	15.025	0.059	50.214	0.952
CSF	Phoenix	182.762	0.270	0.473	0.363	14.353	0.051	143.946	0.964
IDM	I294L1	414.087	0.368	0.538	0.384	2.993	0.064	389.799	0.893
IDM	I90/94	106.421	0.046	0.204	0.161	8.302	0.045	31.795	0.971
IDM	Phoenix	176.835	0.370	0.577	0.448	22.665	0.072	152.224	0.916

Table 6.8: Overall performance of models across the highway datasets.

Model	Error	MSE	RMSE	MAE	MAPE	NRMSE	SSE	R²
CSP	266.055	0.263	0.430	0.320	7.917	0.055	232.296	0.945
CTH	270.424	0.274	0.435	0.322	8.621	0.056	241.246	0.940
TFS	288.230	0.293	0.461	0.337	10.429	0.060	265.179	0.939
CSF	271.867	0.254	0.435	0.324	11.092	0.056	229.596	0.948
IDM	232.448	0.261	0.440	0.331	11.320	0.060	191.273	0.927

The CSP model has demonstrated stable performance across all the highway datasets used for this study, showing relatively low error values across all metrics calculated by the fitness function. The CSP model had the lowest RMSE value of 0.243 and the highest R^2 value of 0.964 in the I90/94 dataset, indicating a strong alignment between the simulated and target trajectories during calibration. However, the MAPE value of 8.949% in the Phoenix dataset suggests that the CSP model struggles to encounter the external factors that affect

the inter-vehicular spacing. Stability has been maintained most of the time and the simulated trajectories generated by the CSP model closely aligns then target trajectories.

The CTH model had slightly higher MSE and RMSE values compared to the CSP model, suggesting a marginally weaker performance in tracking the trajectories. The high MAPE value of 13.556% in the I90/94 dataset implies that the model is more sensitive to speed variations between the leading and the surrounding vehicles. However, the R^2 values consistently remained above 0.940, suggesting that the simulated trajectories were mostly well-aligned with the target trajectories. Overall, the CTH model performs comparably to CSP, although it appears more prone to speed variations in dynamic traffic conditions.

The TFS policy had the highest error metrics across all the highway datasets, evidently showing higher deviations between the simulated and target trajectories. The MAPE value of 15.661% in the I90/94 dataset is significantly higher than the MAPE values of other models, suggesting that the TFS policy struggles to maintain stability in congested traffic conditions. While the R^2 values remain above 0.91, the high error values indicate that the TFS policy is less robust compared to the other models considered in this study. This suggests that TFS may not effectively handle variations in acceleration and deceleration, leading to suboptimal trajectory predictions. Additionally, the relatively higher RMSE and SSE values indicate that errors accumulate over time, further impacting the ability to align itself with the target trajectory in dynamic highway conditions.

The CSF policy has demonstrated overall stable performance by effectively balancing vehicle dynamics and trajectory alignment while prioritizing safety. The CSF model achieved the lowest RMSE value of 0.566 in the I294 dataset, indicating strong predictive accuracy. However, the relatively high MAPE value of 14.533% suggests some difficulties in adapting to varying traffic conditions, particularly in scenarios with abrupt speed changes. Despite this, with R^2 values consistently above 0.94, the CSF model exhibits strong target trajectory tracking capabilities, making it a reliable choice for maintaining smooth and stable traffic flow.

The IDM model has exhibited mixed performance across the highway datasets. The model achieved the lowest RMSE value of 0.204 in the I90/94 dataset, indicating strong trajectory alignment under relatively stable highway conditions. However, the model struggled in the Phoenix dataset, where it had the highest MAPE value of 22.665%, suggesting significant difficulty in adapting to varying traffic conditions and external disturbances. The overall R^2 values remained high, exceeding 0.92, showing that IDM can reasonably align

itself with the target trajectories. However, the MAPE in Phoenix indicates that IDM may be more sensitive to traffic flow variations and abrupt decelerations compared to CSP and CSF.

Based on the overall dataset performance, it can be determined that the CSP and CSF policies are the most reliable control spacing models, having the lowest RMSE values and consistently high R^2 scores. The CTH model, while effective, appears less suitable for scenarios involving frequent speed variations. In contrast, the TFS policy displayed the highest errors, indicating challenges in maintaining stable traffic flow. The IDM model, while effective in stable conditions, exhibited higher errors in complex environments, suggesting a need for refined parameter tuning. Given the calibration results, CSP and CSF are the most appropriate models for simulating car-following behavior, while the TFS policy and IDM may require additional modifications to improve robustness in fluctuating traffic conditions.

Chapter 7: Conclusion

Maintaining appropriate and safe following gap between vehicles is critical for autonomous vehicles. The five most commonly used policies which are Constant Spacing Policy (CSP), Constant Time Headway (CTH), Traffic Flow Stability (TFS), Constant Safety Factor (CSF), and the Intelligent Driver Model (IDM) were calibrated using the genetic algorithm to find the optimized parameters for each policy respectively using the highway datasets from I294, I90/94, and Phoenix Waymo vehicle trajectories for simulating the control spacing models.

The simulated plots comparing trajectories generated by control spacing policies and observed trajectories illustrate how well the generated trajectories align with the observed trajectories. The trajectories simulated by CSP and CSF models closely aligned with the observed vehicle trajectories, demonstrating minimal perturbations in both position and speed of the vehicles across stable traffic conditions. These models effectively and safely maintained the inter-vehicular spacing, achieving smoother trajectory profiles with fewer oscillations. Conversely, the IDM model showed greater variability in certain conditions but the model was able to replicate realistic acceleration and deceleration patterns, making it suitable for dynamic traffic environments. The CTH model was effective in controlled conditions, despite the occasional perturbations under conditions where the surrounding vehicles rapidly change their speeds. The TFS model consistently demonstrated higher trajectory errors, particularly in congested scenarios, indicating its limited reliability in complex traffic conditions.

The performance of the control spacing policies were contingent on the traffic conditions. The CSP and CSF policies were relatively more reliable by consistently achieving the lowest Root Mean Squared Error (RMSE) and highest R^2 values. The CSP model showed stable performance under low-density highway conditions by maintaining uniform spacing effectively with minimal perturbations. The CSF policy was determined to be performing optimally in high-density scenarios, effectively managing critical safety concerns, including abrupt acceleration and braking events, due to the dynamic safety-margin adjustments.

While the CTH policy showed robust performance similar to CSP in stable conditions, it exhibited increased sensitivity and higher errors under scenarios with significant speed variations. This highlights the model's limitations in adapting swiftly to fluctuating speeds. The TFS policy consistently produced higher errors across datasets, reflecting challenges in handling congested, dynamically complex traffic scenarios, and thus was the least reliable for accurate trajectory prediction.

The Intelligent Driver Model (IDM) demonstrated strong performance in accurately simulating realistic driver behavior across diverse traffic conditions. The IDM model was also able to replicate smooth acceleration and deceleration patterns. However, achieving optimal performance required precise calibration, especially in high-density scenarios where dynamic adjustments to speed and spacing are frequent.

In conclusion, the CSP model is recommended for scenarios prioritizing stability and uniform traffic flow, typically in lower-density highway conditions. The CSF policy is effective when safety considerations need to be prioritized, such as dense traffic conditions requiring frequent adjustments to spacing between the surrounding vehicles. The IDM is suitable for accurately modeling realistic vehicle behavior but demands meticulous calibration. Future research should explore hybrid spacing policies integrating multiple strategies to integrate individual models for more adaptive and resilient implementations for self-driving technology.

References

- [1] C. C. C. D. SWAROOP J.K. HEDRICK and P. IOANNOU, “A comparision of spacing and headway control laws for automatically controlled vehicles,” *Vehicle System Dynamics*, vol. 23, no. 1, pp. 597–625, 1994. DOI: [10.1080/00423119408969077](https://doi.org/10.1080/00423119408969077). [Online]. Available: <https://doi.org/10.1080/00423119408969077>.
- [2] C. Wu, Z. Xu, Y. Liu, C. Fu, K. Li, and M. Hu, “Spacing policies for adaptive cruise control: A survey,” *IEEE Access*, vol. 8, pp. 50 149–50 162, 2020. DOI: [10.1109/ACCESS.2020.2978244](https://doi.org/10.1109/ACCESS.2020.2978244).
- [3] M. Treiber, A. Hennecke, and D. Helbing, “Congested traffic states in empirical observations and microscopic simulations,” *Physical Review E*, vol. 62, no. 2, pp. 1805–1824, 2000. DOI: [10.1103/PhysRevE.62.1805](https://doi.org/10.1103/PhysRevE.62.1805).
- [4] G. An and A. Talebpour, “Lane-changing trajectory optimization to minimize traffic flow disturbance in a connected automated driving environment,” in *2019 IEEE Intelligent Transportation Systems Conference (ITSC)*, 2019, pp. 1794–1799. DOI: [10.1109/ITSC.2019.8916942](https://doi.org/10.1109/ITSC.2019.8916942).
- [5] V. Milanés, S. E. Shladover, J. Spring, C. Nowakowski, H. Kawazoe, and M. Nakamura, “Cooperative adaptive cruise control in real traffic situations,” *IEEE Transactions on Intelligent Transportation Systems*, vol. 15, no. 1, pp. 296–305, 2014. DOI: [10.1109/TITS.2013.2278494](https://doi.org/10.1109/TITS.2013.2278494).
- [6] S. Moon, I. Moon, and K. Yi, “Design, tuning, and evaluation of a full-range adaptive cruise control system with collision avoidance,” *Control Engineering Practice*, vol. 17, no. 4, pp. 442–455, 2009, ISSN: 0967-0661. DOI: <https://doi.org/10.1016/j.conengprac.2008.09.006>. [Online]. Available: <https://www.sciencedirect.com/science/article/pii/S0967066108001548>.
- [7] R. Rajamani and C. Zhu, “Semi-autonomous adaptive cruise control systems,” *Vehicular Technology, IEEE Transactions on*, vol. 51, pp. 1186–1192, Oct. 2002. DOI: [10.1109/TVT.2002.800617](https://doi.org/10.1109/TVT.2002.800617).

- [8] D. Chen, S. Ahn, M. Chitturi, and D. Noyce, “Truck platooning on uphill grades under cooperative adaptive cruise control (cacc),” *Transportation Research Part C: Emerging Technologies*, vol. 94, pp. 50–66, 2018, ISTTT22, ISSN: 0968-090X. DOI: <https://doi.org/10.1016/j.trc.2017.08.025>. [Online]. Available: <https://www.sciencedirect.com/science/article/pii/S0968090X17302346>.
- [9] D. Yanakiev and I. Kanellakopoulos, “Variable time headway for string stability of automated heavy-duty vehicles,” in *Proceedings of 1995 34th IEEE Conference on Decision and Control*, vol. 4, 1995, 4077–4081 vol.4. DOI: [10.1109/CDC.1995.479245](https://doi.org/10.1109/CDC.1995.479245).
- [10] G. J. L. Naus, R. P. A. Vugts, J. Ploeg, M. J. G. van de Molengraft, and M. Steinbuch, “String-stable cacc design and experimental validation: A frequency-domain approach,” *IEEE Transactions on Vehicular Technology*, vol. 59, no. 9, pp. 4268–4279, 2010. DOI: [10.1109/TVT.2010.2076320](https://doi.org/10.1109/TVT.2010.2076320).
- [11] D. L. Luu, C. Lupu, L. S. Ismail, and H. Alshareefi, “Spacing control of cooperative adaptive cruise control vehicle platoon,” in *2020 IEEE International Conference on Automation, Quality and Testing, Robotics (AQTR)*, 2020, pp. 1–6. DOI: [10.1109/AQTR49680.2020.9129997](https://doi.org/10.1109/AQTR49680.2020.9129997).
- [12] A. Talebpour and H. S. Mahmassani, “Influence of connected and autonomous vehicles on traffic flow stability and throughput,” *Transportation Research Part C: Emerging Technologies*, vol. 71, pp. 143–163, 2016, ISSN: 0968-090X. DOI: <https://doi.org/10.1016/j.trc.2016.07.007>. [Online]. Available: <https://www.sciencedirect.com/science/article/pii/S0968090X16301140>.
- [13] G. Cesari, G. Schildbach, A. Carvalho, and F. Borrelli, “Scenario model predictive control for lane change assistance and autonomous driving on highways,” *IEEE Intelligent Transportation Systems Magazine*, vol. 9, no. 3, pp. 23–35, 2017. DOI: [10.1109/MITS.2017.2709782](https://doi.org/10.1109/MITS.2017.2709782).
- [14] M. Wang, S. P. Hoogendoorn, W. Daamen, B. van Arem, and R. Happee, “Game theoretic approach for predictive lane-changing and car-following control,” *Transportation Research Part C: Emerging Technologies*, vol. 58, pp. 73–92, 2015, ISSN: 0968-090X. DOI: <https://doi.org/10.1016/j.trc.2015.07.009>. [Online]. Available: <https://www.sciencedirect.com/science/article/pii/S0968090X15002491>.
- [15] Y. Zheng, S. E. Li, K. Li, F. Borrelli, and J. K. Hedrick, “Distributed model predictive control for heterogeneous vehicle platoons under unidirectional topologies,” *IEEE Transactions on Control Systems Technology*, vol. 25, no. 3, pp. 899–910, 2017. DOI: [10.1109/TCST.2016.2594588](https://doi.org/10.1109/TCST.2016.2594588).

- [16] S. Zhao and K. Zhang, “A distributionally robust stochastic optimization-based model predictive control with distributionally robust chance constraints for cooperative adaptive cruise control under uncertain traffic conditions,” *Transportation Research Part B: Methodological*, vol. 138, pp. 144–178, 2020, ISSN: 0191-2615. DOI: <https://doi.org/10.1016/j.trb.2020.05.001>. [Online]. Available: <https://www.sciencedirect.com/science/article/pii/S0191261520303155>.
- [17] G. An and A. Talebpour, “Vehicle platooning control for merge coordination: A hybrid acc-dmpc approach,” in *2022 IEEE 25th International Conference on Intelligent Transportation Systems (ITSC)*, 2022, pp. 1611–1616. DOI: [10.1109/ITSC55140.2022.9922330](https://doi.org/10.1109/ITSC55140.2022.9922330).
- [18] A. Talebpour, H. S. Mahmassani, and S. H. Hamdar, “Effect of information availability on stability of traffic flow: Percolation theory approach,” *Transportation Research Part B: Methodological*, vol. 117, pp. 624–638, 2018, TRB:ISTTT-22, ISSN: 0191-2615. DOI: <https://doi.org/10.1016/j.trb.2017.09.005>. [Online]. Available: <https://www.sciencedirect.com/science/article/pii/S0191261517308226>.
- [19] B. van Arem, C. J. G. van Driel, and R. Visser, “The impact of cooperative adaptive cruise control on traffic-flow characteristics,” *IEEE Transactions on Intelligent Transportation Systems*, vol. 7, no. 4, pp. 429–436, 2006. DOI: [10.1109/TITS.2006.884615](https://doi.org/10.1109/TITS.2006.884615).
- [20] R. Rajamani, H.-S. Tan, B. K. Law, and W.-B. Zhang, “Demonstration of integrated longitudinal and lateral control for the operation of automated vehicles in platoons,” *IEEE Transactions on Control Systems Technology*, vol. 8, no. 4, pp. 695–708, 2000. DOI: [10.1109/87.852914](https://doi.org/10.1109/87.852914).
- [21] R. Sipahi, S.-I. Niculescu, and I. I. Delice, “Asymptotic stability of constant time headway driving strategy with multiple driver reaction delays,” in *2009 American Control Conference*, 2009, pp. 4898–4903. DOI: [10.1109/ACC.2009.5160482](https://doi.org/10.1109/ACC.2009.5160482).
- [22] R. Donà, K. Mattas, Y. He, G. Albano, and B. Ciuffo, “Multianticipation for string stable adaptive cruise control and increased motorway capacity without vehicle-to-vehicle communication,” *Transportation Research Part C: Emerging Technologies*, vol. 140, p. 103687, 2022, ISSN: 0968-090X. DOI: <https://doi.org/10.1016/j.trc.2022.103687>. [Online]. Available: <https://www.sciencedirect.com/science/article/pii/S0968090X22001280>.
- [23] B. Ciuffo, K. Mattas, M. Makridis, *et al.*, “Requiem on the positive effects of commercial adaptive cruise control on motorway traffic and recommendations for future automated driving systems,” *Transportation Research Part C: Emerging Technologies*, vol. 130,

- p. 103 305, 2021, ISSN: 0968-090X. DOI: <https://doi.org/10.1016/j.trc.2021.103305>. [Online]. Available: <https://www.sciencedirect.com/science/article/pii/S0968090X21003144>.
- [24] K. Santhanakrishnan and R. Rajamani, “On spacing policies for highway vehicle automation,” *IEEE Transactions on Intelligent Transportation Systems*, vol. 4, no. 4, pp. 198–204, 2003. DOI: [10.1109/TITS.2003.821341](https://doi.org/10.1109/TITS.2003.821341).
- [25] P. Ioannou, Z. Xu, S. Eckert, D. Clemons, and T. Sieja, “Intelligent cruise control: Theory and experiment,” in *Proceedings of 32nd IEEE Conference on Decision and Control*, 1993, 1885–1890 vol.2. DOI: [10.1109/CDC.1993.325521](https://doi.org/10.1109/CDC.1993.325521).
- [26] S. Darbha and K. Rajagopal, “Intelligent cruise control systems and traffic flow stability,” *Transportation Research Part C: Emerging Technologies*, vol. 7, no. 6, pp. 329–352, 1999, ISSN: 0968-090X. DOI: [https://doi.org/10.1016/S0968-090X\(99\)00024-8](https://doi.org/10.1016/S0968-090X(99)00024-8). [Online]. Available: <https://www.sciencedirect.com/science/article/pii/S0968090X99000248>.
- [27] J. Wang and R. Rajamani, “Should adaptive cruise-control systems be designed to maintain a constant time gap between vehicles?” *IEEE Transactions on Vehicular Technology*, vol. 53, no. 5, pp. 1480–1490, 2004. DOI: [10.1109/TVT.2004.832386](https://doi.org/10.1109/TVT.2004.832386).
- [28] A. Maxim, C. F. Caruntu, and C. Lazar, “Cruise and headway control for vehicle platooning using a distributed model predictive control algorithm,” in *2017 21st International Conference on System Theory, Control and Computing (ICSTCC)*, 2017, pp. 146–151. DOI: [10.1109/ICSTCC.2017.8107025](https://doi.org/10.1109/ICSTCC.2017.8107025).
- [29] A. Kesting, M. Treiber, M. Schönhof, and D. Helbing, “Adaptive cruise control design for active congestion avoidance,” *Transportation Research Part C: Emerging Technologies*, vol. 16, no. 6, pp. 668–683, 2008, ISSN: 0968-090X. DOI: <https://doi.org/10.1016/j.trc.2007.12.004>. [Online]. Available: <https://www.sciencedirect.com/science/article/pii/S0968090X08000028>.
- [30] S. Li, K. Li, R. Rajamani, and J. Wang, “Model predictive multi-objective vehicular adaptive cruise control,” *IEEE Transactions on Control Systems Technology*, vol. 19, no. 3, pp. 556–566, 2011. DOI: [10.1109/TCST.2010.2049203](https://doi.org/10.1109/TCST.2010.2049203).
- [31] P. Nilsson, O. Hussien, A. Balkan, *et al.*, “Correct-by-construction adaptive cruise control: Two approaches,” *IEEE Transactions on Control Systems Technology*, vol. 24, no. 4, pp. 1294–1307, 2016. DOI: [10.1109/TCST.2015.2501351](https://doi.org/10.1109/TCST.2015.2501351).

- [32] P. Barooah, P. G. Mehta, and J. P. Hespanha, “Mistuning-based control design to improve closed-loop stability margin of vehicular platoons,” *IEEE Transactions on Automatic Control*, vol. 54, no. 9, pp. 2100–2113, 2009. DOI: [10.1109/TAC.2009.2026934](https://doi.org/10.1109/TAC.2009.2026934).
- [33] R. Delpiano, J. C. Herrera, J. Laval, and J. E. Coeymans, “A two-dimensional car-following model for two-dimensional traffic flow problems,” *Transportation Research Part C: Emerging Technologies*, vol. 114, pp. 504–516, 2020, ISSN: 0968-090X. DOI: <https://doi.org/10.1016/j.trc.2020.02.025>. [Online]. Available: <https://www.sciencedirect.com/science/article/pii/S0968090X18317996>.
- [34] Y. Zhou, S. Ahn, M. Chitturi, and D. A. Noyce, “Rolling horizon stochastic optimal control strategy for acc and cacc under uncertainty,” *Transportation Research Part C: Emerging Technologies*, vol. 83, pp. 61–76, 2017, ISSN: 0968-090X. DOI: <https://doi.org/10.1016/j.trc.2017.07.011>. [Online]. Available: <https://www.sciencedirect.com/science/article/pii/S0968090X17301997>.
- [35] P. Y. Li and A. Shrivastava, “Traffic flow stability induced by constant time headway policy for adaptive cruise control vehicles,” *Transportation Research Part C: Emerging Technologies*, vol. 10, no. 4, pp. 275–301, 2002, ISSN: 0968-090X. DOI: [https://doi.org/10.1016/S0968-090X\(02\)00004-9](https://doi.org/10.1016/S0968-090X(02)00004-9). [Online]. Available: <https://www.sciencedirect.com/science/article/pii/S0968090X02000049>.
- [36] A. Delis, I. Nikolos, and M. Papageorgiou, “Macroscopic traffic flow modeling with adaptive cruise control: Development and numerical solution,” *Computers and Mathematics with Applications*, vol. 70, no. 8, pp. 1921–1947, 2015, ISSN: 0898-1221. DOI: <https://doi.org/10.1016/j.camwa.2015.08.002>. [Online]. Available: <https://www.sciencedirect.com/science/article/pii/S0898122115003703>.
- [37] Y. Zhang, B. Kosmatopoulos, P. Ioannou, and C. Chien, “Using front and back information for tight vehicle following maneuvers,” *IEEE Transactions on Vehicular Technology*, vol. 48, no. 1, pp. 319–328, 1999. DOI: [10.1109/25.740110](https://doi.org/10.1109/25.740110).
- [38] I. Kilic, A. Yazici, O. Yildiz, M. Özçelikors, and A. Ondoan, “Intelligent adaptive cruise control system design and implementation,” *2015 10th System of Systems Engineering Conference, SoSE 2015*, pp. 232–237, Jul. 2015. DOI: [10.1109/SYSoSE.2015.7151967](https://doi.org/10.1109/SYSoSE.2015.7151967).
- [39] Federal Highway Administration (FHWA), *Third Generation Simulation (TGSIM) Data*, Available: https://catalog.data.gov/dataset/?q=Third+Generation+Simulation+Data&sort=views_recent+desc&publisher=Federal+Highway+

[`Administration&organization=dot-gov&ext_location=&ext_bbox=&ext_prev_extent=`](#). Accessed: Nov. 25, 2024, 2024.

- [40] A. Talebpour, H. S. Mahmassani, and S. H. Hamdar, “Third generation simulation data (tgSim): A closer look at the impacts of automated driving systems on human behavior,” Federal Highway Administration, University of Illinois at Urbana-Champaign, Urbana, Illinois 61801, Tech. Rep. FHWA-JPO-24-133, May 2024, The project CORs were Rachel James and John Hourdos. The JPO Program Manager was Hyungjun Park.
- [41] R. Ammourah, P. Beigi, B. Fan, *et al.*, “Introduction to the third generation simulation dataset: Data collection and trajectory extraction,” *Transportation Research Record*, pp. 1–17, 2024. DOI: [10.1177/0361198124125757](https://doi.org/10.1177/0361198124125757).
- [42] Y. Zhang, D. Monzer, N. Li, *et al.*, *Coexistence in motion: Unveiling the behavioral dynamics of humans and highly automated vehicles in naturalistic mixed traffic*, Presented at the Transportation Research Board (TRB) 103rd Annual Meeting, Paper No. TRBAM-25-05831, Washington, D.C., Jan. 2025.
- [43] D. Swaroop and J. K. Hedrick, “Constant spacing strategies for platooning in automated highway systems,” *Journal of Dynamic Systems, Measurement, and Control*, vol. 121, no. 3, pp. 462–470, Sep. 1999, ISSN: 0022-0434. DOI: [10.1115/1.2802497](https://doi.org/10.1115/1.2802497). eprint: https://asmedigitalcollection.asme.org/dynamicsystems/article-pdf/121/3/462/5779606/462_1.pdf. [Online]. Available: <https://doi.org/10.1115/1.2802497>.
- [44] P. Ioannou and C. Chien, “Autonomous intelligent cruise control,” *IEEE Transactions on Vehicular Technology*, vol. 42, no. 4, pp. 657–672, 1993. DOI: [10.1109/25.260745](https://doi.org/10.1109/25.260745).
- [45] J. Wang and R. Rajamani, “The impact of adaptive cruise control systems on highway safety and traffic flow,” *Proceedings of the Institution of Mechanical Engineers, Part D: Journal of Automobile Engineering*, vol. 218, no. 2, pp. 111–130, 2004. DOI: [10.1243/095440704772913918](https://doi.org/10.1243/095440704772913918). eprint: <https://doi.org/10.1243/095440704772913918>. [Online]. Available: <https://doi.org/10.1243/095440704772913918>.
- [46] J. Zhao and A. El Kamel, “Coordinated throttle and brake fuzzy controller design for vehicle following,” in *13th International IEEE Conference on Intelligent Transportation Systems*, 2010, pp. 659–664. DOI: [10.1109/ITSC.2010.5625158](https://doi.org/10.1109/ITSC.2010.5625158).
- [47] S. Thede, “An introduction to genetic algorithms,” *Journal of Computing Sciences in Colleges*, vol. 20, Oct. 2004.